

Fall 12-14-2018

Development of Chloroquine-containing HPMA Copolymers for Drug Delivery

Fei Yu

University of Nebraska Medical Center

Tell us how you used this information in this [short survey](#).

Follow this and additional works at: <https://digitalcommons.unmc.edu/etd>

 Part of the [Medicinal Chemistry and Pharmaceutics Commons](#)

Recommended Citation

Yu, Fei, "Development of Chloroquine-containing HPMA Copolymers for Drug Delivery" (2018). *Theses & Dissertations*. 307.

<https://digitalcommons.unmc.edu/etd/307>

This Dissertation is brought to you for free and open access by the Graduate Studies at DigitalCommons@UNMC. It has been accepted for inclusion in Theses & Dissertations by an authorized administrator of DigitalCommons@UNMC. For more information, please contact digitalcommons@unmc.edu.

Development of Chloroquine-containing HPMA Copolymers for Drug Delivery

by

Fei Yu

A DISSERTATION

Presented to the Faculty of
the University of Nebraska Graduate College
in Partial Fulfillment of the Requirements
for the Degree of Doctor of Philosophy

Pharmaceutical Sciences Graduate Program

Under the Supervision of Professor David Oupický

University of Nebraska Medical Center
Omaha, Nebraska

September, 2018

Supervisory Committee:

Martin Conda-Sheridan, Ph.D.

Maneesh Jain, Ph.D.

Rongshi Li, Ph.D.

Acknowledgments

I would like to sincerely thank my mentor, Dr. David Oupický for his constant support, guidance and encouragement during my Ph.D. study. I am extremely lucky to have Dr. Oupický as my mentor who truthfully cares about my work, my life and my future. He is always willing to share his knowledge, listen to my idea, discuss my results and inspire me to resolve the problems. His passion, professional attitude and dedication to pharmaceutical sciences encourage me to be a great scientist. I appreciate his mentorship during the past 4 years.

I would also like to sincerely thank my graduate supervisory committees, Dr. Martin Conda-Sheridan, Dr. Rongshi Li and Dr. Maneesh Jain for their guidance, valuable suggestions, encouragement, as well as their help with my career development throughout my study in UNMC.

My special gratitude goes to my group members. I would like to thank Dr. Jing Li for her endless help with animal study, thank Dr. Zhenghong Peng for his help with synthesis, thank Dr. Yan Wang, Ying Xie, Dr. Yazhe Wang, Yu Hang for their help with biological assays. I also want to thank Yi Chen, Richard Lee Sleightholm, Lee Jaramillo, Shrey Kanvinde, Suthida Boonsith, Weimin Tang and Ao Yu for their help in and out of the lab. I want to thank Daniela Machová for her help. I really enjoy the time we spent together.

I would like to express my gratitude to Ed Ezell from UNMC NMR Facility for all his help with chemical structure determination and equipment operation. I also want to thank UNMC Advanced Microscopy Core Facility and Tissue Facility. I would like to thank Dr. Amar Natarajan and Dr. David Kelly for their help with high-throughput screening. I would also like to thank Dr. DJ Murry, Dr. Jered Garrison, and Dr. Wei Fan and Wenting Zhang in Dr. Garrison's lab for their endless help with LC-MS. I also want to thank the Department of Pharmaceutical Sciences, Graduate Study for helping me finish my study.

I would like to thank Graduate Assistantship/Fellowship, Program of Excellence of UNMC Graduate Study and Presidential Graduate Fellowship of University of Nebraska Foundation for their financial support and encouragement. I would also like to thank Berndt Travel Award for their generous support.

Last but not least, I would like to thank all my family. I would like to thank my parents, Haifang Wang and Chuanyi Yu for their concern and support. I want to thank my husband, Bin Yang, who is a very good chemist, for his endless love and support. I am very lucky to have him listen to me all the time and talk about my study.

I appreciate all the help from everybody that makes me a better person.

Abstract

Development of Chloroquine-containing HPMA Copolymers for Drug Delivery

Fei Yu, Ph.D.

University of Nebraska Medical Center, 2018

Supervisor: David Oupický, Ph.D.

Synthetic polymers have been extensively explored for improved delivery of anticancer agents. Polymers can be designed as either carriers of existing drugs or as polymeric drugs with intrinsic pharmacological activity. Advantages of such polymeric drugs include common positive features of polymer-drug conjugates, such as targeted delivery of drugs, altered pharmacokinetic and biodistribution, improved drug safety, but also favorable pharmacological activities due to multivalent receptor-ligand interactions.

Chloroquine (CQ) and hydroxychloroquine (HCQ) are safe drugs that have been in clinical use for longer than six decades. In addition to their antimalarial and antirheumatoid use, CQ and HCQ are known to synergistically enhance the activity of multiple anticancer drugs via complementary mechanisms of action so that they are applied in numerous clinical trials. In this study, we proposed that using the polymeric drug concept in the development of CQ-containing polymers will allow us to improve the pharmacological activity.

We first synthesized copolymers based on *N*-(2-hydroxypropyl)methacrylamide (HPMA) and methacryloyl-hydroxychloroquine (MA-CQ) as pCQ that exhibited lowered cytotoxicity, enhanced inhibition of cancer cell migration and invasion, improved antimetastatic activity *in vivo*, and prolonged animal survival when compared with parent HCQ. These results suggest the potential of pCQ used for combination anticancer therapy to achieve simultaneous antimetastasis effect. Therefore, we then developed reduction-responsive camptothecin (CPT)-pCQ copolymers as pCQCPT that were used for codelivery of CPT and pCQ. The *in vivo* study showed that pCQCPT

exhibited significantly enhanced inhibitory activity on tumor growth and antimetastasis activity when compared to CPT. In addition, we investigated the role of the linkage between CQ and polymer backbone by using ester in pCQ and a stable amide and triazole ring by copolymerization of HPMA and methacrylamido methyl triazole chloroquine (MA-tCQ) as NpCQ. NpCQ showed similar inhibitory activity of pCQ on cancer cell migration, suggesting that pCQ functions as a pharmacologically active polymer drug that does not require the release of the small molecule HCQ. Overall, this study provides clear impetus for further development of pCQ as a new class of antimetastatic polymer agents with possibly unique mechanism of action that is not found in HCQ.

Table of Contents

Acknowledgments	i
Abstract	iii
Table of Contents	v
List of Figures	ix
List of Schemes	xiii
List of Tables	xiv
List of Abbreviations	xv
1 Introduction.....	1
1.1 Synthetic polymers for anticancer drug delivery system	2
1.1.1 Degradable synthetic polymers for anticancer drug delivery.....	2
1.1.1.1 Poly(α -hydroxy acids).....	3
1.1.1.2 Poly(lactones)	5
1.1.2 Stimuli-responsive synthetic polymers for anticancer drug delivery	8
1.2 HPMA copolymers for anticancer drug delivery	11
1.2.1 Traditional HPMA-drug conjugates in clinical trials	12
1.2.2 New generation of HPMA copolymer-drug conjugates.....	14
1.2.2.1 pH-triggered degradable HPMA copolymer-drug conjugates	15
1.2.2.2 Reductively degradable HPMA copolymer-drug conjugates.....	17
1.2.2.3 Other spacers used in HPMA copolymer-drug conjugates	18
1.3 Polymeric drugs for cancer treatment	24
1.3.1 Polymeric drugs with anticancer activities	24

1.3.2	Pharmaceutical ingredients with newly discovered bioactivities.....	26
1.4	CQ for cancer treatment.....	27
1.4.1	CQ/HCQ monotherapy	28
1.4.2	Combination therapy with CQ/HCQ.....	30
1.4.3	Mechanism of action.....	35
1.4.3.1	Inhibition of autophagy	35
1.4.3.2	Inhibition of CXCL12/CXCR4 signaling pathway	37
1.4.3.3	Effects on tumor microenvironment	37
2	Synthesis and characterization of CQ-containing HPMA polymers.....	39
2.1	Synthesis of MA-CQ.....	40
2.2	Synthesis of pCQ by free radical polymerization	44
2.3	Synthesis of RpCQ by RAFT polymerization	47
2.4	Synthesis of <i>N</i> -propargyl methacrylamide (PPMA)	50
2.5	Synthesis of CQ-N ₃	52
2.6	Synthesis of methacrylamido methyl triazole chloroquine (MA-tCQ).....	65
2.7	Synthesis of non-degradable CQ-containing polymers by free radical polymerization (FNpCQ)	67
2.8	Synthesis of non-degradable CQ-containing polymers by RAFT polymerization of HPMA and MA-tCQ (RNpCQ)	68
2.9	Synthesis of non-degradable CQ-containing polymers from clickable poly(HPMA- <i>co</i> -PPMA) (pHP) copolymers	70
2.9.1	Investigation of CTA for polymerization of pHP copolymers.....	70

2.9.2	Synthesis of pHP.....	71
2.9.3	Synthesis of non-degradable CQ-containing HPMA copolymers (CNpCQ) by click reaction of CQ-N ₃ and pHP	74
2.9.4	Synthesis of poly(hydroxypropyl methacrylate- <i>co</i> -PPMA) (pHPte) copolymers by RAFT polymerization	77
2.9.5	Synthesis of non-degradable CQ-containing HPMAte copolymers (pHPte-CQ) by click reaction of CQ-N ₃ and pHPte.....	80
2.10	Synthesis of CQ- and CPT-containing HPMA copolymers.....	82
2.11	Synthesis of diblock PLA-pCQ copolymers	87
3	Effect of polymeric CQ on cancer metastasis.....	93
3.1	Inhibition of cancer cell migration and experimental lung metastasis by polymeric chloroquine pCQ.....	95
3.1.1	Cell culture.....	95
3.1.2	Cytotoxicity of the polymers.....	95
3.1.3	Inhibition of autophagy by polymers	97
3.1.4	pCQ effect on cell surface expression of CXCR4	100
3.1.5	pCQ effect on CXCR4 redistribution.....	101
3.1.6	pCQ effect on the CXCR4/CXCL12 axis	103
3.1.7	Antimetastatic activity <i>in vivo</i>	108
3.1.8	Survival study	112
3.2	Clicked CQ copolymers for inhibition of cancer cell migration.....	114
3.2.1	Cytotoxicity of NpCQ polymers	115

3.2.2	Effect of NpCQ on 4T1 cancer cell migration	116
3.3	CPT-containing reduction-responsive polymeric CQ for combinational treatment of breast cancer	121
3.3.1	Cytotoxicity of polymers	122
3.3.2	Anticancer effect <i>in vivo</i>	124
4	Conclusion	128
	References.....	131

List of Figures

- Figure 1.1.** Chemical structure of mPEG-PLLA-PMMD and PTX-loaded nanoparticle.
- Figure 1.2.** Illustration of PTX-loaded Pt-gel.
- Figure 1.3.** Synthesis of CP.
- Figure 1.4.** Schematic illustration of biodegradable photoluminescent polylactide (BPLPL-Cys-PLLA) synthesis and its applications in scaffold imaging and nanoparticle tracking *in vivo*.
- Figure 1.5.** Synthesis route of mPEG-PCL and FA-PCL-PEG.
- Figure 1.6.** Synthetic scheme of reduction-degradable PAA-*g*-PEG amphiphilic graft copolymer.
- Figure 1.7.** Synthesis of PEG-SS-PTMBPEC.
- Figure 1.8.** First-generation HPMA polymer-anticancer drug conjugates used in clinical trials.
- Figure 1.9.** Chemical structure of HPMA copolymer-2-pyrrolinodoxorubicin (left) and HPMA copolymer-THP (right).
- Figure 1.10.** Structure of HPMA copolymer-*N-cis*-aconityl-ADR conjugate (P-aconityl-ADR).
- Figure 1.11.** Synthesis of P-SS-Mce₆.
- Figure 1.12.** Structure of HPMA copolymer-9-AC with azo linker.
- Figure 1.13.** Structure of macromolecular HPMA copolymer conjugates.
- Figure 1.14.** Structure of DIVEMA, ECT-PMA and PAMD.
- Figure 1.15.** Induction of apoptosis in human Burkitt's NHL Raji B cells by crosslinking its CD20 antigens mediated by antiparallel coiled-coil formation at the cell surface.
- Figure 1.16.** Structure of Pluronic.
- Figure 1.17.** Chemical structures of CQ, HCQ and 4-aminoquinoline.

Figure 1.18. Process of autophagy.

Figure 2.1. ^1H NMR and ^{13}C NMR of HCQ in CDCl_3 .

Figure 2.2. ^1H NMR and ^{13}C NMR of MA-CQ in CDCl_3 .

Figure 2.3. ^1H NMR of pHPMA in $\text{DMSO-}d_6$.

Figure 2.4. ^1H NMR of pCQ in $\text{DMSO-}d_6$.

Figure 2.5. ^1H NMR of RpHPMA in $\text{DMSO-}d_6$.

Figure 2.6. ^1H NMR of RpCQ in $\text{DMSO-}d_6$.

Figure 2.7. ^1H NMR and ^{13}C NMR of PPMA in CDCl_3 .

Figure 2.8. ^1H NMR, ^{13}C NMR of CQ- N_3 , COSY Expansion 1, COSY Expansion 2, COSY Expansion 3, COSY Expansion 4, COSY Expansion 5, HSQC, HSQC Expansion 1, HSQC Expansion 2, HSQC Expansion 3, ^{13}C HMBC Expansion 1, ^{13}C HMBC Expansion 2, ^{13}C HMBC Expansion 3, ^{13}C HMBC Expansion 4, ^{15}N HMBC 1, ^{15}N HMBC 2, ^{15}N HMBC Expansion 1, ^{15}N HMBC Expansion 2, and ^{15}N HMBC Expansion 3 in CDCl_3 .

Figure 2.9. ^1H NMR and ^{13}C NMR of MA-tCQ in CDCl_3 .

Figure 2.10. ^1H NMR of FNpCQ in $\text{DMSO-}d_6$.

Figure 2.11. ^1H NMR of RNpCQ in $\text{DMSO-}d_6$.

Figure 2.12. Typical ^1H NMR spectrums of pHP polymers in $\text{DMSO-}d_6$.

Figure 2.13. GPC spectrums of pHP polymers.

Figure 2.14. GPC spectrums of pHP-CQ polymers and comparison of pHP to the corresponding pHP-CQ.

Figure 2.15. Typical ^1H NMR spectrums of pHPte polymers in $\text{DMSO-}d_6$.

Figure 2.16. GPC spectrums of pHPte copolymers.

Figure 2.17. GPC spectrums of pHPte-CQ polymers and comparison of pHPte to the corresponding pHPte-CQ.

Figure 2.18. ^1H NMR of MA-SS-OH and MA-SS-CPT in CDCl_3 .

Figure 2.19. ^1H NMR of pCQCPT, pCPT, pCQ_C in $\text{DMSO-}d_6$.

Figure 2.20. ^1H NMR of 4-(dodecyl trithiocarbonyl)-4-cyano-1-pentanol in CDCl_3 , PLA-CTA in CDCl_3 and PLA-pCQ10H in $\text{DMSO-}d_6$.

Figure 2.21. GPC spectrums of pCQ-PLA polymers.

Figure 3.1. Cytotoxicity of pCQ. Cell viability of pCQ, HCQ and pHPMA was determined using CellTiter-Blue Assay.

Figure 3.2. Effect of pCQ on autophagy in U2OS and 4T1 cells.

Figure 3.3. Effect of pCQ on expression of surface CXCR4 receptors in U2OS cells.

Figure 3.4. Effect of pCQ on redistribution of the CXCR4 receptors under stimulation with CXCL12.

Figure 3.5. Inhibition of CXCL12-induced cell invasion.

Figure 3.6. Inhibition of pERK by pCQ.

Figure 3.7. Inhibition of FBS-induced cell migration.

Figure 3.8. Antimetastatic activity of pCQ in experimental 4T1 lung metastasis model.

Figure 3.9. Toxicity evaluation of pCQ *in vivo*.

Figure 3.10. (A) Survival curve of experimental lung metastasis model of the 4T1 breast cancer.

(B) Body weight changes of the animals treated by PBS, HCQ and pCQ16.7.

Figure 3.11. Cytotoxicity of CQ-containing polymers in 4T1 cells at CQ concentration of $30\ \mu\text{M}$.

Figure 3.12. Inhibition of FBS induced 4T1 migration. Inhibition of FBS-induced 4T1 cell migration utilizing transwell assay.

Figure 3.13. Inhibition of 4T1 cell migration utilizing wound healing assay.

Figure 3.14. Cytotoxicity of pCQCPT, pCPT, pCPT+pCQ_C, CPT and CPT+pCQ_C.

Figure 3.15. Tumor growth curve of mice treated with CPT, pCPT, pCPT+pCQ_C, and pCQCPT.

Figure 3.16. Percentage of animal body weight compared to day 8 during treatment (n=5).

Figure 3.17. Average number of surface lung metastases.

Figure 3.18. Representative images of histological analysis of tumor sections stained with H&E (4 ×) and Ki67 (40 ×).

List of Schemes

Scheme 2.1. Synthesis of MA-CQ.

Scheme 2.2. Synthesis of pCQ by free radical polymerization.

Scheme 2.3. Synthesis of RpCQ by RAFT polymerization.

Scheme 2.4. Synthesis of PPMA.

Scheme 2.5. Synthesis of CQ-N₃.

Scheme 2.6. Synthesis of MA-tCQ by click chemistry.

Scheme 2.7. Synthesis of FNpCQ.

Scheme 2.8. Synthesis of noncleavable RNpCQ by RAFT polymerization.

Scheme 2.9. Synthesis of pHP by RAFT polymerization.

Scheme 2.10. Synthesis of CNpCQ.

Scheme 2.11. Synthesis of pHPte by RAFT polymerization.

Scheme 2.12. Synthesis of pHPte-CQ by click chemistry.

Scheme 2.13. Synthesis of MA-SS-CPT.

Scheme 2.14. Synthesis of pCQCPT.

Scheme 2.15. Synthesis of 4-(dodecyl trithiocarbonyl)-4-cyano-1-pentanol, PLA-CTA and PLA-pCQ.

Scheme 3.1. Chemical structure of pCQCPT, pCPT and pCQ_C used in combination delivery study.

List of Tables

Table 1.1. Preclinical *in vivo* research combining anticancer drugs with CQ/HCQ.

Table 2.1. Characterization of pCQ polymers.

Table 2.2. Characterization of RpCQ polymers.

Table 2.3. Characterization of F/RNpCQ polymers.

Table 2.4. Characterization of pHP polymer with different chain transfer agent.

Table 2.5. Synthesis and characterization of pHP.

Table 2.6. Summary of CNpCQ.

Table 2.7. Synthesis and characterization of pHPte.

Table 2.8. Summary of pHPte-CQ.

Table 2.9. Summary of pCQCPT, pCPT and pCQ_C.

Table 2.10. Summary of PLA-pCQ.

Table 3.1. Summary of polymer characterization of NpCQ study.

List of Abbreviations

^1H NMR - proton nuclear magnetic resonance

2D NMR - two-dimensional NMR

9-AC - 9-aminocamptothecin

^{13}C NMR - carbon 13 NMR

AIBN - azobisisobutyronitrile

APC - allophycocyanin

ATG5/7 - autophagy related 5/7

ATRA - atom transfer radical addition

BPLALs - biodegradable photoluminescent polylactones

BPLP-Cys-PLLA - biodegradable photoluminescent polylactones-polycystamine-poly(L-lactic acid)

calcd - calculated

CMC - critical micelle concentration

COSY - homonuclear correlation spectroscopy

CP - chondroitin sulfate-g-poly(ϵ -caprolactone)

CPDT - 2-cyano-2-propyl dodecyl trithiocarbonate

CPT - camptothecin

CQ - chloroquine

CQ-N₃ - CQ azide

CTA - chain transfer agent

CTPA - 4-cyano-4-[(ethylsulfanylthiocarbonyl)sulfanyl] pentanoic acid

CuAAC - copper (I)-catalyzed azide-alkyne cycloaddition

CXCL12 - C-X-C motif chemokine ligand 12

CXCR4 - C-X-C chemokine receptor type 4

DBU - 1,8-diazabicyclo[5.4.0]undec-7-ene

DCM - dichloromethane

Dex - dextran

DEX - dexamethasone

DIVEMA - maleic anhydride

DMAP - 4-dimethylaminopyridine

DMEM - Dulbecco's Modified Eagle Medium

DMF - dimethylformamide

DMSO - dimethyl sulfoxide

DOX - doxorubicin

DPPA - diphenylphosphoryl azide

DTT - 1,4-dithiothreitol

ECT-PMA - end carboxyl-trithiocarbonate functionalized poly(maleic anhydride)

EDC·HCl - *N*-(3-dimethylaminopropyl)-*N*'-ethylcarbodiimide hydrochloride

EDTA - disodium dihydrogen ethylenediaminetetraacetate

EGFR - epidermal growth factor receptor

EMEM - Eagle's Minimum Essential Medium

EO - ethylene oxide

EPR - enhanced permeability and retention

ERK - extracellular signal-regulated kinases

FA-PCL-PEG - folate-conjugated poly(ϵ -caprolactone)-poly(ethylene glycol)

FBS - fetal bovine serum

FDA - Food and Drug Administration

FNpCQ - non-degradable CQ-containing polymers synthesized by free radical polymerization

GAPDH - glyceraldehyde-3-phosphate dehydrogenase

GPC - gel permeation chromatography

HCQ - hydroxychloroquine

HMBC - heteronuclear multiple bond correlation

HSQC - heteronuclear single quantum correlation

HPMA - *N*-(2-hydroxypropyl)methacrylamide

HPMAte - hydroxypropyl methacrylate

HRP - horseradish peroxidase

IgG - immunoglobulin G

IP - intraperitoneal

MAA - methacrylic acid

MA-CQ - methacryloyl-hydroxychloroquine

MA-SS-OH - mono-methacrylated dithiodiethanol

MA-tCQ - methacrylamido methyl triazole chloroquine

MAPK - mitogen-activated protein kinase

Mce₆ - mesochlorin e₆

MCL-1 - induced myeloid leukemia cell differentiation protein

MDR - multidrug-resistant cancer

MitC - Mitomycin C

mPEG-PLA - poly(ethylene glycol)-poly(lactic acid)

mPEG-PLLA-PMMD - poly(ethylene glycol)-poly(L-lactide)-poly(3(S)-methyl-morpholine-2,5-dione)

NaAs - sodium ascorbate

NMR - nuclear magnetic resonance

NpCQ - non-degradable pCQ

PAA - poly(amido amine)

PAMD - polymer of AMD3100

PBS - phosphate-buffered saline

PCL - poly(ϵ -caprolactone)

pCQ - polymeric chloroquine

pCQ_C - pCQ copolymer used in co-delivery of CPT and pCQ project

pCQCPT - camptothecin-conjugated pCQ copolymers

PD - pharmacodynamic

PDEA - poly(2-(diethyl amino)ethyl methacrylate)

PDI - polydispersity

pDTC - poly(dithiolane trimethylene carbonate)

PEG - poly(ethylene glycol)

PEI - polyethylenimine

Pen-Strep - Penicillin-Streptomycin

PEO-*b*-(CL-*g*-SP) - poly(ethylene oxide)-*b*-poly(ϵ -caprolactone-*grafted*-spermine)

PGA - poly(glycolic acid)

pHP - poly(HPMA-*co*-PPMA)

pHPMA - HPMA polymer synthesized by free radical polymerization

pHPte - poly(hydroxypropyl methacrylate-*co*-PPMA)

PK - pharmacokinetic

PK1, PK2, P-DOX - DOX-conjugated HPMA copolymers

PLGA - poly(lactic-*co*-glycolic acid)

PLA - poly(lactic acid)

PO - propylene oxide

PPA - propargyl amine

PPMA - *N*-propargyl methacrylamide

PTMBPEC - poly(2,4,6-trimethoxybenzylidene-pentaerythritol carbonate)

PTX - paclitaxel

RAFT - reversible addition-fragmentation chain transfer

RGD4C - ACDCRGDCFCG

RNpCQ - non-degradable CQ-containing polymers synthesized by RAFT polymerization

ROS - reactive oxygen species

RpCQ - pCQ synthesized by RAFT polymerization

RpHPMA - pHPMA synthesized by RAFT polymerization

SCID - severe combined immune deficiency

SD - standard deviation

shRNA - short hairpin RNA

siRNA - small interfering RNA

THF - tetrahydrofuran

THP - pirarubicin

TLR9/NF- κ B - toll like receptor 9/nuclear factor-kappaB

TMC - trimethylene carbonate

PBLA - poly(β -benzyl-L-aspartate)

ZnPc - zinc(II) phthalocyanine

1 Introduction

Polymers have played an irreplaceable role in pharmaceuticals for spatiotemporal delivery of therapeutics. Polymers contribute not only in conventional drug formulations, but also in drug delivery systems to meet the demand of emergence of potent and specific therapeutics [1]. Polymers are used as excipients to compress, coat, and encapsulate bioactive agents in traditional pharmaceutical industry. Drug delivery systems request specific targeting, precise intracellular transport, tunable pharmacokinetics and pharmacodynamics to maintain drug concentration at expected concentration for certain period of time [2, 3]. Since the extensive study of enhanced permeability and retention (EPR) effect, polymers have been widely applied in cancer therapy as materials of nanocarriers or polymeric conjugates [4]. Polymers tethered therapeutics can be either polymeric drugs with intrinsic pharmacological activities to provide their own therapeutic benefits or biodegradable polymer-drug conjugates to improve release kinetics [5, 6]. There are several successful polymeric conjugates/nanomedicines of anticancer therapeutics that have been approved by the FDA and a lot of products are under clinical trials, such as Doxil (liposomal doxorubicin (DOX)), Abraxane (albumin-bound paclitaxel (PTX)), Myocet (liposome-encapsulated DOX, approved in Europe and Canada), Eligard (poly(D,L-lactide-*co*-glycolide) encapsulated leuprolide), DaunoXome (liposome-encapsulated daunorubicin), DepoCyt (liposomal cytarabine), Oncaspar (Pegylated asparaginase), Marqibo (liposome-encapsulated vincristine), Onivyde (liposomal irinotecan), Genexol-PM (PTX-loaded polymeric micelle, approved in Europe and Korea) and Ontak (engineered protein combining IL-2 and diphtheria toxin) [7]. Moreover, polymer-based combination anticancer therapy draws more and more attention for treatment of advanced cancer. Versatile combinational anticancer strategies, such as chemotherapeutic combination, nucleic acid-based co-delivery, intrinsic sensitive and extrinsic stimulus combinational patterns can achieve synergistic effect through multiple-target therapy [8]. This introduction will include synthetic polymers for anticancer drug delivery system with the focus on application of *N*-(2-Hydroxypropyl)

methacrylamide (HPMA) polymers to anticancer drug delivery, polymeric drugs and chloroquine (CQ) for cancer treatment.

1.1 Synthetic polymers for anticancer drug delivery system

Both natural and synthetic polymers have been extensively studied in drug delivery system. Natural polymers, especially carbohydrates, are widely used not only for nanoformulation, but also as excipients [9]. However, synthetic and semi-synthetic polymers are more flexible to be tuned in physical, chemical and biological properties to meet the requirements of specific application [10]. To release drugs, polymers are destructible in certain spatiotemporal circumstance. Biodegradable synthetic polymers request hydrolytical or proteolytical labile bonds in their backbone or crosslinker to release encapsulated or conjugated drugs after cleavage [1]. Synthetic biodegradable polymers include poly(α -hydroxy acids), poly(lactones), poly(orthoesters), poly(phospho esters), poly(carbonates), poly(anhydrides), poly(urethanes), poly(phosphazenes), poly(alkyl cyano acrylates), and poly(amino acids) [11]. Moreover, the requirement for delivery of therapeutic agents to specific intracellular organelles accelerates development of stimuli-responsive polymeric materials [12]. The following introduction will focus on advances in biodegradable and stimuli-responsive synthetic polymers for anticancer drug delivery.

1.1.1 Degradable synthetic polymers for anticancer drug delivery

Degradable synthetic polymers assist anticancer drug delivery through diverse forms, such as polymer-agents conjugates, polymeric nanoparticles, polymeric micelles, polymerosomes, polyplexes, polymer-lipid hybrid, etc. As all the delivery system, polymeric delivery system for anticancer drugs aims to alter the pharmacokinetic (PK) and pharmacodynamic (PD) profiles, improve drug release in targeted tissue and subcellular organelles, and minimize systemic side effects [13]. Examples of synthetic biodegradable polymers for anticancer drug delivery will be provided and I will focus on most widely investigated poly(α -hydroxy acids) and poly(lactones).

1.1.1.1 Poly(α -hydroxy acids)

Poly(α -hydroxy acids) are the most common biocompatible and biodegradable polymers in clinical medicine [14]. Poly(glycolic acid) (PGA), poly(lactic acid) (PLA) and poly(lactic-co-glycolic acid) (PLGA) are most widely explored in this class. FDA has approved PLGA encapsulated leuprolide as Eligard, which further inspired the development of PLGA formulation [11]. Except for delivery of small molecule, PLGA nanoparticles can be used for protein delivery, such as trastuzumab, to improve the target efficiency, PK profile and tumor penetration [15]. For theranostic purpose, hollow CuS nanoparticles and PTX were encapsulated in PLGA microspheres and labeled with radioiodine-131, which resulted in higher antitumor efficacy compared to monotherapies and guidance of near-infrared laser irradiation [16].

Nowadays, this class of polymers are often copolymerized or functionalized with hydrophilic moieties to achieve targeted delivery or specific purpose for challenging cancer treatment. Zhao et al. synthesized triblock poly(ethylene glycol)-poly(L-lactide)-poly(3(S)-methylmorpholine-2,5-dione) (mPEG-PLLA-PMMD) that presented lower critical micelle concentration (CMC), positive-shifted zeta-potential, better drug loading efficiency and stability compared to the diblock mPEG-PLLA (Figure 1.1). The elimination half-life for Taxol, PTX-loaded mPEG-PLLA nanoparticle, and PTX-loaded mPEG-PLLA-PMMD nanoparticle were 1.194 h, 1.547 h, and 1.941 h, respectively, due to the stabilization of triblock polymeric micelles by the hydrogen bonding of PMMD. This further revealed the potential of triblock copolymer mPEG-PLLA-PMMD as a promising carrier for targeted chemodrug delivery [17].

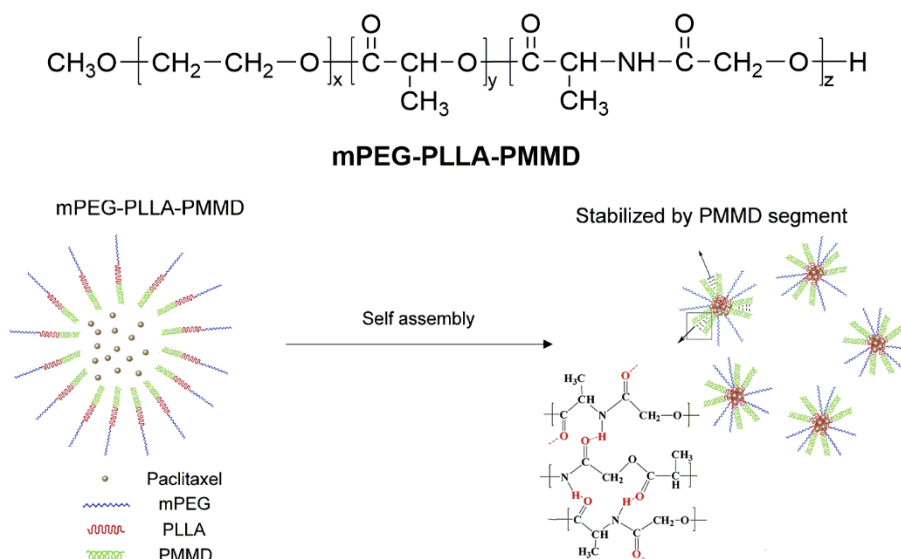


Figure 1.1. Chemical structure of mPEG-PLLA-PMMD and PTX-loaded nanoparticle. (Reproduced from [17].)

Poly(α -hydroxy acids) are also used in combination delivery of anticancer agents. Wang et al. applied methoxy poly(ethylene glycol)-poly(lactide-*co*-glycolide) mPEG-PLA based nanoparticles for co-delivery of hydrophilic DOX and hydrophobic PTX, which showed synergistic effect on suppression of cancer cell growth compared to DOX or PTX alone [18]. Zhang et al. applied PLGA-PEG for co-delivery of cisplatin and wortmannin to synergistically enhance chemoradiotherapy and reverse resistance in platinum resistant ovarian cancer [19]. PEG-PLGA was also used to covalently conjugate Pt(IV) and co-delivery PTX by micelles (Figure 1.2), which further exhibited as gel for sustained release of Pt and PTX. The PTX-loaded Pt-gel showed a well-controlled sustained release profile for 2.5 months and synergistic anticancer effect [20].

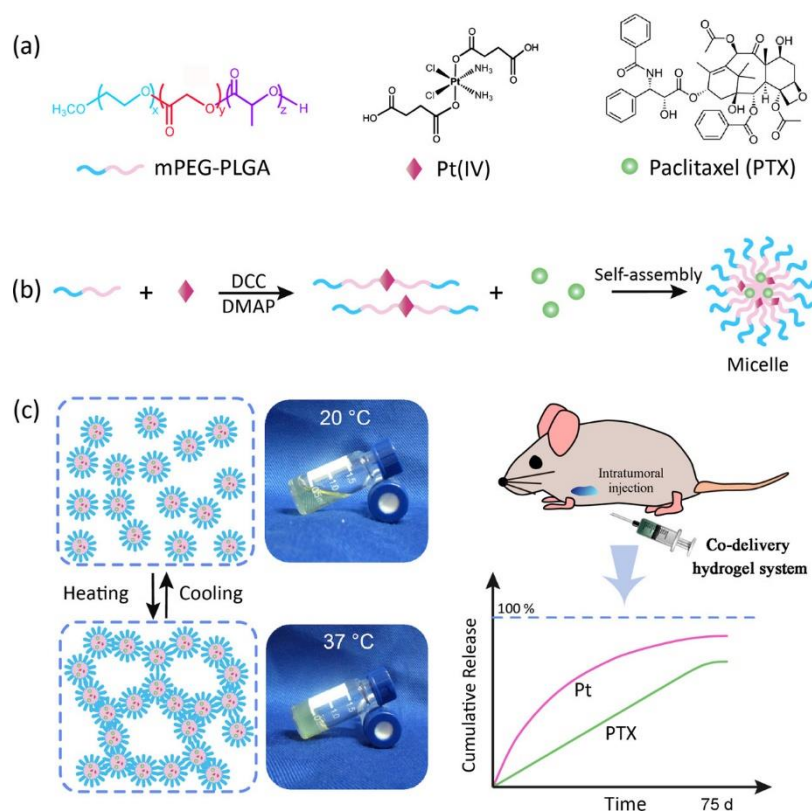


Figure 1.2. Illustration of PTX-loaded Pt-gel. (Reproduced from [20].)

1.1.1.2 Poly(lactones)

The most commonly studied poly(lactones) is poly- ϵ -caprolactone (PCL), which exhibits ester link hydrolysis but with a slower rate of degradation than poly(hydroxy acid) [11].

Similar to PLA and PLGA, PCL is also modified with hydrophilic block to form self-assembled nanoparticles or micelles, or novel delivery strategy. PCL-PEG was deposited on biocompatible substrates by plasma deposition with *cis*-platinum incorporated for local delivery of anticancer agent [21]. Garg et al. prepared poly(ethylene oxide)-*b*-poly(ϵ -caprolactone-*grafted*-spermine) (PEO-*b*-(CL-*g*-SP)) micelles modified with cholesterol group in the core and with RGD4C peptide on the shell for delivery of MCL-1 siRNA to breast cancer [22]. Liu et al. synthesized chondroitin sulfate-*g*-poly(ϵ -caprolactone) (CP) copolymers via atom transfer radical addition (ATRA), which exhibited self-assemble to micelle for encapsulation of camptothecin

(CPT) (Figure 1.3). CPT-loaded micelles showed CD44 targeted delivery that was promising for lung cancer treatment [23].

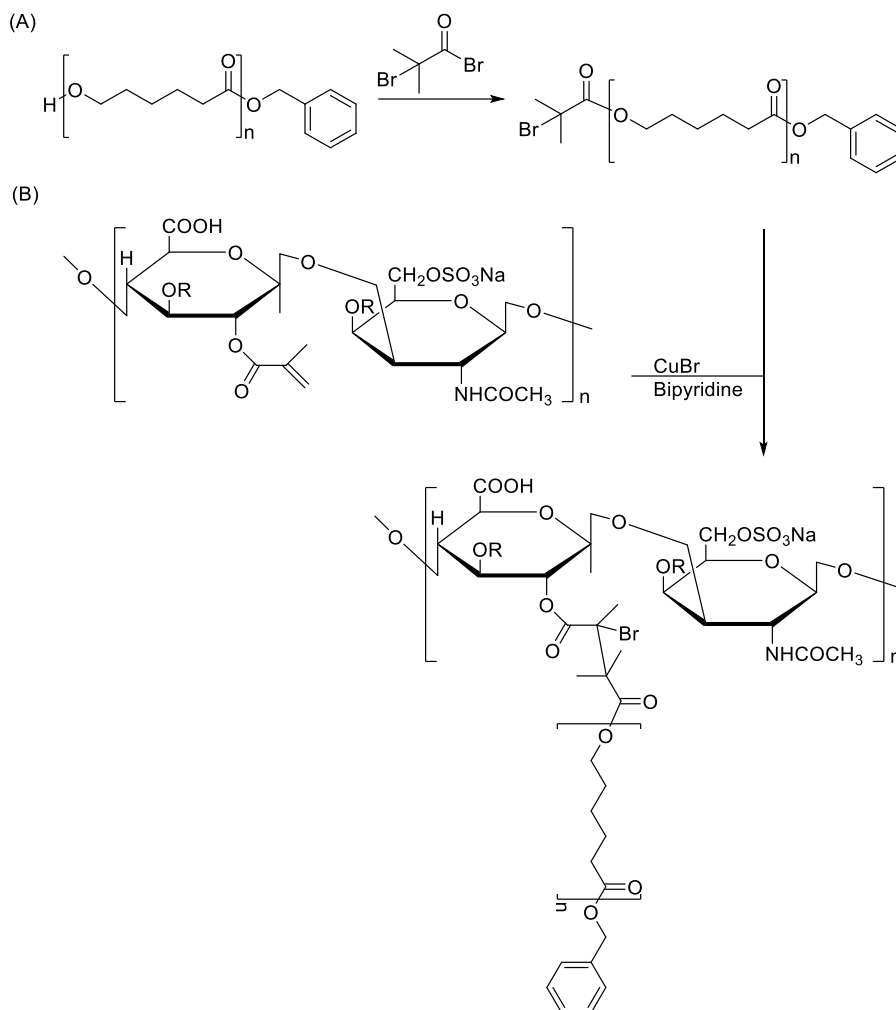


Figure 1.3. Synthesis of CP. (Reproduced from [23].)

PCL copolymers are also widely used in combination delivery of multiple therapeutic agents. PEG-*b*-PCL micelles were loaded with PTX, cyclophamide and gossypol, which enhanced tumor growth inhibition by intraperitoneal (IP) combination delivery for ovarian cancer treatment [24]. Docetaxel, everolimus and LY294002 were loaded in PEG-PCL nanoparticles tailored for lymphatic uptake and metastatic melanoma [25]. Stefan's group developed histone deacetylase

inhibitor conjugated PCL copolymers to prepared DOX loaded micelles for combination cancer therapy [26, 27].

Xie et al. developed a series of biodegradable poly(lactone) copolymers possessing photostable and intrinsic photoluminescence without conjugation or encapsulation of fluorescent dyes or quantum dots, which were promising for *in vivo* imaging and theranostic study. This biodegradable photoluminescent polylactones (BPLALs) were copolymerized with lactide to form BPLP-PLLA. The resulting BPLP-PLLA remained intrinsic photoluminescence and was further fabricated to nanoparticle, which retained detectable fluorescence for 4 weeks and was able to be monitored for the degradation in mice [28].

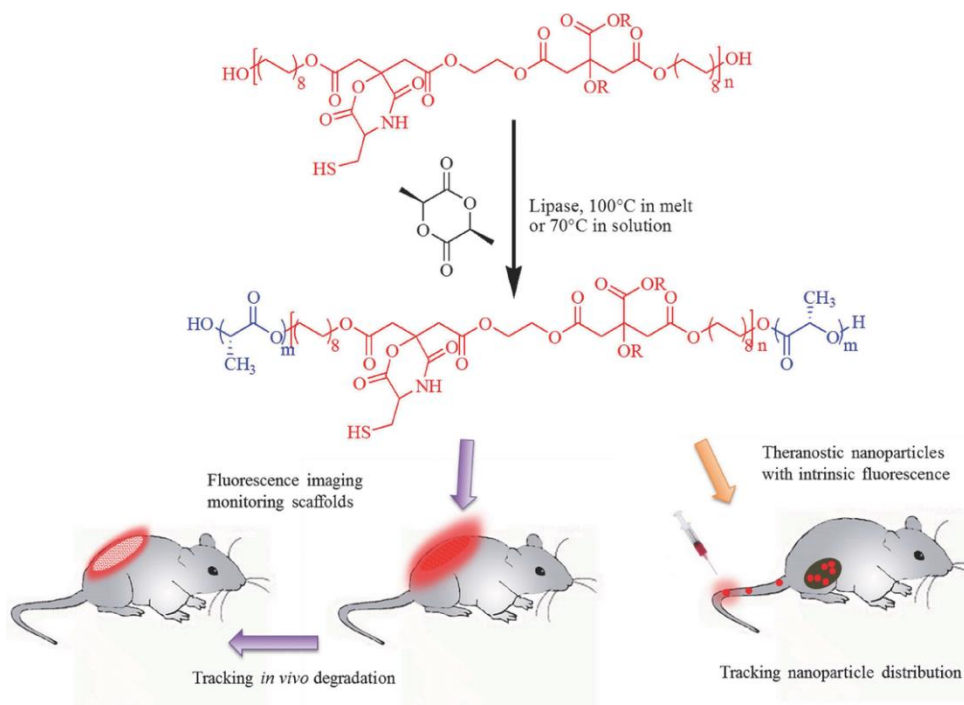


Figure 1.4. Schematic illustration of biodegradable photoluminescent polylactide (BPLPL-Cys-PLLA) synthesis and its applications in scaffold imaging and nanoparticle tracking *in vivo*. (Reproduced from [28].)

Yang et al. developed an implantable active-targeting micelle-in-nanofiber device by usage of folate-conjugated poly(ϵ -caprolactone)-poly(ethylene glycol) (FA-PCL-PEG) copolymers for

encapsulation of DOX, which resulted in micelles that was embedded in electrospun fibers. The folate receptor targeted micelles were sustained released from the fiber and accumulated around the tumor. The tumor suppression rate and survival of animals of the DOX-loaded nanofiber were higher than DOX alone or blank nanofiber [29].

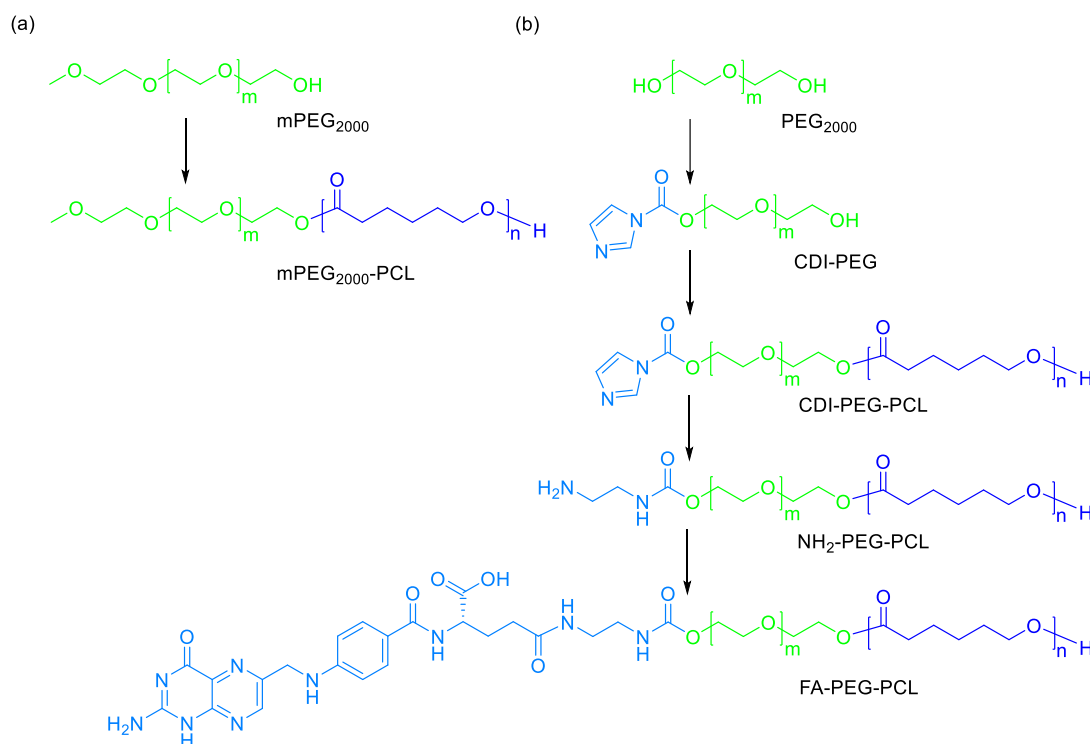


Figure 1.5. Synthesis route of mPEG-PCL and FA-PCL-PEG. (Reproduced from [29].)

Other than PCL, poly(*p*-dioxanone) was another type of poly(lactones) being investigated. Saltzman's group synthesized poly(ω -pentadecalactone-*co-p*-dioxanone) using *Candida antarctica* lipase B as the catalyst instead of metal catalysts that were difficult to remove during the polymer purification processes. These copolyesters were used for both drug and gene delivery [30].

1.1.2 Stimuli-responsive synthetic polymers for anticancer drug delivery

There have been increasing numbers of studies on development of stimuli-responsive polymers over the past decades. The strategies of development of most stimuli-responsive polymer-based systems depend on abnormal tumor microenvironment or variable properties of cancer cells

[31, 32]. Stimuli-responsive polymers can be applied with various bioactive molecules by chemical conjugation or physical mixing. The stimuli can be physiological and externally applied, which hinge on the intention of design. Moreover, the polymer can be responsive to more than one stimulus. The environmental stimuli that the polymers are respond to include (1) physical change, such as temperature, pH, ionic strength, solvents, radiation, electric field, mechanical stress, pressure, sonic radiation and magnetic field, (2) biochemical change, such as redox, hypoxia, enzyme substrate and affinity ligand [12, 32]. The following introduction will cover some of the recent reports on stimuli-polymer based drug delivery systems with focus on redox-responsive systems.

Development of redox-sensitive polymers for cancer therapy achieves remarkable progress for cytoplasmic drug and gene delivery based on the fact that redox potential in the cytoplasm of tumor cells is 2-3 orders magnitude higher than that in the blood circulation [32-34]. Disulfide linker is the most frequently used redox responsive moiety in polymers. Disulfide moieties in polymers exhibit fast breakage to intracellular reducing environment through thiol-disulfide exchange reaction, while rather stable property under extracellular conditions and during workup [33]. Disulfide bonds can exist in monomers, between polymers and therapeutic agents, and between blocks of polymers. In addition, boronates, sulfides, thioethers and thioketals are reactive oxygen species (ROS) responsive functional groups that are sensitive to superoxides, hydrogen peroxide, hydroxyl radicals, and peroxy radicals [35, 36].

Zhang's group developed micelles fabricated by poly(amido amine)-*g*-PEG (PAA-*g*-PEG) copolymer containing disulfide linkages through the backbone (Figure 1.6), which was used for delivery of DOX. The *in vitro* study showed that the drug release of the micelles was less than 25% within 24 h in normal condition, compared to 100% release within 10 h in presence of 1,4-dithiothreitol (DTT). The *in vivo* study showed that the DOX micelles showed stronger accumulation and better anticancer effect than DOX·HCL [37, 38].

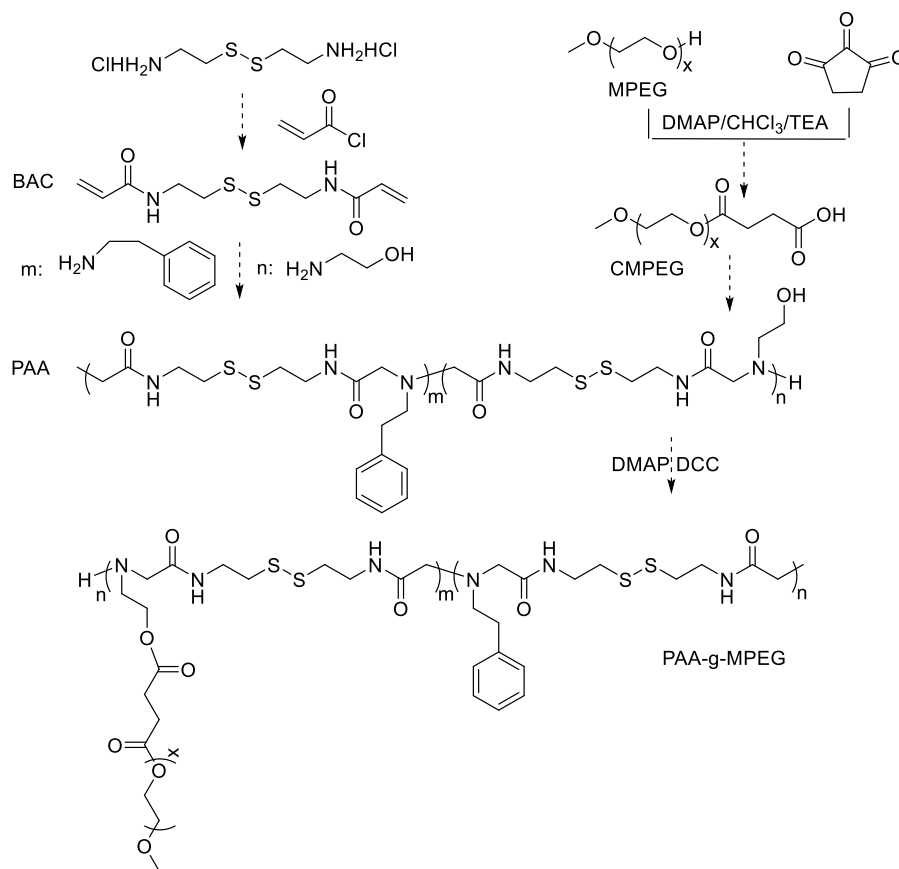


Figure 1.6. Synthetic scheme of reduction-degradable PAA-g-PEG amphiphilic graft copolymer. (Reproduced from [37].)

Zhong's group developed series of reduction-sensitive polymers and dual-stimuli biodegradable polymers for targeted delivery of anticancer therapeutics, including reduction-responsive PEG-ss-PCL [39], PCL-g-ss-PEG [40], dextran-SS-PCL (Dex-SS-PCL) [41], PEG-*b*-poly(dithiolane trimethylene carbonate) (PEG-*b*-pDTC) [34], cRGD functionalized cRGD-PEG-P(CL-DTC) [42], cNGQGEQc-functionalized cNGQ-PEG-poly(trimethylene carbonate-DTC) (cNGQ-PEG-P(TMC-DTC)) [43], cRGD-PEG-P(TMC-g-SS-mertansine) [44], dual-responsive PEG-SS-poly(2-(diethyl amino)ethyl methacrylate) (PEG-SS-PDEA) [45], PEG-SS-poly(2,4,6-trimethoxybenzylidene-pentaerythritol carbonate) (PEG-SS-PTMBPEC, Figure 1.7) [46], and thiolated derivative of PEG-PAA-PDEA, PEG-PAA(SH)-PDEA [47]. These polymers were used

for fabrication of redox-responsive micelles for delivery of PTX, DOX and other therapeutics for cancer treatment and achieved targeted delivery.

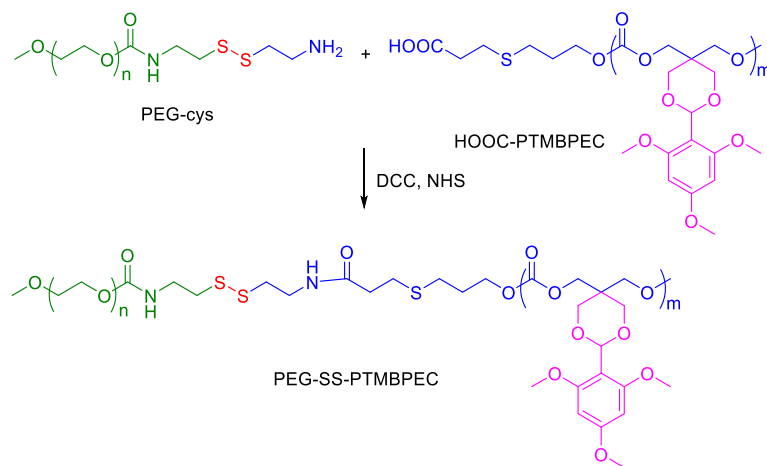


Figure 1.7. Synthesis of PEG-SS-PTMBPEC. (Reproduced from [46].)

Photo-sensitive moieties and targeting molecules are also combined with redox-responsive strategy. Gao developed polymeric micelles based on diblock mPEG-poly(β -benzyl-L-aspartate) (mPEG-PBLA) copolymers consisting of DOX by acid-labile hydrazine linker and zinc(II) phthalocyanine (ZnPc) by redox-responsive disulfide linker [48]. Conte et al. developed PEGylated nanoparticles using PLGA-SS-PEG polymers for enhancing lung cancer cell uptake [49]. Liu et al. synthesized diblock folate-PEG-PCL-SS-CPT for targeted delivery of CPT by micelle [50]. Gulfam et al. combined mPEG-PCL with click chemistry by clicking a redox-responsive bis(alkyne) to mPEG-PCL-azidoPCL to form the crosslinked core for encapsulation of drugs [51]. Future developments of stimuli-responsive polymers will lead to intelligent materials that communicate with biological systems in a manageable manner [52].

1.2 HPMA copolymers for anticancer drug delivery

The HPMA polymer is a very unique synthetic polymer in biomedical applications. Developed by Dr. Kopeček and colleagues at the Czech Academy of Sciences in the mid-1970s, HPMA copolymer was the first synthetic polymer-based drug conjugate to enter clinical trial.

HPMA has been developed as both hydrogel and therapeutic conjugates due to its excellent water-solubility, non-immunogenicity and non-toxicity [53]. With insight of EPR effect, HPMA copolymers are extensively studied for cancer drug delivery with the goal of altering drug PK and cellular trafficking, enhancing tumor uptake and *in vivo* anticancer activity [54]. The following introduction will bring up the classic HPMA-drug conjugates, as well as the advances of development of HPMA carriers.

1.2.1 Traditional HPMA-drug conjugates in clinical trials

There were 6 HPMA copolymer conjugates that have entered clinical trials as anticancer agents (Figure 1.8) [55]. Different from most of the polymers discussed above, backbone of HPMA polymer is non-degradable carbon-carbon bond. All of the conjugates exhibited molecular weight less than 40 kDa to guarantee eventual renal elimination, while fit in the size range required by EPR effect at the same time [55]. Both PK1 and PK2 were referred as P-DOX, and DOX was released by cathepsin B through enzymatic cleavage of GFLG. Addition of galactosamine to PK2 was to create active targeting towards liver hepatocytes, however, the level of the conjugate accumulated in liver tumor was lower than that in healthy tissues. PK1 and PK2 did show lower systemic toxicity and improved efficacy as expected, but the clinical trials discontinued in 2008 due to lack of improvement of anticancer activities [56].

PNU166945 was HPMA copolymer conjugated PTX that was cleavable by hydrolysis. The clinical trial was discontinued due to the neurotoxicity that was commonly caused by free PTX. The free PTX was from ester bond breakage and impurities (unreacted PTX) from manufacturing process [57]. PCNU166148, also known as MAG-CPT, was developed to overcome the low solubility and high toxicity of free CPT. The linker of MAG-CPT was different from the GFLG linker used in the previous polymer conjugates. CPT was modified by glycine, which was reacted with glycylohexanoyl spacer on HPMA polymers. Unfortunately, MAG-CPT showed serious

bladder toxicity but did not show clinical antitumor activity, which may be resulted from the excretion of MAG-CPT from kidney, as well as the inappropriate release rate [58].

AP5280 and AP5346 were HEMA polymer conjugated with carboplatin analogue and oxaliplatin analogue, respectively. AP5280 showed longer half-live time and minimized renal toxicity and myelosuppression in patients that were typically observed with cisplatin and carboplatin in clinical [59-61]. However, there is no further report on the clinical results of these two drugs.

These unsuccessful examples revealed that the polymer conjugates have to process long circulation time and certain serum stability [55]. Thus, studies on the new generation of HEMA copolymer-drug conjugates were carried out.

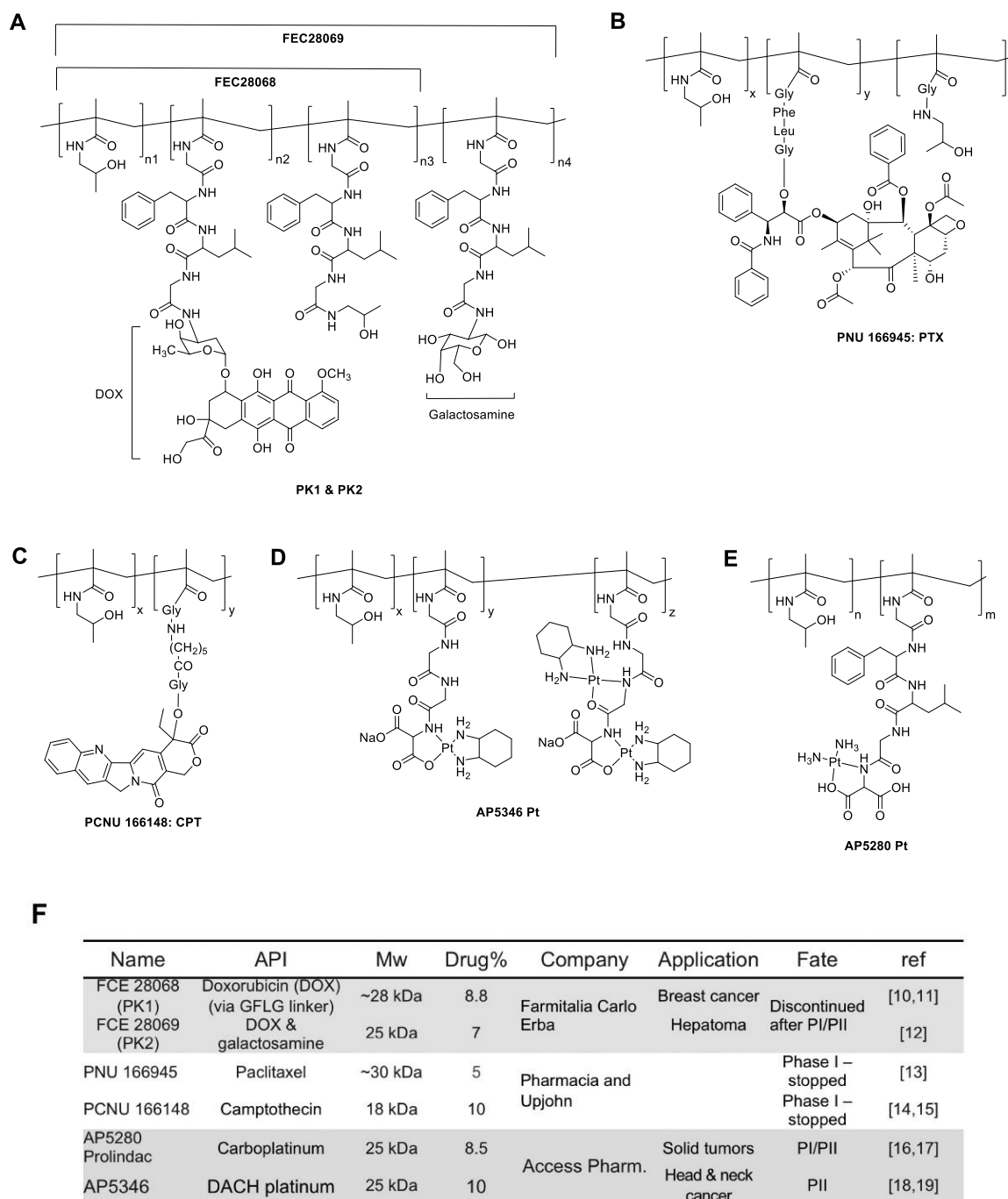


Figure 1.8. First-generation HPMA polymer-anticancer drug conjugates used in clinical trials.

(Reproduced from [55].)

1.2.2 New generation of HPMA copolymer-drug conjugates

To break out the limitation on circulation time of the traditional HPMA copolymers, researchers have designed macromolecular therapeutics with diverse architectures and morphologies. Furthermore, responsive spacers/linkers to cancer cell or tumor microenvironment were applied to accomplishing the controlled release/activation of anticancer drugs. The spacers can be in the backbone or between polymers and drugs to achieve long circulation and targeted activation of drugs.

1.2.2.1 pH-triggered degradable HPMA copolymer-drug conjugates

The fact that the pH of tumor microenvironment and the intracellular pH in endosome and lysosome is lower than the pH of normal tissue and blood circulation is well established. In fact, the final destination of polymer conjugates are endosome and lysosome after internalization into tumor cells. Therefore, several linkers/spacers that are liable to hydrolysis in acidic environment are designed [54].

Hydrazone is the most widely used pH-triggered linker used in the HPMA copolymer conjugates. Hydrazone bond is stable at physiological pH and the hydrolysis rate increases at low pH. Of course, the stability depends on the chemical structure tethering to hydrazone bond. Compared to the traditional HPMA copolymer conjugates using GFLF as spacer, conjugates with hydrazone showed higher DOX loading ratio and better water solubility. Release of DOX was no more than 8% at pH 7.4 for 48 h, compared to 50% release at pH 5 for 4 h. Moreover, the *in vivo* anticancer effect of the hydrazone conjugates was better than that of GFLG conjugates [62, 63]. Except for DOX, 2-pyrrolinodoxorubicin and pirarubicin (THP) were also conjugated to HPMA copolymer by hydrazone bond (Figure 1.9). THP showed similar release profile to DOX conjugates, targeted accumulation and enhanced uptake in tumor tissue [64, 65].

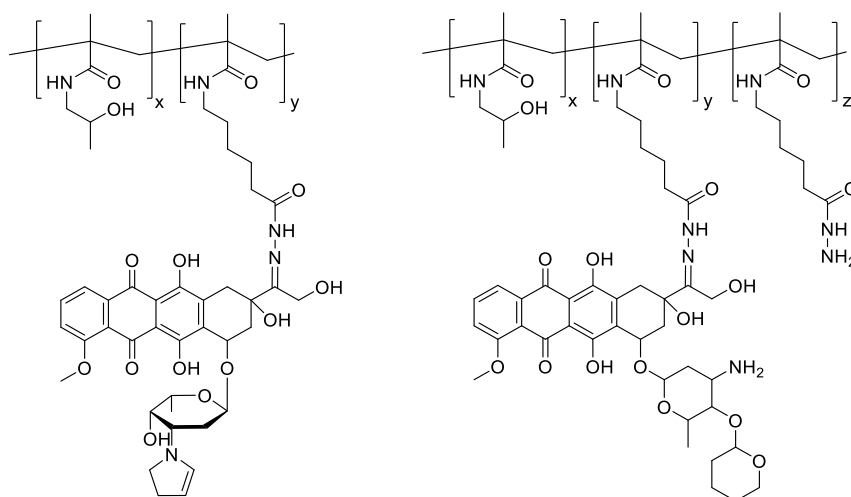


Figure 1.9. Chemical structure of HPMA copolymer-2-pyrrolinodoxorubicin (left) and HPMA copolymer-THP (right). (Reproduced from [64, 65].)

Other than DOX, docetaxel was also bound to HPMA copolymer by hydrazone bond [66]. Furthermore, two or more therapeutic agents were tethered to HPMA copolymers simultaneously for combination drug delivery, such as DOX with dexamethason (DEX) [67], and DOX with Mitomycin C (MitC) [68]. Another pH sensitive linker used in HPMA polymer conjugation is *cis*-aconityl (Figure 1.10), which showed faster release of DOX than DOX conjugates with hydrazone [69, 70].

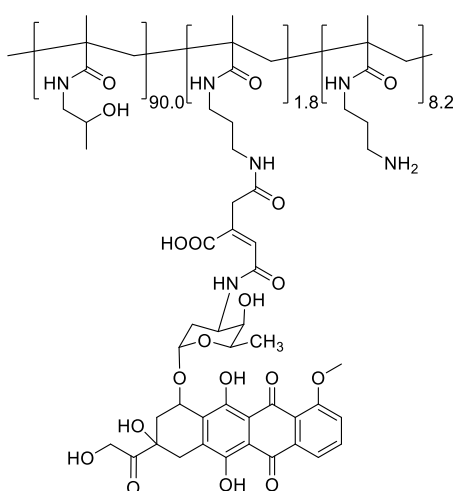


Figure 1.10. Structure of HPMA copolymer-*N-cis*-aconityl-ADR conjugate (P-aconityl-ADR).

(Reproduced from [69].)

1.2.2.2 Reductively degradable HPMA copolymer-drug conjugates

To minimize the off-target release of anticancer drugs and systemic toxicity, reductive-responsive linker disulfide bond is extensively applied. Kopeček's group conjugated photosensitizer mesochlorin e_6 (Mce₆) to HPMA copolymer by disulfide bond (P-SS-Mce₆) (Figure 1.11). Degradation of the polymer was time dependent and an increase in the quantum yield of singlet oxygen generation upon exposure to DTT was occurred at the same time [71].

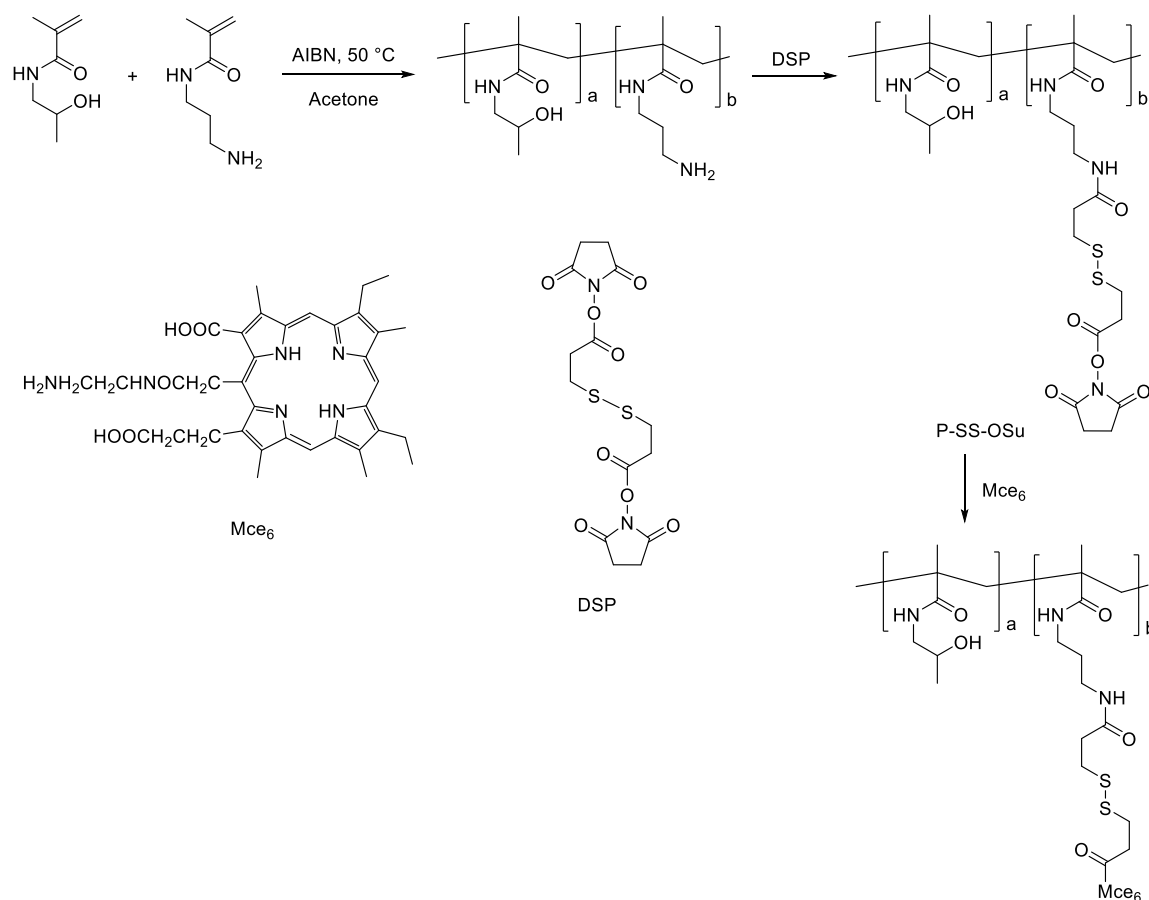


Figure 1.11. Synthesis of P-SS-Mce₆. (Reproduced from [71].)

Kopeček's group also developed HPMA copolymer-9-aminocamptothecin (9-AC) conjugates for colon-specific delivery using peptide-aromatic azo bonds as reductive-degradable linker (Figure 1.12). By oral administration, the conjugates were stable to gastrointestinal enzymes due to the steric hindrance so that the release and absorption were minimized in the small intestine. The azido bond was cleaved in presence of azoreductase in colon to release 9-AC. As a result, antitumor efficacy was enhanced due to the prolonged colon tumor exposure to higher localized drug concentration [72-75].

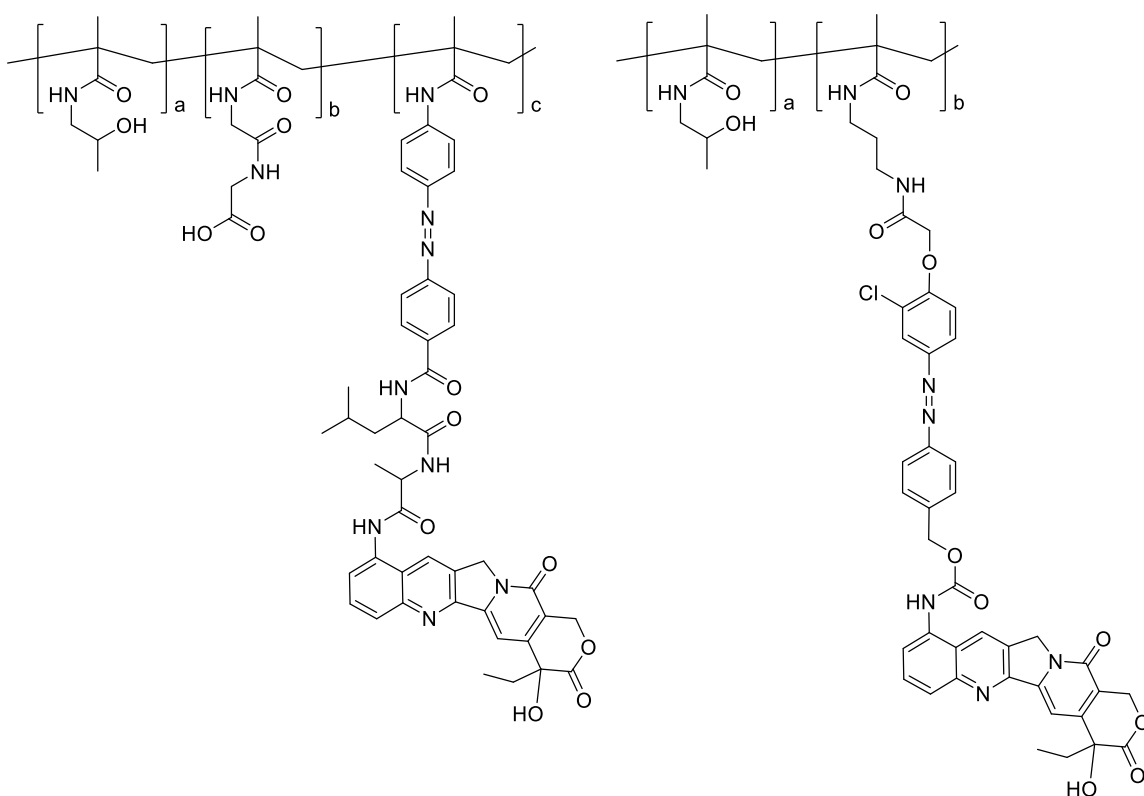


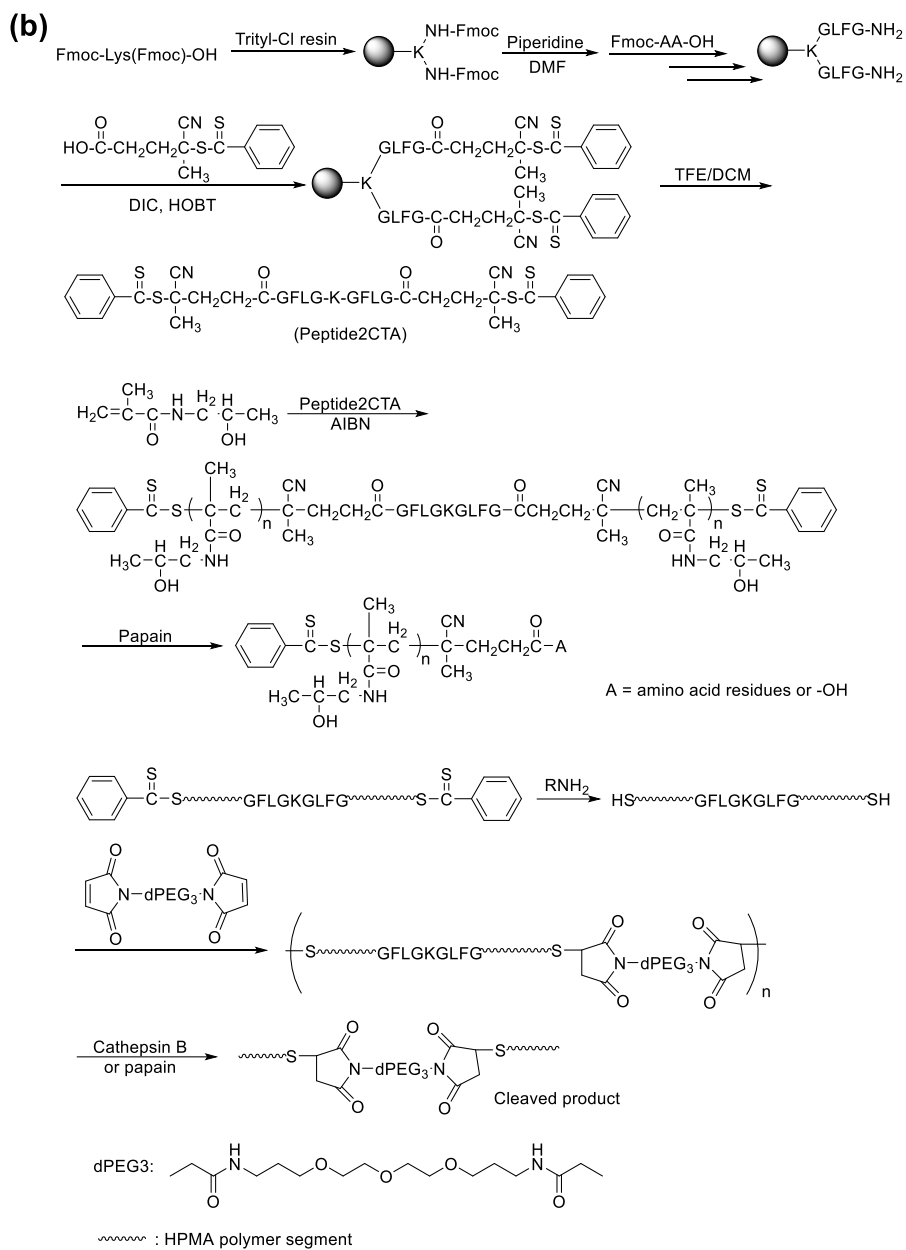
Figure 1.12. Structure of HPMA copolymer-9-AC with azo linker. (Reproduced from [73, 74].)

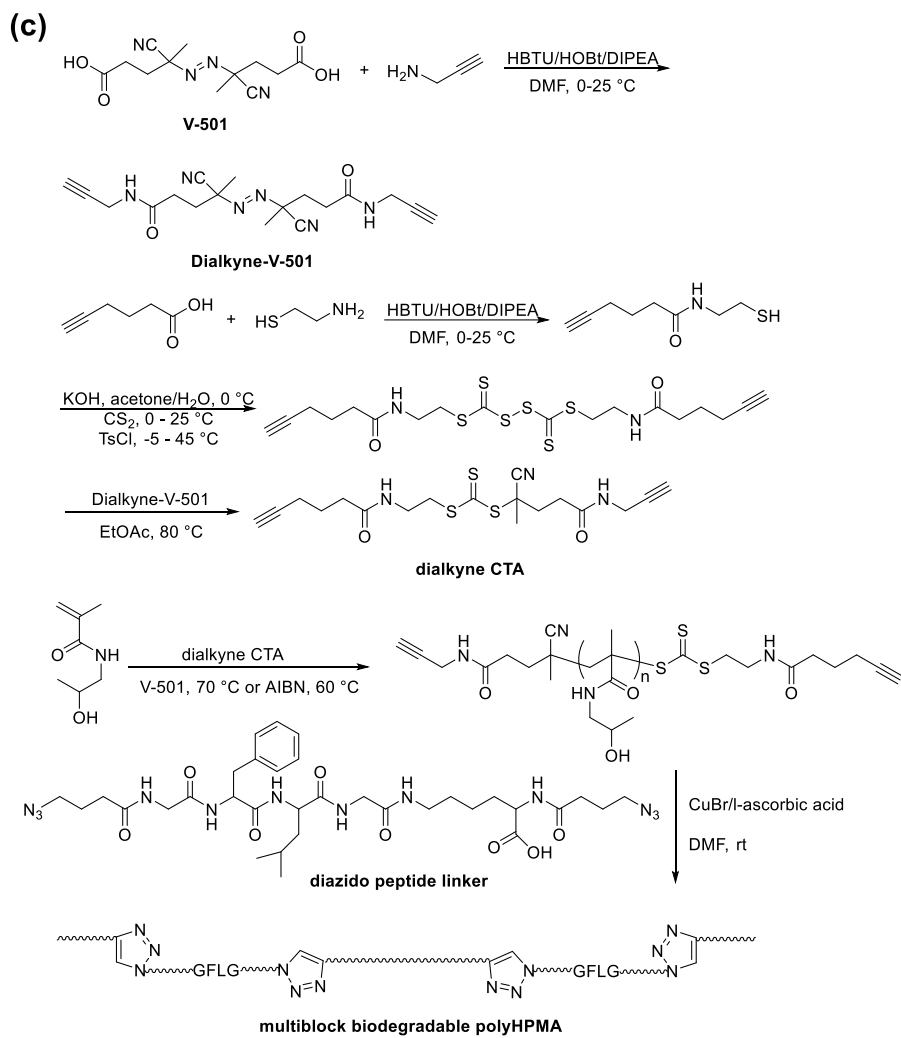
1.2.2.3 Other spacers used in HPMA copolymer-drug conjugates

The cleavable linkers/spacers are normally located between polymer and drug to carry the therapeutic agents to the desired sites and release them. To elongate the circulation time of the polymers, linkers are also applied to increasing the size of the HPMA conjugates. The goal of

synthesis of macromolecular HPMA copolymer is on the basis of the correlation of the molecular weight and drug accumulation in tumor. By addition of glycyphenylalanylleucylglycine side chain and the N^2, N^5 -bis(*N*-methacryloyl glycyphenylalanylleucylglycyl)ornithine crosslinker, Kopeček's group prepared conjugates with molecular weight up to 1230 kDa (Figure 1.13a). The drug accumulation of 160 kDa conjugates was more than 2 times higher than that of the 22 kDa conjugates [76].

Thanks to the advances of Reversible Addition-Fragmentation chain Transfer (RAFT) polymerization, HPMA polymers can be synthesized in a well-defined way and with flexible end-group modification. Kopeček's group developed a series of functional chain transfer agents (CTA) for conjugation of the HPMA backbone by different chemistry. GLFG was included in the CTA as enzymatic cleavable Peptide2CTA. After polymerization by Peptide2CTA, free thiol group was exposed and conjugated to bismaleimide by thiol-ene chemistry (Figure 1.13b). The molecular weight of the conjugates was up to 260 kDa with Cathepsin B responsive cleavage [77]. Dialkyne CTA was synthesized for preparation of alkyne terminated HPMA copolymers, which were clicked with diazide terminated GFLG linker by azide-alkyne click chemistry (Figure 1.13c). The resulted multi-block polymer had the molecular weight of 290 kDa [78]. Moreover, CTA with one alkyne end and another azide-transferrable end was designed and applied to HPMA copolymerization. The resulted heterotelechelic HPMA copolymers underwent click chemistry and obtained macromolecules larger than 200 kDa (Figure 1.13d) [79]. These studies significantly enhanced the plasma half-life of the conjugates. Click chemistry is widely explored for macromolecule conjugation due to its high specificity.





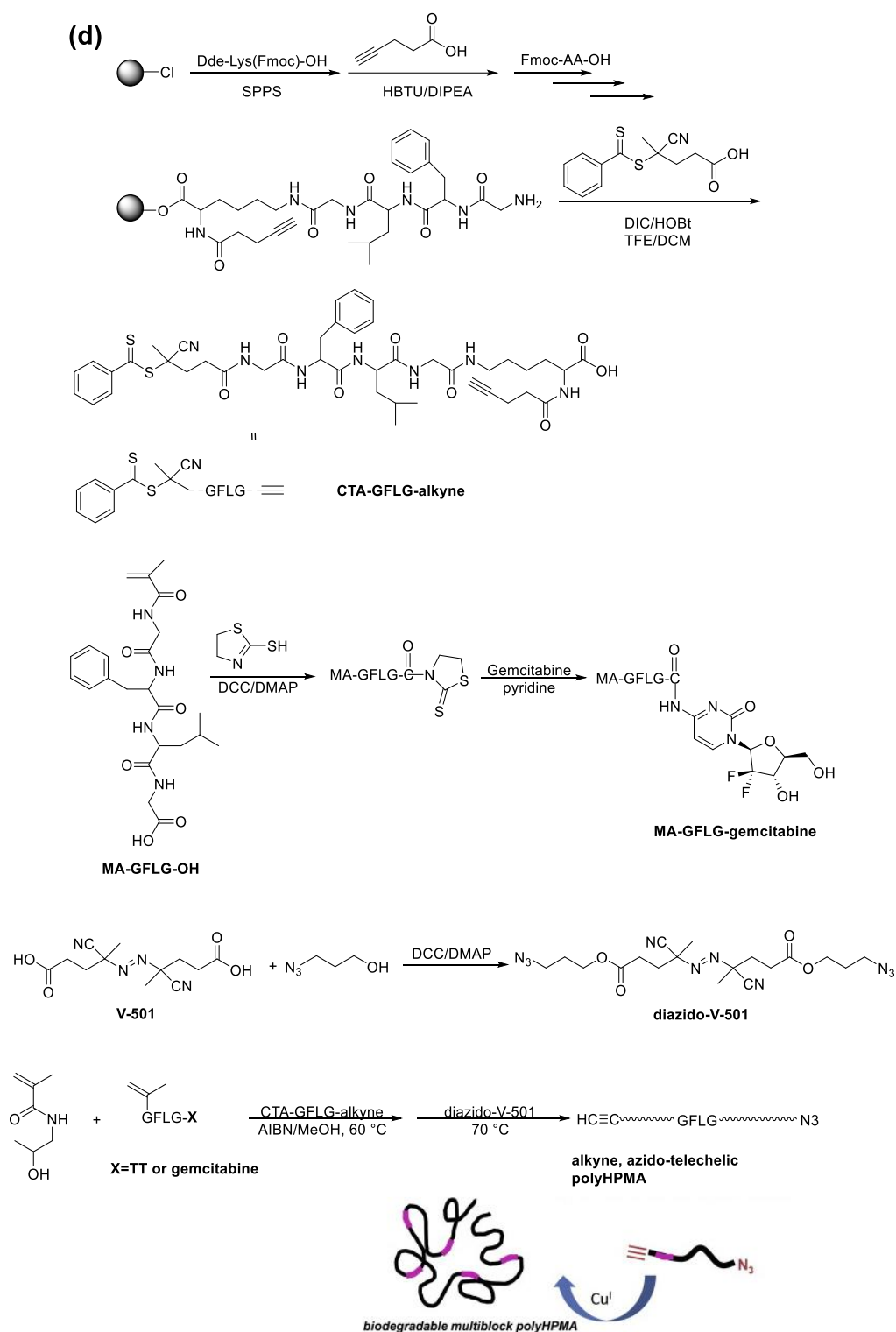


Figure 1.13. Structure of macromolecular HPMA copolymer conjugates. (Reproduced from [76-79].)

1.3 Polymeric drugs for cancer treatment

Instead of inert drug carriers, polymeric drugs are polymers that exhibit pharmacological activities that do not need to release small therapeutic agents [5]. The most significant difference between polymeric drug and polymeric conjugate is that polymeric drug has intrinsic bioactivity, but polymer of conjugate is an inactive carrier for delivery of conjugated molecules. The development of synthetic polymeric drug started several decades ago, additionally, some polymeric carriers are found to be biologically active instead of being inert in recent studies [80]. One of the biggest advantages of the polymeric drug versus the small molecule is that polymeric drug fits the size range of protein so that the repeating units can bind to the targets by complex set of multivalent interactions, which results in enhanced activation or inhibition of related signaling pathways [81]. Traditional examples of polymeric drugs include sequestrants to bind and remove harmful substances from the organism [82, 83]. Recent examples include polymeric drugs aimed at treating cancer, modulating hemostasis, or using as antiviral agents [84-89]. Polymeric drugs with activities towards cancer will be discussed briefly.

1.3.1 Polymeric drugs with anticancer activities

The first anticancer polymeric drug in clinical trials was a copolymer of divinyl ether and maleic anhydride (DIVEMA) (Figure 1.14), which was known for its wide variety of biological activities including induction of cancer cell apoptosis and interferon release, and to activate macrophages to promote the killing of tumor cells. However, DIVEMA failed in the early clinical trials due to the severe systemic toxicity [90].

Inspired by DIVEMA, polycations, polyanions, poly(amido amine)s and polysaccharides have been studied for their direct anticancer activity, immune-stimulation activity, and synergistic antineoplastic activity. Polyethylenimine (PEI) showed agglutination activity on kidney tumor cells *in vitro* and remarkable antitumor activity *in vivo*. PEI is the most widely used carrier for gene

delivery, however, its systemic toxicity is still noteworthy [91]. End carboxyl-trithiocarbonate functionalized poly(maleic anhydride) (ECT-PMA) (Figure 1.14) showed higher and selective cytotoxicity, apoptotic and necrotic effects on HeLa cells at relatively low concentrations [92]. Our group developed series of polymer of AMD3100 (PAMD), which is a multivalent CXCR4 antagonist as well as a cationic gene carrier (Figure 1.14) [93].

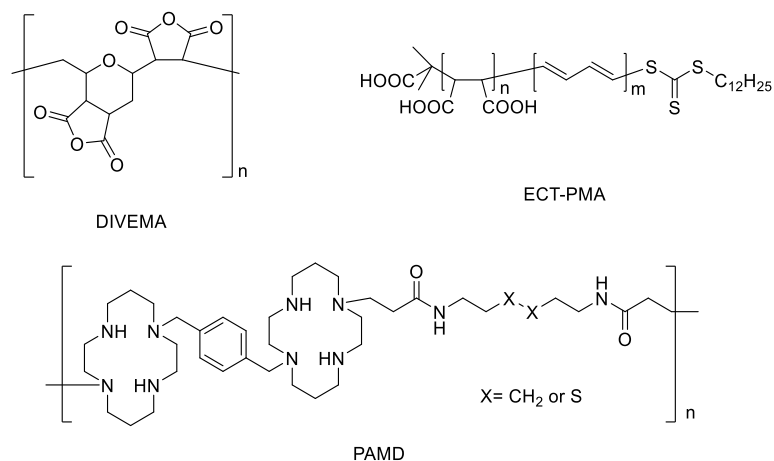


Figure 1.14. Structure of DIVEMA, ECT-PMA and PAMD. (Reproduced from [90, 92, 93].)

HPMA copolymers are also harnessed as polymeric drugs. Kopeček's group developed polymeric drugs that contained peptide CCK that formed antiparallel coiled-coil heterodimers in presence of peptide CCE. By treatment of Fab'-CCE with human Burkitt's NHL Raji B cells, CCE was present on the cell surface due to the attachment of Fab's to CD20. After treatment of CCK-polymer, CD20 antibody (Fab's) was crosslinked via recognition of CCK and CCE followed by formation of heterodimeric coiled coils, which induced apoptosis of human Burkitt's NHL Raji B cells by crosslinking antigens on the cell surface (Figure 1.15) [84]. The *in vivo* study showed that intravenous injection of Fab'-CCE followed by CCK-polymer improved survival in SCID mice bearing human B cell NHL xenografts [94]. CXCR4 is a chemokine receptor highly related to cancer metastasis. Kopeček's group designed multivalent HPMA copolymer containing CXCR4 inhibiting peptide BKT140 and showed remarkably higher inhibitory activity than free peptide [95].

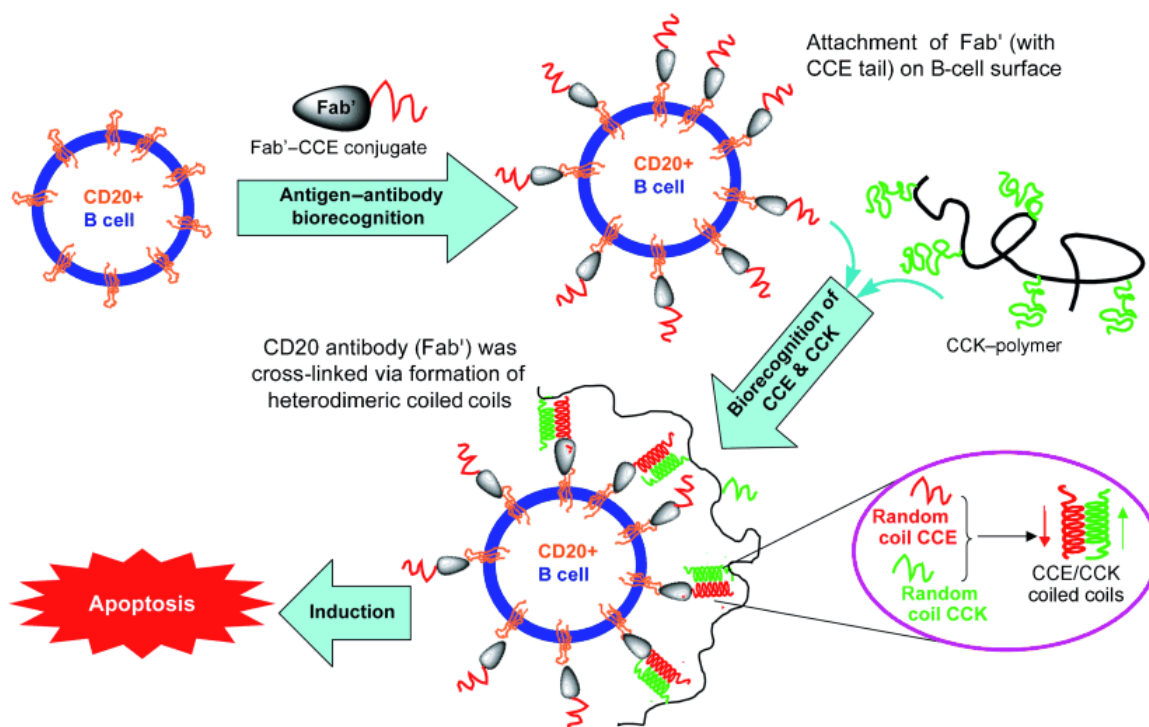


Figure 1.15. Induction of apoptosis in human Burkitt's NHL Raji B cells by crosslinking its CD20 antigens mediated by antiparallel coiled-coil formation at the cell surface. (Reproduced from [84].)

1.3.2 Pharmaceutical ingredients with newly discovered bioactivities

When we talk about biomaterials, we always emphasize that the materials used as drug carriers are biocompatible polymers with non-immunogenicity, which means the materials have minimized interaction with tissues and no unwanted immune response [80]. However, with the comprehensive investigation of the materials, the activities of biomaterials that used to be unintentionally ignored have emerged. The natural polymers and chemically modified natural polymers, such as chitosan and its derivatives, hyaluronic acid and its derivatives, chondroitin sulfate are known for their activities towards cancer treatment including delay of tumor progression and interaction with chemokine receptors [80]. The most well-known synthetic polymeric biomaterial exhibiting anticancer activities is Pluronic block copolymers. Pluronics are triblock copolymer developed by Kabanov's group consisting of hydrophilic ethylene oxide (EO) and

hydrophobic propylene oxide (PO) with the order of EO-PO-EO (Figure 1.16) [96]. Pluronic block copolymers were found to dramatically sensitize the multidrug-resistant cancer (MDR) tumors to various anticancer agents. The mechanism of sensitization includes inhibition of drug efflux transporters, diminution drug sequestration in acidic vesicles, inhibition of glutathione/glutathione S-transferase detoxification system, and enhancement of pro-apoptotic signaling and mitigate anti-apoptotic cellular defense [96, 97].

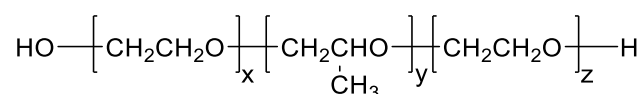


Figure 1.16. Structure of Pluronic.

1.4 CQ for cancer treatment

CQ and HCQ are 4-aminoquinoline drugs that have been in clinical use for more than 60 years (Figure 1.17) [98]. CQ was discovered as an antimalarial drug, to which a hydroxy group was added generating HCQ with decreased toxicity [99]. Both CQ and HCQ are currently used for the treatment of inflammation and autoimmune disease including rheumatoid arthritis, discoid lupus erythematosus and amoebic hepatitis [100, 101].

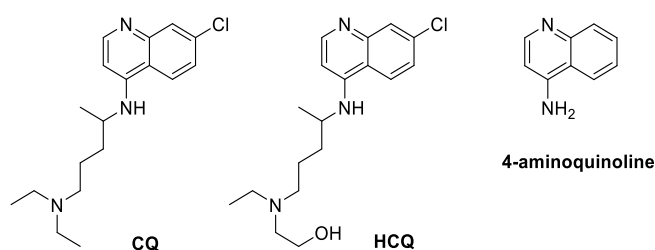


Figure 1.17. Chemical structures of CQ, HCQ and 4-aminoquinoline.

CQ and HCQ have been extensively studied for cancer treatment *in vitro* and *in vivo*. Numbers of clinical trials have been carried out using CQ or HCQ, alone or in combination with other cancer treatment because CQ and HCQ are known to synergistically enhance activity of multiple treatments [102-105]. Although the mechanism of action is not fully understood, the

preclinical studies show evidence that CQ and HCQ have multiple mechanisms of action that may complement each other, which include inhibition of autophagy, inhibition of cancer cell signaling pathways, and modulation of tumor microenvironment [106]. The *in vivo* preclinical and clinical cases of CQ and HCQ for cancer treatments, and the mechanism studies will be discussed as follows.

1.4.1 CQ/HCQ monotherapy

A lot of *in vivo* studies showed promising anticancer activity by using CQ/HCQ alone in various cancer types. Back in 1960s, Hiraki's group applied CQ to experimental animal tumors of Brown-Pearce cancer and Yoshida sarcoma. CQ inhibited growth of tumor and increased survival rate of rabbits bearing Brown-Pearce cancer by daily administration of chloroquine diphosphate of 10 mg/kg [107]. Zheng et al found that CQ (25 or 50 mg/kg) reduced tumor volume and prolonged survival time in CT26-bearing mice via induction of apoptosis [108]. Kim et al. showed CQ suppressed growth of glioma in an orthotopic human glioblastoma mouse model by activation of p53 and induction of apoptosis [109]. CQ was reported to inhibit SK-MEL23 melanoma growth in NOD-SCID mice by the dose of 25 mg/kg [110]. Maes discovered that CQ normalized tumor vessel structure via autophagy-independent mechanism and reduced melanoma tumor growth [111].

Not only on primary tumor, CQ also showed effect on metastasis. Jiang et al applied CQ (25, 50 mg/kg) to 4T1 tumor implanted mice and found that CQ significantly inhibited growth of primary tumor and improved the survival. Moreover, the metastasis of tumor cells to lungs was inhibited [112].

The most extensively studied mechanism of CQ related to cancer is autophagy inhibition. Yang et al. discovered that autophagy was required for pancreatic cancer growth. Inhibition of autophagy by chloroquine resulted in robust tumor regression and prolonged survival in pancreatic cancer xenografts [113]. Song et al. observed that CQ impaired the clonogenic capacity of CD133+ liver cancer stem cell by inhibition of autophagy and reduced the tumor volume [114]. Jutten et al.

discovered there was correlation between expression of epidermal growth factor receptor (EGFR) and autophagy. CQ (60 mg/kg) reduced the glioblastoma tumor size [115]. It was also proven that CQ improved survival of animal bearing autophagy-dependent breast tumor MDA-MB-231 but not autophagy-independent breast tumor MCF-7 [116].

Other than the above, a very recent paper revealed that CQ (75 mg/kg) worked as an anticancer immune modulator that ameliorate tumor immune microenvironment and enhanced antitumor T-cell immunity, which suggested a new anticancer mechanism of CQ [117].

However, there are different opinions towards the effects of CQ/HCQ. Also back in 1960s, CQ were found to have more infiltrating tendency in transplantable mouse tumors (a spontaneous mammary carcinoma, Bashford carcinoma 63 and Ehrlich ascites tumor) with the dose of 0.2 mg/2 days [118]. Dutta et al. showed CQ (45 mg/kg) enhanced the tumor growth of R3230AC mammary adenocarcinoma in rats pre-treated with CQ for 7 days, followed by 18 days treatment of CQ after implantation of tumor [119]. It is not surprising that different mechanisms are involved in the activity of CQ. Loehberg et al. found that CQ (3.5 mg/kg) significantly reduced the incidence of *N*-methyl-*N*-nitrosourea-induced mammary tumors in the animal models, however, CQ had no effect in BALB/c p53-null mammary epithelium model, which indicated the connection of function between p53 and CQ [120]. The relationship between p53 and CQ was further proven by Maclean et al that CQ impaired spontaneous lymphoma development in *Atm*-deficient mice but not in p53-deficient mice [121].

Autophagy and lysosome function are highly related to tumor progression. However, it was reported that disruption of lysosome function by CQ resulted in promoted tumor growth and metastasis in *Drosophila* [122]. Sun et al. found that CQ inhibited hepatocarcinoma growth in the tumor-forming stage but promoted hepatocarcinogenesis in its early stage called dysplastic stage, which were resulted from the interaction of the activity of autophagy and reactive oxygen species (ROS) [123]. Rosenfeldt et al. reported that HCQ significantly promoted tumor formation in mice

containing oncogenic Kras but lacking p53, which emphasized the consideration of types of malignant disease when targeting autophagy by HCQ [124].

There are several clinical trials using CQ/HCQ alone, including CQ on small cell lung cancer, HCQ on B-cell chronic lymphocytic leukemia, HCQ on prostate cancer, HCQ on pancreatic cancer, and HCQ on breast cancer. But no exciting results have been disclosed yet.

1.4.2 Combination therapy with CQ/HCQ

Cancer is a disease involving a combination of interconnected disease pathways, dynamic changes in the genome, and sophisticated tumor microenvironment [31, 125, 126]. Due to the cellular and molecular complexity of cancer and tumor microenvironment, a single drug therapy strategy is not sufficient for effective treatments [127]. Combination chemotherapy for cancer was developed to increase response and tolerability and overcome drug resistance [128, 129]. Current research focusing on combining anticancer drugs aims at maximizing efficacy while minimizing systemic toxicity through the delivery of lower drug doses [130-132]. Drug resistance and clinical relapse are normally the result of complicated cellular pathways with multiple redundancies or alternative routes activated in response to the activation or inhibition of a pathway, which promotes the emergence of resistant cells [133]. The rationale underlying combination chemotherapy is to co-administer drugs with different molecular mechanisms to shut down the targeted cellular pathways, thus increasing the activity of killing cancer cells while reducing the likelihood of drug resistance and minimizing overlapping toxicity [134]. Over 3,700 clinical trials aimed at developing drug combination therapies were approved by the FDA from 2008 to 2013 and the number is increasing [135].

Almost all cancer therapies have been applied in combination with CQ/HCQ, which consist of small molecules of chemotherapeutic agents, antibodies, hormones and radiotherapy. There are

thousands of papers about preclinical combination research and some studies consisting of *in vivo* work with the FDA approved therapies are summarized here (Table 1.1).

Table 1.1. Preclinical *in vivo* research combining anticancer drugs with CQ/HCQ.

Cancer type	CQ/HCQ	Intervention	Year of publication
Glioma	CQ	Bevacizumab	2012 [136]
	CQ	Vandetanib	2013 [137]
	CQ	Temozolomide	2014 [138]
	CQ	Temozolomide (+curcumin)	2015 [139]
Neuroblastoma	CQ	Hyperthermia	1990 [140]
Neuroendocrine neoplasms	CQ	Everolimus	2018 [141]
Melanoma	CQ	Cyclophosphamide	1971 [142]
	CQ	Radiotherapy	1971 [142]
	CQ	Caloric restriction	2012 [143]
	HCQ	Temsirolimus	2013 [144]
Breast cancer	CQ	5-FU	1978 [145]
	CQ	5-FU (+6-propyl-thiouracil)	1979 [146]
	CQ	Everolimus	2012 [147]
	CQ	Panobinostat	2012 [148]
	CQ	Nelfinavir Celecoxib	2012 [149]

	CQ	Rapamycin	2013 [150]
	HCQ	Gefitinib	2013 [151]
	CQ	Trastuzumab	2013 [152]
	CQ	Radiotherapy	2013 [153]
	CQ	Cyclophosphamide (+Adriamycin)	2014 [154]
	HCQ	Tamoxifen and faslodex	2014 [155]
	CQ	Carboplatin	2016 [156]
Lymphoma	CQ	Cyclophosphamide	2007 [157]
	CQ	Crizotinib	2015 [158]
Oesophageal carcinoma	CQ	Cisplatin	2014 [159]
Gastric carcinoma	CQ	Cisplatin	2015 [160]
Hypopharyngeal carcinoma	CQ	Cisplatin	2015 [160]
Hepatocarcinoma	CQ	Oxaliplatin	2011 [161]
	CQ	Sorafenib	2011 [162]
	CQ	5-FU	2012 [163]
	CQ	Bortezomib	2012 [164]
	CQ	Sorafenib	2012 [165]

	CQ	Transcatheter arterial chemoembolization	2013 [166]
	CQ	Doxorubicin	2018 [167]
Colon cancer	CQ	Bortezomib	2009 [168]
	CQ	Vorinostat	2010 [169]
	CQ	5-FU	2012 [170]
	CQ	High dose interleukin-2	2012 [171]
	CQ	Oxaliplatin (+Bevacizumab)	2013 [172]
	CQ	Bevacizumab (+oxaliplatin)	2013 [172]
	CQ	Temsirolimus	2014 [173]
	CQ	Photodynamic therapy	2014 [174]
Pancreatic cancer	CQ	Gemcitabine	2014 [175]
Leukemia	CQ	Imatinib	2009 [176]
	CQ	Daunorubicin	2010 [177]
Ascitic tumor	CQ	Etoposide	1982 [178]
	CQ	Sunitinib	2014 [179]
Renal carcinoma	CQ	Temsirolimus	2012 [180]
	CQ	Sunitinib	2018 [181]

Lung cancer	HCQ	Erlotinib	2013 [182]
	CQ	Gefitinib	2014 [183]
		(+akt inhibitor)	
	CQ	Crizotinib	2014 [184]
	HCQ	Crizotinib	2015 [185]
	CQ	Gefitinib	2015 [186]
CQ	Afatinib	2017 [187]	
Ovarian cancer	CQ	Cisplatin	2017 [188]
Myeloma	CQ	Carfilzomib	2016 [189]

There are more than 16 clinical trials of CQ combination therapy and over 49 clinical trials of HCQ combination therapy for primary tumor, cancer metastasis and refractory or relapsed tumor, which consist of glioma, myeloma, pancreatic cancer, ductal carcinoma, lung cancer, breast cancer, neoplasm, prostate cancer, renal cell carcinoma, lymphoma, leukemia, colon cancer, melanoma, hepatocellular carcinoma, etc. The summary can be found in reference [106]. CQ/HCQ is very promising for cancer treatment, especially as combination treatment with other therapies.

1.4.3 Mechanism of action

It is increasingly accepted that the anticancer activity of CQ/HCQ includes multiple mechanisms of action that may complement each other. According to the preclinical studies, these mechanisms include autophagy inhibition, inhibition of signaling pathways (TLR9/NF- κ B, CXCL12/CXCR4, p53), inhibition of cholesterol metabolism, immunomodulation, normalization of tumor vasculature and disruption of the cancer cell interplay [106, 190].

1.4.3.1 Inhibition of autophagy

CQ and HCQ are weak bases with pKa 10.18, 8.38 for CQ, and 9.67, 8.27 for HCQ [191]. As lysosomotropic agents, they are often used to enhance the transfection of non-viral gene delivery vectors *in vitro* [192]. In red blood cells infected with malaria, CQ enters digestive vacuole (pH4.7) by simple diffusion and gets protonated. Then protonated CQ accumulates in food vacuole and inhibits polymerization of heme to hemozoin, resulting in toxic heme accumulation and oxidative damage in parasite, and finally leads to parasite death.

Autophagy inhibition is the most well studied anticancer activity of CQ. Autophagy controls cellular homeostasis by lysosomal degradation of cytoplasmic components, including invading pathogens, cytotoxic protein and damaged organelles to ensure cell survival under stressful conditions such as hypoxia, starvation and organelle damage [193]. The progress of autophagy is shown in Figure 1.18 [103]. Initially, components needed to be recycled in cytoplasm are engulfed within a vesicle called autophagosome. Fusion of autophagosome and lysosome generates autolysosome, where the components are degraded by various lysosomal hydrolytic enzymes. Degradation generates energy and nutrients that are recycled for macromolecular synthesis. CQ inhibits autophagy by neutralization of the acidic lysosomal compartment and inhibition of lysosomal hydrolytic enzymes.

Autophagy actually suppresses tumor in early carcinogenesis because it protects the cell by sequestering and eliminating defective cellular components such as abnormal mitochondria [194]. In advanced stages of cancer, pro-survival autophagy is induced in response to stressful conditions including starvation, hypoxia, even anticancer treatment. Therefore, inhibition of autophagy is a promising anticancer strategy.

Inhibition of autophagy by CQ or shRNA-mediated knockdown of ATG5 or ATG7 suppressed the proliferation of cancer lines [113, 195]. Autophagy is also known to be associated with therapeutic resistance so that CQ can resensitize tumor cells to chemotherapy and radiation.

Although CQ and HCQ were initially tested in cancer treatment owing to their ability to inhibit autophagy, it is known that their therapeutic effects also involve other mechanisms [196-198].

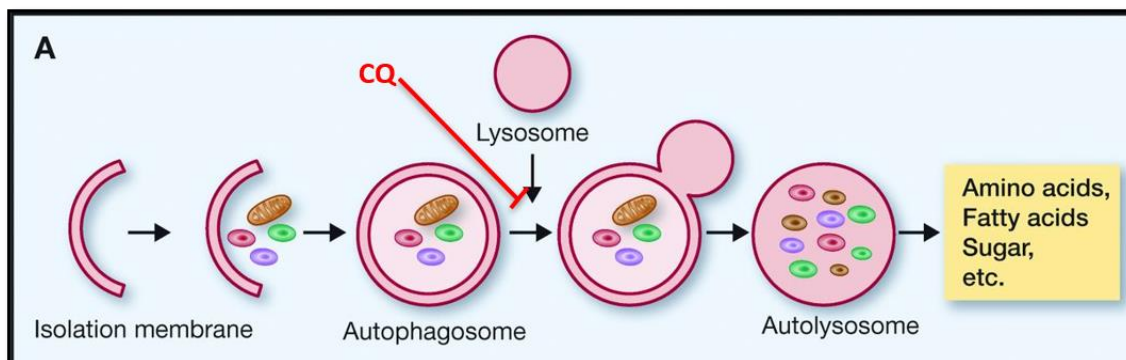


Figure 1.18. Process of autophagy. (Reproduced from [103].)

1.4.3.2 Inhibition of CXCL12/CXCR4 signaling pathway

The ability of CQ and its derivatives like HCQ to inhibit CXCR4 has been also recognized and successfully utilized in the treatment of several types of solid tumors [175, 199]. For example, CQ and HCQ inhibited CXCL12-mediated pancreatic cancer cell invasion and proliferation *in vitro* and contributed to the inhibition of pancreatic cancer stem cells via reduced phosphorylation of the extracellular signal regulated kinase (pERK) and signal transducer and activator of transcription 3 (STAT3). The CXCR4 inhibition by CQ translated into potent anti-metastatic effect *in vivo* when combined with a chemotherapeutic gemcitabine [175].

1.4.3.3 Effects on tumor microenvironment

Maes et al. found that CQ normalized tumor vessels, resulting in reduced tumor hypoxia, cancer cell invasion, intravasation, and spreading and improved the delivery and efficacy of chemotherapeutics. The fact that CQ did not sensitize tumor cells to cisplatin *in vitro* but only *in vivo* proved that the anticancer effect was autophagy-independent but due to the cancer vessel normalization that improved the delivery of cisplatin to the tumor core because of improved perfusion and decreased interstitial fluid pressure in tumor [111].

More recently, Chen et al. reported that CQ (75 mg/kg) worked as an anticancer immune modulator that ameliorate tumor immune microenvironment and enhanced antitumor T-cell immunity, which suggested a new anticancer mechanism of CQ [117].

It may be still too early to conclude the effect of CQ/HCQ in cancer treatment, however, the clinical trials encourage the explore of application of CQ/HCQ. By taking advantage of polymeric drugs, we designed several CQ-containing copolymers for cancer treatment. The synthesis, characterization, and biological activities will be introduced in the following chapters.

2 Synthesis and characterization of CQ-containing HPMA polymers

The pharmacological activity of CQ has been illuminated by different mechanisms of action on various types of cancer, which makes CQ promising for cancer therapy. However, CQ is a poor inhibitor or modulator (mM). In this study, we proposed using the concept of polymeric drugs to synthesize CQ-containing polymers for improvement of activities.

We designed several CQ-containing polymers from methacrylate and methacrylamide derivatives of HCQ. We firstly proposed methacryloyl-hydroxychloroquine (MA-CQ) with ester bond connecting CQ and polymer backbone as pCQ. But ester bond made pCQ susceptible to degradation *in vivo*, which meant that we were unable to unequivocally dissect the therapeutic contribution of the polymeric versus small molecule form HCQ. Therefore, we designed non-cleavable CQ-containing polymers NpCQ from methacrylamido methyl triazole chloroquine (MA-tCQ) utilizing click chemistry and RAFT polymerization. Moreover, to achieve codelivery of cytotoxic CPT and pCQ, we synthesized a pCQ polymer containing reduction-cleavable CPT for combination cancer therapy. In addition, a diblock pCQ-PLA copolymer was synthesized and used for physically encapsulation of PTX.

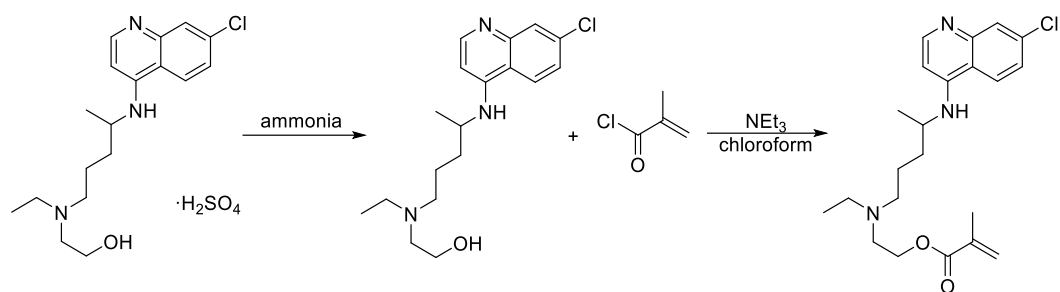
The methods of preparation of small molecules and polymers will be demonstrated, and the results will be discussed in each subsection of this chapter. All the characterization including nuclear magnetic resonance (NMR), mass and gel permeation chromatography (GPC) spectrums will be interpreted as well.

Hydroxychloroquine sulfate, methacrylic acid (MAA), methacryloyl chloride, chloroform-*d* (CDCl₃), and dimethyl sulfoxide-*d*₆ (DMSO-*d*₆) were purchased from ACROS Organics (Fair Lawn, NJ). Propargyl amine (PPA), diphenylphosphoryl azide (DPPA), copper (II) sulfate (CuSO₄), sodium ascorbate (NaAs), *N*-(3-dimethylaminopropyl)-*N'*-ethylcarbodiimide hydrochloride (EDC·HCl), triethylamine, 2-cyano-2-propyl dodecyl trithiocarbonate (CPDT), azobisisobutyronitrile (AIBN), 4-dimethylaminopyridine (DMAP), sodium sulfate, sodium

carbonate, sodium chloride, dimethylformamide (DMF), and dimethyl sulfoxide (DMSO) were purchased from Sigma-Aldrich (St. Louis, MO). 1,8-diazabicyclo[5.4.0]undec-7-ene (DBU) was purchased from Alfa Aesar (Ward Hill, MA). HPMA was purchased from Polysciences (Warrington, PA). Disodium dihydrogen ethylenediaminetetraacetate (EDTA), magnesium sulfate (MgSO_4), 1,4-dioxane, chloroform, dichloromethane (DCM), methanol, ethyl acetate, tetrahydrofuran (THF) and hexane were obtained from Fisher (Fair Lawn, NJ) without further purification.

NMR was performed by Bruker-Avance-III HD 500 MHz or 600 MHz and the data was processed by TopSpin 3.5 (Bruker). The mass spectrum was obtained by a Waters e2695 system equipped with a Waters 2489 absorption detector and a Waters Qtof Micro electrospray ionization mass spectrometer, or a Shimadzu liquid chromatograph mass spectrometer. For all the water soluble cationic polymers, the molecular weight of each sample was tested by GPC with 0.1 M sodium acetate buffer (pH 5.0) as running eluent, using Agilent 1260 Infinity LC system equipped with a miniDAWN TREOS multi-angle light scattering (MALS) detector and an Optilab T-rEX refractive index detector from Wyatt Technology (Santa Barbara, CA). The column TSKgel G3000PWXL-CP (Part No. 0021873, Tosoh Bioscience LLC, King of Prussia, PA) was used at a flow rate of 0.5 mL/min, 25 °C. Results were analyzed using Astra 6.1 software from Wyatt Technology. For all the hydrophobic polymers, the molecular weight was tested by gel permeation chromatography with 10 mM LiBr DMF as eluent, using the same Agilent 1260 Infinity LC system equipped with MALS detector and an Optilab T-rEX refractive index detector from Wyatt Technology (Santa Barbara, CA). The column PLgel 5 μm MIXED-C (Part No. 1110-6500, Polymer Laboratories, UK) was used at a flow rate of 0.5 mL/min, 45 °C. Results were analyzed using Astra 6.1.

2.1 Synthesis of MA-CQ



Scheme 2.1. Synthesis of MA-CQ.

DCM (20 mL) was added to aqueous solution (20 mL) of hydroxychloroquine sulfate (3.0 g, 6.9 mmol). Ammonium hydroxide (30% aq., 2.5 mL, 21 mmol) was added dropwise to the mixture with vigorously stirring for 30 min. The mixture was then transferred to a separatory funnel. DCM layer was drained and another 10 mL of DCM was added to extract the HCQ. The DCM layers were combined and washed with brine (20 mL). After drying with anhydrous sodium sulfate, DCM was evaporated by rotavap and viscous colorless paste was obtained (1.38 g, 59%). ¹H NMR (500 MHz, Chloroform-*d*) δ 8.45 (d, *J* = 5.4 Hz, 1H), 7.90 (d, *J* = 2.1 Hz, 1H), 7.73 (d, *J* = 8.9 Hz, 1H), 7.28 (dd, *J* = 9.0, 2.2 Hz, 1H), 6.36 (d, *J* = 5.4 Hz, 1H), 5.17 (d, *J* = 7.7 Hz, 1H), 3.65 – 3.68 (m, 1H), 3.61 (s, 1H), 3.55 (t, *J* = 5.6, 1.2 Hz, 2H), 2.47 – 2.59 (m, 6H), 1.68 – 1.71 (m, 1H), 1.52 – 1.61 (m, 3H), 1.27 (d, *J* = 6.4 Hz, 3H), 0.98 (t, *J* = 7.1 Hz, 3H). ¹³C NMR δ 151.58, 149.23, 148.98, 134.57, 128.09, 124.78, 121.59, 117.22, 98.91, 77.37, 77.11, 76.86, 58.49, 54.83, 53.37, 52.96, 48.21, 47.42, 34.04, 23.84, 20.07, 11.51.

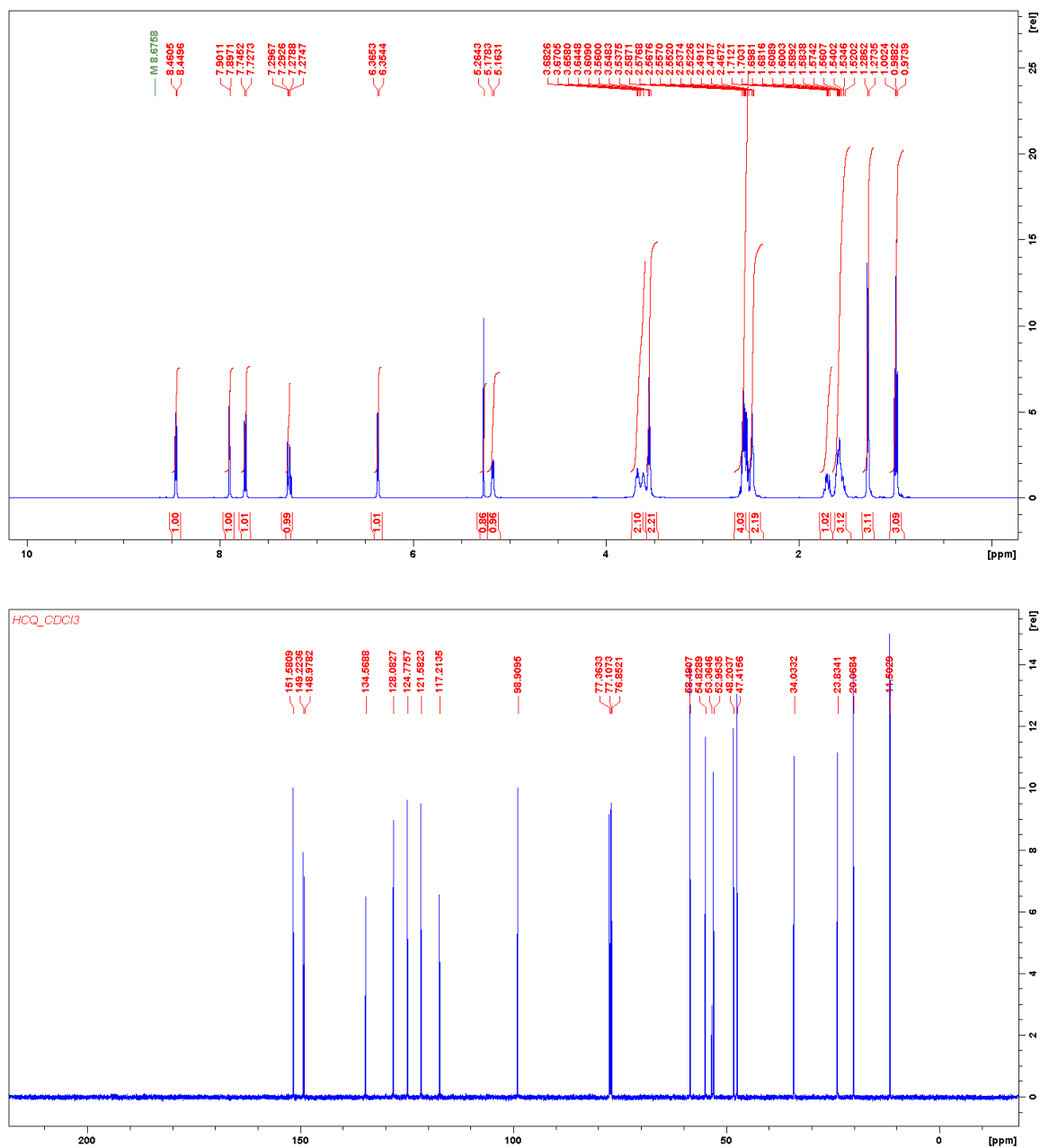
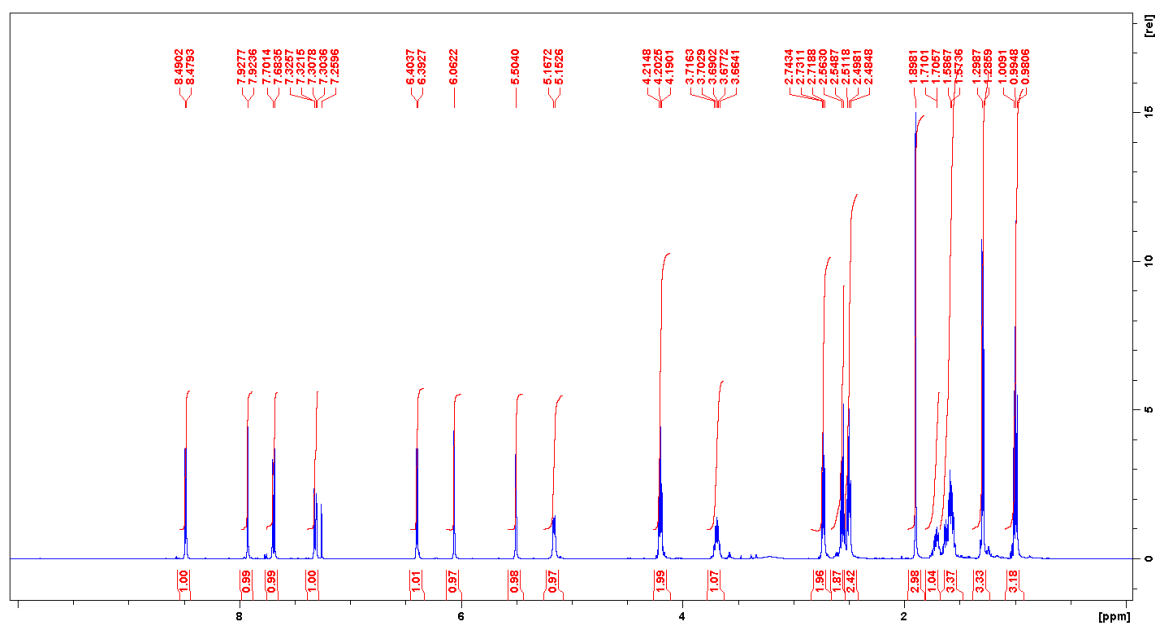


Figure 2.1. ¹H NMR and ¹³C NMR of HCQ in CDCl₃.

The desalted HCQ (2.0 g, 5.95 mmol) and triethylamine (1.92 g, 2.4 mL, 19 mmol) were dissolved in anhydrous chloroform (100 mL) and cooled down in the ice bath. Methacryloyl chloride (1.99 g, 1.84 mL, 19 mmol) was dissolved in anhydrous chloroform (100 mL) and added to the HCQ dropwise with vigorously stirring at 0 °C. The mixture was stirred overnight while the temperature rising to room temperature. The reaction mixture was washed with saturated sodium

carbonate (2×50 mL) and brine (50 mL). The resulted organic layer was concentrated and purified by silica gel chromatography with DCM:methanol (10:1) as eluent to give the MA-CQ (0.96 g, 40%) as a light yellow paste. The mass $[M+H]^+$ of MA-CQ was found at 404.03 (calcd. 404.21). ^1H NMR (500 MHz, CDCl_3) δ 8.48 (d, $J = 5.5$ Hz, 1H), 7.92 (d, $J = 2.2$ Hz, 1H), 7.69 (d, $J = 9.0$ Hz, 1H), 7.32 (dd, $J = 8.9, 2.2$ Hz, 1H), 6.39 (d, $J = 5.6$ Hz, 1H), 6.06 (s, 1H), 5.50 (s, 1H), 5.16 (d, $J = 7.4$ Hz, 1H), 4.20 (td, $J = 6.1, 2.1$ Hz, 2H), 3.69 (m, 1H), 2.73 (t, $J = 6.2$ Hz, 2H), 2.56 – 2.48 (m, 4H), 1.89 (s, 3H), 1.74 – 1.51 (m, 4H), 1.29 (d, $J = 6.3$ Hz, 3H), 0.99 (t, $J = 7.1$ Hz, 3H). ^{13}C NMR δ 167.45, 151.32, 149.52, 148.66, 136.23, 135.02, 127.97, 125.61, 125.11, 121.56, 117.21, 99.06, 77.37, 77.11, 76.86, 62.76, 53.71, 51.43, 48.44, 48.20, 34.15, 24.14, 20.19, 18.28, 11.68.



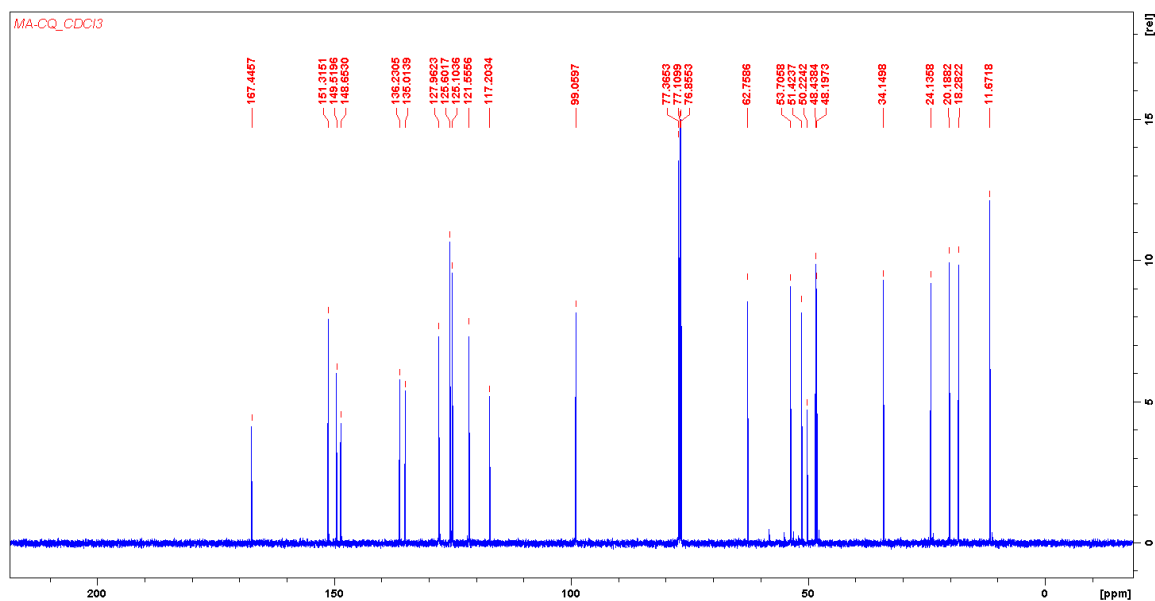
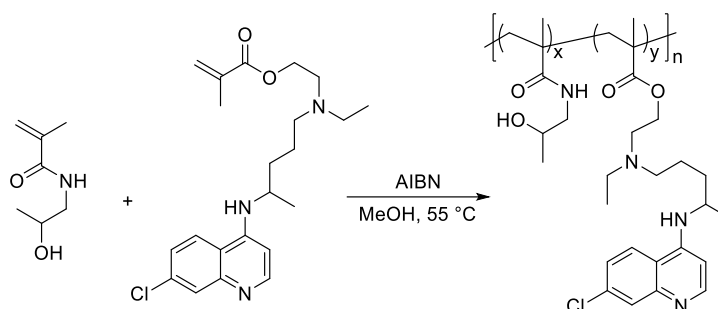


Figure 2.2. ^1H NMR and ^{13}C NMR of MA-CQ in CDCl_3 .

MA-CQ was prepared by direct acylation of hydroxyl of HCQ with methacryloyl chloride. MA-CQ was purified by silica column chromatography using DCM and methanol as eluents and characterized by ^1H NMR, ^{13}C NMR and mass spectrometry. Selective substitution of the hydroxyl group and the absence of substitution of the secondary alkyl/aryl amine in HCQ were confirmed by NMR analysis. Chemical shifts of the aromatic quinoline protons and protons adjacent to the secondary amine were identical in HCQ and MA-CQ. In contrast, the chemical shifts of the methylene protons adjacent to the hydroxyl group changed from 3.55 to 4.20 ppm as a result of the esterification of the hydroxyl group in HCQ. The chemical shifts at 6.06 and 5.50 of the methylene protons, as well as the integration ratio of the protons indicated the formation of methacrylate. Moreover, ^{13}C NMR signals at 167.45 further supported the conclusion of methacrylate formation.

2.2 Synthesis of pCQ by free radical polymerization



Scheme 2.2. Synthesis of pCQ by free radical polymerization.

Polymers with different CQ content were obtained by changing the monomer ratio of MA-CQ to HPMA in the reagents. Typically, MA-CQ (40 mg, 0.099 mmol), HPMA (57 mg, 0.4 mmol) and AIBN (4 mg, 0.025 mmol) were dissolved in methanol (1 mL) and purged by nitrogen for 30 min. After stirred at 55 °C overnight, the polymer was precipitated out by adding the mixture to cold diethyl ether under vigorous stirring. The precipitates were collected and re-dissolved in methanol. The precipitation step was repeated twice and the polymers were dialyzed against water (MWCO: 8,000) for 2 days. The pCQ polymers were obtained by lyophilization. The pHPMA polymer with CQ content as 0% was synthesized as control. The molecular weight of the polymers was tested by GPC as water soluble cationic polymers. The content of CQ in polymer pCQ16.7 was calculated by the integration ratio of protons on CQ (δ 8.38, 7.77, 6.53) and HPMA (δ 4.70, 3.68, 2.91) using pHPMA as reference:

$$\text{mol\% of CQ} = \frac{(1.66+1+0.99)/4}{(1.66+1+0.99)/4 + (4.59+5.26+8.50)/4} \times 100\% = 16.7\%.$$

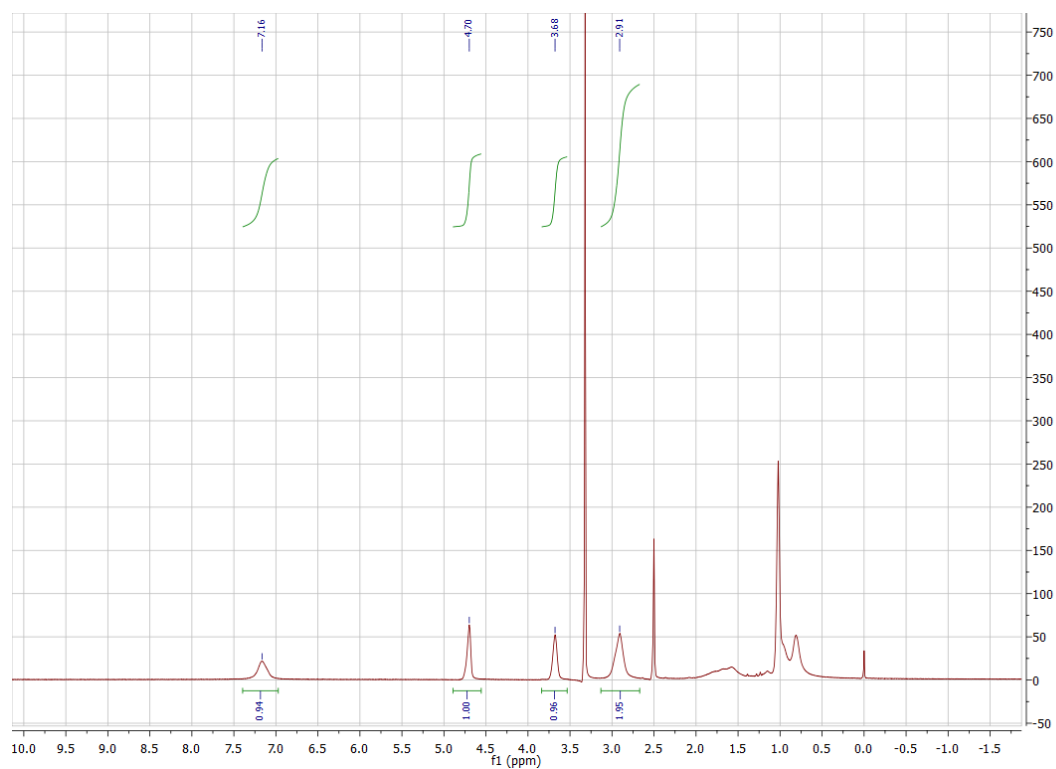


Figure 2.3. ^1H NMR of pHPMA in $\text{DMSO-}d_6$.

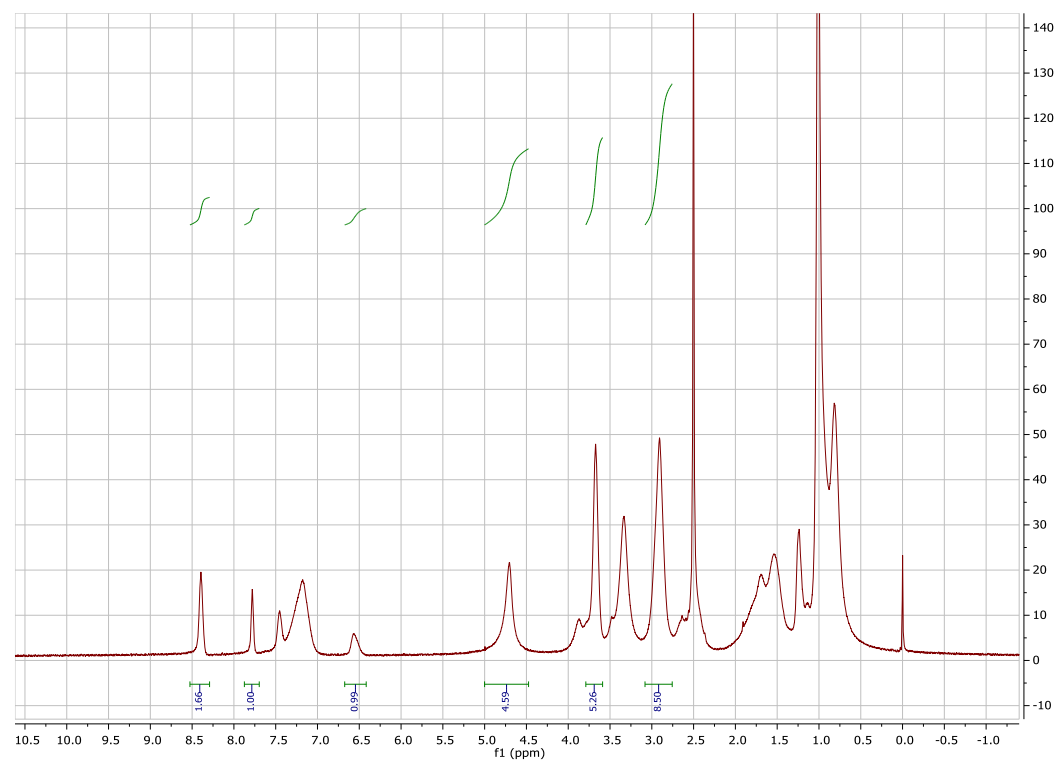


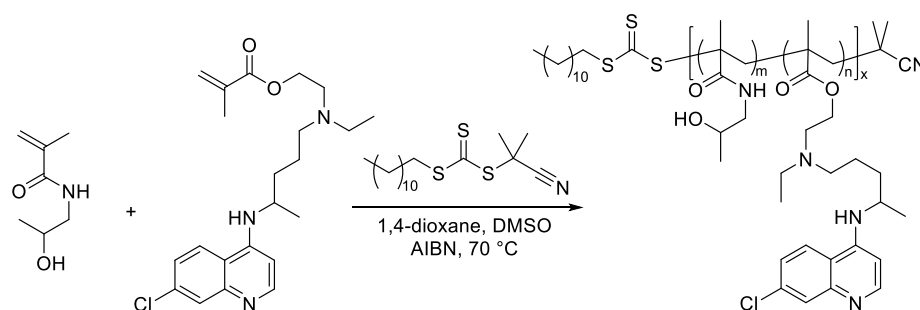
Figure 2.4. ^1H NMR of pCQ in $\text{DMSO-}d_6$.

The MA-CQ and HPMA were copolymerized by free radical polymerization using AIBN as the initiator. By changing the molar ratio of MA-CQ and HPMA in the feed, we were able to obtain pCQ copolymers with different MA-CQ content from 0-20% (mol%). Considering the pharmacological activity and solubility, we picked pCQ10.0 and pCQ16.7 for further study. Negative control pHPMA with no expected pharmacologic activity was synthesized and used for further study. The properties were summarized in Table 2.1.

Table 2.1. Characterization of pCQ polymers.

	CQ content (mol%)		M_n (kDa)	M_w/M_n	P_n
	In feed	In copolymer			
pHPMA	0	0	33.9	1.6	235
pCQ10.0	9.1	10.0	18.4	1.5	109
pCQ16.7	20.0	16.7	18.9	1.8	101

2.3 Synthesis of RpCQ by RAFT polymerization



Scheme 2.3. Synthesis of RpCQ by RAFT polymerization.

To obtain better controlled CQ-containing polymers, we applied RAFT polymerization to synthesis by using CPDT as chain transfer agent (CTA). The procedure of preparing RpCQ was very similar to pCQ. Typically, MA-CQ (80.8 mg, 0.2 mmol), HPMA (143.0 mg, 1.0 mmol), CPDT (4.1 mg, 4.2 μ L, 0.012 mmol) and AIBN (0.5 mg, 0.003 mmol) were dissolved in the 1:1 mixture of 1,4-dioxane and DMSO (100 mg/mL) and purged by argon for 30 min. After stirred in a flame

sealed ampule at 70 °C for 16 h, the reaction was terminated in liquid nitrogen and the polymer was precipitated out by adding to cold diethyl ether under vigorous stirring. The precipitates were collected and re-dissolved in dimethylformamide (DMF). The precipitation step was repeated twice and the polymers were dialyzed against water (MWCO: 3,500) for 2 days. The RpCQ polymers were obtained by lyophilization. The RpHPMA polymer with CQ content as 0% was synthesized using the same CTA as control. The molecular weight of the polymers was tested by GPC as water soluble cationic polymers. The content of CQ in polymer pCQ-16.7 was calculated by the integration ratio of protons on CQ (δ 8.38, 7.77, 6.54) and HPMA (δ 4.71, 3.68, 2.91) using RpHPMA as reference:

$$\text{mol\% of CQ} = \frac{(1.74 + 0.95 + 1)/4}{[(1.74 + 0.95 + 1)/4 + (4.77 + 5.99 + 9.60)/4]} \times 100\% = 15.3\%.$$

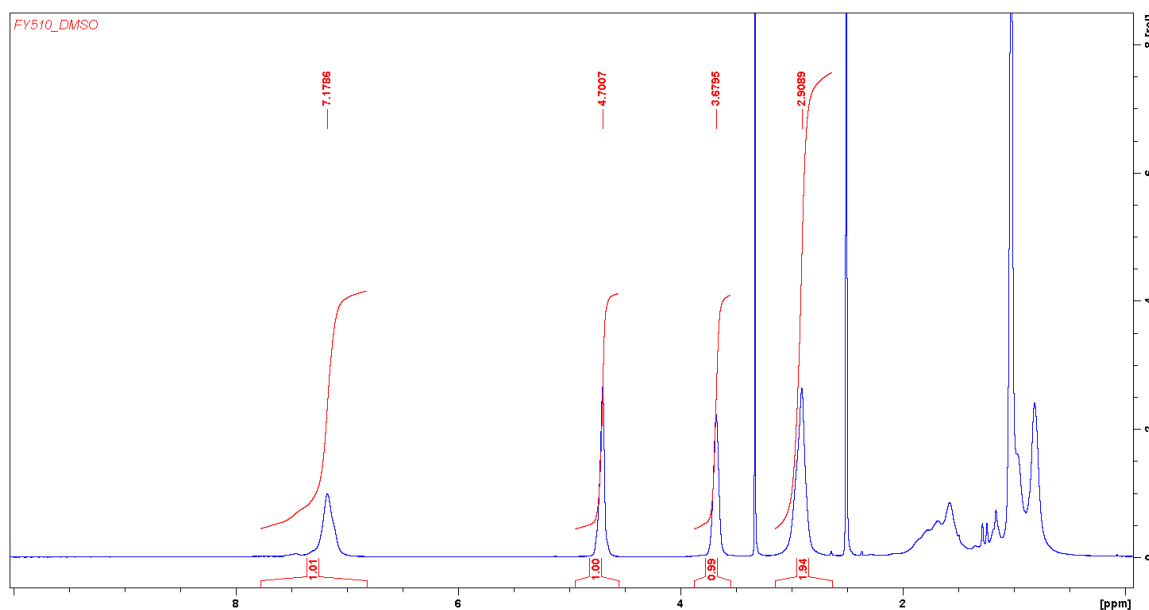


Figure 2.5. ¹H NMR of RpHPMA in DMSO-*d*₆.

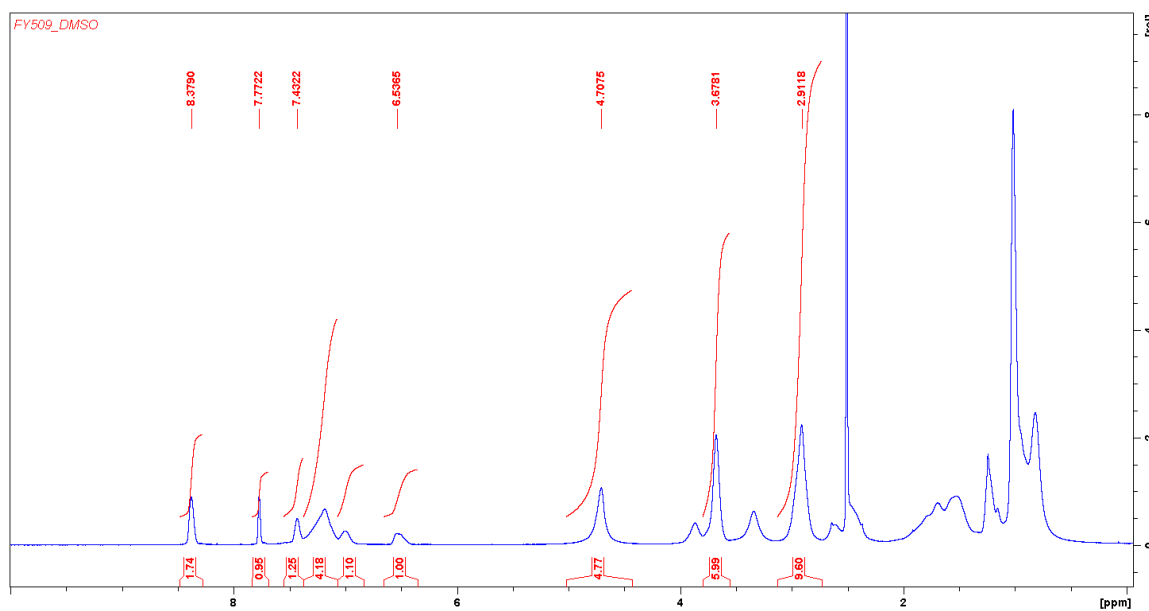


Figure 2.6. ^1H NMR of RpCQ in DMSO- d_6 .

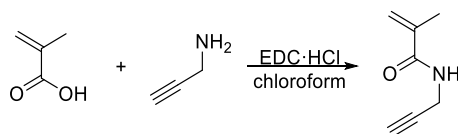
RAFT polymerization resulted in well-defined RpHPMA and RpCQ polymers with low polydispersity (PDI) compared to pCQ. As shown in Table 2.2, RpHPMA and RpCQ possessed lower PDI and better controlled CQ content than pCQ polymers, indicating the successful application of RAFT polymerization.

Synthesis and characterization of pCQ copolymers with ester bond between CQ and backbone of the polymers were discussed in section 2.1-2.3. Our initial studies showed that pCQ copolymers demonstrated unexpectedly enhanced inhibitory activity of cancer cell migration and experimental lung metastasis as polymeric drugs when compared to HCQ. However, the ester bond between CQ and backbone made pCQ susceptible to degradation *in vivo*, which meant that we were unable to unequivocally dissect the therapeutic contribution of the polymeric versus small molecule form HCQ. The goal of the following study (section 2.4-2.9) was to synthesize non-degradable CQ-containing polymer (NpCQ) and to compare its pharmacologic activity with the degradable pCQ.

Table 2.2. Characterization of RpCQ polymers.

	CQ content (mol%)		M_n (kDa)	M_w/M_n	P_n
	In feed	In copolymer			
RpHPMA	0	0	10.7	1.1	75
RpCQ	16.7	15.3	17.7	1.1	97

2.4 Synthesis of *N*-propargyl methacrylamide (PPMA)



Scheme 2.4. Synthesis of PPMA.

MAA (20 mmol, 1721 mg, 1687 μ L) and EDC·HCl (30 mmol, 5751 mg) were dissolved in anhydrous chloroform (60 mL) and stirred at room temperature for 30 min. The mixture was cooled down in ice bath followed by addition of propargyl amine (PPA, 13.33 mmol, 734 mg, 854 μ L) dissolved in chloroform (15 mL). After stirring overnight, the resulting product was concentrated and purified by column chromatography with DCM as eluent. The final product was white solid with the yield of 55%. ^1H NMR (500 MHz, CDCl_3) δ 1.95 (s, 3H), 2.22 (t, $J = 2.52$ Hz, 1H), 4.08 (dd, $J = 2.52, 5.25$ Hz, 2H), 5.35 (s, 1H), 5.71 (s, 1H), 6.20 (s, 1H). ^{13}C NMR δ 18.63, 29.48, 71.69, 79.64, 120.32, 139.45, 168.09.

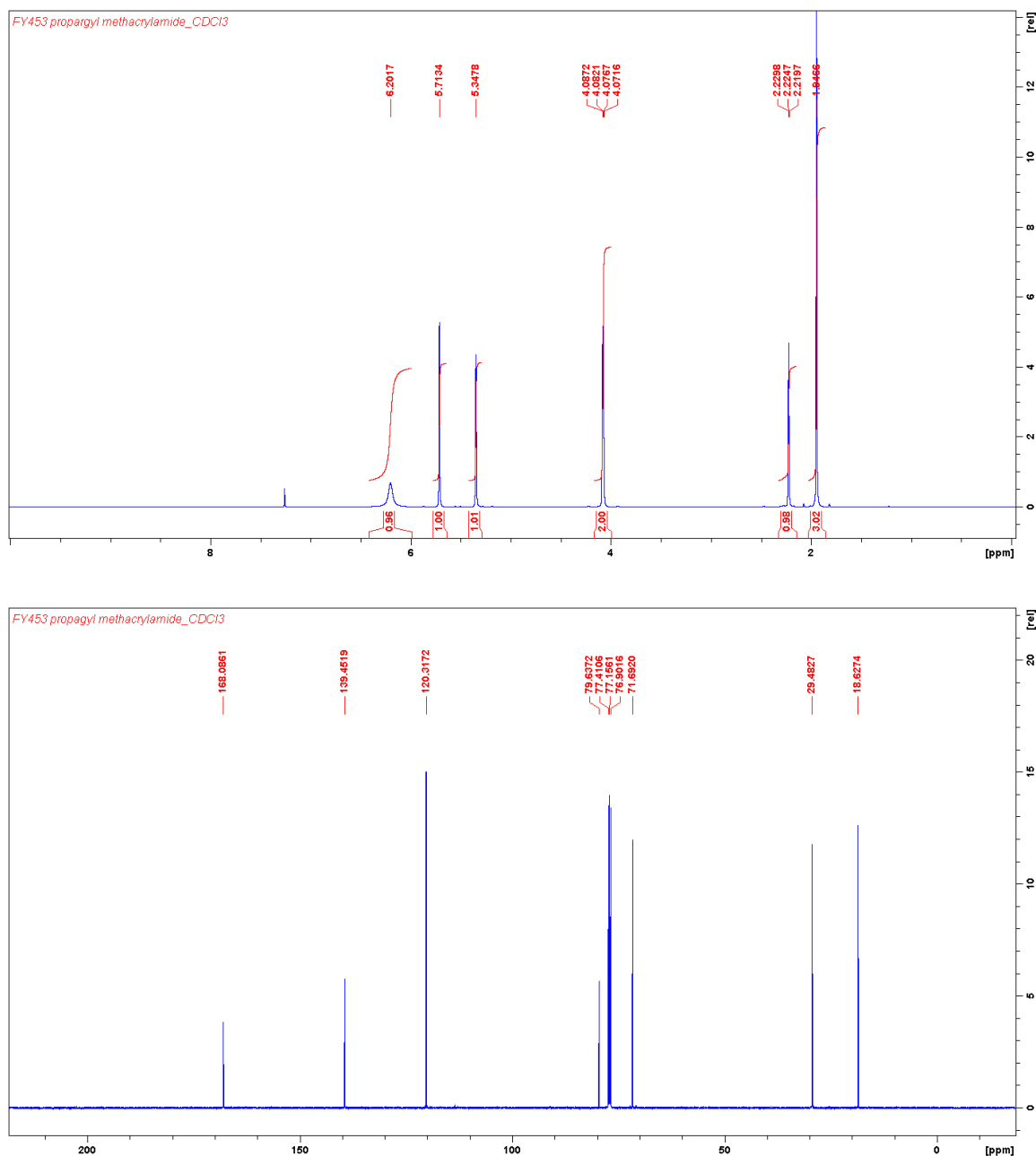
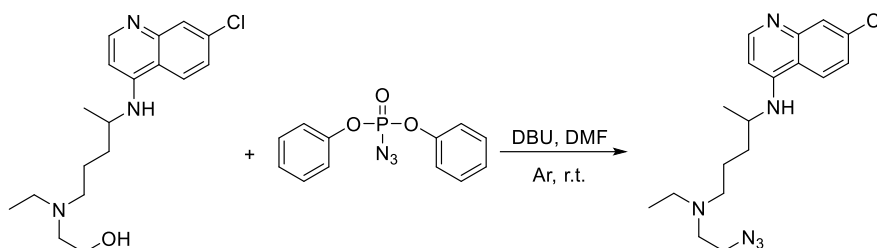


Figure 2.7. ^1H NMR and ^{13}C NMR of PPMA in CDCl_3 .

We first attempted PPMA synthesis using methacryloyl chloride and PPA with triethylamine as a base but 90% of the product was an undesired Michael addition byproduct. Instead, coupling of MAA and PPA with EDC·HCl was performed to obtain PPMA with the yield of 55%. The signals at 5.71 and 5.35 confirmed the existence of methylene protons. The amide proton was shown at 6.20 as a broad peak. PPMA exhibited two functional groups, methacrylamide

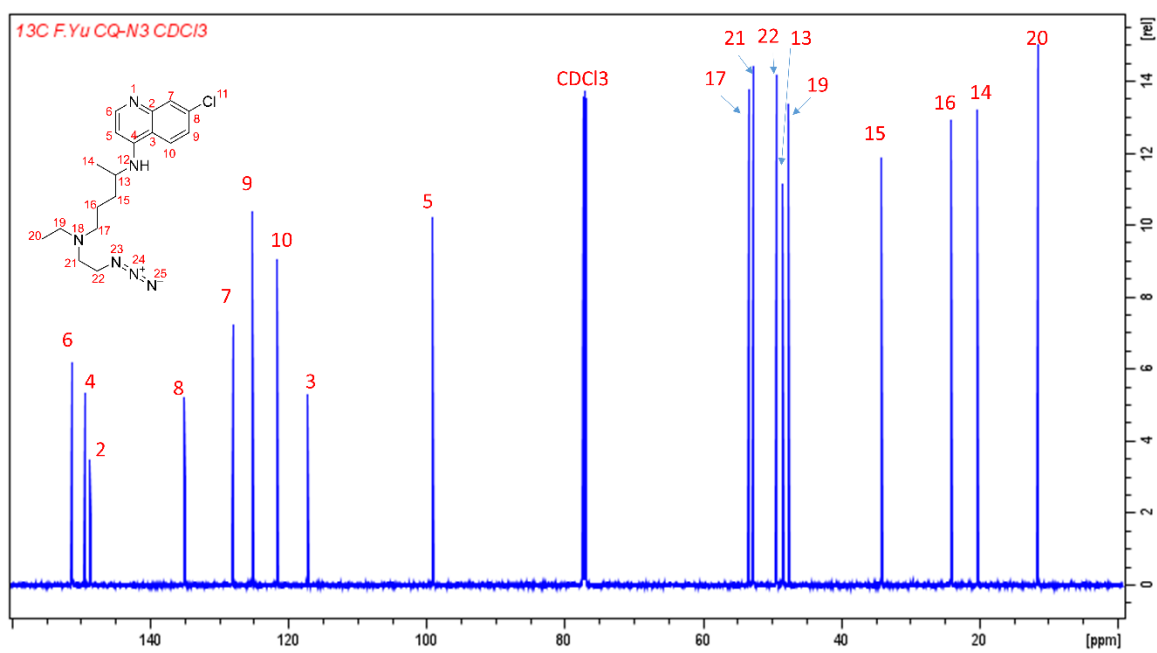
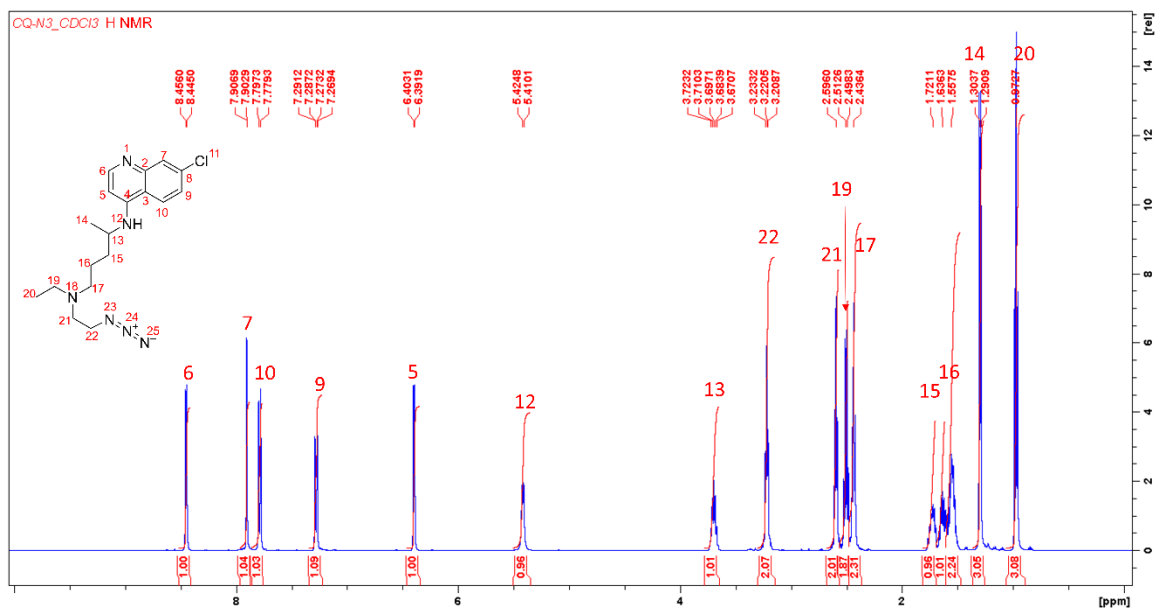
for polymerization and alkyne for click chemistry, which benefited the non-cleavable modification of polymers.

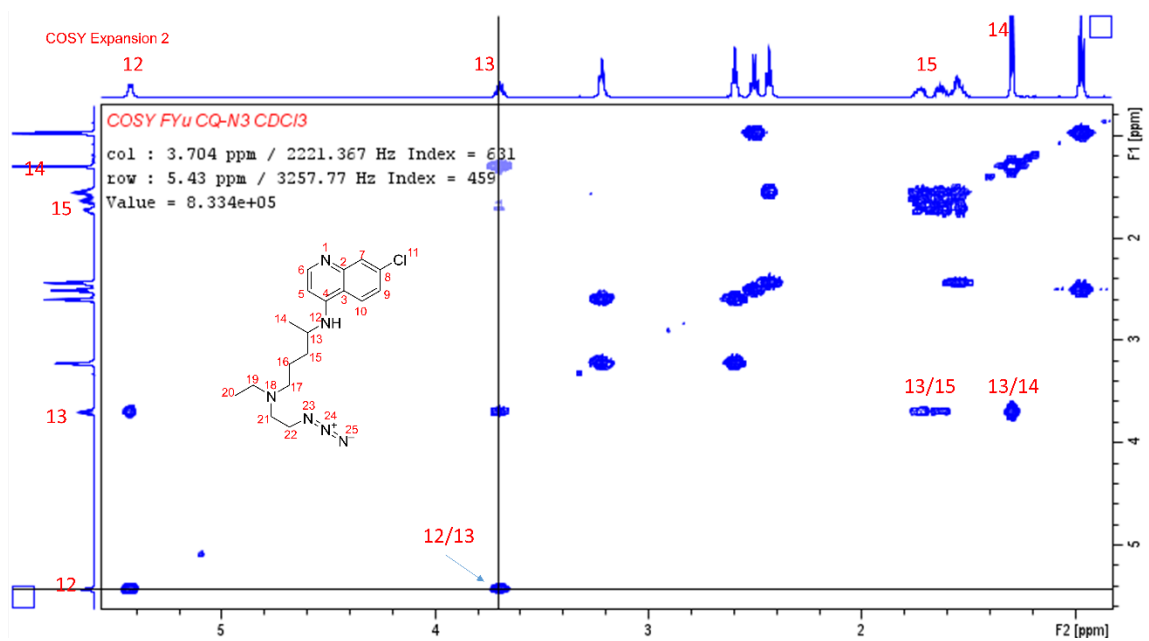
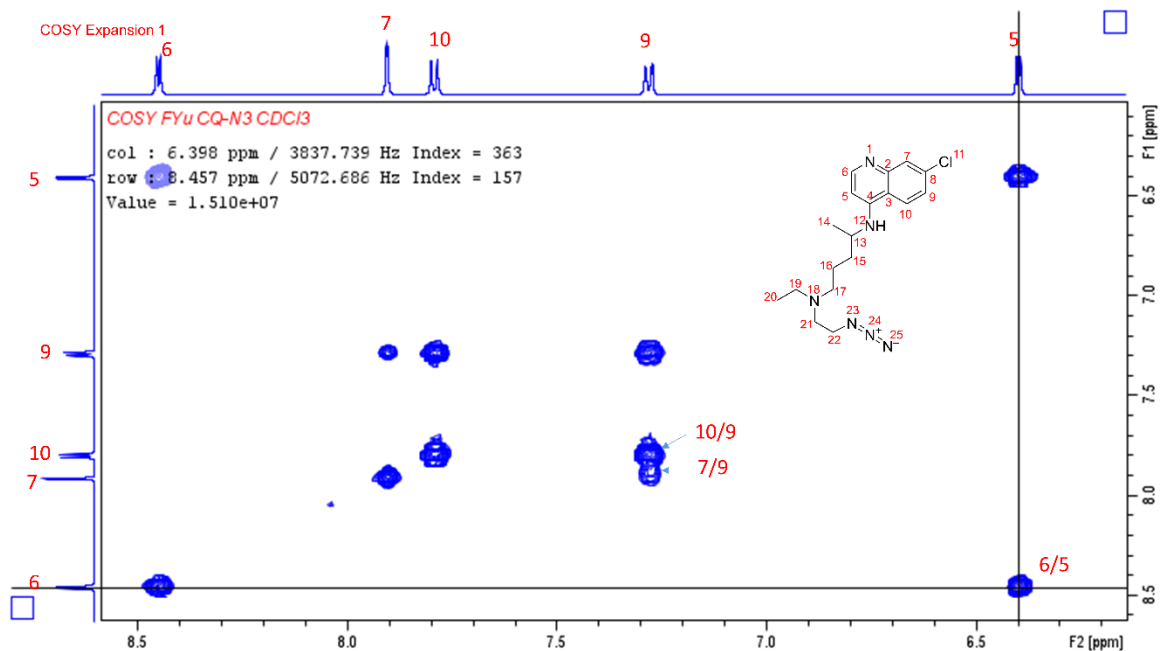
2.5 Synthesis of CQ-N₃

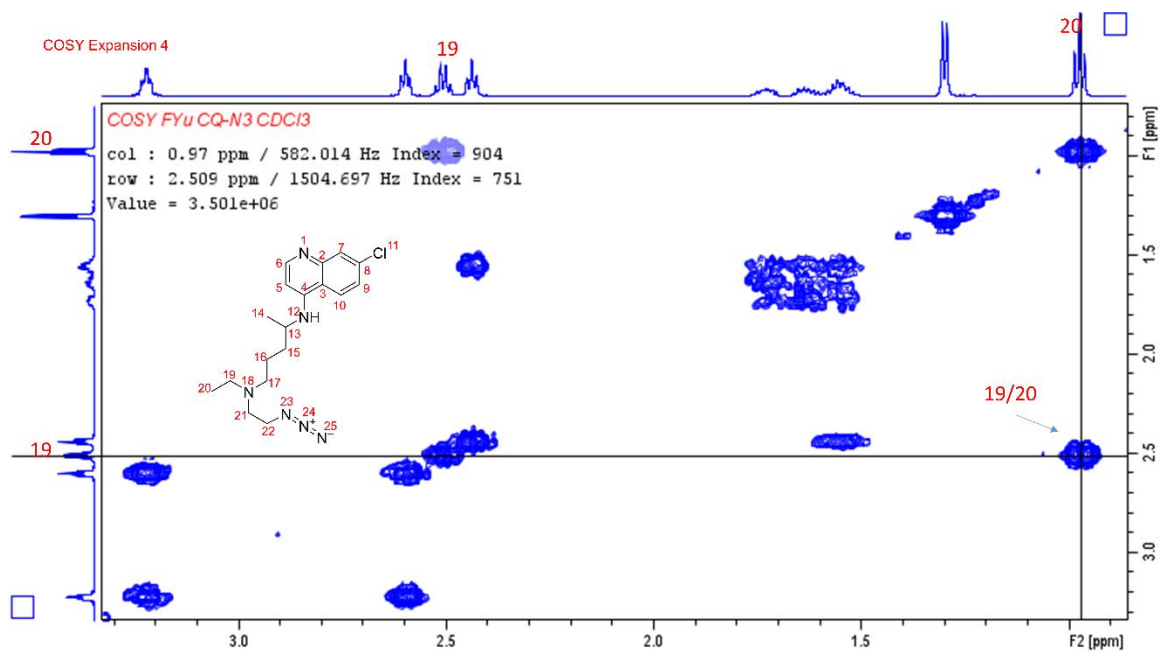
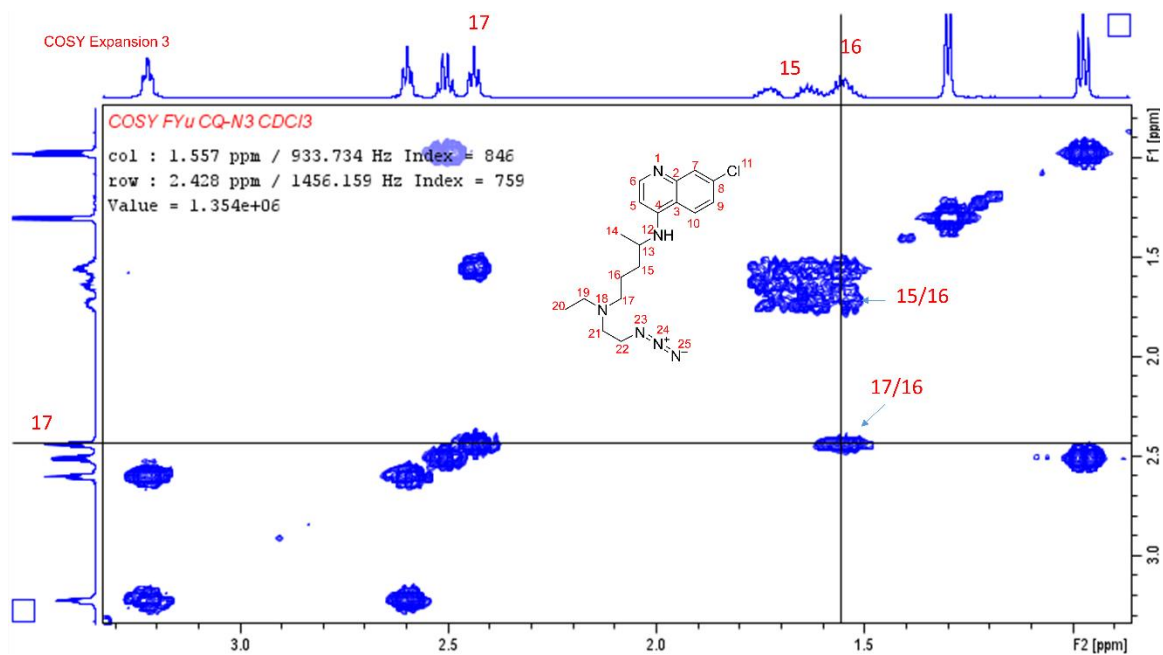


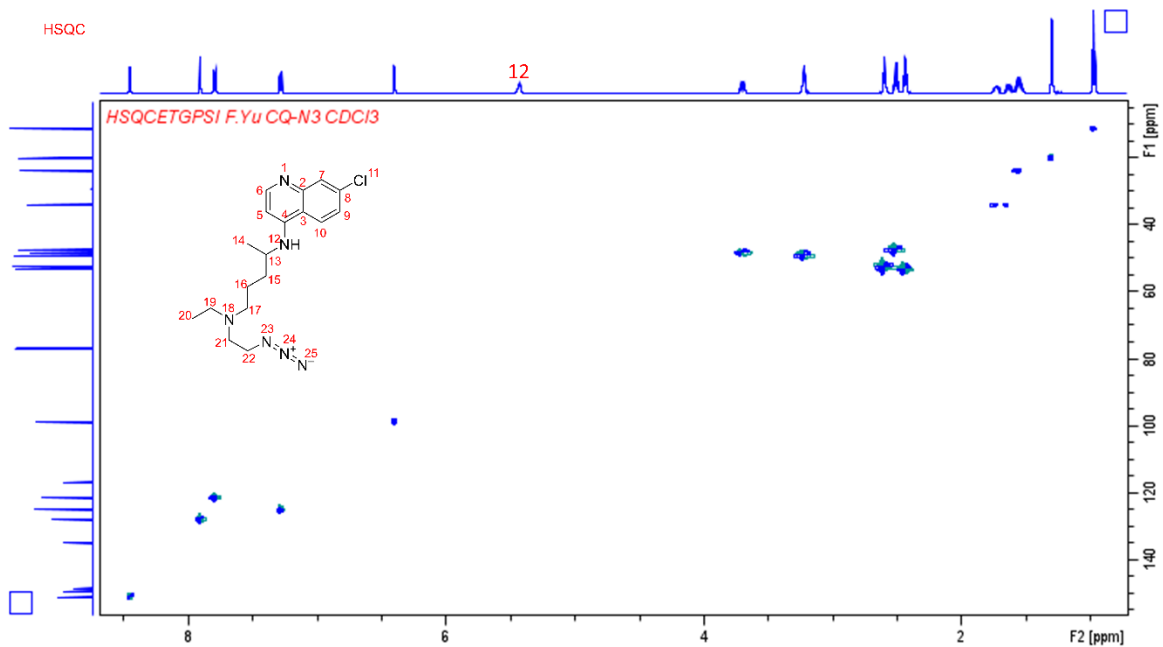
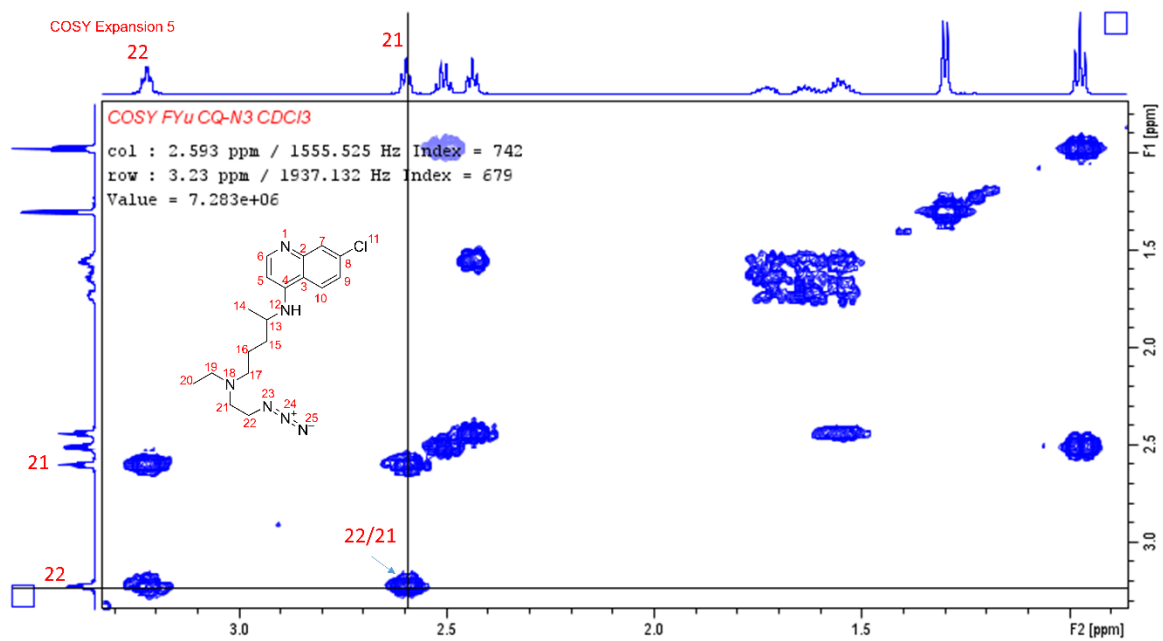
Scheme 2.5. Synthesis of CQ-N₃.

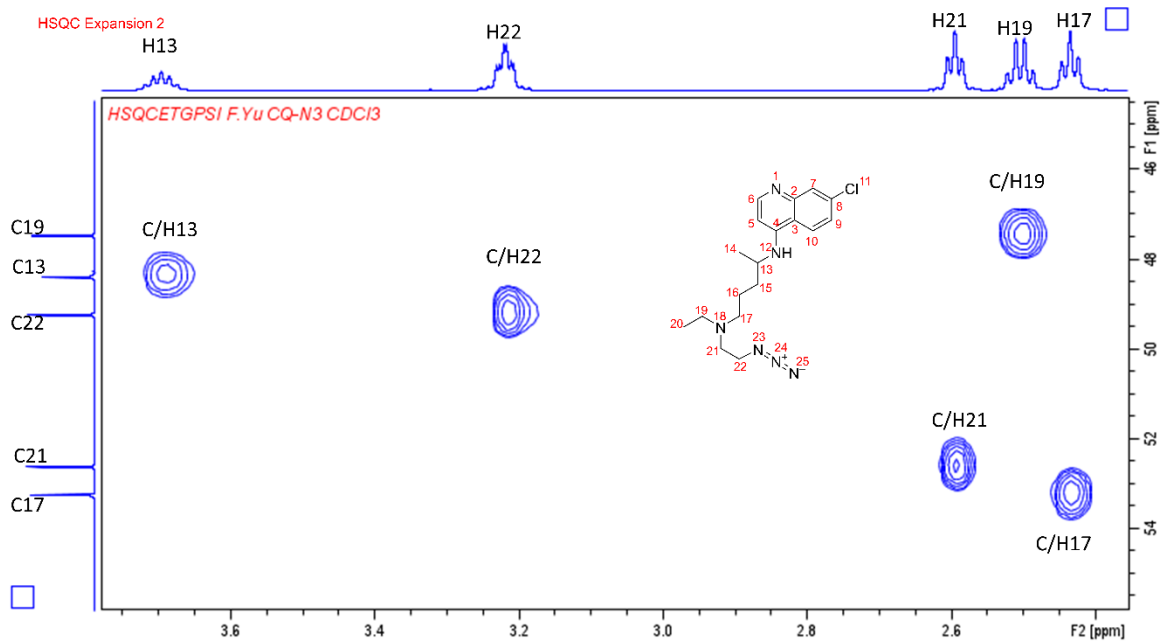
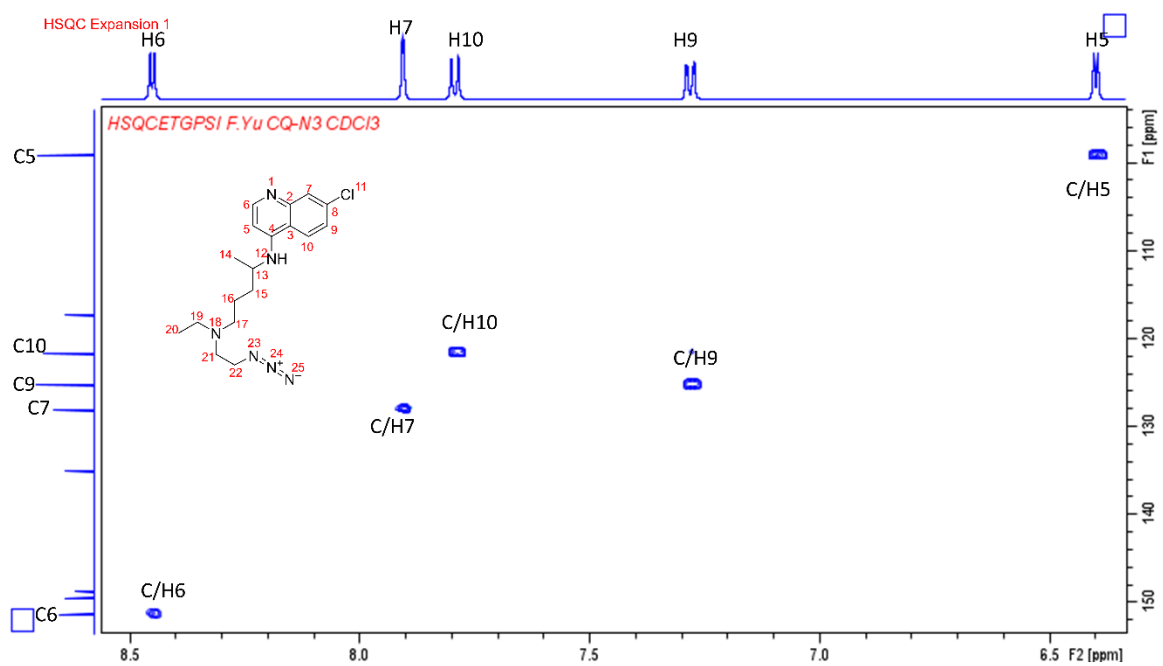
HCQ (360 mg, 1.07 mmol) and DPPA (338.5 mg, 1.23 mmol, 265 μ L) were dissolved in dimethylformamide under argon (Ar). Then DBU (190 mg, 1.23 mmol, 186 μ L) was added and stirred for 48 h. The resulting product was diluted by DCM (50 mL) and washed by deionized water (50 mL) twice and brine (50 mL). The organic phase was dried through sodium sulfate and evaporated by rotavap. The final product was purified by column chromatography with DCM:methanol (10:1) as eluent. CQ-N₃ was light yellow solid with yield of 70%. The mass $[M+H]^+$ of CQ-N₃ was found to be 361.28 (calcd 361.19). ¹H NMR (500 MHz, CDCl₃) δ 8.45 (d, J = 5.5 Hz, 1H), 7.91 (d, J = 2.2 Hz, 1H), 7.79 (d, J = 9.0 Hz, 1H), 7.28 (dd, J = 8.9, 2.2 Hz, 1H), 6.40 (d, J = 5.6 Hz, 1H), 5.42 (d, J = 7.6 Hz, 1H), 3.70 (hept, J = 6.5 Hz, 1H), 3.22 (td, J = 6.1, 1.7 Hz, 2H), 2.60 (t, J = 5.9 Hz, 2H), 2.51 (q, J = 7.1 Hz, 2H), 2.44 (t, J = 6.9 Hz, 2H), 1.79 – 1.69 (m, 1H), 1.69 – 1.49 (m, 3H), 1.30 (d, J = 6.4 Hz, 3H), 0.98 (t, J = 7.1 Hz, 3H). ¹³C NMR δ 151.31, 149.50, 148.71, 135.03, 128.08, 125.18, 121.60, 117.23, 99.13, 53.39, 52.76, 49.38, 48.53, 47.61, 34.21, 24.12, 20.28, 11.57.

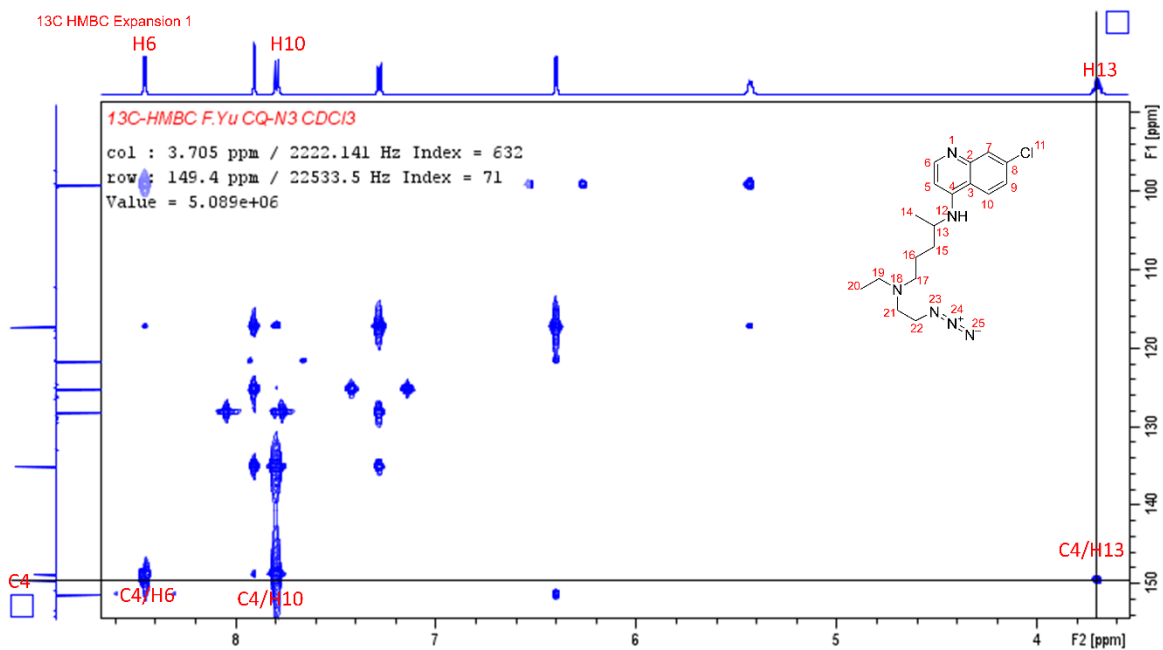
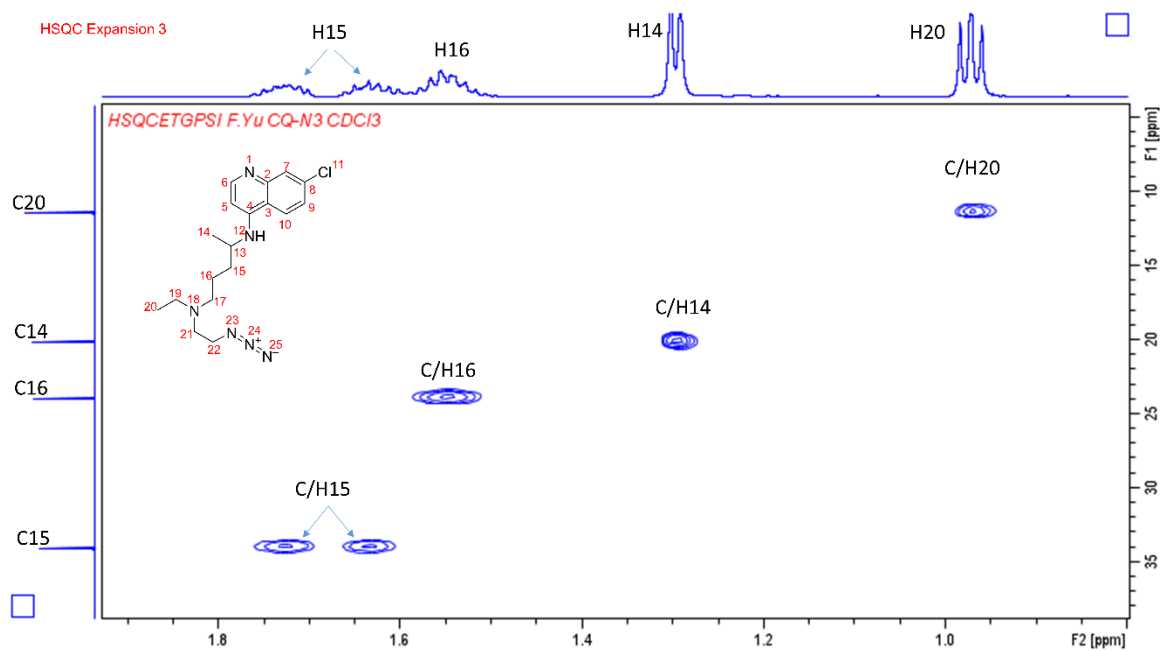


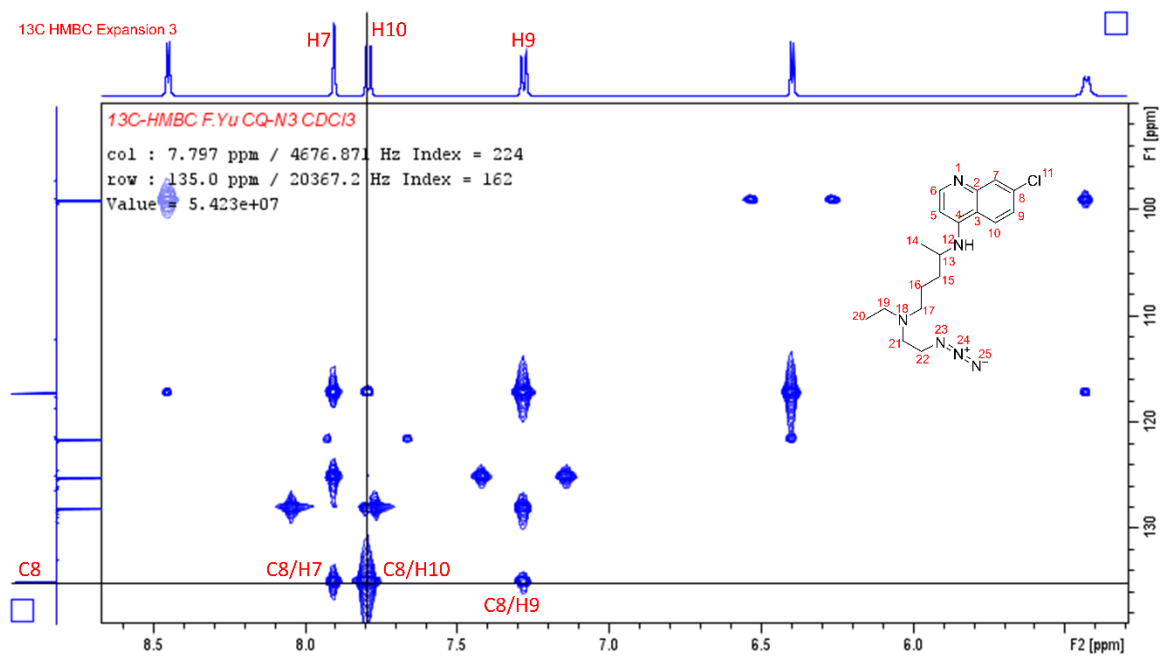
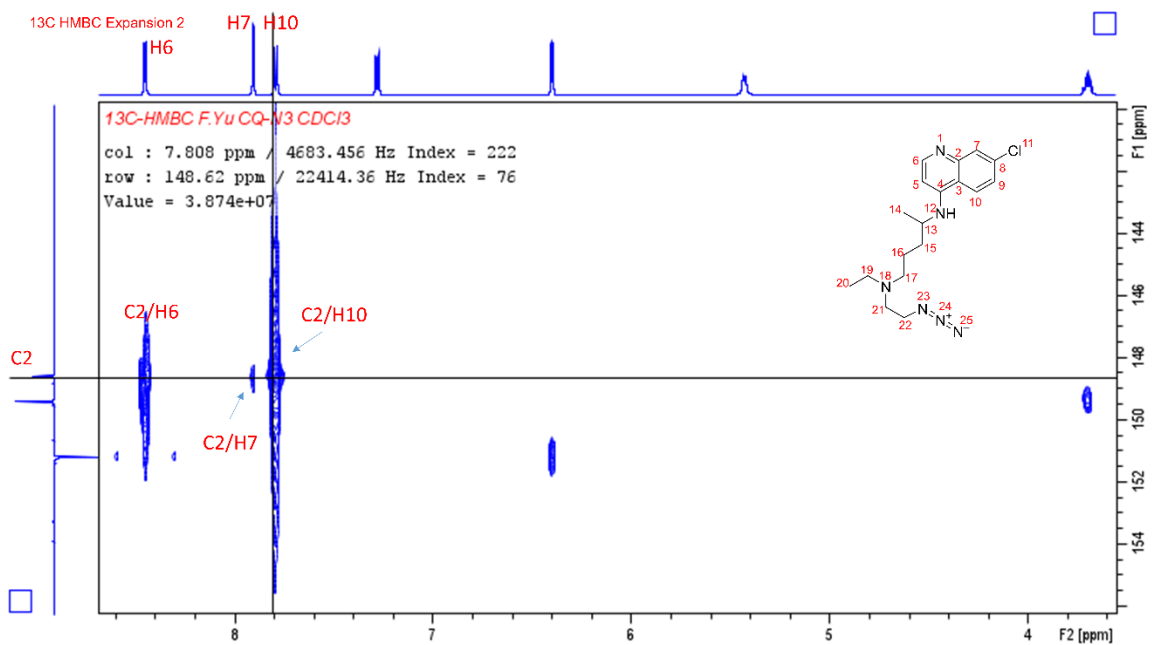


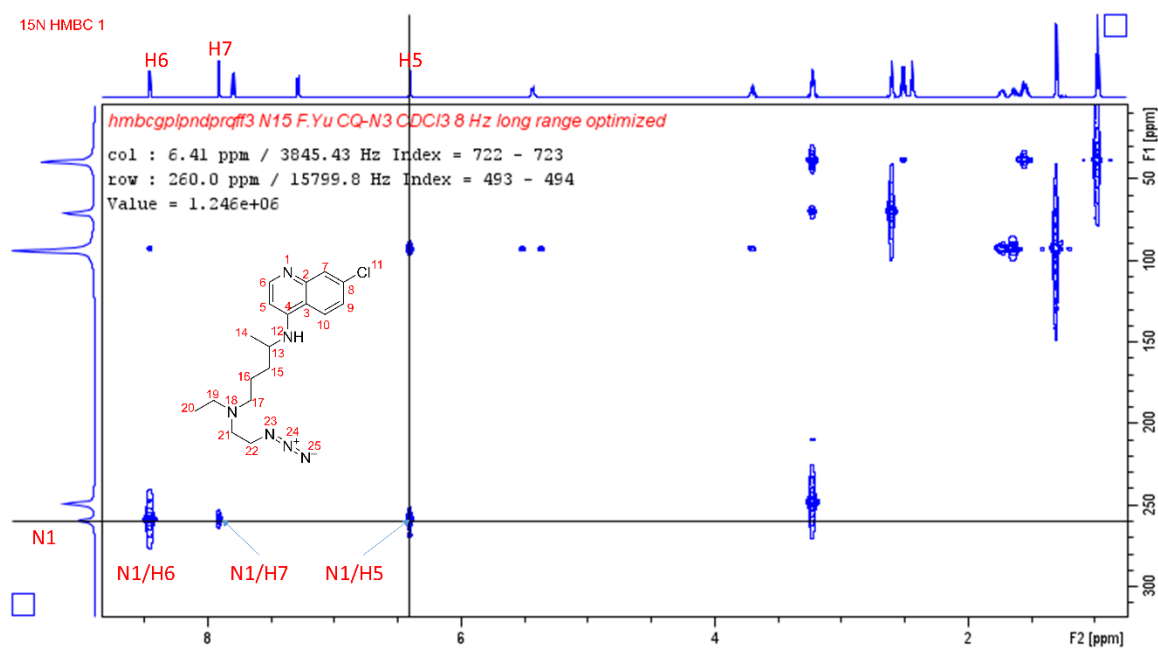
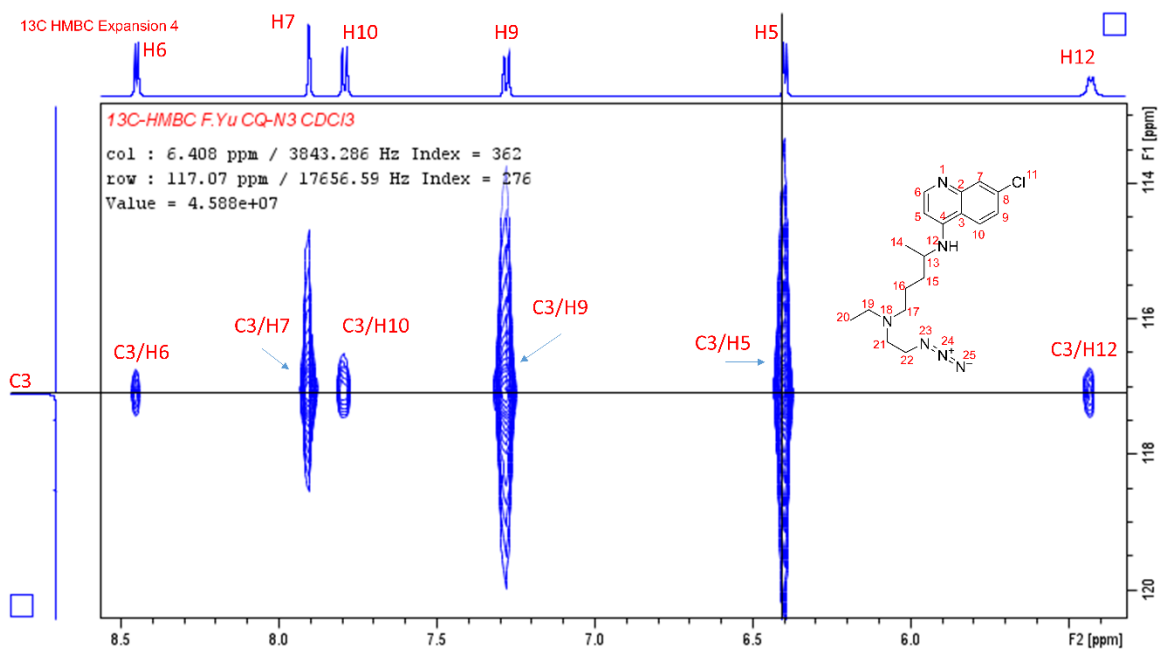


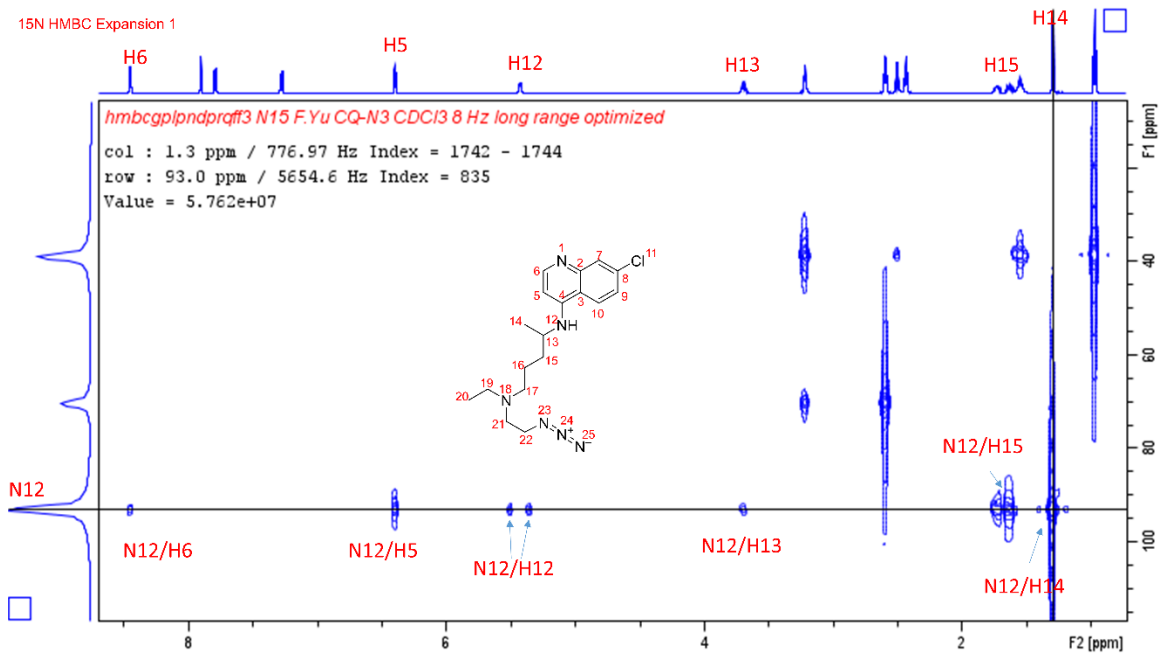
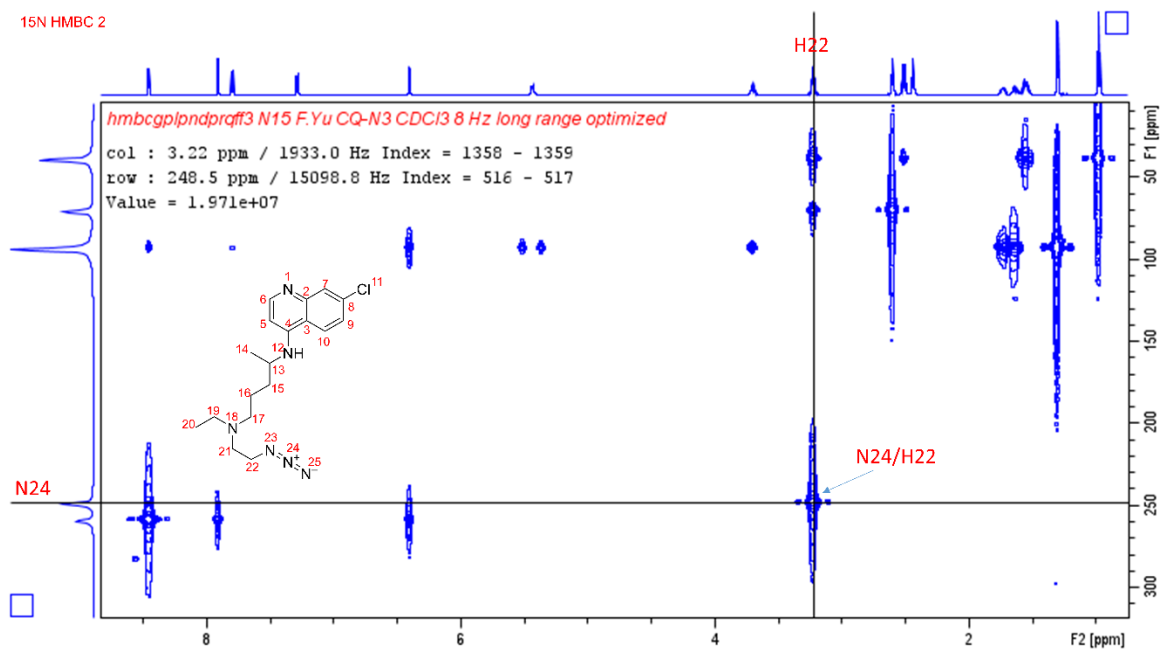












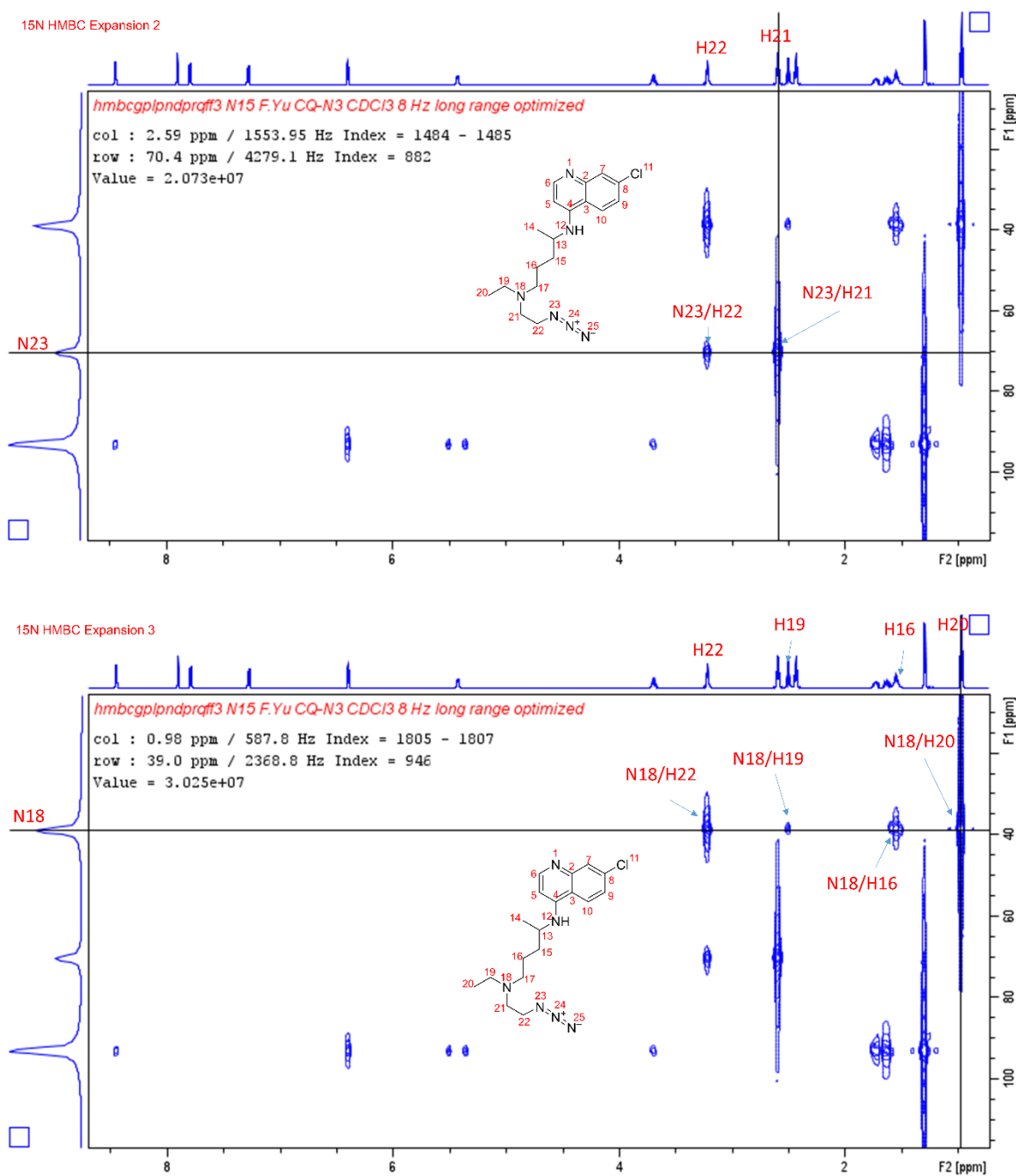


Figure 2.8. ^1H NMR, ^{13}C NMR of CQ-N₃, COSY Expansion 1, COSY Expansion 2, COSY Expansion 3, COSY Expansion 4, COSY Expansion 5, HSQC, HSQC Expansion 1, HSQC Expansion 2, HSQC Expansion 3, ^{13}C HMBC Expansion 1, ^{13}C HMBC Expansion 2, ^{13}C HMBC Expansion 3, ^{13}C HMBC Expansion 4, ^{15}N HMBC 1, ^{15}N HMBC 2, ^{15}N HMBC Expansion 1, ^{15}N HMBC Expansion 2, and ^{15}N HMBC Expansion 3 in CDCl_3 .

Instead of the traditional alcohol-tosylate-azide route that gave very low yield of the product (<10%), DPPA was used for conversion of HCQ to CQ-N₃ in a single step and yield of 70%. The conversion of hydroxyl group to azido group was confirmed by ¹H NMR from the chemical shifts of the methylene protons adjacent to the hydroxyl group from 3.55 to 3.22. Still, the proton and the ¹³C signals of the aromatic ring kept identical, which meant the aromatic structure was preserved during reaction.

To further confirm the substitution of the azido group, we performed 2D NMR to support the chemical structure of CQ-N₃. All the chemical shifts and multiplicity of coupled peaks allowed us to start our H spectrum assignments using the two-dimensional homonuclear correlation spectroscopy (COSY) spectrum. COSY Expansion 1 of the aromatic region showed the fused ring system with the more downfield H6 due to proximity to N1 and correlation to H5. Meta coupling between H7 and H9, and H9 COSY correlations to H10 further supported the assignment of the aromatic ring. In the continuing upfield, we can see amine H12 coupling to H13, with further COSY correlations of H13 to H15 and H14 in COSY Expansion 2. H15 and H16 generated a crowded but discernable COSY cluster, which helped the assignment of H17 in COSY Expansion 3. Characteristic triplet and quartet coupling patterns allowed us to pick out H20 and H19. That leaves the two downfield multiplets as H22 and H21. Assignment of these two protons was determined by data from the ¹³C heteronuclear multiple bond correlation (HMBC) experiment as follows.

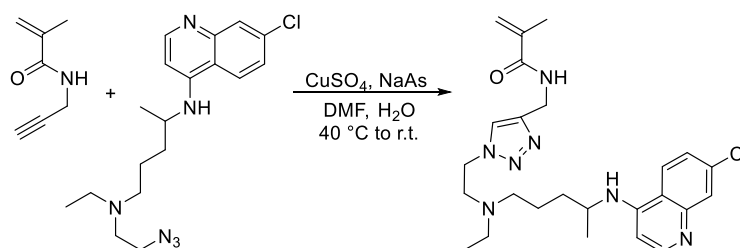
The ¹³C Heteronuclear single quantum correlation (¹³C HSQC) 2D spectrum allowed us to use the proton assignments to label the carbon atom they are covalently bonded to. In HSQC spectrum, there was no carbon correlation for the H12 at 5.43 ppm, which further confirmed it was the amine proton. Carbon peaks were assigned in HSQC Expansion 1 according to the correlation to proton peaks. From HSQC Expansion 2, we can see that aliphatic carbons covalently bonded to N were chemically shifted downfield. In HSQC Expansion 3, it was notable that steric constraints resulted in magnetically non-equivalent H15.

The ^{13}C HMBC was optimized at 8 Hz coupling for 3-bond coherence transfer. HMBC Expansion 1 showed 3-bond H correlations to aromatic quaternary C4 from H6, H10 and most important identifier, H13. External projection in carbon dimension was Attached Proton Test (APT) experiment, phased with methylene/quaternary peaks as positive and methyl/methane as negative. HMBC Expansion 2 showed quaternary C2 3-bond correlations to H6 and H10, with a much weaker vicinal 2-bond correlation to H7. Similarly, HMBC Expansion 3 showed strong 3-bond correlation of C8 to H10, as well as weaker 2-bond vicinal coupling of C8 to H7 and H9. From HMBC Expansion 4, we can see the well connected bridgehead Carbon, C3, with 3-bond correlations to H5, H7, H9 and H12, as well as weaker vicinal 2-bond to H10 and unexpected 4-bond to H6 resulted from enhanced correlation intensity of duplicity of coupling pathways.

^{15}N HMBC was optimized for expected strength of long range J -coupling. However, the geometry influenced by the lone pair of electrons means that 3-bond is not always the strongest correlation observed. As shown in ^{15}N HMBC 1, the coupling of vicinal N1/H6 was stronger than that of 3-bond N1/H7 and N1/H5. The ^{15}N HMBC 2 showed a strong 3-bond correlation from N24 to H22, which confirmed its assignment. The ^{15}N HMBC Expansion 1 clearly showed the very well connected H12 as note of the observed doublet due to direct ~ 90 Hz J -coupling to H, and weak 4-bond correlation back to H6. The ^{15}N HMBC was an “inverse” detected experiment in that we detected the ^{15}N nucleus through its magnetic coupling to the more sensitive nearby H isotope. Strong 3-bond response from N23 to H21 and a weaker vicinal 2-bond to H22 were observed in ^{15}N HMBC Expansion 2. N18 with its expected 3-bond correlations to H22, H16 and H20, and weaker 2-bond to H19 were also detected in ^{15}N HMBC Expansion 3. N15 has a large chemical shift range, with two prevalent reference points, $\text{CH}_3\text{-NO}_2$ and liquid NH_3 . We expanded ^{15}N HMBC observation sweep width, doubled indirect dimension digitization, increased number of acquisitions, optimized long range delay to 2.75 HZ and started looking for a long range correlation to N25. A very weak 4-bond correlation was detected to the closest H22. Strength of detection

depended on how close the J -optimized delay was to the actual strength of coupling and residual magnetization remaining after the requisite delay time. Small coupling required a longer delay between polarization transfer pulses with attendant decrease in signal remaining to be detected. We were only able to observe the chemical shift of our supposed N25 as shown in 15N HMBC Expansion 3.

2.6 Synthesis of methacrylamido methyl triazole chloroquine (MA-tCQ)



Scheme 2.6. Synthesis of MA-tCQ by click chemistry.

CQ-N₃ (343 mg, 0.95 mmol) and PPMA (185 mg, 1.5 mmol) were dissolved in DMF (2.5 mL). CuSO₄ (8 mg, 0.05 mmol) was dissolved in deionized water (0.4 mL) and added into the DMF solution. After the reaction mixture was degassed for 30 min, NaAs (40 mg, 0.2 mmol) dissolved in deionized water (0.4 mL) was added to the above reaction mixture under N₂. The reaction was taken at 40 °C for 2 h and at room temperature overnight with stirring. The resulting mixture was diluted by DCM (50 mL) and washed by EDTA aqueous solution (50 mM, 50 mL) twice, water (50 mL) and brine (50 mL). The organic phase was dried through sodium sulfate and evaporated by rotavap. The final product was purified by column chromatography with DCM:methanol (10:1) as eluent. The final yield was 65%. The mass $[M+H]^+$ of MA-tCQ was found at 484.12 (calcd 484.26). ¹H NMR (500 MHz, CDCl₃) δ 8.38 (d, $J = 5.6$ Hz, 1H), 8.05 (d, $J = 9.0$ Hz, 1H), 7.85 (d, $J = 2.2$ Hz, 1H), 7.65 (s, 1H), 7.41 – 7.34 (m, 1H), 7.24 (dd, $J = 9.0, 2.2$ Hz, 1H), 6.33 (d, $J = 5.7$ Hz, 1H), 6.03 (d, $J = 7.8$ Hz, 1H), 5.69 (s, 1H), 5.25 (s, 1H), 4.53 (dd, $J = 15.1, 6.0$ Hz, 1H), 4.40 (dd, $J = 15.1, 5.7$ Hz, 1H), 4.26 (qt, $J = 13.6, 6.0$ Hz, 2H), 3.60 (p, $J = 6.5$ Hz, 1H), 2.76 (qt, $J =$

13.4, 5.9 Hz, 2H), 2.43 (q, $J = 7.1$ Hz, 2H), 2.36 (dt, $J = 10.6, 5.0$ Hz, 2H), 1.88 (s, 2H), 1.52 – 1.31 (m, 3H), 1.19 (d, $J = 6.3$ Hz, 3H), 0.84 (t, $J = 7.1$ Hz, 3H). ^{13}C NMR δ 168.65, 151.41, 148.30, 145.72, 144.49, 139.45, 136.42, 125.80, 125.40, 123.82, 123.29, 120.40, 116.85, 98.52, 77.32, 77.07, 76.81, 53.27, 53.08, 49.27, 48.82, 47.31, 35.18, 33.82, 24.31, 19.98, 18.69, 11.56.

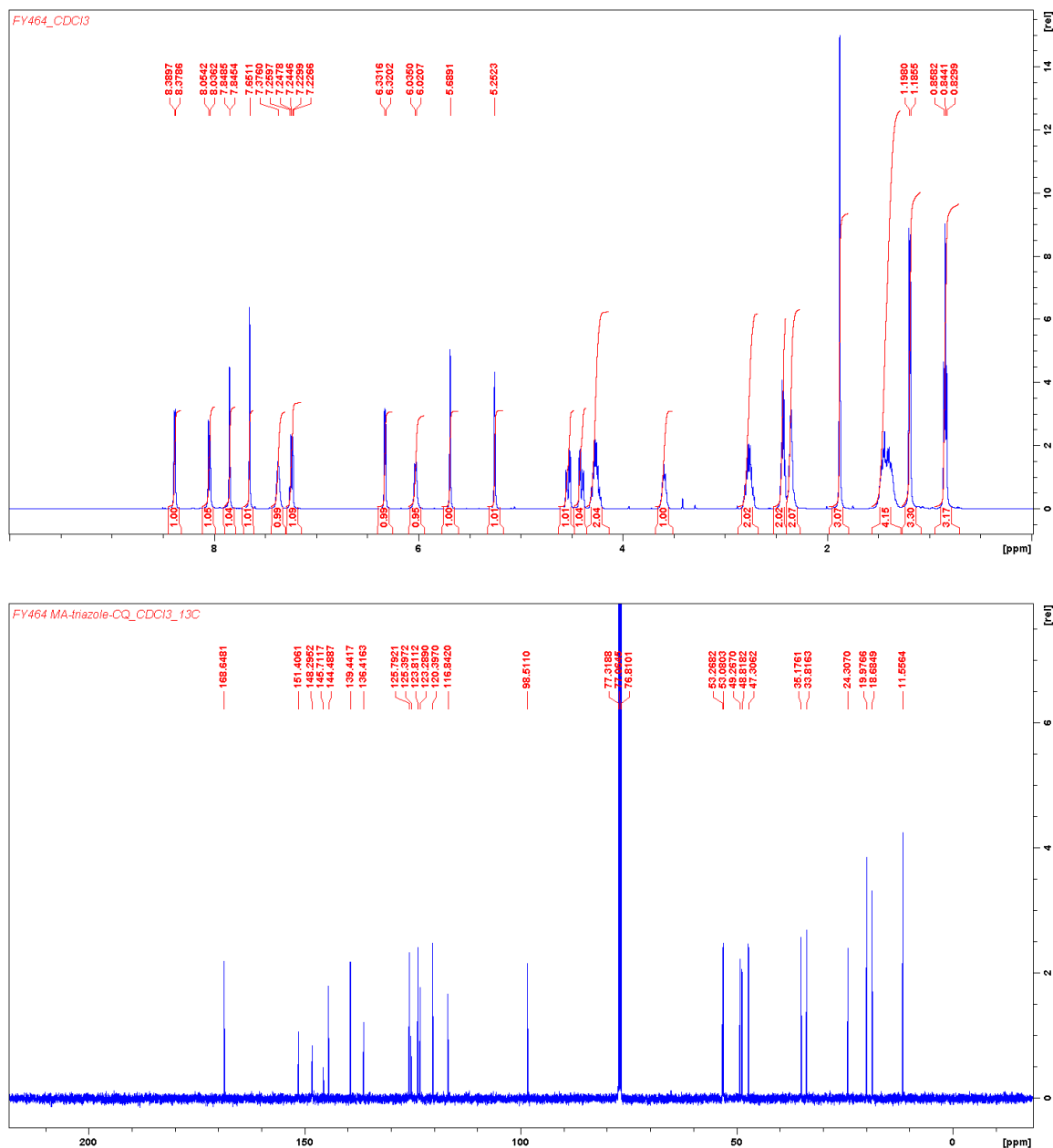
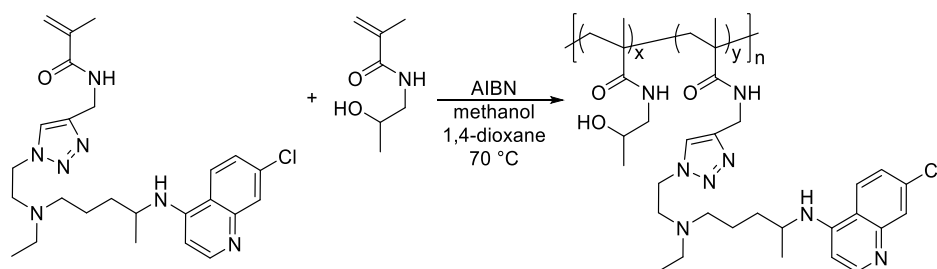


Figure 2.9. ^1H NMR and ^{13}C NMR of MA-tCQ in CDCl_3 .

Once PPMA and CQ-N₃ were obtained, we approached the synthesis of NpCQ by two strategies, either by direct copolymerization or post-polymerization conjugation. To directly polymerize the noncleavable CQ monomer, MA-tCQ was synthesized by copper (I)-catalyzed azide-alkyne cycloaddition (CuAAC) reaction between PPMA and CQ-N₃. We used CuAAC reaction instead of the copper-free click chemistry for two main reasons. First, copper-free click chemistry needs to introduce a cyclooctyne into the structure, which may decrease the water solubility of the polymer. Second, we wanted to keep the impact on the structure as low as possible so that CuAAC generating triazole ring was applied. The ¹H NMR spectrum confirmed the formation of the monomer as evidenced from the presence of the proton signal at δ 7.65, which indicated the formation of the triazole ring. Moreover, the proton signals at δ 5.69 and 5.25 of the methylene protons, as well as the ratio of integration confirmed the successful cycloaddition. Furthermore, ¹³C NMR signals at 120.40 and 123.81 indicating the carbons in the triazole ring further supported the conclusion of the click product formation.

2.7 Synthesis of non-degradable CQ-containing polymers by free radical polymerization (FNpCQ)



Scheme 2.7. Synthesis of FNpCQ.

Polymers with different CQ content were obtained by changing the monomer ratio of MA-tCQ to HPMA in the reagents, which was similar to the preparation of pCQ. Typically, MA-tCQ (70 mg, 0.145 mmol), HPMA (103 mg, 0.72 mmol) and AIBN (2.85 mg, 0.017 mmol) were dissolved in methanol:1,4-dioxane (1:1, 100mg/mL) and purged by nitrogen for 30 min. After

stirred in a sealed ampule at 70 °C overnight, the polymer was precipitated out by adding the mixture to cold diethyl ether under vigorous stirring. The precipitates were collected and re-dissolved in methanol. The precipitation step was repeated twice and the polymers were dialyzed against water (MWCO: 3,500) for 2 days. The FNpCQ polymers were obtained by lyophilization. The content of CQ in FNpCQ was calculated by the integration ratio of protons on CQ (δ 8.37, 7.42, 6.92, 6.50) and HPMA (δ 4.72, 3.68) using pHPMA as reference:

$$\text{mol\% of CQ} = [(1.78+1.04+1.18+1)/5]/[(1.78+1.04+1.18+1)/5+(4.77+5.35)/2] \times 100\% = 16.5\%$$

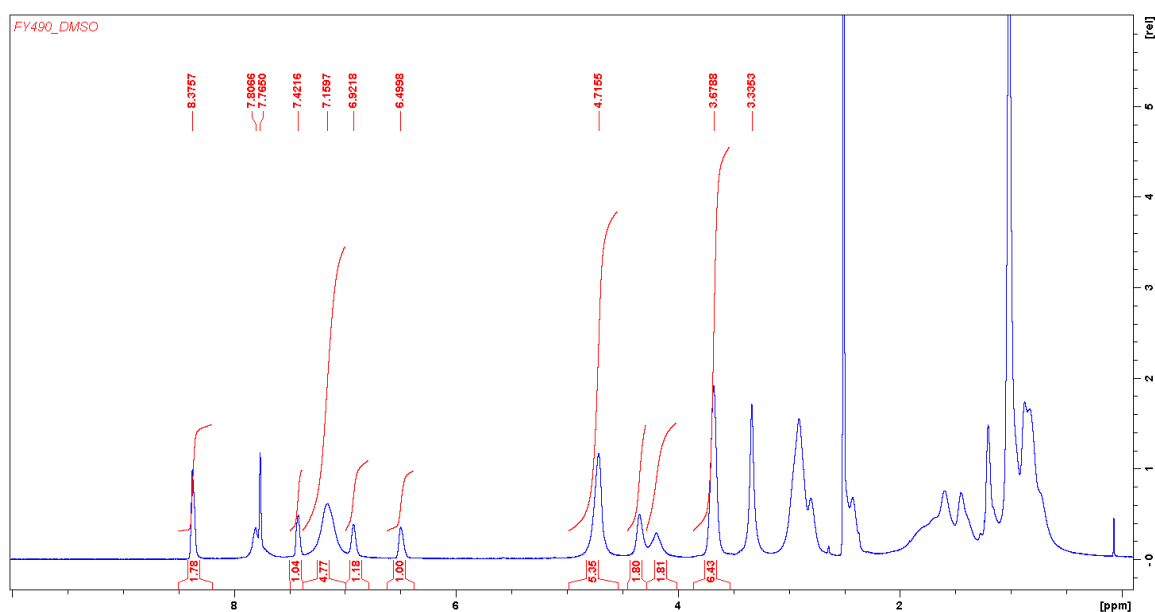
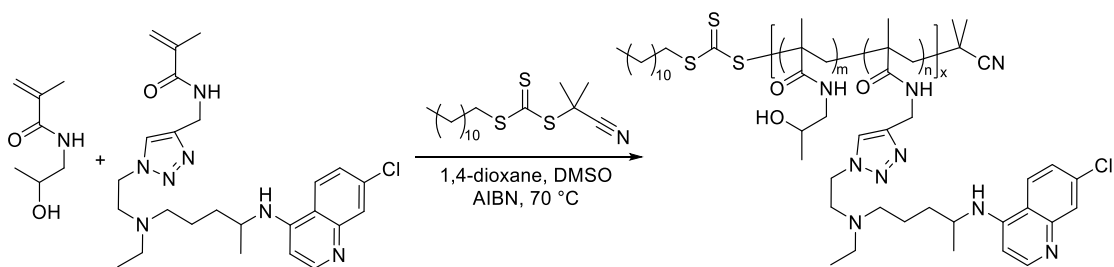


Figure 2.10. ^1H NMR of FNpCQ in DMSO- d_6 .

2.8 Synthesis of non-degradable CQ-containing polymers by RAFT polymerization of HPMA and MA-tCQ (RNpCQ)



Scheme 2.8. Synthesis of noncleavable RNpCQ by RAFT polymerization.

Procedure of Synthesizing RNpCQ was the same as RpCQ. MA-tCQ (70 mg, 0.15 mmol), HPMA (103 mg, 0.72 mmol), CPDT (3.0 mg, 3.03 μ L, 0.0087 mmol) and AIBN (0.36 mg, 0.0022 mmol) were dissolved in DMSO and 1,4-dioxane and followed the same protocol as RpCQ. The content of CQ in RNpCQ was calculated by the integration ratio of protons on CQ (δ 8.38, 7.44, 7.16, 6.52) and HPMA (δ 7.16, 4.71) using RpHPMA as reference:

$$\text{mol\% of CQ} = [(1.85+1.13+1.24+1)/5] / [(1.85+1.13+1.24+1)/5 + (5.28+5.94)/2] \times 100\% = 15.7\%.$$

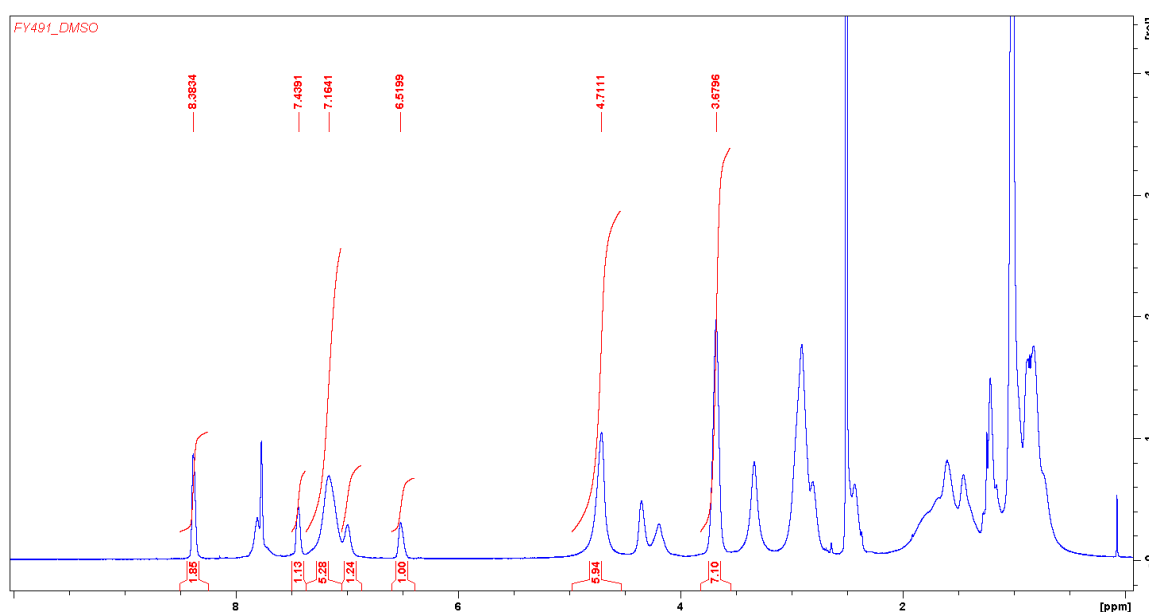


Figure 2.11. ^1H NMR of RNpCQ in DMSO- d_6 .

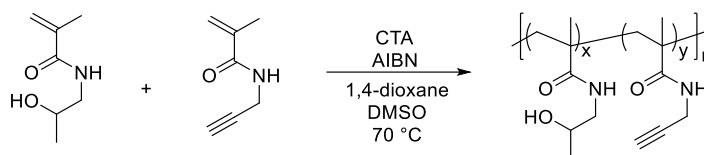
The properties of FNpCQ and RNpCQ were summarized in Table 2.3. RAFT polymerization obviously gave better control of polymers than free radical polymerization with the polydispersity value of 1.1 versus 1.4. Despite of that, NpCQ possessed closer CQ content of in feed and in copolymer than that of RNpCQ. The CQ content in both polymers can be adjusted by changing the ratio of HPMA and MA-tCQ in feed with the CQ content less than 25%.

Table 2.3. Characterization of F/RNpCQ polymers.

	CQ content (mol%)		M_n (kDa)	M_w/M_n	P_n
	In feed	In copolymer			
FNpCQ	16.7	16.6	22.9	1.4	115
RNpCQ	16.7	15.7	20.3	1.1	103

2.9 Synthesis of non-degradable CQ-containing polymers from clickable poly(HPMA-co-PPMA) (pHP) copolymers

2.9.1 Investigation of CTA for polymerization of pHP copolymers



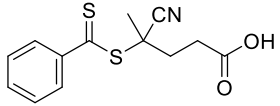
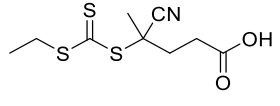
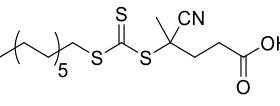
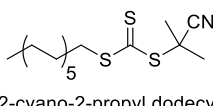
Scheme 2.9. Synthesis of pHP by RAFT polymerization.

RAFT polymerization was applied to synthesizing clickable pHP copolymers. Due to different monomer compatibility of RAFT agents, four CTAs were tested in the polymerization of pHP with PPMA content as 20% (mol%) [200]. One dithiobenzoate and three trithiocarbonates CTAs were chosen due to their reported compatibility to methacrylamides (Table 2.4). The molar ratio of HPMA/PPMA/CTA/initiator was fixed at 80/20/1/0.25. HPMA, PPMA, AIBN and the CTAs were dissolved in 1,4-dioxane/DMSO (1/1, v/v, 100 mg/mL) and transferred to prescored ampules. The ampules were flame sealed after purged with nitrogen for 30 min. The polymerization was conducted at 70 °C for 16 h and terminated in liquid nitrogen. The polymers were precipitated in cold diethyl ether for three times and dried under vacuum. The composition of each polymer was analyzed by ^1H NMR. The molecular weight of the polymers was tested by GPC as water soluble cationic polymers.

As shown in Table 2.4, 4-cyano-4-(phenyl-carbonothioylthio) pentanoic acid resulted in lowest yield and the product was not enough for characterization. Polymers prepared by CPDT

demonstrated highest yield, closest theoretical molecular weight (M_{th}) and M_w of the copolymer, as well as acceptable PDI and PPMA content. One thing needed to be noticed was that the yield, instead of conversion rate was shown here and some polymers were lost during precipitation. Based on these results, we used CPDT for further PPMA polymerization.

Table 2.4. Characterization of pHP polymer with different chain transfer agent.

CTA	$[HPMA]_0/[PPMA]_0/[CTA]_0/[I]_0$	M_{th} (kDa)	M_w (kDa)	PDI	PPMA in feed/ in polymer (mol%)	Yield (%)
 4-cyano-4-(phenyl-carbonothioylthio) pentanoic acid	80/20/1/0.25	13.9	-	-	20/-	11
 4-cyano-4-[(ethylsulfanylthiocarbonyl) sulfanyl]pentanoic acid	80/20/1/0.25	13.9	7.5	1.1	20/19.7	21
 4-cyano-4-[(dodecyl sulfanylthiocarbonyl) sulfanyl]pentanoic acid	80/20/1/0.25	13.9	9.3	1.2	20/20.0	37
 2-cyano-2-propyl dodecyl trithiocarbonate	80/20/1/0.25	13.9	13.6	1.2	20/19.7	44

2.9.2 Synthesis of pHP

The pHP copolymers were prepared using CPDT as CTA reagent and AIBN as initiator. The copolymers were synthesized with a range of molecular weights of 7-56 kDa and different PPMA contents of 0-40 (Table 2.5). The procedure was the same as shown in 2.9.1. Typical 1H NMR spectrum was shown in Figure 2.12. The properties of pHP were summarized in Table 2.5 and GPC spectrums were shown in Figure 2.13.

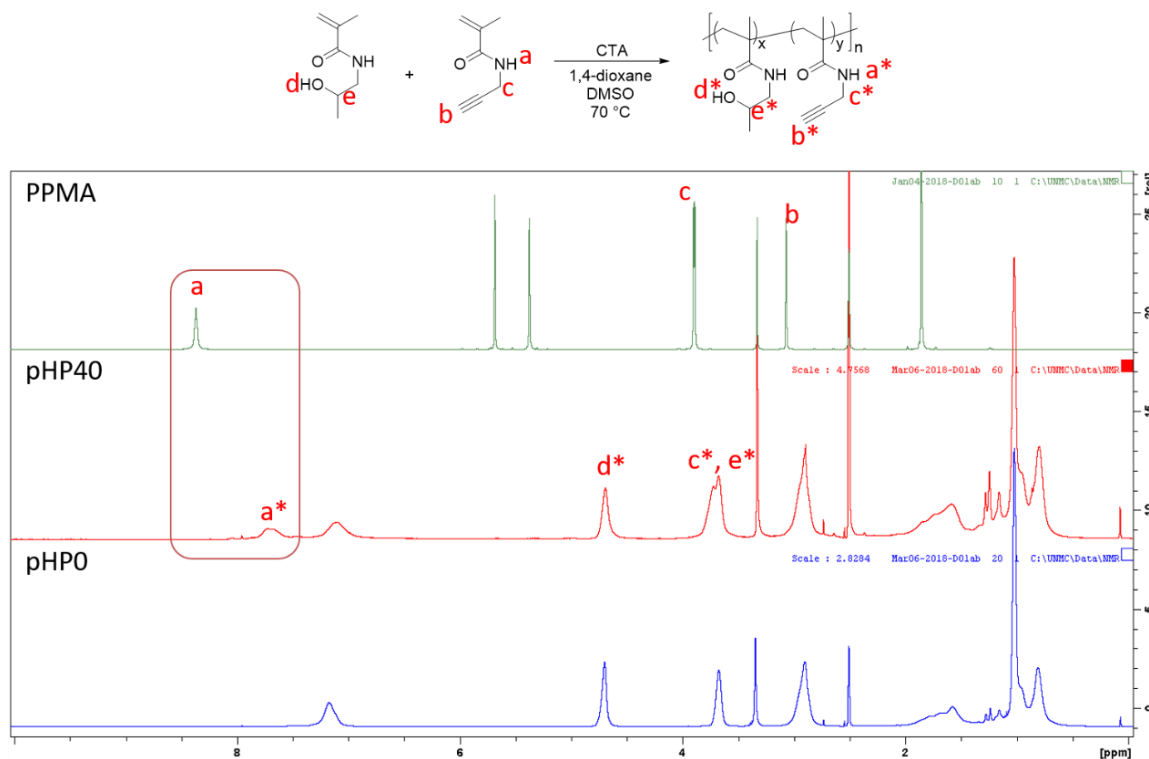


Figure 2.12. Typical ^1H NMR spectra of pHP polymers in $\text{DMSO-}d_6$.

The ^1H NMR spectra of PPMA, pHP40 and pHP0 were stacked in Figure 2.12 to quantify the alkyne content. Integration ratio of proton d^* from HPMA and proton a^* from PPMA were applied for calculation of alkyne content. From pHP0 to pHP40, the PDI was increasing, the difference of PPMA in feed and in copolymer was increasing, yet the yield was decreasing. These may due to the influence of PPMA on the activity of CTA. And the copolymers were well-controlled when the PPMA content was not more than 20%. By comparing pHP20L, pHP20, pHP20M, pHP20H, we found that the yield was decreasing, PDI, and the difference between M_{th} and M_w were increasing, which suggested that we were able to better control the copolymer within the molecular weight probably less than 20 kDa. The GPC spectra showed pHP20H and pHP20M with broader peaks and earlier retention time than the other peaks, which were corresponding to their higher molecular weight and larger PDI than the other polymers. The spectra of pHP0, pHP5 and pHP10 showed that the three polymers had similar size but

increasing PDI, which were in agreement with the data reported. The only problem was that the calculated molecular weight of pHP20L was smaller than that of pHP40, however, retention time of pHP20L was earlier than that of pHP40, which may be caused by the different interaction between the columns and polymers with different hydrophilicity.

Table 2.5. Synthesis and characterization of pHP.

Sample	[HPMA] ₀ /[PPMA] ₀ / [CTA] ₀ /[I] ₀	M_{th} (kDa)	M_w (kDa)	PDI	PPMA in feed/ in copolymer (mol%)	Yield (%)
pHP0	100/0/1/0.25	14.3	14.8	1.1	0/0	62
pHP5	95/5/1/0.25	14.2	16.7	1.2	5/4.3	60
pHP10	90/10/1/0.25	14.1	14.3	1.2	10/9.9	58
pHP20	80/20/1/0.25	13.9	13.6	1.2	20/19.7	44
pHP40	60/40/1/0.25	13.5	11.3	1.4	40/24.4	26
pHP20L	80/20/2/0.5	7.0	7.8	1.2	20/16.5	58
pHP20M	80/20/0.5/0.125	27.8	23.8	1.4	20/19.5	39
pHP20H	80/20/0.25/0.0625	55.6	38.1	1.4	20/20.6	33

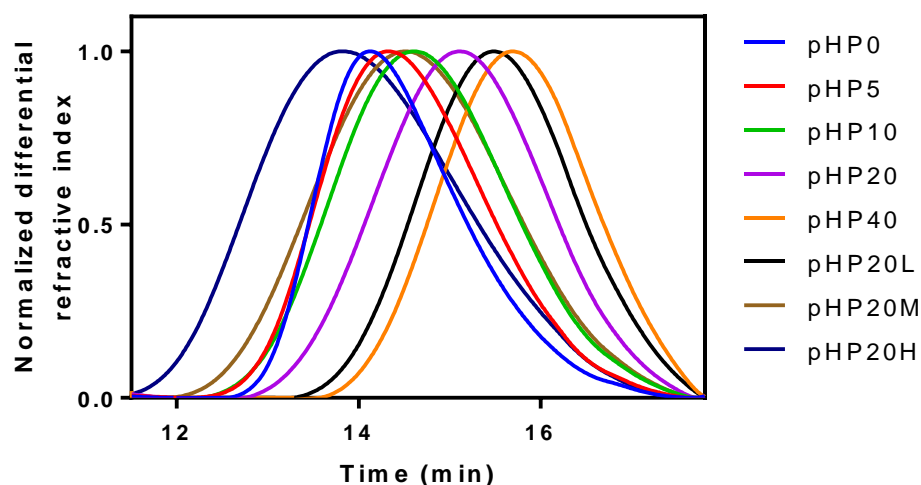
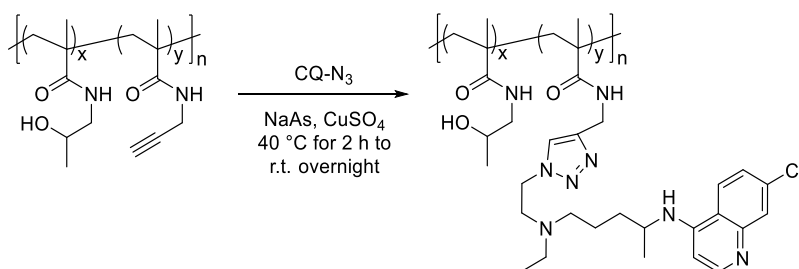


Figure 2.13. GPC spectrums of pHP polymers.

2.9.3 Synthesis of non-degradable CQ-containing HPMA copolymers (CNpCQ) by click reaction of CQ-N₃ and pHP



Scheme 2.10. Synthesis of CNpCQ.

Except for direct polymerization of MA-tCQ and HPMA, non-degradable pCQ was also able to be synthesized by click reaction of pHP and CQ-N₃ to obtain CNpCQ. To conduct click reaction, pHP, CQ-N₃ (1.1 equiv. of alkyne amount in pHP) and CuSO₄ (0.1 equiv. of CQ-N₃) were dissolved in water containing 10% DMF under nitrogen in Schlenk tube. The reaction mixture was purged by nitrogen for 30 min. NaAs (0.4 equiv. of CQ-N₃) was added before the tube was merged in 40 °C oil bath. The reaction mixture was stirred at 40 °C for 2 h and cooled down to room temperature (r.t.) overnight. The resulting product was washed by 50 mM EDTA aqueous solution

twice and water once to remove the copper ion, followed by dialysis against water (MWCO: 3,500) for 3 days. The final product was obtained by lyophilization. The molecular weight was obtained by GPC and CQ content was calculated by ^1H NMR as previously described.

The CQ content was mainly in accordance with the corresponding alkyne content as shown in Table 2.6 except for pHP5-CQ, which was possibly due to the limitation of the characterization. By comparing each pHP copolymers before and after click reaction in GPC, we were able to confirm that the molecular weight of each pHP-CQ was higher than that of corresponding pHP, which further verified the successful of click chemistry. The pHP-CQ copolymers exhibited broader peak than corresponding pHP, which may due to the difference in charge and hydrophilicity.

Table 2.6. Summary of CNpCQ.

Sample	M_w (kDa)	PPMA in polymer (mol%)	CQ content (mol%)
pHP0	14.8	0	-
pHP5-CQ	16.7	4.3	1
pHP10-CQ	14.3	9.9	9.0
pHP20-CQ	13.6	19.7	20.0
pHP40-CQ	11.3	24.4	26.8
pHP20L-CQ	7.8	16.5	16.5
pHP20M-CQ	23.8	19.5	21.7
pHP20H-CQ	38.1	20.6	23.6

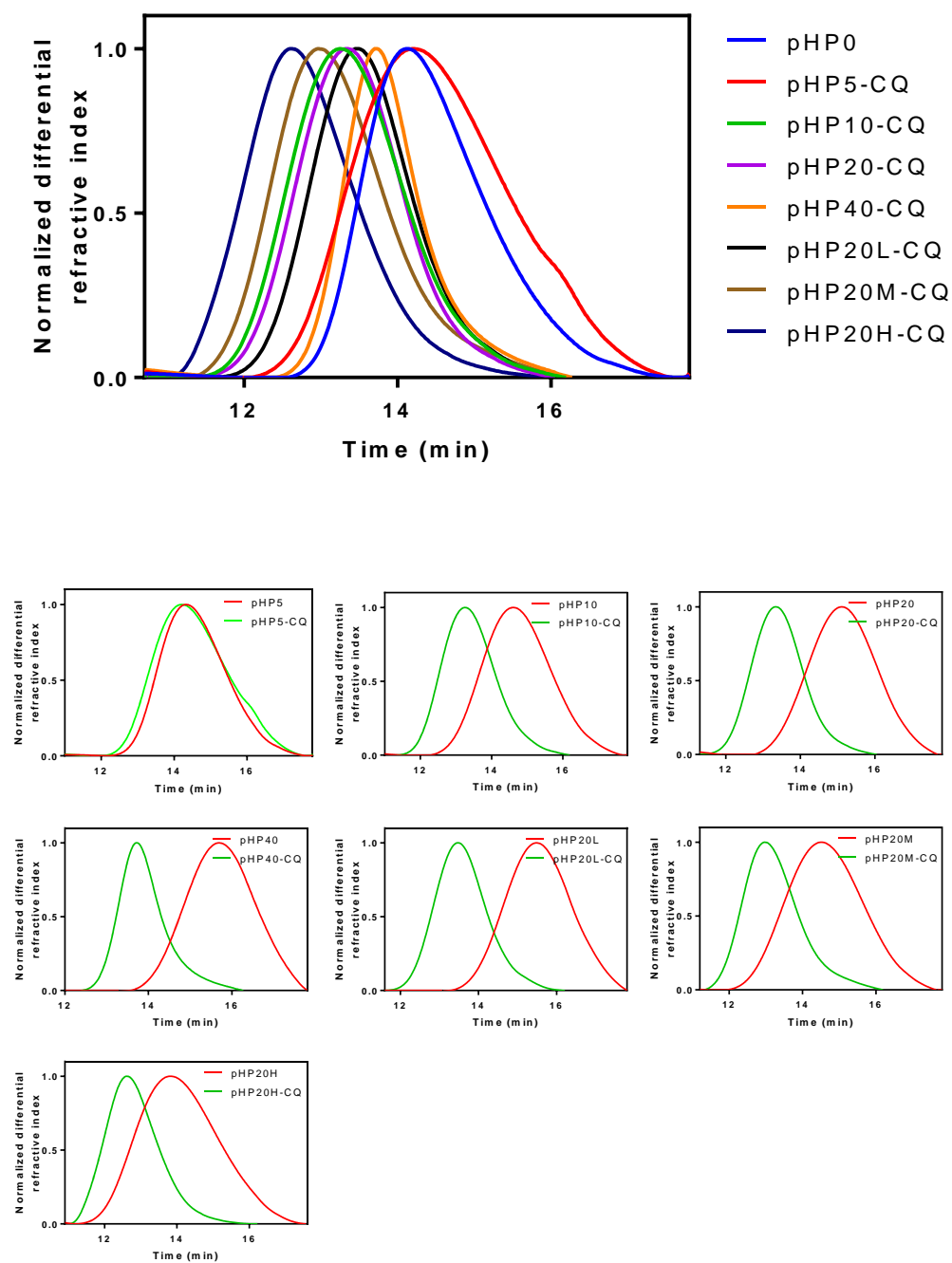
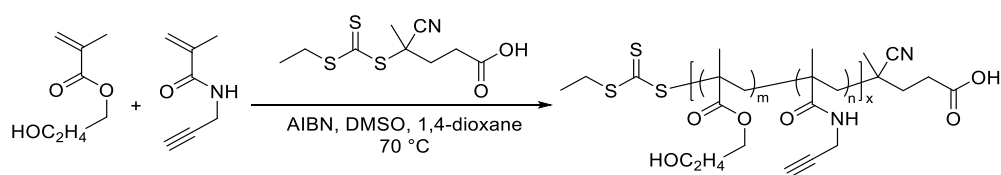


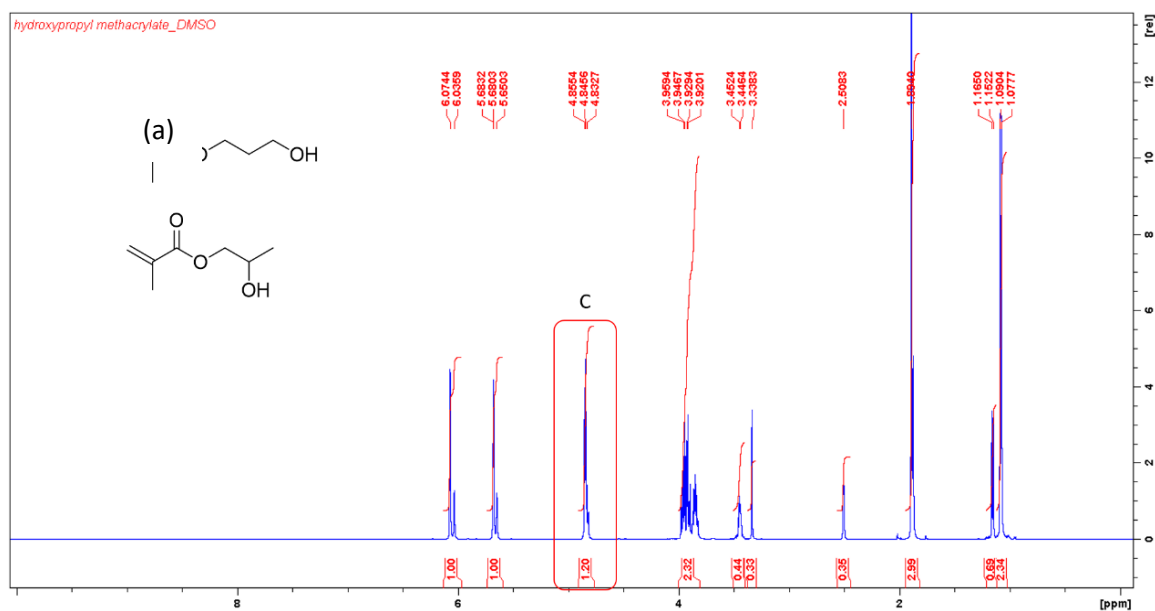
Figure 2.14. GPC spectrums of pHP-CQ polymers and comparison of pHP to the corresponding pHP-CQ.

2.9.4 Synthesis of poly(hydroxypropyl methacrylate-*co*-PPMA) (pHPte) copolymers by RAFT polymerization

To explore the application of clickable polymers, we studied the polymerization of PPMA and hydroxypropyl methacrylate (HPMAte) by RAFT polymerization with 4-cyano-4-[(ethylsulfanylthiocarbonyl)sulfanyl] pentanoic acid (CTPA) as CTA. The investigation was taken out followed the similar principle of pHP. Typical ^1H NMR spectrum was shown in Figure 2.15. The properties of pHPte were summarized in Table 2.7 and GPC spectrums were shown in Figure 2.16.



Scheme 2.11. Synthesis of pHPte by RAFT polymerization.



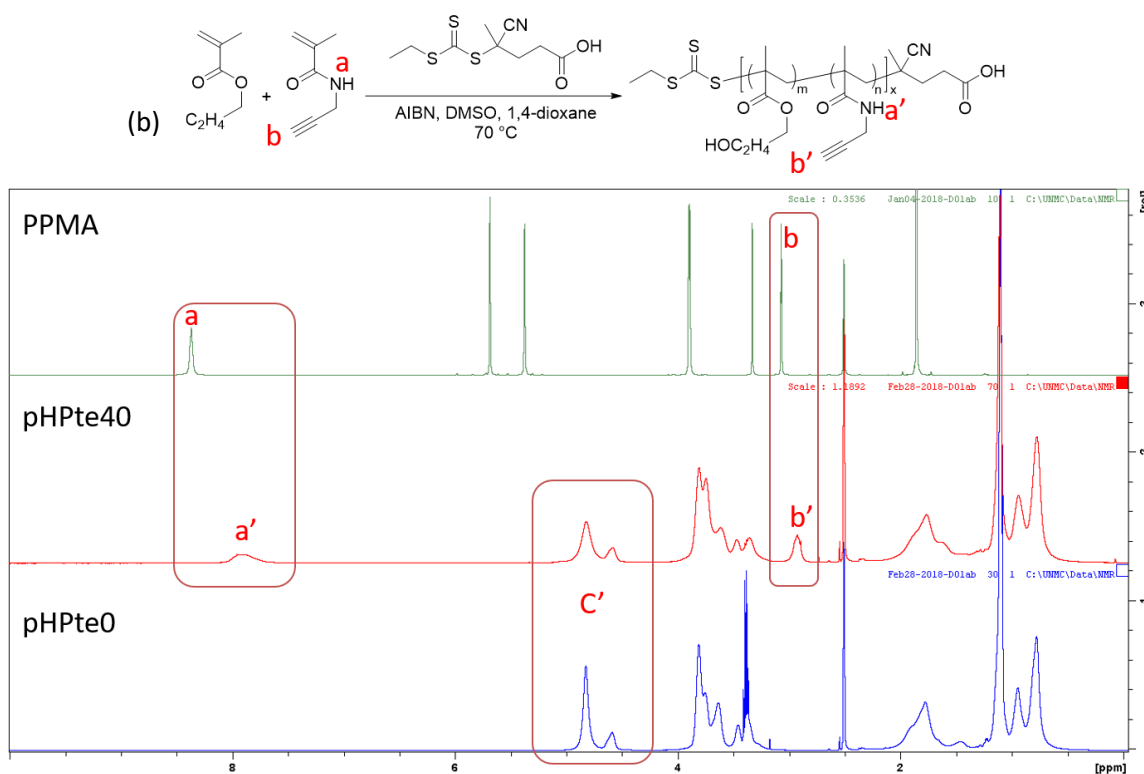


Figure 2.15. Typical ^1H NMR spectrums of pHPte polymers in $\text{DMSO-}d_6$.

Table 2.7. Synthesis and characterization of pHPte.

Sample	$[\text{HPMte}]_0/[\text{PPMA}]_0/$ $[\text{CTA}]_0/[\text{I}]_0$	M_{th} (kDa)	M_{w} (kDa)	PDI	PPMA in	
					feed/ in polymer (mol%)	Yield (%)
pHPte0	100/0/1/0.25	14.4	17.6	1.1	0/0	52
pHPte5	95/5/1/0.25	14.3	19.2	1.1	5.0/4.8	94
pHPte10	90/10/1/0.25	14.2	19.9	1.1	10.0/8.3	94
pHPte20	80/20/1/0.25	14.0	20.5	1.1	20.0/15.3	95
pHPte40	60/40/1/0.25	13.6	16.9	1.2	40.0/28.0	71

pHPte20L	80/20/2/0.5	7.2	9.0	1.1	20.0/16.7	89
pHPte20M	80/20/0.5/0.125	28.0	32.9	1.2	20.0/16.7	79
pHPte20H	80/20/0.25/0.0625	55.9	51.2	1.1	20.0/15.3	74

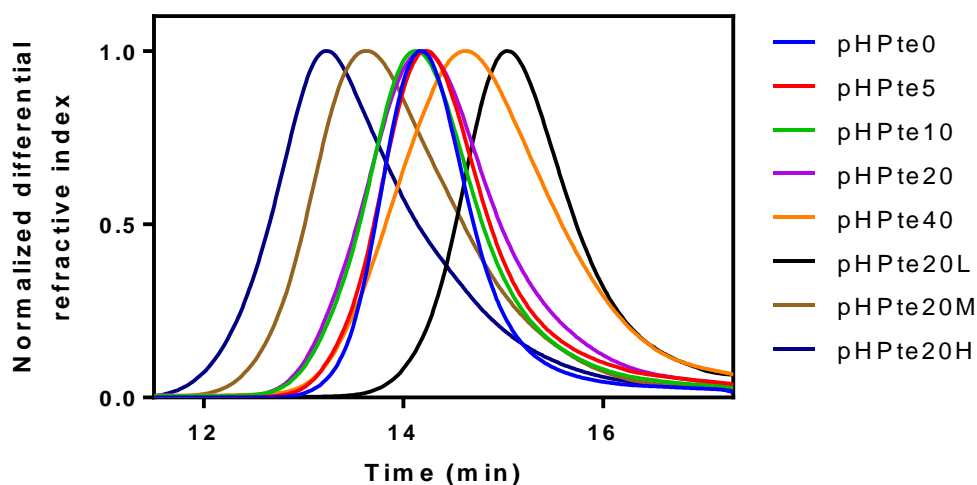
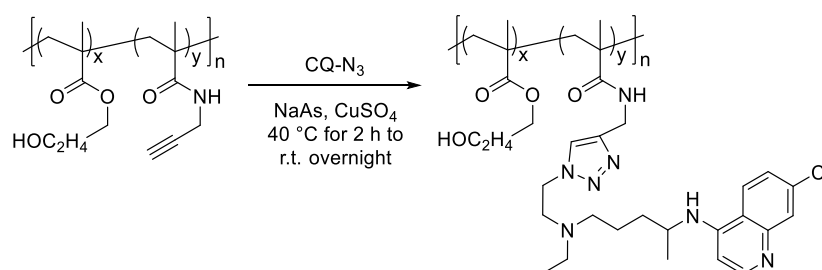


Figure 2.16. GPC spectrums of pHPte copolymers.

The ^1H NMR spectrums of PPMA, pHPte40 and pHPte0 were stacked in Figure 2.15 to quantify the alkyne content. Proton signals C' from 4.5 to 5.0 belonged to HPMate, and according to the ^1H NMR of HPMate, the integration ratio of these protons to each methylene proton was 1.2:1 because HPMate used here was mixture of two monomers. Therefore, the proton a' and b' from PPMA and proton signals C' from HPMate were applied for calculation of alkyne content. PDI of all the polymers were similar. And the copolymers were well-controlled when the PPMA content was not more than 20%. By comparing pHPte20L, pHPte20, pHPte20M, pHPte20H, we found that the yield trended decreasing. PDI, and the difference between M_{th} and M_w were controllable. The GPC spectrums showed pHPte20H and pHPte20M with broader peaks and earlier retention time than the other peaks, which were corresponding to their higher molecular weight than the other polymers. The spectrum of pHPte20L showed it had smallest molecular weight,

which was also in accordance with the results. The spectrums of pHPte5, pHPte10 and pHPte20 showed very close retention time and similar size, which were in agreement with the data reported.

2.9.5 Synthesis of non-degradable CQ-containing HPMAte copolymers (pHPte-CQ) by click reaction of CQ-N₃ and pHPte



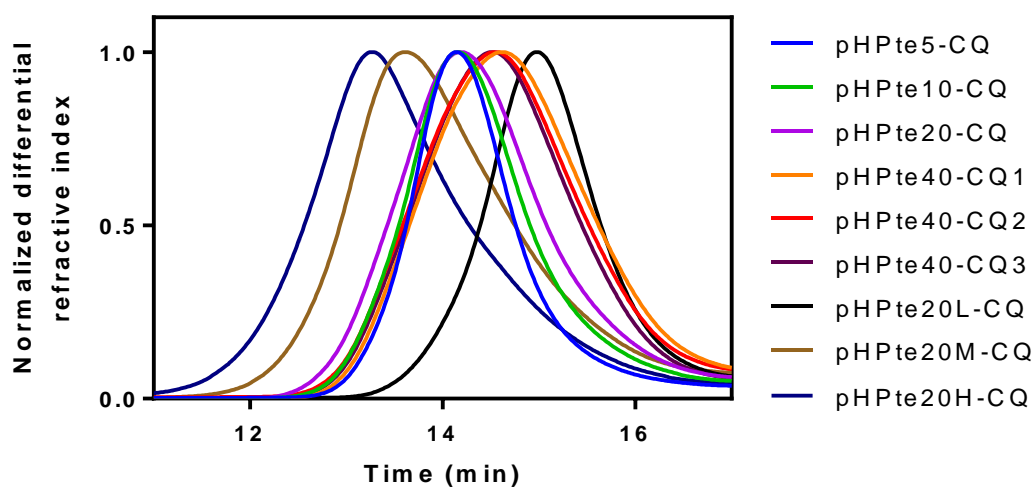
Scheme 2.12. Synthesis of pHPte-CQ by click chemistry.

Click reaction of pHPte and CQ-N₃ was also investigated similar to CNpCQ. The pHPte polymer, CQ-N₃ (1.2 equiv. of alkyne amount in pHPte) and CuSO₄ (0.1 equiv. of CQ-N₃) were dissolved in DMF under nitrogen in Schlenk tube. The reaction mixture was purged by nitrogen for 30 min. NaAs (0.4 equiv. of CQ-N₃) dissolved in water was added before the tube was merged in 40 °C oil bath. The reaction was taken out at 40 °C for 2 h and cooled down to room temperature (r.t.) overnight. The resulting product was dialyzed against DMF containing 50 mM EDTA aqueous solution (20%) for 1 day and against DMF for 2 days (MWCO: 3,500). The final product was obtained by precipitated in cold diethyl ether for twice. The molecular weight was obtained by GPC and CQ content was calculated by ¹H NMR as previously described.

In addition, pHPte40-CQ1, pHPte40-CQ2 and pHPte40-CQ3 were pHPte40 polymers click with CQ-N₃ as 1.2, 0.5, 0.25 equiv. of alkyne to study the reactivity of click chemistry of CQ-N₃ and alkyne polymer.

Table 2.8. Summary of pHPte-CQ.

Sample	M_w (kDa)	PPMA in polymer (mol%)	CQ content (mol%)
pHPte0	17.6	0	-
pHPte5-CQ	19.2	4.8	3.2
pHPte10-CQ	19.9	8.3	6.7
pHPte20-CQ	20.5	15.3	11.6
pHPte40-CQ1	16.9	28.0	29.4
pHPte40-CQ2	16.9	28.0	20.1
pHPte40-CQ3	16.9	28.0	11.7
pHPte20L-CQ	9.0	16.7	14.8
pHPte20M-CQ	32.9	16.7	14.8
pHPte20H-CQ	51.2	15.3	11.8



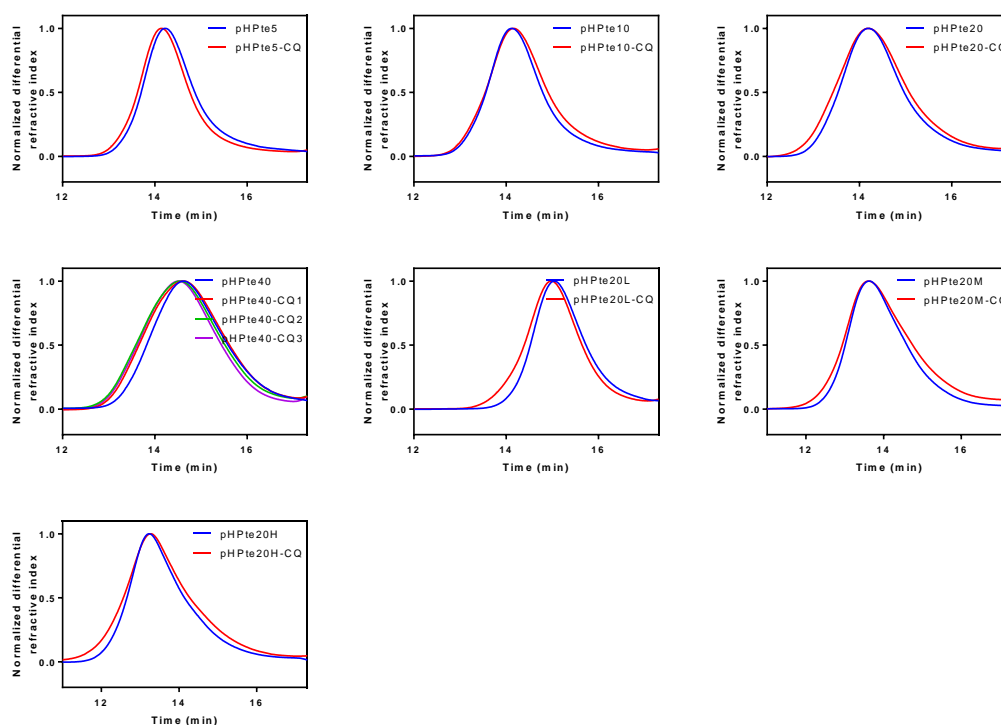


Figure 2.17. GPC spectra of pHPte-CQ polymers and comparison of pHPte to the corresponding pHPte-CQ.

The CQ content was mainly in accordance with the corresponding alkyne content as shown in Table 2.8. However, the clicked CQ content was less than alkyne content. Polymers pHPte40-CQ1, pHPte40-CQ2 and pHPte40-CQ3 were pHPte40 reacted with different ratio of CQ-N₃. The final CQ content were proportional to the quantity of CQ-N₃ reagent, which proved that the CQ content can be controlled. We were unable to compare each pHPte copolymers before and after click reaction in GPC spectrums in this case, which may due to the GPC column efficiency.

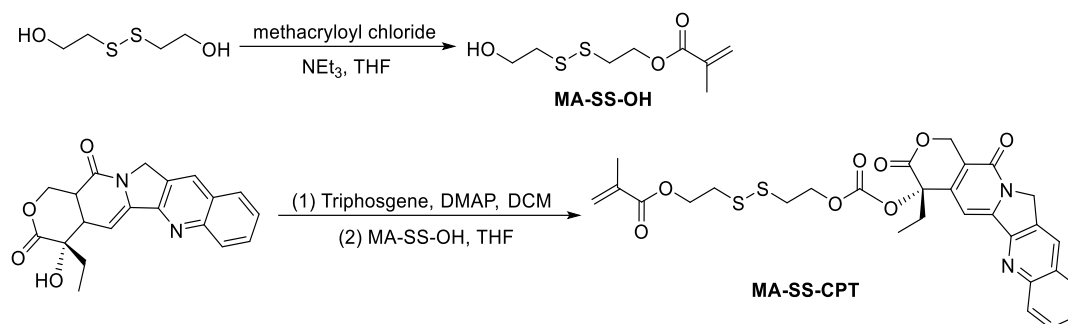
2.10 Synthesis of CQ- and CPT-containing HPMA copolymers

The CQ- and CPT-containing HPMA copolymer (pCQCPT) was created to achieve co-delivery of pCQ and CPT to inhibit cancer metastasis and progression. CPT was linked to the

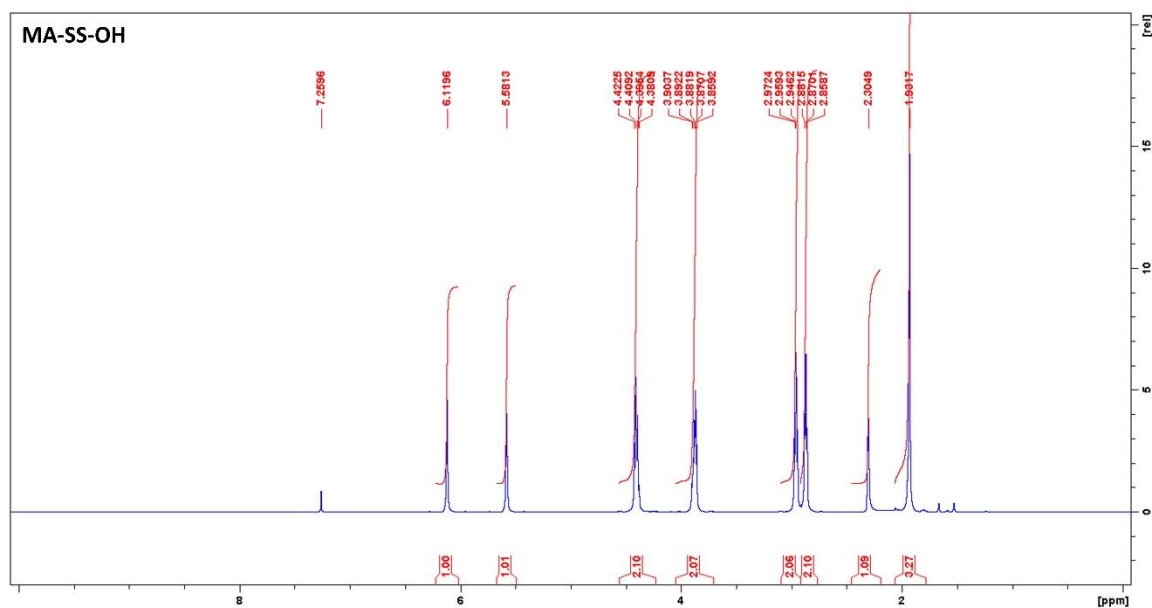
backbone of the polymer via reduction-responsive disulfide bond that was able to be cleaved in cytoplasm.

MA-SS-CPT was synthesized according to the protocol reported by Liu et al [201]. Briefly, dithiodiethanol was selectively methacrylated on one hydroxyl group, followed by the connection of CPT by carbonate bond (Scheme 2.13). To synthesize the mono-methacrylated dithiodiethanol (MA-SS-OH), 2,2'-dithiodiethanol (3.08 g, 20 mmol) and triethylamine (3.04 g, 4.19 mL, 30 mmol) were dissolved in THF (100 mL) and cooled down to 0 °C in ice-water bath, to which methacryloyl chloride (2.09 g, 1.95 mL, 20 mmol) in THF (50 mL) was added dropwise under vigorous stirring. The reaction mixture was warmed up to room temperature and stirred overnight. After filtration and evaporation of all the solvents, the resulting product was dissolved in ethyl acetate (50 mL) and washed by water (20 mL \times 2) and brine (20 mL \times 1). The organic layer was dried over MgSO₄ and concentrated. The final product was obtained by column chromatograph using ethyl acetate/hexane (1/2, v/v) as eluent. The ¹H NMR of MA-SS-OH (Figure 2.18) confirmed the structure. ¹H NMR (500 MHz, CDCl₃) δ 6.12 (s, 1H), 5.58 (s, 1H), 4.40 (q, J = 7.1 Hz, 2H), 3.88 (dt, J = 11.6, 5.8 Hz, 2H), 2.96 (t, J = 6.7 Hz, 2H), 2.87 (t, J = 5.8 Hz, 2H), 2.30 (d, J = 3.7 Hz, 1H), 1.93 (s, 3H). The reduction-responsive CPT monomer (MA-SS-CPT) was prepared by esterification of CPT and MA-SS-OH. Typically, CPT (0.1 g, 0.287 mmol) and DMAP (0.106 g, 0.865 mmol) was dissolved in anhydrous DCM (2.5 mL) under argon. Triphosgene (28.3 mg, 0.096 mmol) was added and stirred for 30 min at room temperature. MA-SS-OH (70 mg, 0.316 mmol) in anhydrous THF (0.75 mL) was added dropwise to CPT and stirred overnight in dark. The reaction suspension was filtered and concentrated by rotavap, which was then dissolved in ethyl acetate (5 mL) and washed by HCl (1 M, 2.5 mL \times 2), water (2.5 mL \times 1) and brine (2.5 mL \times 1). The organic layer was dried over MgSO₄ and concentrated. The final product was obtained by column chromatograph using ethyl acetate as eluent. ¹H NMR (500 MHz, Chloroform-d) δ 8.40 (s, 1H), 8.23 (d, J = 8.5 Hz, 1H), 7.94 (dd, J = 8.2, 1.5 Hz, 1H), 7.84 (ddd, J = 8.4, 6.8, 1.5 Hz, 1H),

7.71 – 7.64 (m, 1H), 7.35 (s, 1H), 6.07 (t, $J = 1.3$ Hz, 1H), 5.69 (d, $J = 17.2$ Hz, 1H), 5.54 (t, $J = 1.6$ Hz, 1H), 5.39 (d, $J = 17.1$ Hz, 1H), 5.32 – 5.27 (m, 2H), 4.40 – 4.30 (m, 4H), 2.93 (q, $J = 7.1$, 6.5 Hz, 4H), 2.28 (dq, $J = 14.8$, 7.4 Hz, 1H), 2.15 (dq, $J = 14.7$, 7.5 Hz, 1H), 1.90 (t, $J = 1.3$ Hz, 3H), 1.00 (t, $J = 7.5$ Hz, 3H).



Scheme 2.13. Synthesis of MA-SS-CPT.



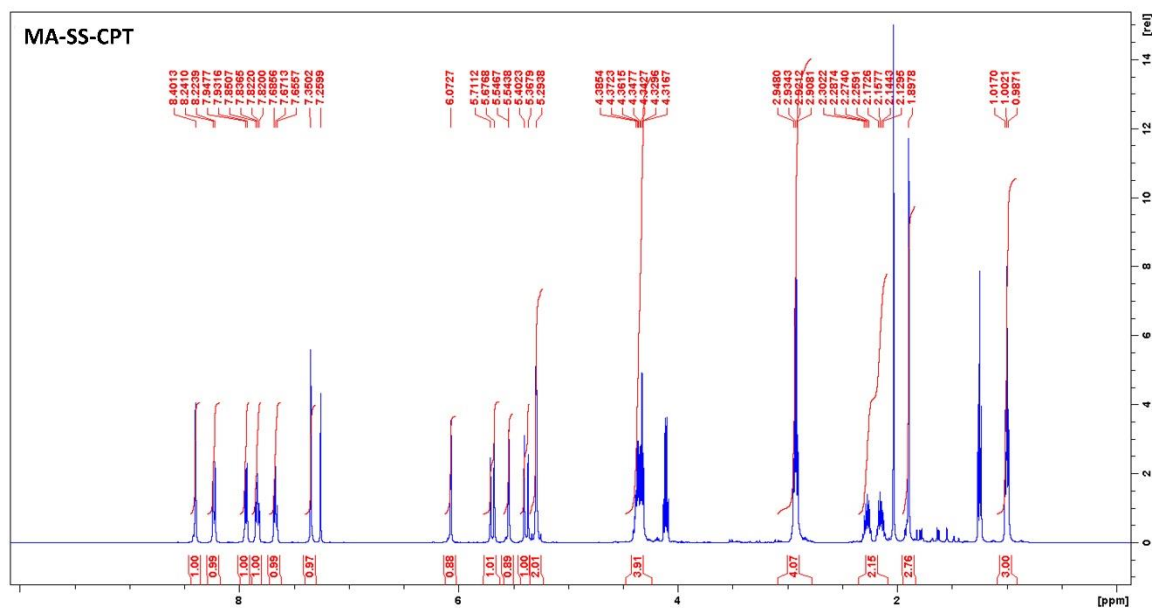
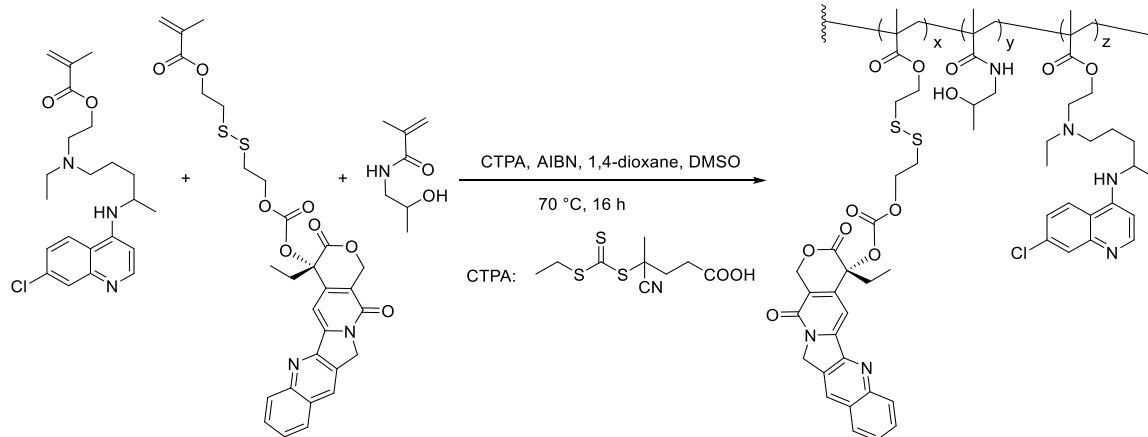


Figure 2.18. ^1H NMR of MA-SS-OH and MA-SS-CPT in CDCl_3 .

CQ- and CPT-containing polymers were synthesized by RAFT polymerization using CTPA as CTA. Typically, HPMA (175 mg, 1.22 mmol), MA-CQ (49 mg, 0.122 mmol), MA-SS-CPT (36.4 mg, 0.061 mmol), CTPA (3.7 mg, 0.01403 mmol) and AIBN (0.58 mg, 0.0035 mmol) were dissolved in DMSO/1,4-dioxane (1/1, 100 mg/mL) under argon in a brown ampule. After purged by argon for 30 min, the ampule was flamed sealed and reaction mixture was stirred at 70 °C for 16 h in the dark. After terminated in liquid nitrogen, the resulting product was precipitated in cold diethyl ether and dialyzed against water for 2 days in the dark. The final product was obtained by lyophilization as pQCQPT. The content of CQ and CPT in the polymer was calculated by ^1H NMR (Figure 2.19). Polymers with only CQ (pCQ_C) or CPT (pCPT) were prepared as control groups followed the same protocol. The characterization of pQCQPT, pCPT and pCQ_C polymers was summarized in Table 2.9.



Scheme 2.14. Synthesis of pCQCPT.

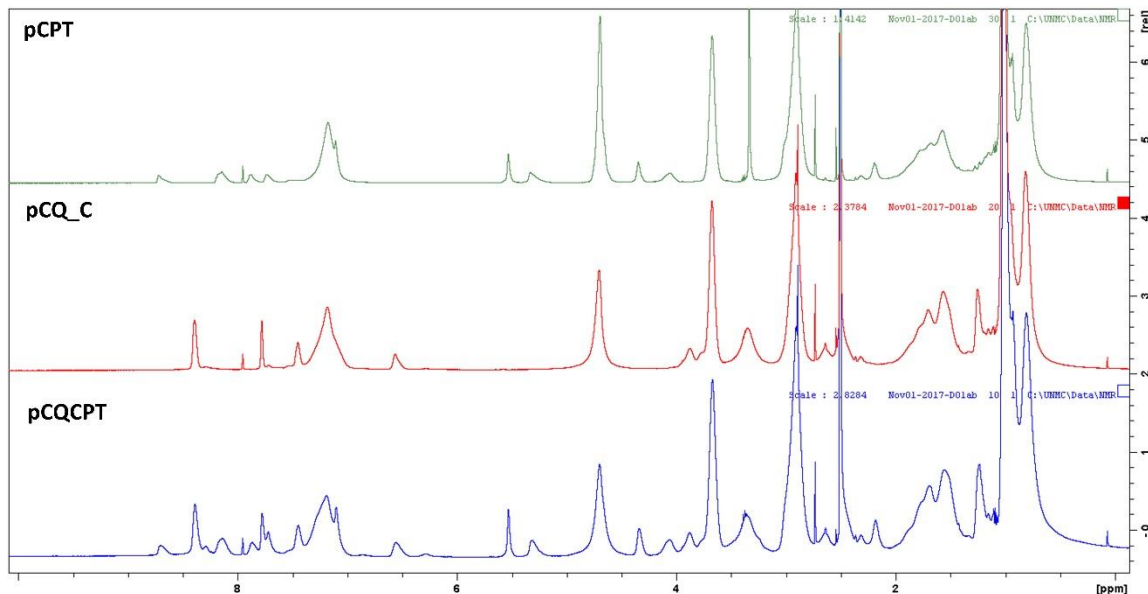


Figure 2.19. ^1H NMR of pCQCPT, pCPT, pCQ_C in $\text{DMSO-}d_6$.

Table 2.9. Summary of pCQCPT, pCPT and pCQ_C.

Sample	M_w (kDa)	PDI	CPT in polymer (w/w%)	CQ in polymer (w/w%)
pCQCPT	20.4	1.02	9.6	18.6

pCPT	23.1	1.20	10.0	-
pCQ_C	15.4	1.05	-	19.7

We synthesized polymers containing CQ and CPT, CQ alone and CPT alone with similar CQ or CPT content for further comparison of their anti-cancer activities. The content of CQ and CPT was obtained from ^1H NMR. Signals representing CPT at 8.15, 7.88, 7.73, 5.54, 5.34, HPMA at 7.18, 4.70 were used to calculate the CPT content. Signals representing CQ at 8.40, 7.78, 6.56, HPMA at 7.19, 4.71 were used for CQ content quantification. Polymers with CPT content higher than 10% and CQ content higher than 20% were obtained but the water solubility was compromised due to the interaction between CPT and CPT, as well as CPT and CQ. We attempted to prepare the diblock pCQ-*b*-pCPT copolymers by RAFT polymerization, however, the reactivity of the macro-pCQ or macro-pCPT was diminished so that we prepared the randomly-arranged pCQCPT.

2.11 Synthesis of diblock PLA-pCQ copolymers

Besides chemical conjugation, anticancer drug can also be encapsulated in the pCQ-containing diblock polymer to achieve co-delivery of cytotoxic drug and pCQ. To obtain diblock amphiphilic copolymers, we synthesized PLA-CTA by ring-opening polymerization with hydroxyl group functionalized chain transfer agent, 4-(dodecyl trithiocarbonyl)-4-cyano-1-pentanol, which was obtained by bis(dodecylsulfanyl thiocarbonyl) disulfide and 4,4'-azobis(4-cyano-1-pentanol) (Scheme 2.15).

Synthesis of 4-(dodecyl trithiocarbonyl)-4-cyano-1-pentanol was reported before [202]. Briefly, bis(dodecylsulfanylthiocarbonyl) (292 mg, 0.53 mmol) and 4,4'-azobis(4-cyano-1-pentanol) (200 mg, 0.79 mmol) were dissolved in ethyl acetate (10 mL) and heated under reflux for 24 h. The resulting product was concentrated under reduced pressure and purified by column chromatography using ethyl acetate/hexane (4/6) as eluent. ^1H NMR indicated the structure of the product as shown in Figure 2.20. ^1H NMR (500 MHz, CDCl_3) δ 3.71 (td, $J = 6.1, 2.4$ Hz, 2H), 3.32

(t, $J = 7.5$ Hz, 2H), 2.31 – 2.22 (m, 1H), 2.14 – 2.02 (m, 1H), 1.88 – 1.79 (m, 5H), 1.68 (p, $J = 7.2$ Hz, 3H), 1.39 (p, $J = 7.0$ Hz, 2H), 1.32 – 1.25 (m, 5H), 1.25 (s, 11H), 0.87 (t, $J = 6.8$ Hz, 3H).

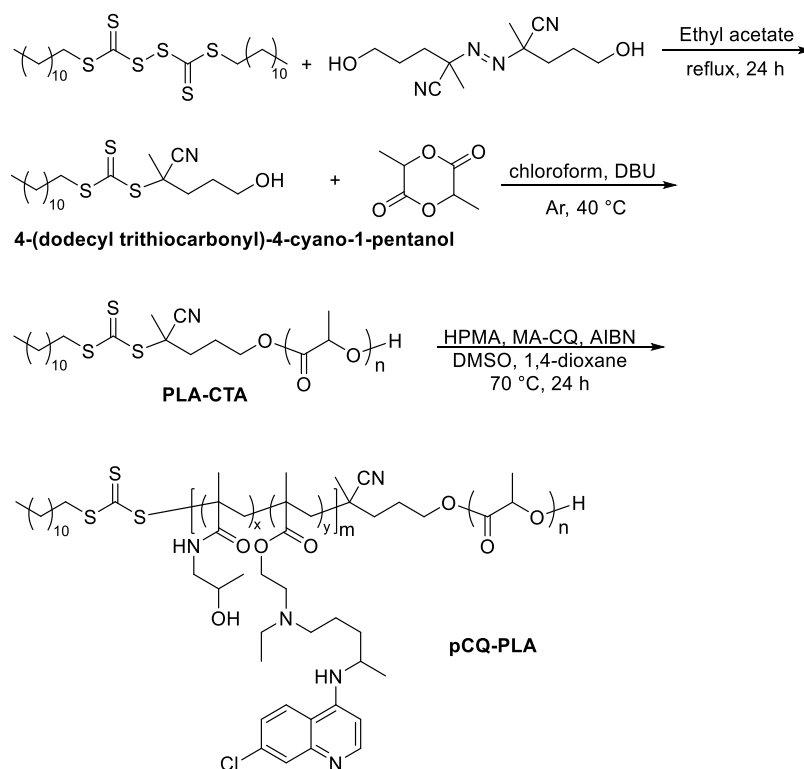
Preparation of PLA-CTA followed the same protocol reported by Du et al [203]. Briefly, L-lactide (2.018 g, 14 mmol), 4-(dodecyl trithiocarbonyl)-4-cyano-1-pentanol (77.94 mg, 0.2 mmol) were charged into a Schlenk tube containing anhydrous chloroform (10 mL) under argon. After merged in 40 °C oil bath with all the solid dissolved, DBU (60.9 mg, 60 μ L, 0.4 mmol) was added. After stirring for 20 min, the reaction was terminated by adding benzoic acid (24.4 mg, 0.2 mmol). The product was precipitated in cold methanol for 3 times. The degree of polymerization of PLA-CTA was calculated by the ratio of integration of proton next to the methyl group on PLA (δ 5.16) to the dodecyl protons on CTA (δ 1.26).

Diblock PLA-pCQ was synthesized by RAFT polymerization similarly as discussed above. A given amount of HPMA, MA-CQ, PLA-CTA and AIBN were dissolved in DMSO/1,4-dioxane (6/4, 100 mg/mL) and sealed in ampules under argon. After stirring at 70 °C for 16 h, the reaction was terminated by merged in liquid nitrogen. The product was obtained by precipitation in cold diethyl ether for 3 times and dried under vacuum. The content of HPMA, CQ, PLA, and the molecular weight was able to be calculated from ^1H NMR according to the integration of protons as discussed before. By changing the ratio of monomers, we got 6 polymers summarized in Table 2.10. The ^1H NMR spectrum of PLA-pCQ10H was shown in Figure 2.20. GPC of all the PLA-pCQ was shown in Figure 2.21.

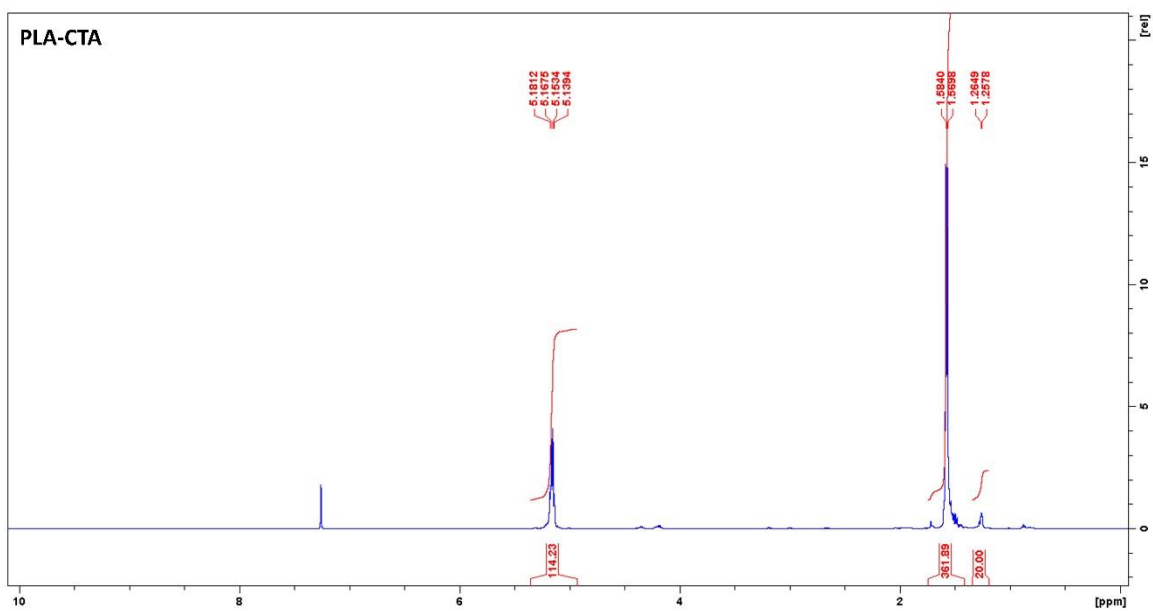
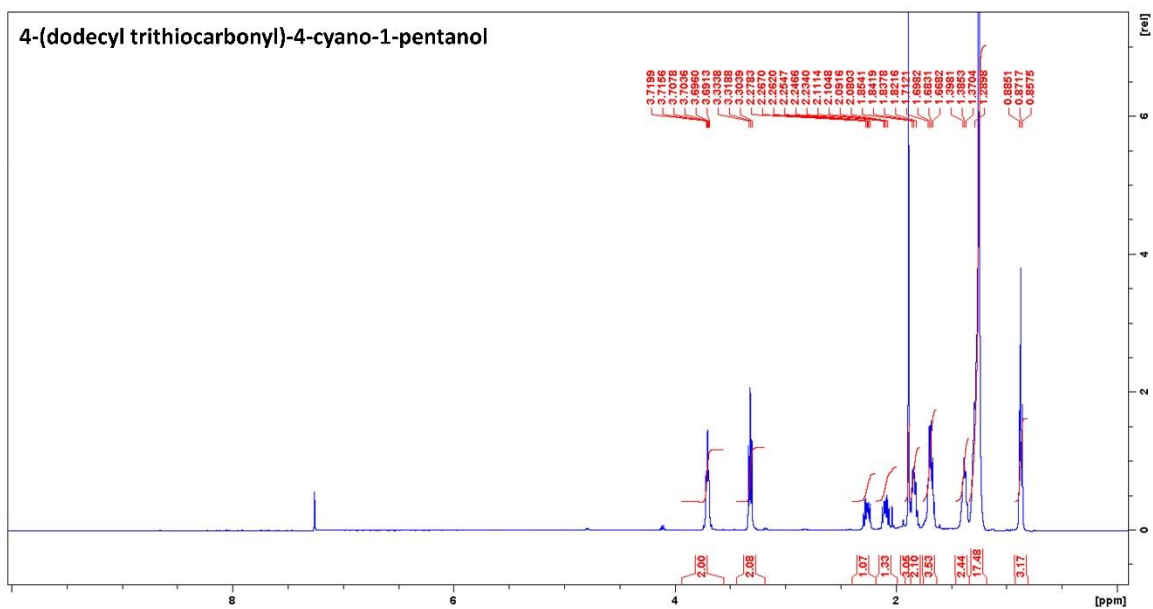
Table 2.10. Summary of PLA-pCQ.

Sample	DP in feed			DP in polymer			M_w (kDa)
	LA	HPMA	CQ	LA	HPMA	CQ	
PLA-pCQ0L	114	50	0	114	41	0	14.1

PLA-pCQ0H	114	100	0	114	86	0	20.5
PLA-pCQ5L	114	50	2.5	114	43	2.4	15.3
PLA-pCQ5H	114	100	5	114	88	4.4	22.6
PLA-pCQ10L	114	50	5	114	34	5.5	15.3
PLA-pCQ10H	114	100	10	114	111	9.3	27.8



Scheme 2.15. Synthesis of 4-(dodecyl trithiocarbonyl)-4-cyano-1-pentanol, PLA-CTA and PLA-pCQ.



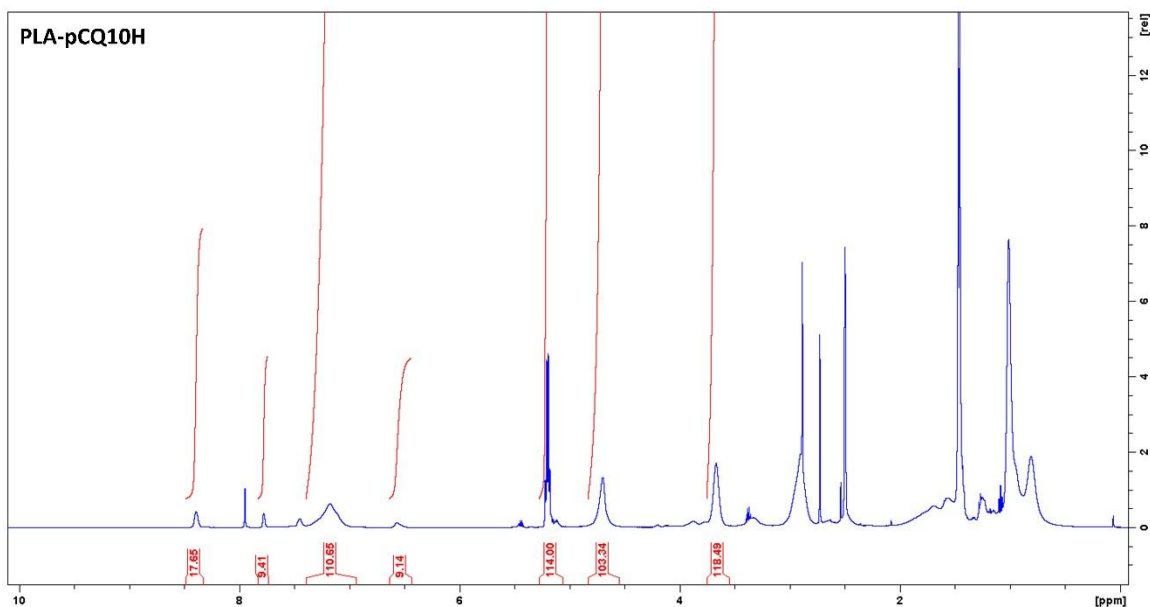


Figure 2.20. ^1H NMR of 4-(dodecyl trithiocarbonyl)-4-cyano-1-pentanol in CDCl_3 , PLA-CTA in CDCl_3 and PLA-pCQ10H in $\text{DMSO}-d_6$.

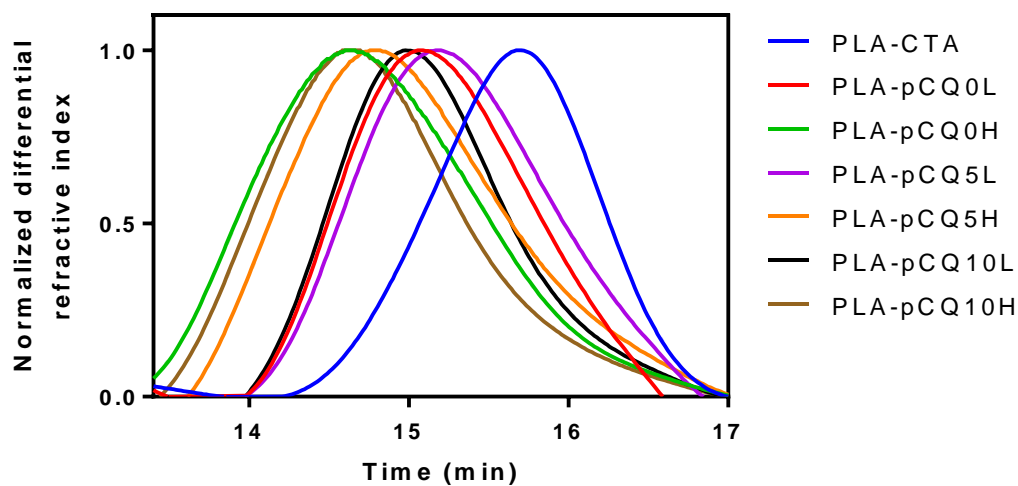


Figure 2.21. GPC spectrums of pCQ-PLA polymers.

The macro PLA-CTA was prepared by ring-opening polymerization and the molecular weight was decided by ^1H NMR. Signals at 1.26 indicated 20 protons on the RAFT agents. Signals at 5.16 and 1.57 with the integration ratio of 1:3 indicated PLA. By setting the integration number

as 20 at 1.26, we were able to quantify the DP as 114. We fixed the molecular weight of PLA at 8.2 kDa and changed the hydrophilic pCQ block by molecular weight and CQ content. Six polymers with CQ content from 0, 5 and 10% and molecular weight of 15 kDa (L) and 20 kDa (H) were prepared by RAFT polymerization utilizing macro PLA-CTA. ^1H NMR of PLA-pCQ10H showed the proton signals of CQ (8.39, 7.78, 7.18), HPMA (4.70) and PLA (5.18), and the integration was applied to calculation of CQ content as described before. The GPC results clearly showed that PLA-CTA had smallest molecular weight among the 7 polymers. PLA-pCQ0H, PLA-pCQ5H and PLA-pCQ10H possessed similar molecular weights. PLA-pCQ0L, PLA-pCQ5L and PLA-pCQ10L exhibited similar molecular weights that were in between of 20 kDa and 8.2 kDa, which were corresponding to the molecular weight calculated from ^1H NMR. We successfully synthesized diblock PLA-pCQ copolymers with controlled CQ content.

3 Effect of polymeric CQ on cancer metastasis

CQ is a classic antimalarial drug that has been in clinical use for decades. CQ was developed from natural product quinine six decades ago and is still widely used for the control of malaria worldwide. Besides its antimalarial properties, a broad spectrum of pharmacological activities, including anti-inflammatory and anticancer activities have been discovered and explored over the years [98]. CQ and HCQ have been recognized as effective autophagy inhibitors that exhibit beneficial anticancer properties [102]. Autophagy controls cellular homeostasis by lysosomal degradation of cytoplasmic components, including invading pathogens, cytotoxic proteins and damaged organelles. In cancer, autophagy provides a survival mechanism to allow cancer cells to support proliferation during metabolic stress [193]. Inhibition of autophagy by CQ can reverse the process and suppress the proliferation of cancer cells. Although CQ and HCQ were initially tested in cancer treatment due to their ability to inhibit autophagy, preclinical studies show that CQ and HCQ have multiple complementary mechanisms of action, including inhibition of autophagy, inhibition of oncogenic signaling pathways such as TLR9/NF- κ B and CXCL12/CXCR4, normalization of tumor vessels, and modulation of tumor micro-environment [111, 117, 198, 204, 205]. Taken together, CQ is a promising multi-functional agent that is well-suited for development of novel combination anticancer strategies.

In this chapter, we report the properties of polymeric CQ (pCQ) as a macromolecular inhibitor of cancer metastasis. We present data evaluating pCQ as inhibitor of cancer cell migration and invasion *in vitro* and its antimetastatic activity *in vivo* in experimental lung metastasis model of breast cancer. Inspired by the unexpected enhanced inhibitory activity of cancer cell migration and experimental lung metastasis of pCQ, we designed and synthesized pCQ polymers containing anticancer drug CPT for combinational treatment of breast cancer. The animal experiment demonstrated the anticancer and anti-metastasis activities of the polymers.

However, it was ester bond between CQ and backbone of copolymers, which made them susceptible to degradation *in vivo*. Therefore, we synthesized non-degradable pCQ (NpCQ) by RAFT polymerization and click chemistry, and compared its pharmacologic activity with the degradable pCQ.

Materials used in this chapter are shown as follows. Phosphate-buffered saline (PBS), Dulbecco's Modified Eagle Medium (DMEM), sodium pyruvate, 1% Pen-Strep, G418, essential amino acids and non-essential amino acids were from Hyclone (Logan, UT). Fetal bovine serum (FBS) was from Atlanta Biologicals (Flowery Branch, GA). Gentamicin was purchased from Gibco (Life Technologies, Grand Island, NY). Eagle's Minimum Essential Medium (EMEM) was obtained from ATCC (Manassas, VA). Nitrocellulose membrane, Novex 10% Tris-Glycine Midi Protein Gels and 12% Tris-Glycine Midi Protein Gels were purchased from Invitrogen (Carlsbad, CA). Gentamicin, enzyme-free cell dissociation buffer and F-12K medium were purchased from Gibco (Life Technologies, Grand Island, NY). Protease and phosphatase inhibitor cocktail, Pierce bicinchoninic acid (BCA) protein assay, RIPA buffer and Pierce ECL Western Blotting Substrate were purchased from ThermoScientific (Waltham, MA). LC3B antibody, phospho-p44/42 MAPK (pERK) rabbit antibody, p44/42 MAPK (ERK) rabbit antibody, GAPDH rabbit antibody and anti-rabbit IgG, and HRP-linked antibody were purchased from Cell Signaling Technology (Beverly, MA). Allophycocyanin (APC) mouse B anti-human CD184 and APC mouse IgG2a, κ isotype control were purchased from BD Biosciences (San Jose, CA). Human and mouse CXCL12 were purchased from Shenandoah Biotechnology (Warwick, PA). Laemmli sample buffer and 2-mercaptoethanol were purchased from Bio-rad (Hercules, CA).

Results are presented as mean \pm standard deviation (SD). The Student's t-test was used to determine the statistical significance of the results obtained in all the studies of this proposal when assessing differences between two groups; ANOVA was used to determine differences among

multiple groups. All statistical analysis was performed using Graphpad Prism v5. A value of $p < 0.05$ was considered statistically significant.

3.1 Inhibition of cancer cell migration and experimental lung metastasis by polymeric chloroquine pCQ

To investigate the properties of polymeric CQ on cancer metastasis, we synthesized pCQ with different CQ content pCQ10.0 and pCQ16.7 from MA-CQ and HPMA by free radical polymerization as reported in Section 2.2 and Table 2.1. Effect of pCQ on cancer cell migration and invasion *in vitro* and metastasis *in vivo* in experimental lung metastasis model of breast cancer was evaluated. Moreover, preliminary mechanism of action of pCQ was also elucidate.

3.1.1 Cell culture

Human epithelial osteosarcoma U2OS cells stably expressing functional EGFP-CXCR4 fusion protein were purchased from Fisher Scientific and cultured in DMEM supplemented with 2mM L-glutamine, 1% Pen-Strep, 0.5 mg/mL G418 and 10% FBS. Mouse breast carcinoma 4T1 was a kind gift from Dr. Fred Miller (Wayne State University) and cultured in DMEM supplemented with 2 mM L-glutamine, 1 mM sodium pyruvate, essential amino acids, non-essential amino acids, gentamycin (0.2 mg/mL) and 10% FBS. Human hepatocellular carcinoma HepG2 cell line was purchased from ATCC (Manassas, VA) and cultured in EMEM with 10% FBS. A549 cells were from Dr. Hillman (Wayne State University) and cultured in F12-K medium with 10% FBS and 1% Pen-Strep. All cells were maintained in an incubator at 37 °C and 5% CO₂.

3.1.2 Cytotoxicity of the polymers

Cytotoxicity was determined using CellTiter-Blue Cell Viability Assay (Promega, Madison, WI) in U2OS, 4T1 and HepG2 cells according to the manufacturer's protocol. Cells were seeded in 96-well plates 24 h prior to treatment at a density of 6000 cells/well for U2OS, 3000

cells/well for 4T1, and 4000 cells/well for HepG2. The medium was then replaced by 100 μ L of serial dilutions of HCQ, pHPMA and pCQ in complete cell culture medium and the cells were incubated for 24 h. To measure cell viability, polymer/drug-containing medium was replaced with a mixture of 100 μ L culture medium and 20 μ L of CellTiter-Blue reagent and the cells were incubated for another 1 h. The fluorescence intensity [I] was measured using SpectraMaxM5e Multi-Mode microplate Reader (Molecular Devices, CA) at 560_{Ex}/590_{Em}. The relative cell viability (%) was calculated as $[I]_{\text{treated}} / [I]_{\text{untreated}} \times 100\%$.

Before evaluating therapeutic activity of pCQ, we first examined its cytotoxicity in three different cell lines using CellTiter-Blue Assay. In addition to the breast cancer cell line 4T1 and osteosarcoma cell line U2OS, we also included human hepatocellular carcinoma cell line HepG2, which is a well-established and frequently used *in vitro* toxicity model for drug screening. As shown in Figure 3.1, HCQ exhibited cytotoxicity in all three cell lines, with IC₅₀ of 22, 28 and 42 μ g/mL in 4T1, U2OS and HepG2 cells, respectively. The corresponding IC₅₀ values expressed as molar concentrations were 70, 88 and 130 μ M, respectively. In contrast to HCQ, both pCQ showed remarkably lowered cytotoxicity. pCQ16.7 had an estimated IC₅₀ >2000 μ g/mL in all three cell lines and the estimated IC₅₀ for pCQ10.0 was >3000 μ g/mL. pHPMA exhibited no toxicity in any of the cell lines within the tested concentration range. Considering the content of HPMA in pCQ, we also compared the cytotoxicity in terms of equivalent CQ concentrations. Both pCQ polymers demonstrated no toxicity at equivalent CQ concentration of 100 μ M and IC₅₀ was >1500 μ M CQ equivalent in all three cell lines. Based on the cytotoxicity findings, we selected 20 μ M HCQ as a safe dose for subsequent biological studies. Concentrations up to 100 μ M CQ equivalent were considered as safe for the pCQ polymers. HPMA copolymers are known to be nontoxic and non-immunogenic and have been widely applied as drug carriers for both small molecule drugs and biomacromolecules [206, 207]. Here we have shown that incorporation of CQ into HPMA copolymers greatly improves its safety in multiple cell lines.

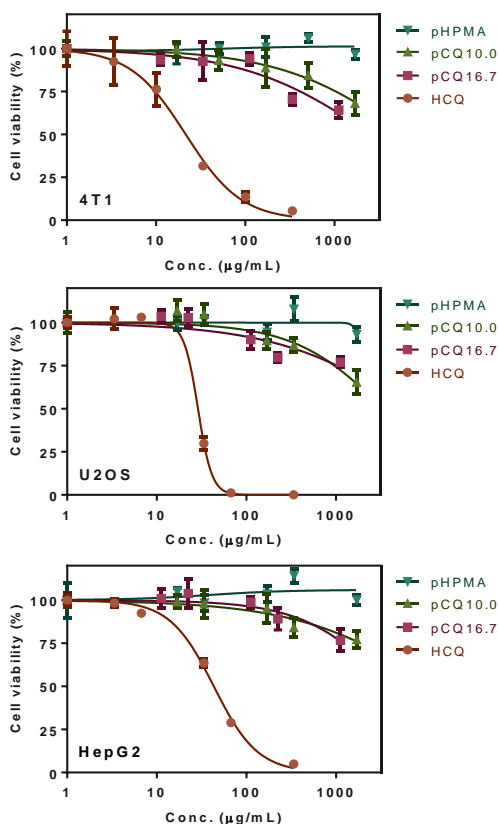


Figure 3.1. Cytotoxicity of pCQ. Cell viability of pCQ, HCQ and pHPMA was determined using CellTiter-Blue Assay. Results are shown as mean cell viability \pm SD (n=3).

3.1.3 Inhibition of autophagy by polymers (This experiment was completed by Richard Lee Sleightholm, MD PhD student in Dr. Oupicky's lab.)

Western blot was used to test the effect of pCQ on autophagy in U2OS and 4T1 cells. Cells were treated with HCQ, pCQ10.0 or pCQ16.7 for 24 h, and then washed with cold PBS, and lysed in ice-cold lysis buffer containing protease and phosphatase inhibitors for 30min. The lysate was centrifuged at 15,000 rpm for 10 min at 4 °C to collect the supernatant. Total protein was extracted with Laemmli lysis buffer according to the suggested protocol and the protein concentration was quantified by the BCA assay. The samples were normalized to the same concentration, loaded and separated on SDS/PAGE gel, transferred to nitrocellulose membranes followed by probing with

LC3B antibody and incubation with anti-rabbit IgG HRP-linked antibody. GAPDH was used as a housekeeping control. Quantification of LC3B levels was performed by ImageJ. The results are shown as mean of duplicate experiment (n=2).

With the goal of assessing possible differences in the mechanism of action between pCQ and CQ, we first evaluated the effect of pCQ on autophagy in U2OS and 4T1 cells. Autophagy is a cell survival mechanism that utilizes degradation and recycling of cellular proteins and cytoplasmic organelles. Damaged proteins or dysfunctional organelles are sequestered into autophagosomes, which then fuse with lysosomes to form autolysosomes where the contents are degraded and recycled. Autophagy is often upregulated in cancers because cancer cells use this mechanism to survive stress and starvation in the tumor microenvironment. Upregulation of autophagy promotes tumorigenesis and tumor aggressiveness [208, 209]. CQ is among several autophagy inhibitors that have been tested in combination with other anticancer drugs [102, 104, 190]. Although the mechanism of action is still not fully understood, CQ is believed to inhibit autophagy in cancer cells by preventing the fusion of autophagosomes and lysosomes. To investigate the effect of pCQ on autophagy, we performed Western blot to quantify the levels of autophagy marker LC3 (microtubule-associated protein 1A/1B-light chain 3). The cytosolic form of LC3 (LC3-I) is converted into LC3-II, which is bound to the autophagosomal membrane, indicating autophagic activity [210]. Monitoring degradation of LC3-II serves as a convenient measure of autophagic activity [32]. The LC3-II degradation was blocked when cells are treated with CQ, which inhibited lysosomal acidification and lead to the accumulation of LC3-II in the cells (Figure 3.2A). Our results show that HCQ treatment resulted in substantial inhibitory activity indicated by the elevated levels of LC3-II in both cell lines. In contrast, pCQ showed only a modest autophagy inhibition in 4T1 cells and no inhibitory activity was observed in U2OS cells. The relative expression of LC3-II and total LC3 expression (i.e., LC3-I + LC3-II) were quantified from the Western blots (Figure 3.2B). HCQ treatment significantly increased LC3-II expression in both

cell lines, with a 4-fold increase observed in 4T1 cells. In contrast, only 1.7- and 1.9-fold increase in LC3-II expression was observed in 4T1 cells treated with pCQ10.0 and pCQ16.7, respectively. Because of the very low LC3-II expression in untreated cells, we have quantified total LC3 levels in the U2OS cells. HCQ treatment resulted in a 5-fold increase in the total LC3 expression, with majority of the increase attributed to the LC3-II. A small non-significant increase (~1.1-fold) in LC3 expression was seen in pCQ-treated U2OS cells. These results clearly suggest that incorporation of HCQ into a polymer resulted in a significant loss of the underlying autophagy inhibitory activity.

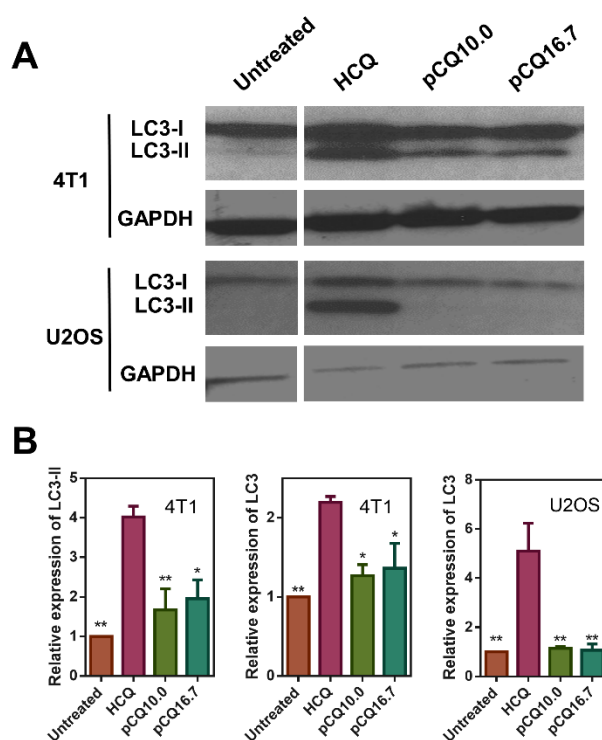


Figure 3.2. Effect of pCQ on autophagy in U2OS and 4T1 cells. Cells were treated with HCQ (20 μ M), pCQ10.0, and pCQ16.7 (100 μ M) for 24 h before Western blot analysis (A). The band intensities from two independent experiments were quantified by ImageJ (B). (* p <0.05, ** p <0.01 vs. HCQ; ANOVA with Tukey's multiple comparison test.)

3.1.4 pCQ effect on cell surface expression of CXCR4

U2OS cells were seeded in T25 culturing flask 18 h prior to treatment. Cells were treated with different concentrations of HCQ, pHPMA and pCQ in HEPES-buffered low-serum medium (DMEM supplemented with 2 mM L-glutamine, 1% penicillin-streptomycin, 1% FBS and 10 mM HEPES) for 90 min and 24 h before flowcytometry analysis. After washing with PBS, cells were dissociated by enzyme-free cell dissociation buffer and stained with allophycocyanin (APC) Mouse B Anti-Human CD184 and APC Mouse IgG2a, κ Isotype Control according to the suggested protocol. FACSCalibur was used to analyze the cells (10,000 events per sample), and data were processed using FlowJo software V7.6.1.

CQ was suggested as a CXCR4 antagonist in various types of cancers only recently [175, 199]. Traditional CXCR4 antagonists like AMD3100 exert their function by specifically binding with the CXCR4 receptors located on the cell surface, thus preventing binding of the chemokine ligand CXCL12. This inhibition of CXCL12 binding then prevents CXCR4 receptor internalization and suppresses activation of the related downstream signaling cascades. CQ and HCQ on the other hand, appear to promote internalization of the surface CXCR4 receptors and their sequestration in the lysosomes, which then makes the receptors inaccessible for binding with extracellular CXCL12 chemokine molecules [175, 211].

To investigate the effect of pCQ on CXCR4 inhibition, we used flow cytometry to quantify the changes in the surface expression of the CXCR4 receptor in U2OS cells after treatment with pCQ. The cells were treated with AMD3100, pCQ, HCQ, and pHPMA for 1.5 h and 24 h prior to incubation with anti-CXCR4 antibody. As shown in Figure 3.3, treatment with the CXCR4-binding compound AMD3100 resulted in a significant decrease in the amount of detectable CXCR4 receptors on the cell surface. In contrast, HCQ (20 μ M) did not cause any significant change in the levels of surface CXCR4 receptors. After 1.5 h of incubation, cells treated with pCQ10.0 exhibited no decrease in the levels of CXCR4 surface expression, while pCQ16.7 resulted in a significant

decrease even at this early time point. The reduction in surface CXCR4 receptor expression with both pCQ10.0 and pCQ16.7 became more pronounced after 24 h. In addition, higher concentrations of pCQ (100 μ M HCQ equivalent) also resulted in a more pronounced decrease in the cell surface CXCR4 levels. As expected, pHPMA did not show any effect on the surface CXCR4 expression. All these data suggest that pCQ is considerably more effective in reducing cell surface CXCR4 than HCQ and that its effect is dependent on the concentration, HCQ content, and time of incubation.

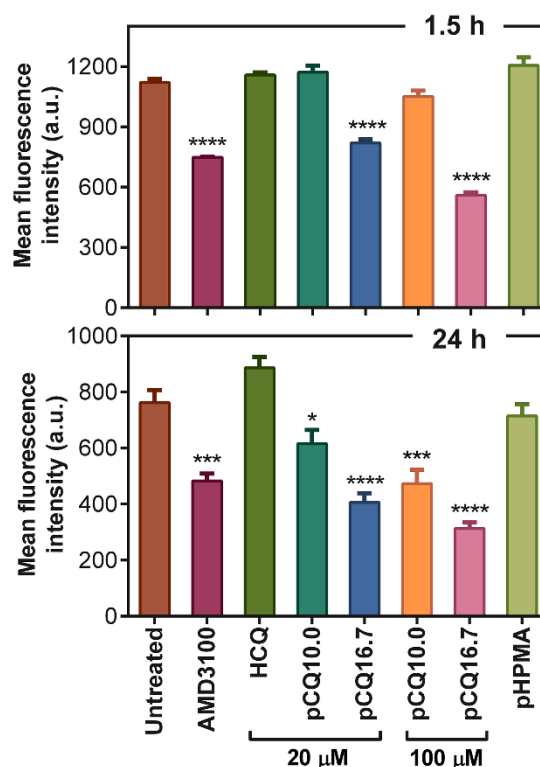


Figure 3.3. Effect of pCQ on expression of surface CXCR4 receptors in U2OS cells. Cells were treated in the absence of CXCL12 with AMD3100, HCQ, pCQ or pHPMA for 1.5 h or 24 h before flow cytometry analysis. (* $p < 0.05$, *** $p < 0.001$, **** $p < 0.0001$ vs. untreated; ANOVA with Tukey's multiple comparison test, $n=2$.)

3.1.5 pCQ effect on CXCR4 redistribution

Further analysis of how pCQ affects the decrease of cell surface CXCR4 expression upon stimulation with CXCL12 was conducted using CXCR4 redistribution assay (Figure 3.4A). U2OS cells stably expressing EGFP-CXCR4 were seeded at a density of 50,000 cells per confocal chamber (Lab-Tek Chambered #1.0 Borosilicate Coverglass 4 chamber System) 18 h prior to treatment. Cells were washed twice with 0.5 mL PBS and incubated with HEPES-buffered low serum medium with AMD3100 (300 nM) or pCQ16.7 (100 μ M) for 30 min before 1 h exposure to CXCL12 (10 nM). Then cells were washed five times using PBS and fixed with 4% paraformaldehyde at room temperature for 20 min. Fixed cells were then washed four times with PBS and stained with 1 μ M Hoechst 33258 solution for 30min before imaging. The images were obtained using Zeiss 800 Airyscan Microscope coupled with 63 \times oil objective and z-axis motor.

U2OS cells expressing EGFP-CXCR4 allow easy tracking of the CXCR4 intracellular distribution. Incubation of the cells with the CXCR4 ligand CXCL12 causes redistribution of the receptor from plasma membrane into intracellular vesicles. This process is prevented by AMD3100 as it binds CXCR4 expressed on the cell surface. The fact that AMD3100 restricts localization of the CXCR4 receptor to the cell surface suggests that the apparent decrease in cell surface expression of CXCR4 determined by flow cytometry in Figure 3.3 is simply a result of AMD3100 preventing binding of the staining anti-CXCR4 antibody to the receptor. In contrast, pCQ promoted CXCR4 internalization into intracellular vesicles, which made the receptor inaccessible for binding with extracellular CXCL12. These results suggest that pCQ may inhibit CXCR4/CXCL12-mediated processes using a different mechanism of action than traditional CXCR4 antagonists like AMD3100. To further support this hypothesis, we also determined the cell surface expression of CXCR4 in the presence of CXCL12 (Figure 3.4B). Upon stimulation with CXCL12, a decrease of surface CXCR4 expression was observed, confirming the data in Figure 3.4A. Cells treated with CXCL12 and the antagonist AMD3100 showed enhanced CXCR4 surface expression when compared with CXCL12-treated cells and the levels were similar to those observed in Figure 3.3.

In contrast, treatment with CXCL12 and pCQ16.7 resulted in further reduction in surface CXCR4 expression, confirming enhanced intracellular localization of the CXCR4 receptors.

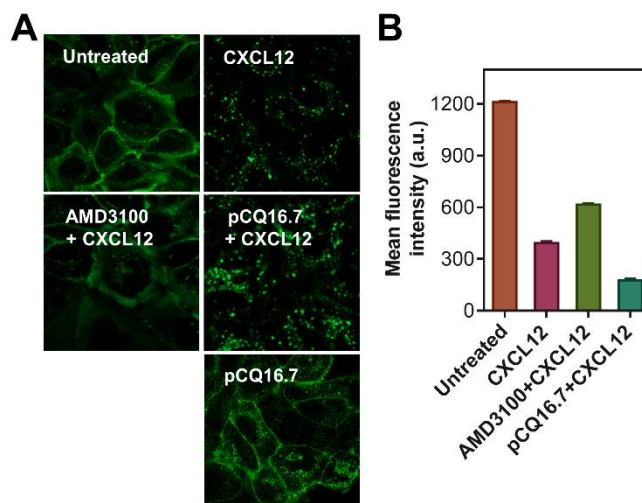


Figure 3.4. Effect of pCQ on redistribution of the CXCR4 receptors under stimulation with CXCL12. (A) U2OS cells overexpressing EGFP-CXCR4 were treated with AMD3100 (300 nM) or pCQ16.7 (100 μ M) for 30 min before exposing to CXCL12 (10 nM) for 1 h. The cells were then fixed and imaged by confocal microscopy (63 \times). (B) Cell surface expression of CXCR4 in U2OS cells measured by flow cytometry. Cells were treated as described above in Figure 3.3.

3.1.6 pCQ effect on the CXCR4/CXCL12 axis

Cell migration assay was used to investigate the effect of pCQ on CXCR4/CXCL12 axis. Porous transwell inserts (pore size 8 μ m, Falcon) were coated with 40 μ L ice-cold diluted Matrigel (1:3 v/v with serum-free medium) and placed in 37 $^{\circ}$ C incubator for 2 h. U2OS cells were trypsinized and resuspended in serum-free medium containing HCQ, pCQ or AMD3100 for 15 min before adding to the inserts at a final concentration of 100,000 cells in 300 μ L medium. Inserts were placed in a 24-well companion plate containing 20 nM CXCL12 in serum-free medium in each well. The cells were then incubated at 37 $^{\circ}$ C and allowed to invade through the Matrigel-coated insert membrane for 18 h. The non-invaded cells on the upper side of the insert membrane

were removed by cotton swabs and the invaded cells attached on the bottom surface were fixed in 100% methanol and stained with 0.2% Crystal Violet solution for 15 min at room temperature. Five different areas under 20× or 40× magnification were randomly selected and imaged using EVOS xl microscope. The number of invaded cells in each area was counted and the results were expressed as average number of invaded cells/imaging area \pm SD (n=5).

The important role of CXCR4/CXCL12 axis as a therapeutic target is often highlighted by its ability to promote migration and invasion of cancer cells as an important step in metastasis. Here, we evaluated *in vitro* activity of pCQ in transwell cell migration and invasion assays. We first applied CXCL12 as chemoattractant in cell invasion of the CXCR4-overexpressing U2OS cells through a layer of Matrigel (Figure 3.5). The results showed that both pCQ10.0 and pCQ16.7 were able to completely inhibit CXCL12-induced cell invasion at 100 μ M concentration. The inhibitory activity was not only considerably higher than activity achieved with safe concentrations of HCQ (~28% inhibition), but even better than the activity of the positive control AMD3100 which showed about 77% inhibition.

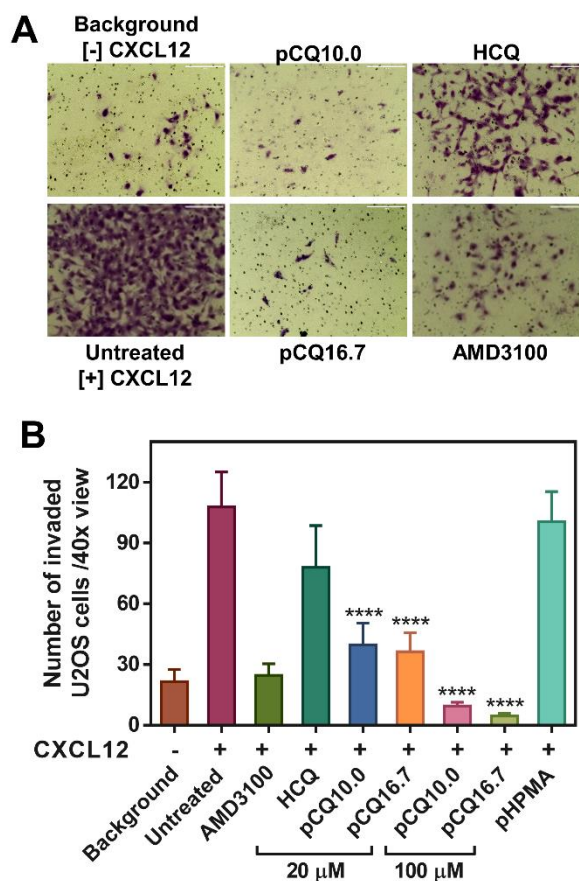


Figure 3.5. Inhibition of CXCL12-induced cell invasion. (A) U2OS cells were treated with pCQ, HCQ or AMD3100 (300 nM) and allowed to invade through a layer of Matrigel upon stimulation with CXCL12 for 18 h. (B) The number of invaded U2OS cells was counted and results are shown as mean number of invaded cells/40 \times view \pm SD ($n \geq 3$). (**** $p < 0.0001$ vs. HCQ; ANOVA with Tukey's multiple comparison test.)

The effect of pCQ on inhibiting CXCL4/CXCL12 chemokine axis was also evaluated by examining the activity on downstream signaling targets of CXCR4. Western blot was used to evaluate the effect of pCQ on inhibiting the phosphorylation of ERK induced by CXCL12 in 4T1 cells. The cells (5×10^6) were seeded 16 h prior to the treatment. The cells were washed with PBS, and incubated with AMD3100 (300 nM), HCQ, or pCQ in serum-free medium for 4 h before 20 min incubation with mouse CXCL12 (100 ng/mL). Total protein was extracted as above and

separated by SDS-PAGE. The samples were transferred to nitrocellulose membrane, followed by probing with pERK antibody and incubation with HRP-linked secondary antibody. GAPDH and ERK were used as housekeeping controls. Quantification of the band intensities was performed by ImageJ. The results are shown as mean of duplicate experiment (n =2).

ERK is one of the key downstream targets phosphorylated upon CXCR4 activation by CXCL12. Upregulation of pERK is directly associated with cancer cell migration and invasion [212]. Here, 4T1 cells were treated with AMD3100 (300 nM), HCQ (20 μ M), or pCQ (100 μ M) for 4 h followed by 20 min incubation with CXCL12 before Western blot analysis. As shown in Figure 3.6, pERK levels more than doubled after CXCL12 stimulation, and AMD3100 could inhibit the process. HCQ showed weaker inhibitory effect on pERK than AMD3100. In contrast, both pCQ10.0 and pCQ16.7 markedly decreased pERK levels, even more so than AMD3100. This finding provides supporting evidence that the mechanism of action of pCQ involves regulating the CXCR4/CXCL12 chemokine axis. The U2OS cells used in this study have impaired ERK signaling and were thus not used in this experiment.

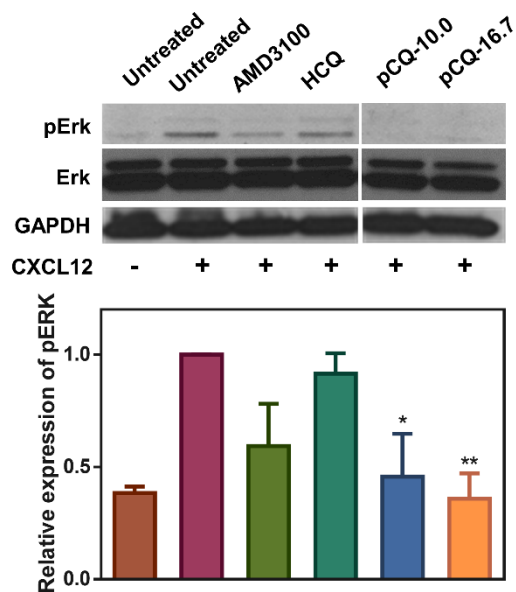


Figure 3.6. Inhibition of pERK by pCQ. 4T1 cells were treated with AMD3100 (300 nM), HCQ (20 μ M), or pCQ (100 μ M) for 4 h followed by 20 min incubation with CXCL12 (100 ng/mL) before lysis (n=2). (* p <0.05, ** p <0.01 vs. CXCL12+ untreated; ANOVA with Tukey's multiple comparison test.)

To further investigate if the inhibitory effect of pCQ on cancer cell motility observed in Figure 3.5 was specifically due to CXCR4 inhibition, we also performed a transwell migration assay using FBS as the chemoattractant. 4T1 cells were trypsinized, washed with PBS, and suspended in serum-free medium containing HCQ, pCQ or AMD3100 for 20 min before adding to the transwell inserts at a final concentration of 50,000 cells in 300 μ L medium. Inserts were then placed in a 24-well companion plate containing medium with 10% FBS in each well. The cells were then incubated at 37 °C and allowed to migrate through the insert membrane for 8 h. The non-migrated cells on the upper side of the membrane were removed by cotton swabs and the migrated cells attached on the bottom surface were fixed, stained, imaged and counted as described above. Results were expressed as average number of migrated cells/imaging area \pm SD (n =6).

FBS contains a complex mixture of proteins that serve as chemoattractants for cancer cells. 4T1 cells were treated with pCQ, HCQ, and AMD3100 and allowed to migrate through the membrane inserts for 8 h (Figure 3.7). Specific CXCR4 inhibitor AMD3100 showed no inhibition of FBS-induced cell migration despite the high concentration (20 μ M) used. In contrast, treatment with HCQ decreased cell migration by ~26%. Both pCQ10.0 and pCQ16.7 demonstrated even greater inhibition of the cell migration than HCQ. For example, pCQ10.0 decreased cell migration by 63% at 20 μ M and by 86% at 100 μ M. These results suggest that the inhibitory activity of pCQ in the cell migration and invasion studies is not CXCR4/CXCL12 specific. It appears that pCQ exerts its effect in a relatively non-specific and broad way that includes effects on other signaling pathways responsible for cancer cell motility.

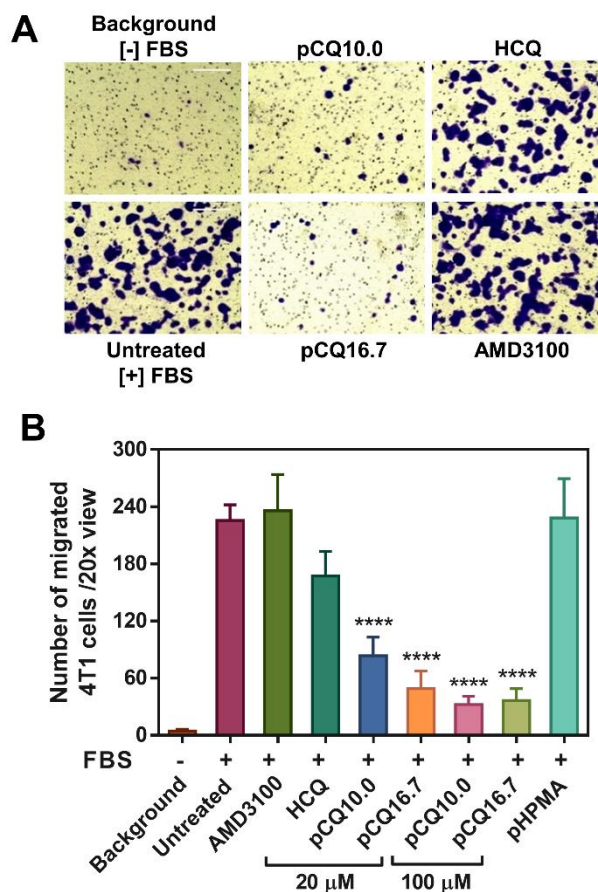


Figure 3.7. Inhibition of FBS-induced cell migration. (A) 4T1 cells were treated with pCQ, HCQ or AMD3100 (20 μ M) and allowed to migrate through porous membrane upon stimulation with FBS for 8 h. (B) The number of migrated 4T1 cells was counted and results are shown as mean number of invaded cells/20 \times view \pm SD ($n \geq 3$). “Background” represents number of randomly migrating cells in the absence of any chemoattractant. “Untreated” represents the number of migrating cells in the presence of FBS. (**** $p < 0.0001$ vs. HCQ; ANOVA with Tukey’s multiple comparison test.)

3.1.7 Antimetastatic activity *in vivo* (This work was completed by Dr. Jing Li, research instructor in Dr. Oupicky’s lab.)

All animal experiments followed a protocol approved by the University of Nebraska Medical Center (UNMC) Institutional Animal Care and Use Committee. Animals were placed in a facility accredited by the Association for Assessment and Accreditation of Laboratory Animal Care upon arrival. A total of 40 female Balb/c mice (8 weeks old) were randomly assigned into five groups (n = 8). Half a million 4T1 cells were treated with HCQ (20 μ M), pCQ10.0 (100 μ M) or pCQ16.7 (100 μ M) for 4 h before intravenous injection via the tail vein (in 100 μ L PBS). The animals were then intravenously administered with HCQ (10 mg/kg or 30 mg/kg), pCQ10.0 (10 mg/kg), or pCQ16.7 (10 mg/kg) on day 3, 5, 7 and 9 for a total of four doses. The animals were sacrificed on day 11, and the lungs were inflated with 30% sucrose followed by fixation in Bouin's solution for 18 h. The lungs were then stored in 70% ethanol before further tissue processing. Each of the five lobes was separated and all surface tumors were counted using dissecting microscope. After counting, the lungs were sectioned and stained with H&E at the UNMC core facility. Major other organs, including heart, liver, spleen and kidneys were also harvested, fixed in 4% paraformaldehyde, sectioned and stained with H&E. Blinded histological analysis of the tissues was conducted by a trained pathologist at the UNMC core facility.

To investigate if the ability of pCQ to inhibit cancer cell migration and invasion *in vitro* translates into decreased metastasis *in vivo*, we used an experimental lung metastasis model of the 4T1 breast cancer. In this model, cancer cells are injected intravenously (i.v.) to colonize the lung and form lung metastasis. After the cell injection, the treatments were given via tail vein i.v. injection. The following five experimental groups were tested: (i) untreated (saline), (ii) HCQ (low dose, 10 mg/kg body weight), (iii) HCQ (high dose, 30 mg/kg), (iv) pCQ10.0 (10 mg/kg HCQ equivalent), and (v) pCQ16.7 (10 mg/kg HCQ equivalent). The lung tumors were allowed to grow for 11 days and the mice were sacrificed. The total tumor burden in the lungs was quantified by counting total number of visible surface lung metastases (regardless of their size) and further analyzed by H&E staining of lung tissue sections. As shown in Figure 3.8A, treatment with low

dose HCQ exhibited no activity, while the high dose HCQ treatment resulted in a decreased number of surface lung metastatic lesions compared to the untreated group, however the difference was not statistically significant. The results with pCQ showed that pCQ16.7 had the highest antimetastatic activity even though only a low dose (10 mg/kg HCQ equivalent) was used. This antimetastatic inhibitory effect was higher even than the control HCQ used at the high dose. Interestingly, pCQ10.0 had no significant effect on the number of lung metastases but the size of the lung tumors in animals treated with pCQ10.0 was smaller than in the untreated animals. The low *in vivo* activity of pCQ10.0 was likely due to insufficient dose and less pronounced and slower effect on changes in the CXCR4 surface expression as suggested by the results in Figure 3.3.

In addition to surface lung metastases, we also evaluated the tumor burden in the lungs by histopathological analysis (Figure 3.8B). H&E staining of the lung sections revealed that the number of metastases in the lungs correlated well with the number of surface lesions. Treatment with pCQ16.7 resulted not only in a decreased number of metastases in the lung, but also smaller sizes of the metastases. Untreated animals typically exhibit signs of mortality related to the tumor burden in the lungs around 14-18 days after injection of the 4T1 cells. We therefore expect the pCQ treatment may improve animal survival since we observed significantly reduced tumor burden in the lungs as late as day 11. These *in vivo* results provide important evidence for antimetastatic activity of pCQ16.7 in 4T1 lung metastatic model, which is one of the most aggressive cancer models in mice. The significant enhancement of antimetastatic activity of pCQ16.7 compared with HCQ was confirmed not only by the overall decrease in the lung metastases, but also by the ability to achieve such effect at a much lower dose than HCQ.

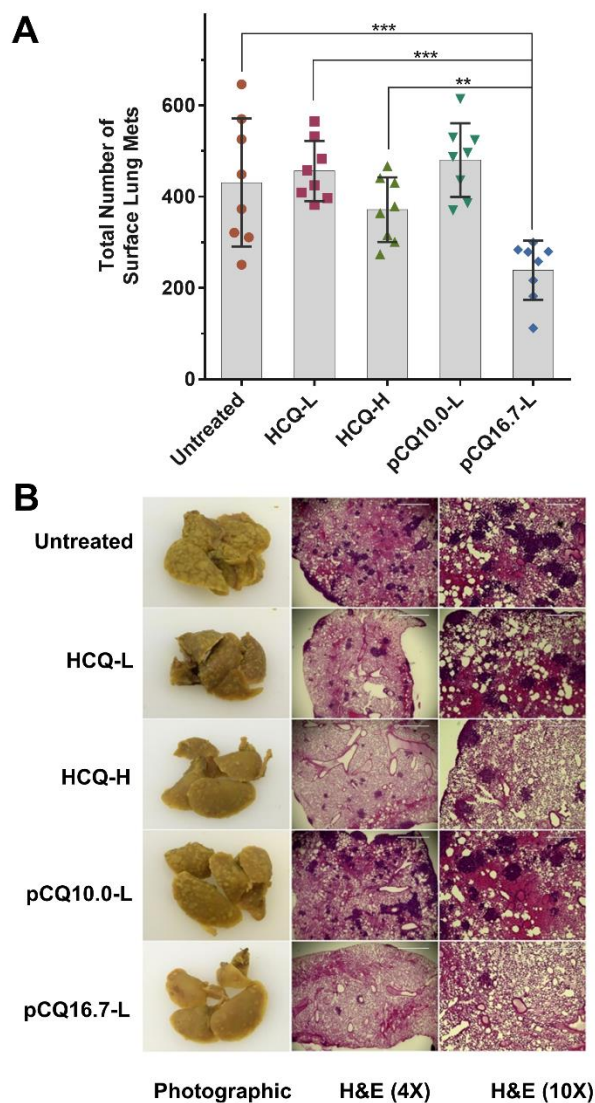


Figure 3.8. Antimetastatic activity of pCQ in experimental 4T1 lung metastasis model. 4T1 cells were injected i.v. in Balb/c mice, followed by 4 i.v. doses of pCQ or HCQ. L = low dose (10 mg/kg HCQ equivalent, H = high dose (30 mg/kg HCQ equivalent). (A) Total number of surface lung metastases. Results shown as average of total number of surface lung mets \pm SD (n = 8) (** p <0.01; *** p <0.001). (B) Representative images of the whole lung and H&E staining of the lung tissue sections (4 \times and 10 \times).

Although exhibiting significantly lowered toxicity *in vitro* compared with HCQ, it was important to investigate the possible toxicity of pCQ *in vivo*. As illustrated in Figure 3.9A, no

apparent loss of body weight was observed in any of the treatment groups until the end of the experiment, indicating that pCQ is well tolerated when given systemically. To further explore the effect on major organs including heart, liver, spleen and kidney, a blinded histopathological examination on H&E stained tissue sections was performed by a pathologist (Figure 3.9B). No significant morphological differences or tissue damage were observed in any of the treatment groups when compared with the untreated controls. These results confirm safety of pCQ16.7 after multiple administered doses *in vivo*.

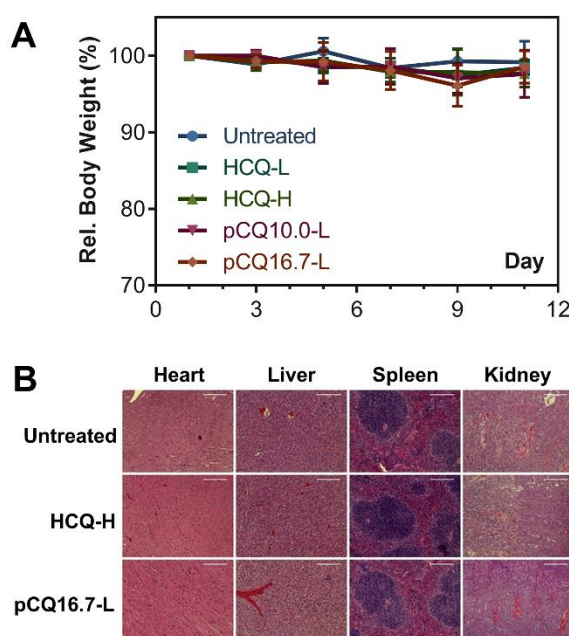


Figure 3.9. Toxicity evaluation of pCQ *in vivo*. (A) Relative body weight. Results shown as % body weight relative to the body weight on day 0. (B) H&E staining of major organs in different treatment groups (heart 20 \times , liver 20 \times , spleen 20 \times , kidney 10 \times).

3.1.8 Survival study (This work was completed by Dr. Jing Li, research instructor in Dr. Oupicky's lab, and Dr. Oupicky's lab in China Pharmaceutical University.)

Animal experiments were performed following rules of Animal Use Committee of China Pharmaceutical University. A total of 24 female Balb/c mice (8 weeks old) were randomly assigned

into three groups ($n = 8$). Half a million 4T1 cells treated with HCQ (20 μM) or pCQ16.7 (100 μM) for 4 h were intravenously injected via the tail vein (in 100 μL PBS). The animals were then intravenously administrated with HCQ (10 mg/kg) or pCQ16.7 (10 mg/kg) on day 3, 5, 7 and 9 for a total of four doses. Animal body weight and survival were monitored.

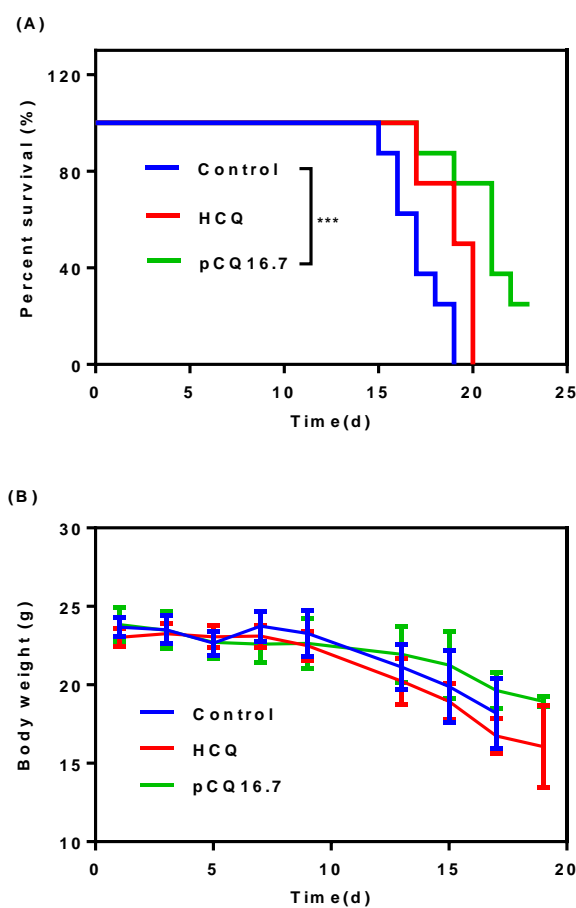


Figure 3.10. (A) Survival curve of experimental lung metastasis model of the 4T1 breast cancer. (B) Body weight changes of the animals treated by PBS, HCQ and pCQ16.7.

Survival curves were shown in Figure 3.10A. All animals in control group treated with PBS died in day 19. The survival of HCQ treated group did not show significant difference compared to control group. The pCQ16.7 treated group prolonged the animal survival compared to control group, with $p < 0.005$ by Logrank Test. However, there was no statistical difference between

the HCQ and pCQ16.7 groups. The body weight changes exhibited that animals in control and HCQ treated groups showed fast decrease after the treatment. However, there was no significant difference among the three groups. This preliminary result demonstrated the therapeutic potential of pCQ on cancer metastasis.

In conclusion, we developed CQ-based polymeric drugs with antimetastatic activity. The pCQ exhibited lowered cytotoxicity, enhanced inhibition of cancer cell migration and invasion, and improved antimetastatic activity *in vivo* when compared with parent HCQ. The preliminary survival study showed that pCQ prolonged the survival of animals bearing experimental lung metastasis of 4T1 breast cancer. Although not fully understood yet, our results revealed that pCQ mechanism of action involves, in part, inhibition of the CXCR4/CXCL12 chemokine axis. These results disclose pCQ for combination anticancer therapy to achieve simultaneous antimetastatic effect.

3.2 Clicked CQ copolymers for inhibition of cancer cell migration

We have reported synthesis of pCQ by copolymerization of HPMA and MA-CQ. The reported pCQ copolymers demonstrated unexpectedly enhanced inhibitory activity of cancer cell migration and experimental lung metastasis as polymeric drugs when compared to HCQ. However, CQ was conjugated to the pCQ copolymers through ester bonds, which made them susceptible to degradation *in vivo*, which meant that we were unable to unequivocally dissect the therapeutic contribution of the polymeric versus small molecule form HCQ. The goal of this study was to synthesize non-degradable pCQ (NpCQ) and to compare its pharmacologic activity with the degradable pCQ. The detailed synthesis methods were reported in 2.4-2.9. NpCQ copolymers were synthesized by a combination of click chemistry and RAFT polymerization. Two synthetic strategies were utilized for the preparation of NpCQ. First, direct RAFT polymerization of MA-tCQ was used to obtain RNpCQ, in which R represented RAFT polymerization. Second, a post-modification of alkyne-containing HPMA copolymer (pHP) was accomplished by click reaction of CQ-N₃ to obtain CNpCQ, in which C represented click chemistry. Copolymers used in this study

are summarized in Table 3.1. RpCQ was copolymers synthesized from MA-CQ and HPMA by RAFT polymerization served as control. The inhibitory activity of NpCQ on breast cancer cell migration was investigated.

Table 3.1. Summary of polymer characterization of NpCQ study.

	CQ content (mol %)		M_w (kDa)	M_w/M_n	P_n
	in feed	In copolymer			
RpHPMA	-	-	10.7	1.1	75
RNpCQ	16.7	15.7	20.3	1.1	103
CNpCQ	-	16.7	21.4	1.2	107
RpCQ	16.7	15.3	17.7	1.1	97
pCQ	20.0	16.7	34.5	1.1	185

3.2.1 Cytotoxicity of NpCQ polymers

Cytotoxicity of CQ-containing copolymers was tested utilizing CellTiter-Blue Cell Viability Assay (Promega, Madison, WI) in 4T1 cells according to the manufacturer's protocol. Cells were seeded in 96-well plates at a density of 6000 cells/well. After 16 h incubation, the medium was replaced by 100 μ L of treatments in complete cell culture medium. The cells were incubated for 24 h. Then the treatment media was replaced by 20 μ L of CellTiter-Blue reagent and the cells were incubated for another 1 h. The fluorescence intensity [I] at 560_{Ex}/590_{Em} was measured by SpectraMaxM5e Multi-Mode microplate Reader (Molecular Devices, CA). The relative cell viability (%) was calculated as $[I]_{\text{treated}} / [I]_{\text{untreated}} \times 100\%$.

HCQ exhibited highest toxicity at 30 μ M in 4T1 cells. At 30 μ M, cell viability of all the polymer-treated groups was higher than 90 % in 4T1 cells, when the cell viability in the HCQ-treated group was 75 % in 4T1 cells (Figure 3.11). NpCQ showed similar cytotoxicity as pCQ,

which indicated that addition of triazole group between CQ and polymer backbone did not significantly influence the cytotoxicity of the copolymer.

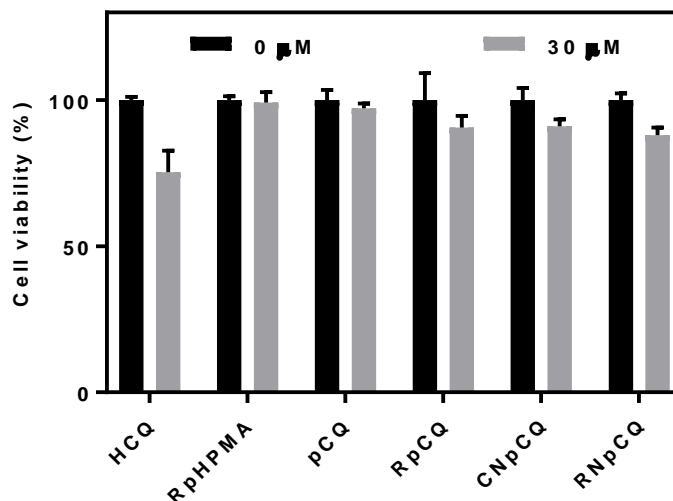


Figure 3.11. Cytotoxicity of CQ-containing polymers in 4T1 cells at CQ concentration of 30 μ M.

3.2.2 Effect of NpCQ on 4T1 cancer cell migration

4T1 cells were suspended in serum-free medium containing HCQ and copolymers after trypsinized and washed with PBS. After 20 min, the cell suspension was added to the transwell inserts at a final concentration of 50,000 cells in 300 μ L medium. Inserts were then placed in a 24-well companion plate containing complete culture media in each well. The cells were then incubated at 37 $^{\circ}$ C for 8 h. The non-migrated cells located on the upper side of the insert membrane were removed by cotton swabs. The migrated cells were attached on the bottom surface and fixed with 100% methanol followed by staining with 0.2% Crystal Violet solution for 15 min at room temperature. Three views/insert under 20 \times magnification were randomly selected and imaged using EVOS xl microscope. The number of migrated cells in each view was counted and the results were expressed as cell migration (%), which was the number of migrated cells in each group/average number of migrated cells in untreated group \times 100% (n=3).

To evaluate the anti-migration effect of the CQ-containing copolymers, we first performed transwell assay using 4T1 cell with fetal bovine serum (FBS) as the chemoattractant. FBS comprises a complex mixture of proteins that provide the chemotactic signals. The cells were treated with HCQ, pHPMA, RNpCQ, CNpCQ, RpCQ and pCQ at equivalent CQ concentration of 20 μ M and allowed to migrate through the membrane inserts for 8 h. All the CQ-containing polymers demonstrated greater inhibition of 4T1 cell migration than HCQ (Figure 3.12). For example, noncleavable CNpCQ and RNpCQ decreased cancer cell migration by 51 % and 49 %, respectively. In comparison, cleavable pCQ and RpCQ decreased cell migration by 55 % and 67 %, respectively. Noncleavable polymers showed similar activity with no significant difference as pCQ, indicating that the introduction of triazole ring between CQ and polymer backbone had negligible impact on the activity of the polymeric drug. Interestingly, cleavable RpCQ prepared by RAFT polymerization showed better effect than pCQ, which may be due to the well-defined polymer structure or the presence of different end groups.

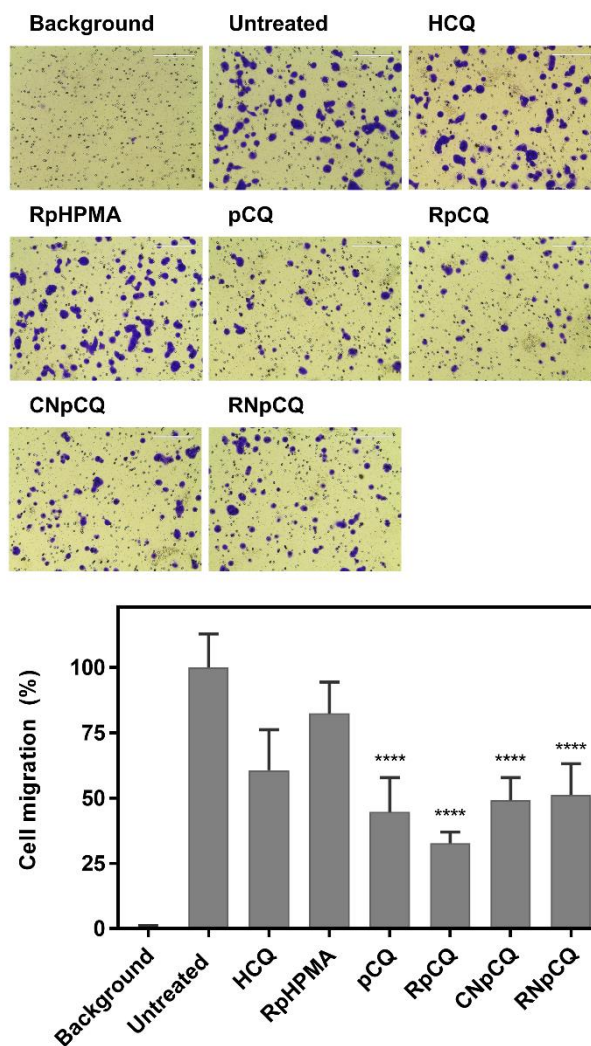


Figure 3.12. Inhibition of FBS induced 4T1 migration. Inhibition of FBS-induced 4T1 cell migration utilizing transwell assay. The number of migrated 4T1 cells was counted in each 20 \times image ($n \geq 3$). Percentage of migrated cell in each treated group relative to the untreated group was shown. Background represented the number of randomly migrated cells in the absence of any chemoattractant. Untreated represented the number of migrated cells in the presence of FBS. (**** $p < 0.0001$ vs. Untreated; One-way ANOVA with Tukey's multiple comparison test.)

To further investigate the inhibitory activity of CQ-containing polymers on 4T1 cell migration, wound healing assay was conducted. 4T1 cells (2×10^5) were seeded in six-well plates

and cultured in complete media overnight to let the confluence reach around 70 %. An artificial wound was created in the monolayer with a micropipette tip (1000 μ L) and the suspended cells were removed. After resting in complete media for 1 h, the wound of the cells were imaged using EVOS xl microscopy (10 \times). Then the cells were treated by HCQ, RpHPMA, CNpCQ, RpCQ and pCQ at equivalent of CQ concentration of 20 μ M in complete media. After 48 h, the cells were rinsed with PBS. Pictures of the wounds were taken by using EVOS xl microscopy (10 \times) (n=3). Here, branched polyethylenimine (PEI, 25 kDa) was used as a control to exclude the possibility that the observed effect is simply a result of sequestration of the chemotactic signals by a polycation. The concentration of PEI applied in this experiment was calculated by the concentration of amine that can be protonated, which means the concentration of the ethylamine units was 40 μ M. After 48 h, the images of the wound were captured and the wound width were compared with the initial wound width. The wound recovery is a measure of the rate of cell migration. All the CQ-containing polymers showed greater inhibition of wound recovery than HCQ.

As shown in Figure 3.13, wound recovery in the HCQ-treated group was 78%, which was not significantly different from untreated group of 75%. CNpCQ and RNpCQ inhibited wound recovery to 45% and 46%, respectively. By contrast, wound recovery of pCQ and RpCQ treated groups were 42% and 37%, respectively. RpCQ exhibited highest inhibitory activity on cancer cell migration. These results are in correspondence with the ones from transwell assay that the noncleavable polymers showed similar inhibitory activity of 4T1 cell migration with no significant difference from pCQ. Furthermore, PEI had no effect on cell migration.

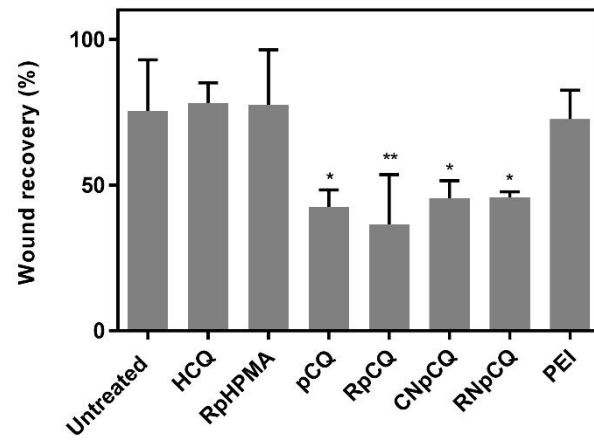
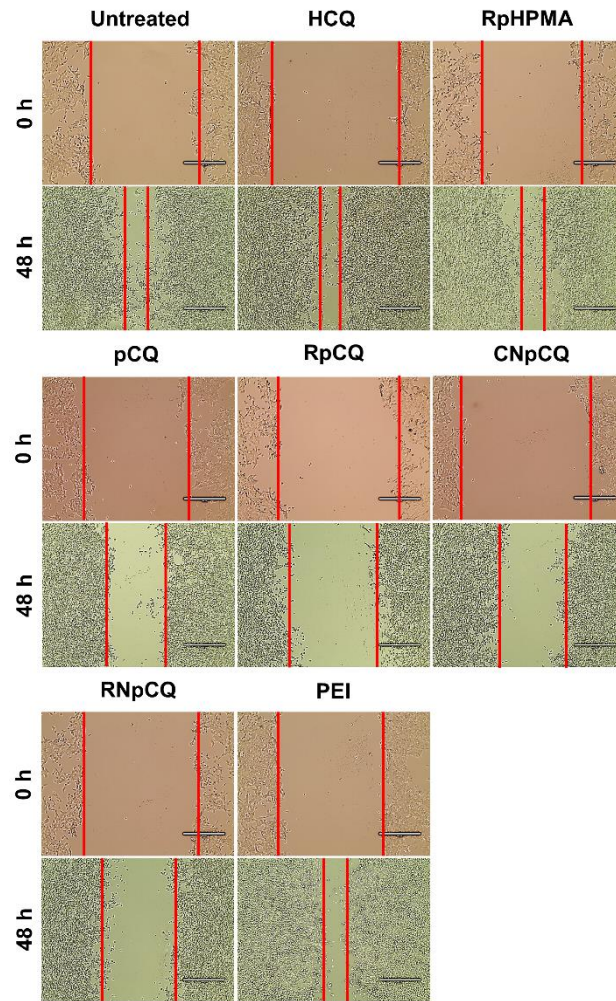


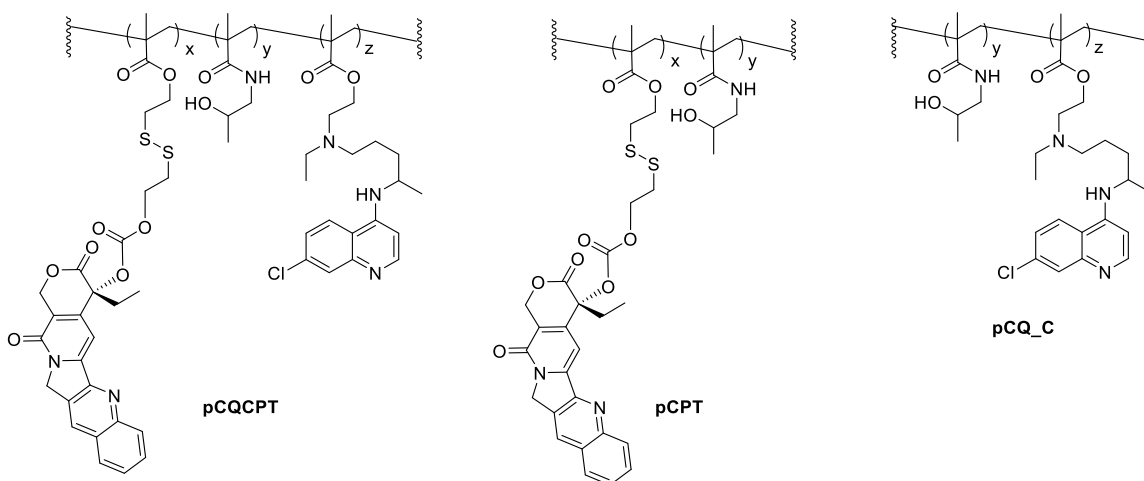
Figure 3.13. Inhibition of 4T1 cell migration utilizing wound healing assay. The wound width was measured in each 10× image ($n \geq 3$). Percentage of wound recovery was shown. (* $p < 0.05$, ** $p < 0.01$ vs. Untreated; One-way ANOVA with Tukey's multiple comparison test.)

In conclusion, an alkyne-containing methacrylamide was successfully synthesized and used as a universal precursor for polymer modification by CuAAC. We compared the antimigratory activity of the synthesized pCQ copolymers prepared by RAFT polymerization to previously reported pCQ in breast cancer cells using transwell and wound healing assays. The results showed that both cleavable and noncleavable pCQ copolymers exhibited enhanced inhibitory activity when compared with HCQ. These findings suggest that pCQ functions as a pharmacologically active polymer drug that does not require the release of the small molecule HCQ to achieve its anti-migration effect on cancer cells. This study provides clear evidence for further development of pCQ as a new class of antimetastatic polymer agents with possibly unique mechanism of action that is not found in HCQ.

3.3 CPT-containing reduction-responsive polymeric CQ for combinational treatment of breast cancer

HPMA copolymer conjugates have been widely developed for anticancer drug delivery. The enhanced antimetastatic activity of pCQ makes it promising for combination treatment of cancer. CPT is a wide-broad anticancer agent, however, its application was restricted by poor water solubility and high systemic toxicity. CPT conjugated HPMA copolymers have been developed using a glycinecyaminohexanoyl spacer. Release of CPT was dependent on the pH. Unfortunately, the polymers showed bladder toxicity and no evidence of antitumor activity in clinical trial. Here, we designed CPT-containing HPMA copolymers with reduction-responsive linkage for targeted release of CPT in tumor tissue based on EPR effect and the fact that redox potential in the cytoplasm of tumor cells is 2-3 orders magnitude higher than that in the blood circulation. The hypothesis is the pCQCPT will achieve targeted delivery of CPT to the tumor site due to the reduction-responsive

release. Also, the combination of pCQ and pCPT will enhance the anticancer activity by inhibition of tumor growth and metastasis.



Scheme 3.1. Chemical structure of pQCQPT, pCPT and pCQ_C used in combination delivery study.

3.3.1 Cytotoxicity of polymers

The cytotoxicity of pQCQPT, pCPT, pCPT+pCQ_C, CPT, and CPT+pCQ_C in 4T1 cells were tested using CellTiter-Blue Cell Viability Assay following the manufacturer's protocol. 4T1 cells were seeded in 96-well plates 24 h prior to treatment at a density of 2000 cells/well. The medium was then replaced by 200 μ L of serial dilutions of pQCQPT, pCPT, pCPT+pCQ_C, CPT, and CPT+pCQ_C in complete cell culture medium and incubated for 48 h. Because the ratio of CPT and CQ was fixed in pQCQPT, all the other groups used the same equivalent of CPT and CQ as the pQCQPT group. The medium was then replaced by 20 μ L of CellTiter-Blue reagent and the cells were incubated for another 1 h. The fluorescence intensity (I) at 560_{ex} and 590_{em} was measured using SpectraMaxM5e Multi-Mode microplate Reader. The relative cell viability (%) was calculated as $[I]_{\text{treated}} / [I]_{\text{untreated}} \times 100 \%$.

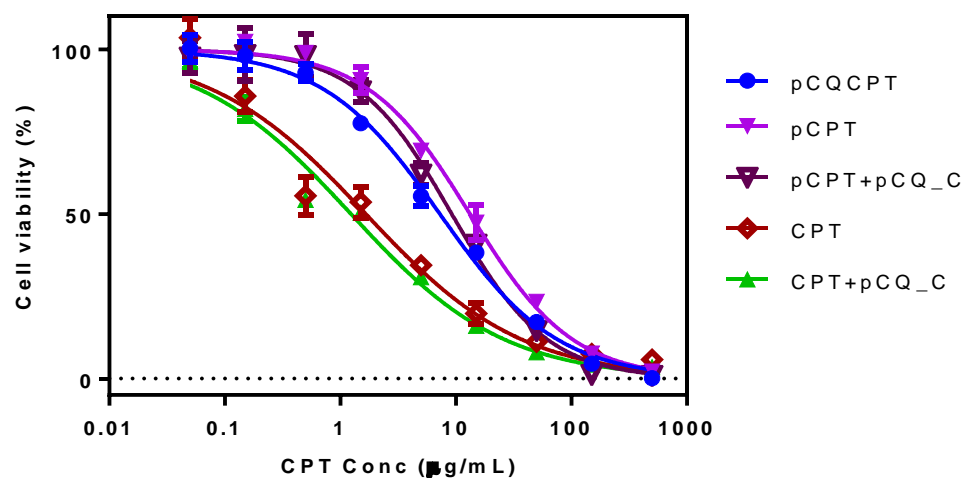


Figure 3.14. Cytotoxicity of pCQCPT, pCPT, pCPT+pCQ_C, CPT and CPT+pCQ_C.

Cancer cell killing effects of CPT and CQ polymer, CPT polymer, physical mixture of CPT polymer and CQ polymer, CPT, and physical mixture of CPT and CQ polymer were first evaluated *in vitro*. As shown in Figure 3.14, CPT and CPT+pCQ_C showed higher cytotoxicity than the other groups with IC50 of 1.66 µg/mL and 1.24 µg/mL as CPT equivalent, respectively. At CPT equivalent of 1.24 µg/mL, the corresponding CQ concentration was 2.40 µg/mL, which should not show any toxicity in 4T1 cells according to our previous study in Section 3.1.1. The cytotoxicity of pCPT, pCPT+pCQ_C and pCQCPT was lower than CPT and CPT+pCQ_C, with the IC50 as 13.3, 9.22 and 7.27 µg/mL, respectively. Addition of pCQ in pCPT polymers enhanced cell killing effect of pCPT by both physically mixing and presenting in the polymers. This may be explained by the fact that in both ways, CPT was inactive in the polymer but active after being released. Therefore, it was not very surprising that pCQCPT and pCPT+pCQ_C showed similar cell killing effect *in vitro*. However, the small molecule of CPT showed higher cytotoxicity than CPT polymer, which may be due to the uptake of the polymer and release of CPT from polymer took longer time than small molecule.

3.3.2 Anticancer effect *in vivo* (This work was completed by Dr. Jing Li, research instructor in Dr. Oupicky's lab)

The protocol of animal experiments was approved by the University of Nebraska Medical Center (UNMC) Institutional Animal Care and Use Committee. Orthotopic 4T1 tumors were established by injecting 4T1 cells (5×10^5) into the mammary fat pad of 8 weeks old female Balb/c mice. When the average tumor volume reached about 50 mm^3 , a total of 25 mice were randomly assigned into 5 groups (n=5) as untreated, CPT, pCPT, pCPT+pCQ_C and pCQCPT. On day 12, 14 and 16, all the treatment groups were injected with 5% glucose containing CPT equivalent of 2 mg/kg (CQ equivalent of 3.9 mg/kg). On day 18 and 20, the dose of CPT was increased to 4 mg/kg (CQ equivalent of 7.8 mg/kg). Tumor growth was monitored by digital calipers, and the volume was calculated as: tumor volume (mm^3) = $0.5 \times \text{length} \times \text{width}^2$. Body weight of the animals were recorded every other day. All the mice were sacrificed on day 23 and tumors, lungs and spleens were collected. Tumors were weighed and used for H&E and Ki-67 staining. Blinded histological analysis of the tissues was conducted by a certified pathologist at the UNMC core facility.

To investigate the anticancer activity of the polymers *in vivo*, we used an orthotopic 4T1 mammary tumor model. As shown in Figure 3.15, untreated group showed fastest tumor development with the average tumor volume of 817 mm^3 at day 23. CPT treated group showed smaller average tumor volume than untreated group after day 16, however, there was no statistical difference of the tumor volume between untreated and CPT groups at day 23. The pCPT, pCPT+pCQ_C and pCQCPT groups showed significantly smaller tumor volume than untreated group with the size of 590, 404 and 443 mm^3 . The pCPT+pCQ_C and pCQCPT groups also showed significantly smaller tumor volume than CPT group at the last day, which indicated better inhibitory activity on tumor growth.

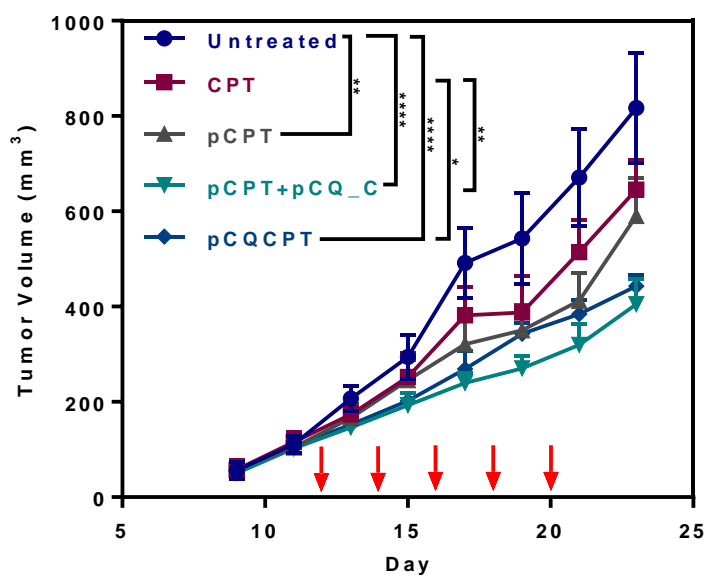


Figure 3.15. Tumor growth curve of mice treated with CPT, pCPT, pCPT+pCQ_C, and pCQCPT.

(* $p < 0.05$, ** $p < 0.01$, **** $p < 0.0001$, two-way ANOVA, $n = 5$.)

Animal body weight was recorded to monitor the toxicity of the treatment. As shown in Figure 3.16, pCQCPT showed toxicity during the first three injections, and pCPT+pCQ_C showed toxicity after the dose increased to 4 mg/kg, which suggested the potential toxicity of the polymers.

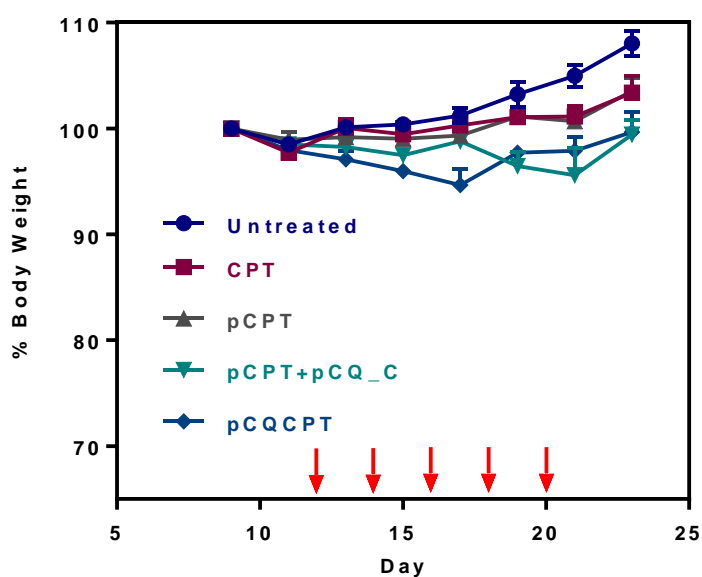


Figure 3.16. Percentage of animal body weight compared to day 8 during treatment (n=5).

This orthotopic 4T1 model used in the therapeutic study also generated lung metastasis. Thus, we evaluated the antimetastatic activity of the polymers by comparing lung metastasis. As shown in Figure 3.17, pQCPT treated group demonstrated significantly decreased number of surface lung metastatic tumor burdens, which indicated the therapeutic activity of pQCPT on primary tumor and metastasis.

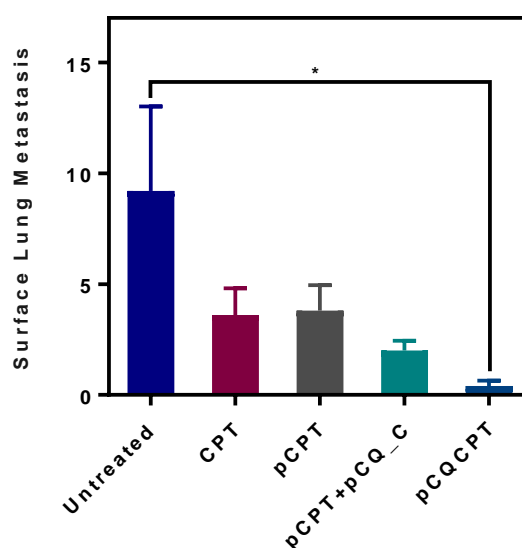


Figure 3.17. Average number of surface lung metastases. (* $p < 0.05$, vs. untreated control, n=5.)

The H&E tumor section showed enhanced necrosis in the pCPT+pCQ_C and pQCPT groups when compared to untreated group. The untreated group showed around 20% necrotic area, but the pCPT+pCQ_C and pQCPT groups showed about 90% necrotic area. However, the immunohistochemical staining of the tumor sections for Ki67 antigen showed that pCPT+pCQ_C and pQCPT groups did not decrease the Ki67 expression in the active tumor area. This suggested that the rate of cell turnover was higher, which may indicate that the treatment was pushing more cells to divide, which could contribute to the higher amount of necrosis in those lesions as most treatments go after actively dividing cells.

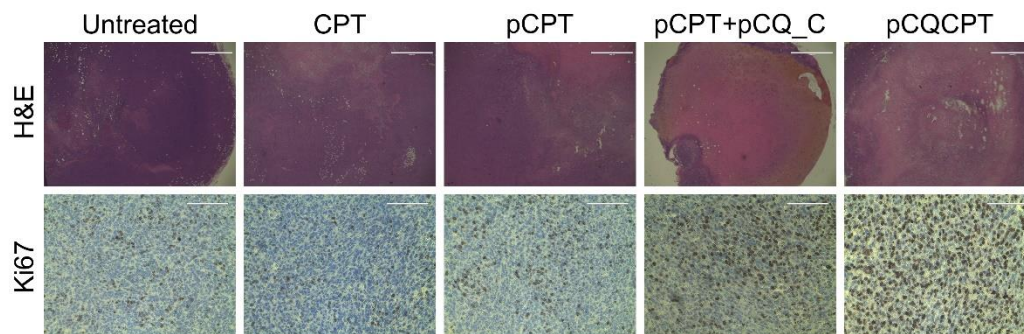


Figure 3.18. Representative images of histological analysis of tumor sections stained with H&E (4 ×) and Ki67 (40 ×).

In conclusion, we successfully synthesized reduction-responsive released pCPT and pCQCPT polymers that were used for codelivery of CPT and pCQ. The *in vivo* study showed that both pCQCPT and the mixture of pCPT+pCQ_C exhibited significantly enhanced inhibitory activity on tumor growth when compared to CPT. Moreover, pCQCPT showed enhanced antimetastasis activity on lung metastasis of breast tumor, which revealed the potential of pCQ in combination with other treatment for cancer therapy.

4 Conclusion

Development of CQ-containing HPMA copolymers is reported in this dissertation. This work is inspired by broad application of CQ and HCQ in clinical trial for cancer treatment and fast development of polymeric drugs. As well-known 4-aminoquinoline antimalarial agents, CQ and HCQ have been proven to be effective in treatment of different cancer types when used alone or in combination with other drugs by potentiating the therapeutic activity of conventional anticancer treatments including radiation therapy, chemotherapy and immunotherapy. Remarkably, CQ and HCQ exhibit their effects on both cancer cells and tumor microenvironment through the multiple complementary mechanism of action. The most studied anticancer effect of CQ and HCQ is autophagy. Other than that, these drugs affect the TLR9, tumor suppressor p53 and CXCR4/CXCL12 signaling pathway axis that are related to tumor cell proliferation, survival, apoptosis and metastasis. In tumor microenvironment, CQ was shown to affect tumor vessel, cancer-associated fibroblasts and the immune cells. To reduce the toxicity and enhance the pharmacological activity of CQ, we transform the small molecules to polymeric drugs, which fits the size range of proteins so that the repeating units can bind to the targets by complex set of multivalent interactions.

HCQ and CQ derivatives were synthesized for preparation of CQ-containing polymers. We first developed MA-CQ and obtained pCQ by free radical polymerization of HPMA and MA-CQ with an ester bond between CQ and the backbone. By comparing pCQ and HCQ, we found pCQ showed lower cytotoxicity, enhanced inhibitory effect of cancer cell migration and invasion, and improved antimetastatic activity *in vivo*. The preliminary survival study revealed that pCQ prolonged the survival of animals bearing experimental lung metastasis of 4T1 breast cancer. Although not fully understood yet, our results showed that pCQ mechanism of action was not exactly the same as HCQ, which involved, at least in part, inhibition of the CXCR4/CXCL12 chemokine axis. These results disclosed pCQ for combination anticancer therapy to achieve

antimetastatic effect. Therefore, we developed the pCQ copolymers conjugating CPT by a reduction-responsive linker as pCQCPT to achieve codelivery of drugs and targeted release of CPT. The animal study showed that both pCQCPT and the mixture of pCPT+pCQ_C demonstrated significantly enhanced inhibitory activity on tumor growth when compared to CPT. In addition, pCQCPT showed enhanced antimetastasis effect on lung metastasis of orthotopic breast tumor. This work further confirmed the potential of pCQ for combination therapy. For further work, the content and ratio of CQ and CPT in polymers can be studied to obtain the optimized polymers that possess better water solubility and anticancer properties. Also, other chemodrugs, such as DOX and cisplatin can be applied to pCQ copolymers. Furthermore, instead of conjugation of anticancer drugs to pCQ polymers, we can physically encapsulate therapeutic agents, such as PTX, by PLA-pCQ polymers as drug loaded nanoparticles. The core-shell structure of the nanoparticles will facilitate the interactions between pCQ and cell surface receptors, as well as targeted delivery of anticancer agents to tumor site through EPR effect.

The pCQ polymers exhibited unexpectedly enhanced inhibitory activity of cancer metastasis, however, CQ was conjugated to the pCQ copolymers through ester bonds that made them susceptible to degradation *in vivo*, which meant that we were unable to unequivocally dissect the therapeutic contribution of the polymeric versus small molecule form HCQ. In this case, non-degradable NpCQ was synthesized and its antimigratory activity was compared to pCQ. CQ derivatives as clickable CQ-N₃ and polymerizable MA-tCQ were designed and synthesized to obtain NpCQ. The results showed that both pCQ and NpCQ copolymers exhibited enhanced inhibitory activity when compared with HCQ. These findings suggest that pCQ functions as a pharmacologically active polymer drug that does not require the release of the small molecule HCQ to achieve its antimigration effect on cancer cells. The pCQ mechanism of action still remains to be studied. We will study the effect of pCQ on signaling pathways that are related to cell motility and migration, such as Rho regulated stress fiber formation. We hope the application of pCQ will

be further explored by acknowledgement of the mechanism in treatment of cancer and other diseases.

References

- [1] W. Liechty, D. Kryscio, B. Slaughter, N. Peppas, Polymers for drug delivery systems, *Annual Review of Chemical and Biomolecular Engineering* 1 (2010) 149.
- [2] R. Siegel, Stimuli sensitive polymers and self regulated drug delivery systems: a very partial review, *Journal of Controlled Release* 190 (2014) 337.
- [3] H. Priya James, R. John, A. Alex, K. Anoop, Smart polymers for the controlled delivery of drugs - a concise overview, *Acta Pharmaceutica Sinica. B* 4(2) (2014) 120.
- [4] B. Pelaz, C. Alexiou, R. Alvarez-Puebla, F. Alves, A. Andrews, S. Ashraf, L. Balogh, L. Ballerini, A. Bestetti, C. Brendel, S. Bosi, M. Carril, W. Chan, C. Chen, X. Chen, X. Chen, Z. Cheng, D. Cui, J. Du, C. Dullin, A. Escudero, N. Feliu, M. Gao, M. George, Y. Gogotsi, A. Grünweller, Z. Gu, N. Halas, N. Hampp, R. Hartmann, M. Hersam, P. Hunziker, J. Jian, X. Jiang, P. Jungebluth, P. Kadhiresan, K. Kataoka, A. Khademhosseini, J. Kopeček, N. Kotov, H. Krug, D. Lee, C. Lehr, K. Leong, X. Liang, M. Ling Lim, L. Liz-Marzán, X. Ma, P. Macchiarini, H. Meng, H. Möhwald, P. Mulvaney, A. Nel, S. Nie, P. Nordlander, T. Okano, J. Oliveira, T. Park, R. Penner, M. Prato, V. Puntès, V. Rotello, A. Samarakoon, R. Schaak, Y. Shen, S. Sjöqvist, A. Skirtach, M. Soliman, M. Stevens, H. Sung, B. Tang, R. Tietze, B. Udugama, J. VanEpps, T. Weil, P. Weiss, I. Willner, Y. Wu, L. Yang, Z. Yue, Q. Zhang, Q. Zhang, X. Zhang, Y. Zhao, X. Zhou, W. Parak, Diverse applications of nanomedicine, *ACS Nano* 11(3) (2017) 2313.
- [5] J. Li, F. Yu, Y. Chen, D. Oupicky, Polymeric drugs: advances in the development of pharmacologically active polymers, *Journal of Controlled Release* 219 (2015) 369.
- [6] E. Connor, I. Lees, D. Maclean, Polymers as drugs—Advances in therapeutic applications of polymer binding agents, *Journal of Polymer Science Part A: Polymer Chemistry* 55(18) (2017) 3146.

- [7] D. Bobo, K. Robinson, J. Islam, K. Thurecht, S. Corrie, Nanoparticle-based medicines: a review of FDA-approved materials and clinical trials to date, *Pharmaceutical Research* 33(10) (2016) 2373.
- [8] L. Miao, S. Guo, C.M. Lin, Q. Liu, L. Huang, Nanoformulations for combination or cascade anticancer therapy, *Advanced Drug Delivery Reviews* 115 (2017) 3.
- [9] K. Liu, X. Jiang, P. Hunziker, Carbohydrate-based amphiphilic nano delivery systems for cancer therapy, *Nanoscale* 8(36) (2016) 16091.
- [10] M. Maitz, Applications of synthetic polymers in clinical medicine, *Biosurface and Biotribology* 1(3) (2015) 161.
- [11] S. Doppalapudi, A. Jain, A.J. Domb, W. Khan, Biodegradable polymers for targeted delivery of anti-cancer drugs, *Expert Opinion on Drug Delivery* 13(6) (2016) 891.
- [12] M. Sun, K. Wang, D. Oupický, Advances in stimulus-responsive polymeric materials for systemic delivery of nucleic acids, *Advanced Healthcare Materials* 7(4) (2018) 1701070.
- [13] K. Ulbrich, K. Holá, V. Šubr, A. Bakandritsos, J. Tuček, R. Zbořil, Targeted drug delivery with polymers and magnetic nanoparticles: covalent and noncovalent approaches, *Release Control, and Clinical Studies, Chemical Reviews* 116(9) (2016) 5338.
- [14] A. Basu, K. Kunduru, J. Katzhendler, A. Domb, Poly(α -hydroxy acid)s and poly(α -hydroxy acid-co- α -amino acid)s derived from amino acid, *Advanced Drug Delivery Reviews* 107 (2016) 82.
- [15] B. Colzani, L. Pandolfi, A. Hoti, P. Iovene, A. Natalello, S. Avvakumova, M. Colombo, D. Prospero, Investigation of antitumor activities of trastuzumab delivered by PLGA nanoparticles, *International Journal of Nanomedicine* 13 (2018) 957.

- [16] Q. Liu, Y. Qian, P. Li, S. Zhang, J. Liu, X. Sun, M. Fulham, D. Feng, G. Huang, W. Lu, S. Song, (131)I-Labeled copper sulfide-loaded microspheres to treat hepatic tumors via hepatic artery embolization, *Theranostics* 8(3) (2018) 785.
- [17] Y. Zhao, J. Li, H. Yu, G. Wang, W. Liu, Synthesis and characterization of a novel polydepsipeptide contained tri-block copolymer (mPEG-PLLA-PMMD) as self-assembly micelle delivery system for paclitaxel, *International Journal of Pharmaceutics* 430(1-2) (2012) 282.
- [18] H. Wang, Y. Zhao, Y. Wu, Y. Hu, K. Nan, G. Nie, H. Chen, Enhanced anti-tumor efficacy by co-delivery of doxorubicin and paclitaxel with amphiphilic methoxy PEG-PLGA copolymer nanoparticles, *Biomaterials* 32(32) (2011) 8281.
- [19] M. Zhang, C. Hagan, Y. Min, H. Foley, X. Tian, F. Yang, Y. Mi, K. Au, Y. Medik, K. Roche, K. Wagner, Z. Rodgers, A. Wang, Nanoparticle co-delivery of wortmannin and cisplatin synergistically enhances chemoradiotherapy and reverses platinum resistance in ovarian cancer models, *Biomaterials* 169 (2018) 1.
- [20] W. Shen, X. Chen, J. Luan, D. Wang, L. Yu, J. Ding, Sustained codelivery of cisplatin and paclitaxel via an injectable prodrug hydrogel for ovarian cancer treatment, *ACS Applied Materials & Interfaces* 9(46) (2017) 40031.
- [21] S. Bhatt, F. Valamanesh, J. Pulpytel, R. Dico, A. Baiyukha, I. Al-dybiat, M. Pocard, F. Arefi-Khonsari, M. Mirshahi, Radio-frequency plasma polymerized biodegradable carrier for in vivo release of cis-platinum, *Oncotarget* 7(36) (2016) 58121.
- [22] S. Garg, A. Falamarzian, M. Vakili, H. Aliabadi, H. Uludağ, A. Lavasanifar, Polymeric micelles for MCL-1 gene silencing in breast tumors following systemic administration, *Nanomedicine* 11(17) (2016) 2319.

- [23] Y. Liu, C. Chiu, H. Chen, S. Chen, L. Wang, Preparation of chondroitin sulfate-g-poly(epsilon-caprolactone) copolymers as a CD44-targeted vehicle for enhanced intracellular uptake, *Molecular Pharmaceutics* 11(4) (2014) 1164.
- [24] H. Cho, T. Lai, G. Kwon, Poly(ethylene glycol)-block-poly(epsilon-caprolactone) micelles for combination drug delivery: evaluation of paclitaxel, cyclophosphamide and doxorubicin in intraperitoneal xenograft models of ovarian cancer, *Journal of Controlled Release* 166(1) (2013) 1.
- [25] B. Doddapaneni, S. Kyryachenko, S. Chagani, R. Alany, D. Rao, A. Indra, A. Alani, A three-drug nanoscale drug delivery system designed for preferential lymphatic uptake for the treatment of metastatic melanoma, *Journal of Controlled Release* 220 (2015) 503.
- [26] R. Kularatne, K. Washington, C. Bulumulla, E. Calubaquib, M. Biewer, D. Oupicky, M.C. Stefan, Histone deacetylase inhibitor (HDACi) conjugated polycaprolactone for combination cancer therapy, *Biomacromolecules* 19(3) (2018) 1082.
- [27] S. Senevirathne, K.E. Washington, J.B. Miller, M.C. Biewer, D. Oupicky, D. Siegwart, M. Stefan, HDAC inhibitor conjugated polymeric prodrug micelles for doxorubicin delivery, *Journal of Materials Chemistry B* 5(11) (2017) 2106.
- [28] Z. Xie, Y. Zhang, L. Liu, H. Weng, R. Mason, L. Tang, K. Nguyen, J. Hsieh, J. Yang, Development of intrinsically photoluminescent and photostable polylactones, *Advanced Materials* 26(26) (2014) 4491.
- [29] G. Yang, J. Wang, Y. Wang, L. Li, X. Guo, S. Zhou, An implantable active-targeting micelle-in-nanofiber device for efficient and safe cancer therapy, *ACS Nano* 9(2) (2015) 1161.
- [30] J. Liu, Z. Jiang, S. Zhang, C. Liu, R. Gross, T. Kyriakides, W. Saltzman, Biodegradation, biocompatibility, and drug delivery in poly(omega-pentadecalactone-co-p-dioxanone) copolyesters, *Biomaterials* 32(27) (2011) 6646.
- [31] D. Hanahan, R. Weinberg, Hallmarks of cancer: the next generation, *Cell* 144(5) (2011) 646.

- [32] A. Hoffman, Stimuli-responsive polymers: Biomedical applications and challenges for clinical translation, *Advanced Drug Delivery Reviews* 65(1) (2013) 10.
- [33] H. Sun, F. Meng, R. Cheng, C. Deng, Z. Zhong, Reduction-sensitive degradable micellar nanoparticles as smart and intuitive delivery systems for cancer chemotherapy, *Expert Opinion on Drug Delivery* 10(8) (2013) 1109.
- [34] Y. Zou, Y. Fang, H. Meng, F. Meng, C. Deng, J. Zhang, Z. Zhong, Self-crosslinkable and intracellularly decrosslinkable biodegradable micellar nanoparticles: A robust, simple and multifunctional nanoplatform for high-efficiency targeted cancer chemotherapy, *Journal of Controlled Release* 244 (2016) 326.
- [35] X. Chen, F. Wang, J.Y. Hyun, T. Wei, J. Qiang, X. Ren, I. Shin, J. Yoon, Recent progress in the development of fluorescent, luminescent and colorimetric probes for detection of reactive oxygen and nitrogen species, *Chemical Society Reviews* 45(10) (2016) 2976.
- [36] C. Tapeinos, A. Pandit, Reactive oxygen species: physical, chemical, and biological structures based on ROS-sensitive moieties that are able to respond to oxidative microenvironments, *Advanced Materials* 28(27) (2016) 5334.
- [37] Y. Sun, X. Yan, T. Yuan, J. Liang, Y. Fan, Z. Gu, X. Zhang, Disassemblable micelles based on reduction-degradable amphiphilic graft copolymers for intracellular delivery of doxorubicin, *Biomaterials* 31(27) (2010) 7124.
- [38] Y. Sun, W. Zou, S. Bian, Y. Huang, Y. Tan, J. Liang, Y. Fan, X. Zhang, Bioreducible PAA-g-PEG graft micelles with high doxorubicin loading for targeted antitumor effect against mouse breast carcinoma, *Biomaterials* 34(28) (2013) 6818.
- [39] H. Sun, B. Guo, R. Cheng, F. Meng, H. Liu, Z. Zhong, Biodegradable micelles with sheddable poly(ethylene glycol) shells for triggered intracellular release of doxorubicin, *Biomaterials* 30(31) (2009) 6358.

- [40] W. Chen, Y. Zou, J. Jia, F. Meng, R. Cheng, C. Deng, J. Feijen, Z. Zhong, Functional poly(ϵ -caprolactone)s via copolymerization of ϵ -caprolactone and pyridyl disulfide-containing cyclic carbonate: controlled synthesis and facile access to reduction-sensitive biodegradable graft copolymer micelles, *Macromolecules* 46(3) (2013) 699.
- [41] H. Sun, B. Guo, X. Li, R. Cheng, F. Meng, H. Liu, Z. Zhong, Shell-sheddable micelles based on dextran-SS-poly(ϵ -caprolactone) diblock copolymer for efficient intracellular release of doxorubicin, *Biomacromolecules* 11(4) (2010) 848.
- [42] Y. Fang, Y. Jiang, Y. Zou, F. Meng, J. Zhang, C. Deng, H. Sun, Z. Zhong, Targeted glioma chemotherapy by cyclic RGD peptide-functionalized reversibly core-crosslinked multifunctional poly(ethylene glycol)-b-poly(ϵ -caprolactone) micelles, *Acta Biomaterialia* 50 (2017) 396.
- [43] Y. Zou, F. Meng, C. Deng, Z. Zhong, Robust, tumor-homing and redox-sensitive polymersomal doxorubicin: a superior alternative to Doxil and Caelyx?, *Journal of Controlled Release* 239 (2016) 149.
- [44] P. Zhong, H. Meng, J. Qiu, J. Zhang, H. Sun, R. Cheng, Z. Zhong, $\alpha v \beta 3$ Integrin-targeted reduction-sensitive micellar mertansine prodrug: superb drug loading, enhanced stability, and effective inhibition of melanoma growth in vivo, *Journal of Controlled Release* 259 (2017) 176.
- [45] J. Zhang, L. Wu, F. Meng, Z. Wang, C. Deng, H. Liu, Z. Zhong, pH and reduction dual-bioresponsive polymersomes for efficient intracellular protein delivery, *Langmuir* 28(4) (2012) 2056.
- [46] W. Chen, P. Zhong, F. Meng, R. Cheng, C. Deng, J. Feijen, Z. Zhong, Redox and pH-responsive degradable micelles for dually activated intracellular anticancer drug release, *Journal of Controlled Release* 169(3) (2013) 171.

- [47] H. Sun, F. Meng, R. Cheng, C. Deng, Z. Zhong, Reduction and pH dual-bioresponsive crosslinked polymersomes for efficient intracellular delivery of proteins and potent induction of cancer cell apoptosis, *Acta Biomaterialia* 10(5) (2014) 2159.
- [48] D. Gao, P. Lo, Polymeric micelles encapsulating pH-responsive doxorubicin prodrug and glutathione-activated zinc(II) phthalocyanine for combined chemotherapy and photodynamic therapy, *Journal of Controlled Release* 282 (2018) 46.
- [49] C. Conte, F. Mastrotto, V. Taresco, A. Tchoryk, F. Quaglia, S. Stolnik, C. Alexander, Enhanced uptake in 2D- and 3D- lung cancer cell models of redox responsive PEGylated nanoparticles with sensitivity to reducing extra- and intracellular environments, *Journal of Controlled Release* 277 (2018) 126.
- [50] C. Liu, J. Yuan, X. Luo, M. Chen, Z. Chen, Y. Zhao, X. Li, Folate-decorated and reduction-sensitive micelles assembled from amphiphilic polymer–camptothecin conjugates for intracellular drug delivery, *Molecular Pharmaceutics* 11(11) (2014) 4258.
- [51] M. Gulfam, T. Matini, P. Monteiro, R. Riva, H. Collins, K. Spriggs, S. Howdle, C. Jerome, C. Alexander, Bioreducible cross-linked core polymer micelles enhance in vitro activity of methotrexate in breast cancer cells, *Biomaterials Science* 5(3) (2017) 532.
- [52] X. Liu, Y. Yang, M. Urban, Stimuli-responsive polymeric nanoparticles, *Macromolecular Rapid Communications* 38(13) (2017) 1700030.
- [53] R. Duncan, M. Vicent, Do HPMA copolymer conjugates have a future as clinically useful nanomedicines? A critical overview of current status and future opportunities, *Advanced Drug Delivery Review* 62(2) (2010) 272.
- [54] P. Chytil, E. Koziolova, T. Etrych, K. Ulbrich, HPMA copolymer-drug conjugates with controlled tumor-specific drug release, *Macromolecular Bioscience* 18(1) (2018) 1700209.

- [55] J. Yang, J. Kopeček, The light at the end of the tunnel—second generation HPMA conjugates for cancer treatment, *Current Opinion in Colloid & Interface Science* 31 (2017) 30.
- [56] R. Williams, Discontinued drugs in 2008: oncology drugs, *Expert Opinion on Investigational Drugs* 18(11) (2009) 1581.
- [57] J. Meerum Terwogt, W. ten Bokkel Huinink, J. Schellens, M. Schot, I. Mandjes, M. Zurlo, M. Rocchetti, H. Rosing, F. Koopman, J. Beijnen, Phase I clinical and pharmacokinetic study of PNU166945, a novel water-soluble polymer-conjugated prodrug of paclitaxel, *Anti-cancer Drugs* 12(4) (2001) 315.
- [58] D. Bissett, J. Cassidy, J. de Bono, F. Muirhead, M. Main, L. Robson, D. Fraier, M. Magne, C. Pellizzoni, M. Porro, R. Spinelli, W. Speed, C. Twelves, Phase I and pharmacokinetic (PK) study of MAG-CPT (PNU 166148): a polymeric derivative of camptothecin (CPT), *British Journal of Cancer* 91(1) (2004) 50.
- [59] J. Rademaker-Lakhai, C. Terret, S. Howell, C. Baud, R. De Boer, D. Pluim, J. Beijnen, J. Schellens, J. Droz, A Phase I and pharmacological study of the platinum polymer AP5280 given as an intravenous infusion once every 3 weeks in patients with solid tumors, *Clinical Cancer Research* 10(10) (2004) 3386.
- [60] J. Rice, J. Gerberich, D. Nowotnik, S. Howell, Preclinical efficacy and pharmacokinetics of AP5346, a novel diaminocyclohexane-platinum tumor-targeting drug delivery system, *Clinical Cancer Research* 12(7 Pt 1) (2006) 2248.
- [61] D. Nowotnik, E. Cvitkovic, ProLindac (AP5346): a review of the development of an HPMA DACH platinum Polymer Therapeutic, *Advanced Drug Delivery Review* 61(13) (2009) 1214.
- [62] T. Etrych, P. Chytil, M. Jelínková, B. Říhová, K. Ulbrich, Synthesis of HPMA copolymers containing doxorubicin bound via a hydrazone linkage. Effect of spacer on drug release and in vitro cytotoxicity, *Macromolecular Bioscience* 2(1) (2002) 43.

- [63] T. Etrych, T. Mrkvan, P. Chytil, Č. Koňák, B. Říhová, K. Ulbrich, N-(2-hydroxypropyl)methacrylamide-based polymer conjugates with pH-controlled activation of doxorubicin. I. New synthesis, physicochemical characterization and preliminary biological evaluation, *Journal of Applied Polymer Science* 109(5) (2008) 3050.
- [64] H. Nakamura, T. Etrych, P. Chytil, M. Ohkubo, J. Fang, K. Ulbrich, H. Maeda, Two step mechanisms of tumor selective delivery of N-(2-hydroxypropyl)methacrylamide copolymer conjugated with pirarubicin via an acid-cleavable linkage, *Journal of Controlled Release* 174 (2014) 81.
- [65] M. Studenovský, K. Ulbrich, M. Ibrahimova, B. Říhová, Polymer conjugates of the highly potent cytostatic drug 2-pyrrolinodoxorubicin, *European Journal of Pharmaceutical Sciences* 42(1) (2011) 156.
- [66] T. Etrych, M. Šírová, L. Starovoytova, B. Říhová, K. Ulbrich, HPMA copolymer conjugates of paclitaxel and docetaxel with pH-controlled drug release, *Molecular Pharmaceutics* 7(4) (2010) 1015.
- [67] H. Krakovičová, T. Etrych, K. Ulbrich, HPMA-based polymer conjugates with drug combination, *European Journal of Pharmaceutical Sciences* 37(3) (2009) 405.
- [68] H. Kostková, T. Etrych, B. Říhová, L. Kostka, L. Starovoytová, M. Kovář, K. Ulbrich, HPMA copolymer conjugates of DOX and mitomycin C for combination therapy: physicochemical characterization, cytotoxic effects, combination index analysis, and anti-tumor efficacy, *Macromolecular Bioscience* 13(12) (2013) 1648.
- [69] W. Choi, P. Kopečková, T. Minko, J. Kopeček, Synthesis of HPMA copolymer containing adriamycin bound via an acid-labile spacer and its activity toward human ovarian carcinoma cells, *Journal of Bioactive and Compatible Polymers* 14(6) (1999) 447.

- [70] J. Reményi, B. Balázs, S. Tóth, A. Falus, G. Tóth, F. Hudecz, Isomer-dependent daunomycin release and in vitro antitumour effect of cis-aconityl-daunomycin, *Biochemical and Biophysical Research Communications* 303(2) (2003) 556.
- [71] V. Cuchelkar, P. Kopečková, J. Kopeček, Synthesis and biological evaluation of disulfide-linked HPMA copolymer-mesochlorin e6 conjugates, *Macromolecular Bioscience* 8(5) (2008) 375.
- [72] S. Sakuma, Z. Lu, P. Kopečková, J. Kopeček, Biorecognizable HPMA copolymer–drug conjugates for colon-specific delivery of 9-aminocamptothecin, *Journal of Controlled Release* 75(3) (2001) 365.
- [73] S. Sakuma, Z. Lu, B. Pecharová, P. Kopečková, J. Kopeček, N-(2-hydroxypropyl)methacrylamide copolymer-9-aminocamptothecin conjugate: colon-specific drug delivery in rats, *Journal of Bioactive and Compatible Polymers* 17(5) (2002) 305.
- [74] S. Gao, Z. Lu, P. Kopečková, J. Kopeček, Biodistribution and pharmacokinetics of colon-specific HPMA copolymer–9-aminocamptothecin conjugate in mice, *Journal of Controlled Release* 117(2) (2007) 179.
- [75] S. Gao, Z. Lu, B. Petri, P. Kopečková, J. Kopeček, Colon-specific 9-aminocamptothecin-HPMA copolymer conjugates containing a 1,6-elimination spacer, *Journal of Controlled Release* 110(2) (2006) 323.
- [76] J. Shiah, M. Dvořák, P. Kopečková, Y. Sun, C. Peterson, J. Kopeček, Biodistribution and antitumour efficacy of long-circulating N-(2-hydroxypropyl)methacrylamide copolymer: doxorubicin conjugates in nude mice, *European Journal of Cancer* 37(1) (2001) 131.
- [77] H. Pan, J. Yang, P. Kopečková, J. Kopeček, Backbone degradable multiblock N-(2-hydroxypropyl)methacrylamide copolymer conjugates via reversible addition–fragmentation chain transfer polymerization and thiol–ene coupling reaction, *Biomacromolecules* 12(1) (2011) 247.

- [78] K. Luo, J. Yang, P. Kopečková, J. Kopeček, Biodegradable multiblock poly[N-(2-hydroxypropyl)methacrylamide] via reversible addition–fragmentation chain transfer polymerization and click chemistry, *Macromolecules* 44(8) (2011) 2481.
- [79] J. Yang, K. Luo, H. Pan, P. Kopečková, J. Kopeček, Synthesis of biodegradable multiblock copolymers by click coupling of RAFT-generated heterotelechelic polyHPMA conjugates, *Reactive and Functional Polymers* 71(3) (2011) 294.
- [80] Y. Yeo, B. Kim, Drug carriers: not an innocent delivery man, *The AAPS Journal* 17(5) (2015) 1096.
- [81] L. Kiessling, J. Gestwicki, L. Strong, Synthetic multivalent ligands as probes of signal transduction, *Angewandte Chemie International Edition* 45(15) (2006) 2348.
- [82] A. Weisman, B. Chou, J. O'Brien, K. Shea, Polymer antidotes for toxin sequestration, *Advanced Drug Delivery Reviews* 90 (2015) 81.
- [83] M. Ivarsson, J. Leroux, B. Castagner, Targeting bacterial toxins, *Angewandte Chemie International Edition* 51(17) (2012) 4024.
- [84] K. Wu, J. Liu, R. Johnson, J. Yang, J. Kopeček, Drug-free macromolecular therapeutics: induction of apoptosis by coiled-coil-mediated cross-linking of antigens on the cell surface, *Angewandte Chemie International Edition* 122(8) (2010) 1493.
- [85] T. Chu, J. Yang, R. Zhang, M. Sima, J. Kopeček, Cell surface self-assembly of hybrid nanoconjugates via oligonucleotide hybridization induces apoptosis, *ACS Nano* 8(1) (2013) 719.
- [86] L. Chan, X. Wang, H. Wei, L. Pozzo, N. White, S. Pun, A synthetic fibrin cross-linking polymer for modulating clot properties and inducing hemostasis, *Science Translational Medicine* 7(277) (2015) 277ra29.

- [87] N. Bertrand, M. Gauthier, C. Bouvet, P. Moreau, A. Petitjean, J. Leroux, J. Leblond, New pharmaceutical applications for macromolecular binders, *Journal of Controlled Release* 155(2) (2011) 200.
- [88] J. Lu, W. Zhao, H. Liu, R. Marquez, Y. Huang, Y. Zhang, J. Li, W. Xie, R. Venkataramanan, L. Xu, S. Li, An improved d- α -tocopherol-based nanocarrier for targeted delivery of doxorubicin with reversal of multidrug resistance, *Journal of Controlled Release* 196 (2014) 272.
- [89] Y. Wang, S. Hazeldine, J. Li, D. Oupicky, Development of functional poly(amido amine) CXCR4 antagonists with the ability to mobilize leukocytes and deliver nucleic acids, *Advanced Healthcare Materials* 4(5) (2015) 729.
- [90] D. Breslow, Biologically active synthetic polymers, *Pure and Applied Chemistry*, 46(2-4) (1976) 103.
- [91] L. Seymour, Review: synthetic polymers with intrinsic anticancer activity, *Journal of Bioactive and Compatible Polymers* 6(2) (1991) 178.
- [92] Z. Rzayev, M. Türk, E. Söylemez, Bioengineering functional copolymers. XXI. Synthesis of a novel end carboxyl-trithiocarbonate functionalized poly(maleic anhydride) and its interaction with cancer cells, *Bioorganic & Medicinal Chemistry* 20(16) (2012) 5053.
- [93] J. Li, D. Oupický, Effect of biodegradability on CXCR4 antagonism, transfection efficacy and antimetastatic activity of polymeric Plerixafor, *Biomaterials* 35(21) (2014) 5572.
- [94] K. Wu, J. Yang, J. Liu, J. Kopeček, Coiled-coil based drug-free macromolecular therapeutics: In vivo efficacy, *Journal of Controlled Release* 157(1) (2012) 126.
- [95] Z. Peng, J. Kopeček, HPMA copolymer CXCR4 antagonist conjugates substantially inhibited the migration of prostate cancer cells, *ACS Macro Letters* 3(12) (2014) 1240.

- [96] A. Kabanov, E. Batrakova, V. Alakhov, Pluronic® block copolymers for overcoming drug resistance in cancer, *Advanced Drug Delivery Reviews* 54(5) (2002) 759.
- [97] D. Alakhova, N. Rapoport, E. Batrakova, A. Timoshin, S. Li, D. Nicholls, V. Alakhov, A. Kabanov, Differential metabolic responses to pluronic in MDR and non-MDR cells: A novel pathway for chemosensitization of drug resistant cancers, *Journal of Controlled Release* 142(1) (2010) 89.
- [98] V. Solomon, H. Lee, Chloroquine and its analogs: A new promise of an old drug for effective and safe cancer therapies, *European Journal of Pharmacology* 625(1) (2009) 220.
- [99] D. Browning, *Pharmacology of chloroquine and hydroxychloroquine, hydroxychloroquine and chloroquine retinopathy*, Springer New York, New York, NY, (2014), 35.
- [100] I. Ben-Zvi, S. Kivity, P. Langevitz, Y. Shoenfeld, Hydroxychloroquine: from malaria to autoimmunity, *Clinical Reviews in Allergy & Immunology* 42(2) (2012) 145.
- [101] S. Lee, E. Silverman, J. Bargman, The role of antimalarial agents in the treatment of SLE and lupus nephritis, *Nature Reviews Nephrology* 7 (2011) 718.
- [102] F. Janku, D. McConkey, D. Hong, R. Kurzrock, Autophagy as a target for anticancer therapy, *Nature Reviews Clinical Oncology* 8(9) (2011) 528.
- [103] T. Kimura, Y. Takabatake, A. Takahashi, Y. Isaka, Chloroquine in cancer therapy: a double-edged sword of autophagy, *Cancer Research* 73(1) (2013) 3.
- [104] Z. Yang, C. Chee, S. Huang, F. Sinicrope, The role of autophagy in cancer: therapeutic implications, *Molecular Cancer Therapeutics* 10(9) (2011) 1533.
- [105] X. Zhang, X. Zeng, X. Liang, Y. Yang, X. Li, H. Chen, L. Huang, L. Mei, S. Feng, The chemotherapeutic potential of PEG-b-PLGA copolymer micelles that combine chloroquine as autophagy inhibitor and docetaxel as an anti-cancer drug, *Biomaterials* 35(33) (2014) 9144.

- [106] C. Verbaanderd, H. Maes, M. Schaaf, V. Sukhatme, P. Pantziarka, V. Sukhatme, P. Agostinis, G. Bouche, Repurposing drugs in oncology (ReDO)—chloroquine and hydroxychloroquine as anti-cancer agents, *Ecancermedicalsecience* 11 (2017) 781.
- [107] H. Kodani, Studies on the treatment of malignant tumors with fibroblast-inhibiting agent part I effects of chloroquine on experimental animal tumors (Brown-Pearce cancer and Yoshida sarcoma), *Okayama Igakkai Zasshi (Journal of Okayama Medical Association)* 77(7) (1965) 949.
- [108] Y. Zheng, Y. Zhao, X. Deng, S. Yang, Y. Mao, Z. Li, P. Jiang, X. Zhao, Y. Wei, Chloroquine inhibits colon cancer cell growth in vitro and tumor growth in vivo via induction of apoptosis, *Cancer Investigation* 27(3) (2009) 286.
- [109] E. Kim, R. Wüstenberg, A. Rübsam, C. Schmitz-Salue, G. Warnecke, E. Bücken, N. Pettkus, D. Speidel, V. Rohde, W. Schulz-Schaeffer, W. Deppert, A. Giese, Chloroquine activates the p53 pathway and induces apoptosis in human glioma cells, *Neuro-Oncology* 12(4) (2010) 389.
- [110] A. Lakhter, R. Sahu, Y. Sun, W. Kaufmann, E. Androphy, J. Travers, S. Naidu, Chloroquine promotes apoptosis in melanoma cells by inhibiting BH3 domain-mediated PUMA degradation, *Journal of Investigative Dermatology* 133(9) (2013) 2247.
- [111] H. Maes, A. Kuchnio, A. Peric, S. Moens, K. Nys, K. De Bock, A. Quaegebeur, S. Schoors, M. Georgiadou, J. Wouters, S. Vinckier, H. Vankelecom, M. Garmyn, A. Vion, F. Radtke, C. Boulanger, H. Gerhardt, E. Dejana, M. Dewerchin, B. Ghesquière, W. Annaert, P. Agostinis, P. Carmeliet, Tumor vessel normalization by chloroquine independent of autophagy, *Cancer Cell* 26(2) (2014) 190.
- [112] P. Jiang, Y. Zhao, X. Deng, Y. Mao, W. Shi, Q. Tang, Z. Li, Y. Zheng, S. Yang, Y. Wei, Antitumor and antimetastatic activities of chloroquine diphosphate in a murine model of breast cancer, *Biomedicine & Pharmacotherapy* 64(9) (2010) 609.

- [113] S. Yang, X. Wang, G. Contino, M. Liesa, E. Sahin, H. Ying, A. Bause, Y. Li, J. Stommel, G. Dell'antonio, J. Mautner, G. Tonon, M. Haigis, O. Shirihai, C. Doglioni, N. Bardeesy, A. Kimmelman, Pancreatic cancers require autophagy for tumor growth, *Genes & Development* 25(7) (2011) 717.
- [114] Y. Song, S. Zhang, X. Guo, K. Sun, Z. Han, R. Li, Q. Zhao, W. Deng, X. Xie, J. zhang, M. Wu, L. Wei, Autophagy contributes to the survival of CD133+ liver cancer stem cells in the hypoxic and nutrient-deprived tumor microenvironment, *Cancer Letters* 339(1) (2013) 70.
- [115] B. Jutten, T. Keulers, M. Schaaf, K. Savelkouls, J. Theys, P. Span, M. Vooijs, J. Bussink, K. Rouschop, EGFR overexpressing cells and tumors are dependent on autophagy for growth and survival, *Radiotherapy and Oncology* 108(3) (2013) 479.
- [116] P. Maycotte, C. Gearheart, R. Barnard, S. Aryal, J. Mulcahy Levy, S. Fosmire, R. Hansen, M. Morgan, C. Porter, D. Gustafson, A. Thorburn, STAT3-mediated autophagy dependence identifies subtypes of breast cancer where autophagy inhibition can be efficacious, *Cancer Research* 74(9) (2014) 2579.
- [117] D. Chen, J. Xie, R. Fiskesund, W. Dong, X. Liang, J. Lv, X. Jin, J. Liu, S. Mo, T. Zhang, F. Cheng, Y. Zhou, H. Zhang, K. Tang, J. Ma, Y. Liu, B. Huang, Chloroquine modulates antitumor immune response by resetting tumor-associated macrophages toward M1 phenotype, *Nature Communications* 9(1) (2018) 873.
- [118] I. Yamaguchi, T. Takahashi, T. Narisawa, K. Karube, S. Majima, Influence of host conditions upon the growth pattern of transplanted tumors, *The Tohoku Journal of Experimental Medicine* 90(3) (1966) 291.
- [119] P. Dutta, R. Karmali, J. Pinto, R. Rivlin, Enhanced growth of mammary adenocarcinoma in rats by chloroquine and quinacrine, *Cancer Letters* 76(2) (1994) 113.

- [120] C. Loehberg, T. Thompson, M. Kastan, K. Maclean, D. Edwards, F. Kittrell, D. Medina, O. Conneely, B. O'Malley, Ataxia telangiectasia-mutated and p53 are potential mediators of chloroquine-induced resistance to mammary carcinogenesis, *Cancer Research* 67(24) (2007) 12026.
- [121] K. Maclean, F. Dorsey, J. Cleveland, M. Kastan, Targeting lysosomal degradation induces p53-dependent cell death and prevents cancer in mouse models of lymphomagenesis, *The Journal of Clinical Investigation* 118(1) (2008) 79.
- [122] C. Chi, H. Zhu, M. Han, Y. Zhuang, X. Wu, T. Xu, Disruption of lysosome function promotes tumor growth and metastasis in *Drosophila*, *The Journal of biological chemistry* 285(28) (2010) 21817.
- [123] K. Sun, X. Guo, Q. Zhao, Y. jing, X. Kou, X. Xie, Y. Zhou, N. Cai, L. Gao, X. Zhao, S. Zhang, J. Song, D. Li, W. Deng, R. Li, M. Wu, L. Wei, Paradoxical role of autophagy in the dysplastic and tumor-forming stages of hepatocarcinoma development in rats, *Cell Death & Disease* 4 (2013) e501.
- [124] M. Rosenfeldt, J. O'Prey, J. Morton, C. Nixon, G. MacKay, A. Mrowinska, A. Au, T. Rai, L. Zheng, R. Ridgway, P. Adams, K. Anderson, E. Gottlieb, O. Sansom, K. Ryan, p53 status determines the role of autophagy in pancreatic tumour development, *Nature* 504 (2013) 296.
- [125] Q. Hu, W. Sun, C. Wang, Z. Gu, Recent advances of cocktail chemotherapy by combination drug delivery systems, *Advanced Drug Delivery Reviews* 98 (2016) 19.
- [126] D. Hanahan, R. Weinberg, The Hallmarks of Cancer, *Cell* 100(1) (2000) 57.
- [127] B. Xiao, L. Ma, D. Merlin, Nanoparticle-mediated co-delivery of chemotherapeutic agent and siRNA for combination cancer therapy, *Expert Opinion on Drug Delivery* 14(1) (2017) 65.
- [128] B. Chabner, T. Roberts, Jr., Timeline: chemotherapy and the war on cancer, *Nature Reviews Cancer* 5(1) (2005) 65.

- [129] V. DeVita, Jr., E. Chu, A history of cancer chemotherapy, *Cancer Research* 68(21) (2008) 8643.
- [130] L. Mayer, T. Harasym, P. Tardi, N. Harasym, C. Shew, S. Johnstone, E. Ramsay, M. Bally, A. Janoff, Ratiometric dosing of anticancer drug combinations: controlling drug ratios after systemic administration regulates therapeutic activity in tumor-bearing mice, *Molecular Cancer Therapeutics* 5(7) (2006) 1854.
- [131] T. Harasym, B. Liboiron, L. Mayer, Drug ratio-dependent antagonism: a new category of multidrug resistance and strategies for its circumvention, *Methods in Molecular Biology* 596 (2010) 291.
- [132] L. Mayer, A. Janoff, Optimizing combination chemotherapy by controlling drug ratios, *Molecular Interventions* 7(4) (2007) 216.
- [133] J. Woodcock, J. Griffin, R. Behrman, Development of novel combination therapies, *The New England Journal of Medicine* 364(11) (2011) 985.
- [134] B. Al-Lazikani, U. Banerji, P. Workman, Combinatorial drug therapy for cancer in the post-genomic era, *Nature Biotechnology* 30(7) (2012) 679.
- [135] M. Wu, M. Sirota, A. Butte, B. Chen, Characteristics of drug combination therapy in oncology by analyzing clinical trial data on ClinicalTrials.gov, *Pacific Symposium on Biocomputing* (2015) 68.
- [136] Y. Hu, M. DeLay, A. Jahangiri, A. Molinaro, S. Rose, W. Carbonell, M. Aghi, Hypoxia-induced autophagy promotes tumor cell survival and adaptation to antiangiogenic treatment in glioblastoma, *Cancer Research* 72(7) (2012) 1773.
- [137] J. Shen, H. Zheng, J. Ruan, W. Fang, A. Li, G. Tian, X. Niu, S. Luo, P. Zhao, Autophagy inhibition induces enhanced proapoptotic effects of ZD6474 in glioblastoma, *British Journal of Cancer* 109(1) (2013) 164.

- [138] E. Golden, H. Cho, A. Jahanian, F. Hofman, S. Louie, A. Schönthal, T. Chen, Chloroquine enhances temozolomide cytotoxicity in malignant gliomas by blocking autophagy, *Neurosurgical Focus* 37(6) (2014) E12.
- [139] A. Zanotto-Filho, E. Braganhol, K. Klafke, F. Figueiró, S. Terra, F. Paludo, M. Morrone, I. Bristot, A. Battastini, C. Forcelini, A. Bishop, D. Gelain, J. Moreira, Autophagy inhibition improves the efficacy of curcumin/temozolomide combination therapy in glioblastomas, *Cancer Letters* 358(2) (2015) 220.
- [140] R. Thomas, D. Vane, J. Grosfeld, P. Faught, The effect of chloroquine and hyperthermia on murine neuroblastoma, *Journal of Pediatric Surgery* 25(9) (1990) 929.
- [141] S. Avniel, G. Leibowitz, V. Doviner, D. Gross, S. Grozinsky-Glasberg, Combining chloroquine with RAD001 inhibits tumor growth in a NEN mouse model, *Endocrine-Related Cancer* 25(6) (2018) 677.
- [142] D. Gaudin, K. Yielding, A. Stabler, J. Brown, The effect of DNA repair inhibitors on the response of tumors treated with x-Ray and alkylating agents, *Proceedings of the Society for Experimental Biology and Medicine* 137(1) (1971) 202.
- [143] L. Harhaji-Trajkovic, K. Arsikin, T. Kravic-Stevovic, S. Petricevic, G. Tovilovic, A. Pantovic, N. Zogovic, B. Ristic, K. Janjetovic, V. Bumbasirevic, V. Trajkovic, Chloroquine-mediated lysosomal dysfunction enhances the anticancer effect of nutrient deprivation, *Pharmaceutical Research* 29(8) (2012) 2249.
- [144] X. Xie, E. White, J. Mehnert, Coordinate autophagy and mTOR pathway inhibition enhances cell death in melanoma, *PloS one* 8(1) (2013) e55096.
- [145] J. Shoemaker, Fifty-five percent complete remission of mammary carcinoma in mice with 5-fluorouracil and chloroquine, *Cancer Research* 38(9) (1978) 2700.

- [146] J. Shoemaker, R. Dagher, Remissions of mammary adenocarcinoma in hypothyroid mice given 5-fluorouracil and chloroquine phosphate, *Journal of the National Cancer Institute* 62(6) (1979) 1575.
- [147] C. Loehberg, P. Strissel, R. Dittrich, R. Strick, J. Dittmer, A. Dittmer, B. Fabry, W. Kalender, T. Koch, D. Wachter, N. Groh, A. Polier, I. Brandt, L. Lotz, I. Hoffmann, F. Koppitz, S. Oeser, A. Mueller, P. Fasching, M. Lux, M. Beckmann, M. Schrauder, Akt and p53 are potential mediators of reduced mammary tumor growth by cloroquine and the mTOR inhibitor RAD001, *Biochemical Pharmacology* 83(4) (2012) 480.
- [148] R. Rao, R. Balusu, W. Fiskus, U. Mudunuru, S. Venkannagari, L. Chauhan, J. Smith, S. Hembruff, K. Ha, P. Atadja, K. Bhalla, Combination of pan-histone deacetylase inhibitor and autophagy inhibitor exerts superior efficacy against triple-negative human breast cancer cells, *Molecular Cancer Therapeutics* 11(4) (2012) 973.
- [149] S. Thomas, N. Sharma, E. Golden, H. Cho, P. Agarwal, K. Gaffney, N. Petasis, T. Chen, F. Hofman, S. Louie, A. Schonthal, Preferential killing of triple-negative breast cancer cells in vitro and in vivo when pharmacological aggravators of endoplasmic reticulum stress are combined with autophagy inhibitors, *Cancer Letters* 325(1) (2012) 63.
- [150] E. Seront, R. Boidot, C. Bouzin, O. Karroum, B. Jordan, B. Gallez, J. Machiels, O. Feron, Tumour hypoxia determines the potential of combining mTOR and autophagy inhibitors to treat mammary tumours, *British Journal of Cancer* 109(10) (2013) 2597.
- [151] W. Dragowska, S. Wepler, J. Wang, L. Wong, A. Kapanen, J. Rawji, C. Warburton, M. Qadir, E. Donohue, M. Roberge, S. Gorski, K. Gelmon, M. Bally, Induction of autophagy is an early response to gefitinib and a potential therapeutic target in breast cancer, *PloS One* 8(10) (2013) e76503.

- [152] S. Cufi, A. Vazquez-Martin, C. Oliveras-Ferraros, B. Corominas-Faja, E. Cuyas, E. Lopez-Bonet, B. Martin-Castillo, J. Joven, J. Menendez, The anti-malarial chloroquine overcomes primary resistance and restores sensitivity to trastuzumab in HER2-positive breast cancer, *Scientific Reports* 3 (2013) 2469.
- [153] J. Ratikan, J. Sayre, D. Schaeue, Chloroquine engages the immune system to eradicate irradiated breast tumors in mice, *International Journal of Radiation Oncology, Biology, Physics* 87(4) (2013) 761.
- [154] S. Lefort, C. Joffre, Y. Kieffer, A. Givel, B. Bourachot, G. Zago, I. Bieche, T. Dubois, D. Meseure, A. Vincent-Salomon, J. Camonis, F. Mechta-Grigoriou, Inhibition of autophagy as a new means of improving chemotherapy efficiency in high-LC3B triple-negative breast cancers, *Autophagy* 10(12) (2014) 2122.
- [155] K. Cook, A. Warri, D. Soto-Pantoja, P. Clarke, M. Cruz, A. Zwart, R. Clarke, Hydroxychloroquine inhibits autophagy to potentiate antiestrogen responsiveness in ER+ breast cancer, *Clinical Cancer Research* 20(12) (2014) 3222.
- [156] D. Liang, D. Choi, J. Ensor, B. Kaiparettu, B. Bass, J. Chang, The autophagy inhibitor chloroquine targets cancer stem cells in triple negative breast cancer by inducing mitochondrial damage and impairing DNA break repair, *Cancer Letters* 376(2) (2016) 249.
- [157] R. Amaravadi, D. Yu, J. Lum, T. Bui, M. Christophorou, G. Evan, A. Thomas-Tikhonenko, C. Thompson, Autophagy inhibition enhances therapy-induced apoptosis in a Myc-induced model of lymphoma, *Journal of Clinical Investigation* 117(2) (2007) 326.
- [158] G. Mitou, J. Frenzel, A. Desquesnes, S. Le Gonidec, T. AlSaati, I. Beau, L. Lamant, F. Meggetto, E. Espinos, P. Codogno, P. Brousset, S. Giuriato, Targeting autophagy enhances the anti-tumoral action of crizotinib in ALK-positive anaplastic large cell lymphoma, *Oncotarget* 6(30) (2015) 30149.

- [159] L. Yu, C. Gu, D. Zhong, L. Shi, Y. Kong, Z. Zhou, S. Liu, Induction of autophagy counteracts the anticancer effect of cisplatin in human esophageal cancer cells with acquired drug resistance, *Cancer Letters* 355(1) (2014) 34.
- [160] H. Zhang, N. Fang, X. Liu, S. Xiong, Y. Liao, W. Jin, R. Song, Y. Wan, Antitumor activity of chloroquine in combination with Cisplatin in human gastric cancer xenografts, *Asian Pacific Journal of Cancer Prevention* 16(9) (2015) 3907.
- [161] Z. Ding, B. Hui, Y. Shi, J. Zhou, Y. Peng, C. Gu, H. Yang, G. Shi, A. Ke, X. Wang, K. Song, Z. Dai, Y. Shen, J. Fan, Autophagy activation in hepatocellular carcinoma contributes to the tolerance of oxaliplatin via reactive oxygen species modulation, *Clinical Cancer Research* 17(19) (2011) 6229.
- [162] Y. Shi, Z. Ding, J. Zhou, B. Hui, G. Shi, A. Ke, X. Wang, Z. Dai, Y. Peng, C. Gu, S. Qiu, J. Fan, Targeting autophagy enhances sorafenib lethality for hepatocellular carcinoma via ER stress-related apoptosis, *Autophagy* 7(10) (2011) 1159.
- [163] X. Guo, D. Li, F. Hu, J. Song, S. Zhang, W. Deng, K. Sun, Q. Zhao, X. Xie, Y. Song, M. Wu, L. Wei, Targeting autophagy potentiates chemotherapy-induced apoptosis and proliferation inhibition in hepatocarcinoma cells, *Cancer Letters* 320(2) (2012) 171.
- [164] B. Hui, Y. Shi, Z. Ding, J. Zhou, C. Gu, Y. Peng, H. Yang, W. Liu, G. Shi, J. Fan, Proteasome inhibitor interacts synergistically with autophagy inhibitor to suppress proliferation and induce apoptosis in hepatocellular carcinoma, *Cancer* 118(22) (2012) 5560.
- [165] S. Shimizu, T. Takehara, H. Hikita, T. Kodama, H. Tsunematsu, T. Miyagi, A. Hosui, H. Ishida, T. Tatsumi, T. Kanto, N. Hiramatsu, N. Fujita, T. Yoshimori, N. Hayashi, Inhibition of autophagy potentiates the antitumor effect of the multikinase inhibitor sorafenib in hepatocellular carcinoma, *International Journal of Cancer* 131(3) (2012) 548.

- [166] L. Gao, J. Song, J. Zhang, X. Zhao, Q. Zhao, K. Sun, W. Deng, R. Li, G. Lv, H. Cheng, L. Wei, Chloroquine promotes the anticancer effect of TACE in a rabbit VX2 liver tumor model, *International Journal of Biological Sciences* 9(4) (2013) 322.
- [167] S. Helmy, M. El-Mesery, A. El-Karef, L. Eissa, A. El Gayar, Chloroquine upregulates TRAIL/TRAILR2 expression and potentiates doxorubicin anti-tumor activity in thioacetamide-induced hepatocellular carcinoma model, *Chemico-biological Interactions* 279 (2018) 84.
- [168] W. Ding, H. Ni, W. Gao, X. Chen, J. Kang, D. Stolz, J. Liu, X. Yin, Oncogenic transformation confers a selective susceptibility to the combined suppression of the proteasome and autophagy, *Molecular Cancer Therapeutics* 8(7) (2009) 2036.
- [169] J. Carew, E. Medina, J. Esquivel, D. Mahalingam, R. Swords, K. Kelly, H. Zhang, P. Huang, A. Mita, M. Mita, F. Giles, S. Nawrocki, Autophagy inhibition enhances vorinostat-induced apoptosis via ubiquitinated protein accumulation, *Journal of Cellular and Molecular Medicine* 14(10) (2010) 2448.
- [170] K. Sasaki, N. Tsuno, E. Sunami, K. Kawai, K. Hongo, M. Hiyoshi, M. Kaneko, K. Muro, N. Tada, T. Nirei, K. Takahashi, J. Kitayama, Resistance of colon cancer to 5-fluorouracil may be overcome by combination with chloroquine, an in vivo study, *Anti-cancer Drugs* 23(7) (2012) 675.
- [171] X. Liang, M. De Vera, W. Buchser, A. Romo de Vivar Chavez, P. Loughran, D. Beer Stolz, P. Basse, T. Wang, B. Van Houten, H. Zeh, M. Lotze, Inhibiting systemic autophagy during interleukin 2 immunotherapy promotes long-term tumor regression, *Cancer Research* 72(11) (2012) 2791.
- [172] M. Selvakumaran, R. Amaravadi, I. Vasilevska, P. O'Dwyer, Autophagy inhibition sensitizes colon cancer cells to antiangiogenic and cytotoxic therapy, *Clinical Cancer Research* 19(11) (2013) 2995.

- [173] M. Kaneko, H. Nozawa, M. Hiyoshi, N. Tada, K. Muro, T. Nirei, S. Emoto, J. Kishikawa, Y. Iida, E. Sunami, N.H. Tsuno, J. Kitayama, K. Takahashi, T. Watanabe, Temsirolimus and chloroquine cooperatively exhibit a potent antitumor effect against colorectal cancer cells, *Journal of Cancer Research and Clinical Oncology* 140(5) (2014) 769.
- [174] M. Wei, M. Chen, K. Chen, P. Lou, S. Lin, S. Hung, M. Hsiao, C. Yao, M. Shieh, Autophagy promotes resistance to photodynamic therapy-induced apoptosis selectively in colorectal cancer stem-like cells, *Autophagy* 10(7) (2014) 1179.
- [175] A. Balic, M. Sorensen, S. Trabulo, B. Sainz, Jr., M. Cioffi, C. Vieira, I. Miranda-Lorenzo, M. Hidalgo, J. Kleeff, M. Erkan, C. Heeschen, Chloroquine targets pancreatic cancer stem cells via inhibition of CXCR4 and hedgehog signaling, *Molecular Cancer Therapeutics* 13(7) (2014) 1758.
- [176] C. Bellodi, M. Lidonnici, A. Hamilton, G. Helgason, A. Soliera, M. Ronchetti, S. Galavotti, K. Young, T. Selmi, R. Yacobi, R. Van Etten, N. Donato, A. Hunter, D. Dinsdale, E. Tirro, P. Vigneri, P. Nicotera, M. Dyer, T. Holyoake, P. Salomoni, B. Calabretta, Targeting autophagy potentiates tyrosine kinase inhibitor-induced cell death in Philadelphia chromosome-positive cells, including primary CML stem cells, *Journal of Clinical Investigation* 119(5) (2009) 1109.
- [177] S. Xiong, H. Li, B. Yu, J. Wu, R. Lee, Triggering liposomal drug release with a lysosomotropic agent, *Journal of Pharmaceutical Sciences* 99(12) (2010) 5011.
- [178] A. Arnold, J. Whitehouse, Interaction of VP16-213 with the DNA repair antagonist chloroquine, *Cancer Chemotherapy and Pharmacology* 7(2-3) (1982) 123.
- [179] A. Abdel-Aziz, S. Shouman, E. El-Demerdash, M. Elgendy, A. Abdel-Naim, Chloroquine synergizes sunitinib cytotoxicity via modulating autophagic, apoptotic and angiogenic machineries, *Chemico-biological Interactions* 217 (2014) 28.

- [180] K. Bray, R. Mathew, A. Lau, J. Kamphorst, J. Fan, J. Chen, H. Chen, A. Ghavami, M. Stein, R. DiPaola, D. Zhang, J. Rabinowitz, E. White, Autophagy suppresses RIP kinase-dependent necrosis enabling survival to mTOR inhibition, *PloS One* 7(7) (2012) e41831.
- [181] M. Li, Y. Xu, W. Lu, Y. Li, S. Tan, H. Lin, T. Wu, Y. Li, S. Wang, Y. Zhao, Chloroquine potentiates the anticancer effect of sunitinib on renal cell carcinoma by inhibiting autophagy and inducing apoptosis, *Oncology Letters* 15(3) (2018) 2839.
- [182] Y. Zou, Y. Ling, J. Sironi, E. Schwartz, R. Perez-Soler, B. Piperdi, The autophagy inhibitor chloroquine overcomes the innate resistance of wild-type EGFR non-small-cell lung cancer cells to erlotinib, *Journal of Thoracic Oncology* 8(6) (2013) 693.
- [183] S. Bokobza, Y. Jiang, A. Weber, A. Devery, A. Ryan, Combining AKT inhibition with chloroquine and gefitinib prevents compensatory autophagy and induces cell death in EGFR mutated NSCLC cells, *Oncotarget* 5(13) (2014) 4765.
- [184] C. Ji, L. Zhang, Y. Cheng, R. Patel, H. Wu, Y. Zhang, M. Wang, S. Ji, C. Belani, J. Yang, X. Ren, Induction of autophagy contributes to crizotinib resistance in ALK-positive lung cancer, *Cancer Biology & Therapy* 15(5) (2014) 570.
- [185] L. You, J. Shou, D. Deng, L. Jiang, Z. Jing, J. Yao, H. Li, J. Xie, Z. Wang, Q. Pan, H. Pan, W. Huang, W. Han, Crizotinib induces autophagy through inhibition of the STAT3 pathway in multiple lung cancer cell lines, *Oncotarget* 6(37) (2015) 40268.
- [186] M. Tang, M. Wu, M. Hwang, Y. Chang, H. Huang, A. Lin, J. Yang, Chloroquine enhances gefitinib cytotoxicity in gefitinib-resistant nonsmall cell lung cancer cells, *PloS One* 10(3) (2015) e0119135.
- [187] X. Hu, S. Shi, H. Wang, X. Yu, Q. Wang, S. Jiang, D. Ju, L. Ye, M. Feng, Blocking autophagy improves the anti-tumor activity of afatinib in lung adenocarcinoma with activating EGFR mutations in vitro and in vivo, *Scientific Reports* 7(1) (2017) 4559.

- [188] J. Zhu, Y. Zheng, H. Zhang, J. Zhu, H. Sun, Low concentration of chloroquine enhanced efficacy of cisplatin in the treatment of human ovarian cancer dependent on autophagy, *American Journal of Translational Research* 9(9) (2017) 4046.
- [189] V. Jarauta, P. Jaime, O. Gonzalo, D. de Miguel, A. Ramirez-Labrada, L. Martinez-Lostao, A. Anel, J. Pardo, I. Marzo, J. Naval, Inhibition of autophagy with chloroquine potentiates carfilzomib-induced apoptosis in myeloma cells in vitro and in vivo, *Cancer Letters* 382(1) (2016) 1.
- [190] M. King, I. Ganley, V. Flemington, Inhibition of cholesterol metabolism underlies synergy between mTOR pathway inhibition and chloroquine in bladder cancer cells, *Oncogene* 35(34) (2016) 4518.
- [191] R. Schroeder, J. Gerber, Chloroquine and hydroxychloroquine binding to melanin: some possible consequences for pathologies, *Toxicology Reports* 1 (2014) 963.
- [192] S. Bhattarai, E. Muthuswamy, A. Wani, M. Brichacek, A. Castañeda, S. Brock, D. Oupicky, Enhanced gene and siRNA delivery by polycation-modified mesoporous silica nanoparticles loaded with chloroquine, *Pharmaceutical Research* 27(12) (2010) 2556.
- [193] K. Degenhardt, R. Mathew, B. Beaudoin, K. Bray, D. Anderson, G. Chen, C. Mukherjee, Y. Shi, C. Gelinas, Y. Fan, D.A. Nelson, S. Jin, E. White, Autophagy promotes tumor cell survival and restricts necrosis, inflammation, and tumorigenesis, *Cancer Cell* 10(1) (2006) 51.
- [194] M. Cicchini, V. Karantza, B. Xia, Molecular pathways: autophagy in cancer--a matter of timing and context, *Clinical Cancer Research* 21(3) (2015) 498.
- [195] J. Guo, H. Chen, R. Mathew, J. Fan, A. Strohecker, G. Karsli-Uzunbas, J. Kamphorst, G. Chen, J. Lemons, V. Karantza, H. Coller, R. Dipaola, C. Gelinas, J. Rabinowitz, E. White, Activated Ras requires autophagy to maintain oxidative metabolism and tumorigenesis, *Genes & Development* 25(5) (2011) 460.

- [196] P. Boya, R. Gonzalez-Polo, D. Poncet, K. Andreau, H. Vieira, T. Roumier, J. Perfettini, G. Kroemer, Mitochondrial membrane permeabilization is a critical step of lysosome-initiated apoptosis induced by hydroxychloroquine, *Oncogene* 22(25) (2003) 3927.
- [197] P. Maycotte, S. Aryal, C. Cummings, J. Thorburn, M. Morgan, A. Thorburn, Chloroquine sensitizes breast cancer cells to chemotherapy independent of autophagy, *Autophagy* 8(2) (2012) 200.
- [198] C. Eng, Z. Wang, D. Tkach, L. Toral-Barza, S. Ugwonali, S. Liu, S. Fitzgerald, E. George, E. Frias, N. Cochran, R. De Jesus, G. McAllister, G. Hoffman, K. Bray, L. Lemon, J. Lucas, V. Fantin, R. Abraham, L. Murphy, B. Nyfeler, Macroautophagy is dispensable for growth of KRAS mutant tumors and chloroquine efficacy, *Proceedings of the National Academy of Sciences of the United States of America* 113(1) (2016) 182.
- [199] J. Kim, M. Yip, X. Shen, H. Li, L. Hsin, S. Labarge, E. Heinrich, W. Lee, J. Lu, N. Vaidehi, Identification of anti-malarial compounds as novel antagonists to chemokine receptor CXCR4 in pancreatic cancer cells, *PloS One* 7(2) (2012) e31004.
- [200] G. Moad, E. Rizzardo, S. Thang, Living radical polymerization by the RAFT process, *Australian Journal of Chemistry* 58(6) (2005) 379.
- [201] X. Hu, J. Hu, J. Tian, Z. Ge, G. Zhang, K. Luo, S. Liu, Polyprodrug amphiphiles: hierarchical assemblies for shape-regulated cellular internalization, trafficking, and drug delivery, *Journal of the American Chemical Society* 135(46) (2013) 17617.
- [202] K. Uk, Y. Chang, S. Jin, Y. Ho, One-step synthesis of block copolymers using a hydroxyl-functionalized trithiocarbonate RAFT agent as a dual initiator for RAFT polymerization and ROP, *Journal of Polymer Science Part A: Polymer Chemistry* 51(4) (2013) 774.

- [203] N. Du, W. Guo, Q. Yu, S. Guan, L. Guo, T. Shen, H. Tang, Z. Gan, Poly(d,l-lactic acid)-block-poly(N-(2-hydroxypropyl)methacrylamide) nanoparticles for overcoming accelerated blood clearance and achieving efficient anti-tumor therapy, *Polymer Chemistry* 7(36) (2016) 5719.
- [204] J. Levy, C. Towers, A. Thorburn, Targeting autophagy in cancer, *Nature Reviews Cancer* 17(9) (2017) 528.
- [205] J. Sandholm, J. Tuomela, J. Kauppila, K. Harris, D. Graves, K. Selander, Hypoxia regulates Toll-like receptor-9 expression and invasive function in human brain cancer cells in vitro, *Oncology Letters* 8(1) (2014) 266.
- [206] J. Kopeček, Polymer–drug conjugates: Origins, progress to date and future directions, *Advanced Drug Delivery Reviews* 65(1) (2013) 49.
- [207] R. Duncan, Polymer therapeutics: Top 10 selling pharmaceuticals - what next?, *Journal of Controlled Release* 190 (2014) 371.
- [208] E. White, The role for autophagy in cancer, *The Journal of Clinical Investigation* 125(1) (2015) 42.
- [209] Y. Kondo, T. Kanzawa, R. Sawaya, S. Kondo, The role of autophagy in cancer development and response to therapy, *Nature Reviews Cancer* 5 (2005) 726.
- [210] N. Mizushima, T. Yoshimori, B. Levine, Methods in mammalian autophagy research, *Cell* 140(3) (2010) 313.
- [211] F. Yu, Y. Xie, Y. Wang, Z. Peng, J. Li, D. Oupický, Chloroquine-containing HPMA copolymers as polymeric inhibitors of cancer cell migration mediated by the CXCR4/SDF-1 chemokine axis, *ACS Macro Letters* 5(3) (2016) 342.
- [212] Y. Alsayed, H. Ngo, J. Runnels, X. Leleu, U. Singha, C. Pitsillides, J. Spencer, T. Kimlinger, J. Ghobrial, X. Jia, G. Lu, M. Timm, A. Kumar, D. Côté, I. Veilleux, K. Hedin, G. Roodman, T.

Witzig, A. Kung, T. Hideshima, K. Anderson, C. Lin, I. Ghobrial, Mechanisms of regulation of CXCR4/SDF-1 (CXCL12)-dependent migration and homing in multiple myeloma, *Blood* 109(7) (2007) 2708.